

**Further Development of
the Module ATHLET-CD
of the Code Package AC²**

Further Development of the Module ATHLET-CD of the Code Package AC²

Liviusz Lovasz
Livia Tiborcz
Peter Pandazis
Christophe D'Alessandro
Yann Périn
Thorsten Hollands
Kin Wing Wong
Andreas Wielenberg

March 2022

Remark

This report refers to the research project RS1574 which has been funded by the Federal Ministry for the Environment, Nature, Conservation, Nuclear Safety and Consumer Protection (BMUV).

The work was conducted by the GRS. The authors are responsible for the content of the report.

The report reflects the views and opinion of GRS and are not necessarily those of the BMUV.

Keywords

AC², ATHLET-CD, code system, severe accident

Abstract

As part of the reactor safety research funded by the German government, the ATHLET-CD computer code system is being developed for safety analyses of nuclear power plants with pressurised and boiling water reactors and for the evaluation of plant-internal emergency protection measures. The objective is to provide a largely mechanistic analysis tool for a realistic simulation of severe accidents in water-cooled nuclear reactors. Furthermore, the performance of the code system should allow realistic analyses of beyond-design-basis accidents as well as the simulation of advanced core destruction with an extended model scope to be carried out in reasonable computing time.

ATHLET-CD is based on the ATHLET thermal-hydraulic models. On the basis of the ATHLET models, it is possible to derive the initial and boundary conditions for the calculation of accidents with ATHLET-CD directly from previous transients. The current version of ATHLET is fully integrated in ATHLET-CD. ATHLET-CD contains modules for the simulation of fuel rod and control element destruction in pressurised and boiling water reactors, models for the description of phenomena in the lower plenum, as well as modules for the release and transport of fission products and aerosols in the cooling circuit, including the decay of nuclide inventories and chemical reactions in the gas phase. Within the framework of project RS1574, models were further developed or newly implemented in the following subject areas and the following quality assurance measures were carried out:

- Core destruction and relocation of the core meltdown
- Fission product transport
- Phenomena in the lower plenum and simulation of ex-vessel cooling
- Extension of the documentation, improvement of the user-friendliness
- Extension and automation of the test base
- Customer support and bug fixes

With this work, the quality of the recalculations of transients, accidents and accident sequences in nuclear reactors and of tests could be significantly increased. In addition, the overall robustness of ATHLET-CD could be improved.

During the reporting period, two versions were released and distributed to numerous users.

Kurzfassung

Umfassende Sicherheitsanalysen von Stör- und Unfallabläufen in Kernkraftwerken erfordern den Einsatz von Rechenprogrammen, die entsprechend dem jeweils aktuellen Stand von Wissenschaft und Technik eine möglichst realitätsnahe Simulation der Abläufe und der sich einstellenden Zustände erlauben. Diese Forderung wird sowohl für Auslegungsstörfälle als auch für auslegungsüberschreitende Ereignisse erhoben. Die Gesellschaft für Anlagen- und Reaktorsicherheit (GRS) gGmbH entwickelt hierzu u.a. das Programmsystem AC², das die Programme ATHLET (**A**nalyse der **T**hermohydraulik von **L**ecks und **T**ransienten), ATHLET-CD (**C**ore **D**egradation) und COCOSYS (**C**ontainment **C**ode **S**ystem) umfasst. Der Fokus dieses Vorhabens lag auf der Weiterentwicklung und Verbesserung von ATHLET-CD.

Übergeordnetes Ziel der Weiterentwicklung von ATHLET-CD war ein signifikant verbessertes Simulationsprogramm zur Beurteilung der Sicherheit der in Deutschland noch laufenden bzw. im Ausland betriebenen, in Bau befindlichen und geplanten Kernkraftwerke bereitzustellen. Um das Gesamtziel der umfassenden Verbesserung von ATHLET-CD zu erreichen, wurde das Vorhaben in vier Arbeitsziele gegliedert, die den jeweiligen Arbeitspaketen zugeordnet waren:

- AP1: Verbesserung und Erweiterung der Modelle für den Reaktorkern
- AP2: Simulation der Spätphase
- AP3: Arbeiten zur Reaktoranwendung
- AP4: Querschnittsaufgaben

AP1: Verbesserung und Erweiterung der Modelle für den Reaktorkern

Die Vorgänge im Reaktorkern haben großen Einfluss auf alle anderen Unfallabläufe und spielen somit eine überaus wichtige Rolle für die gesamte Entwicklung eines Unfalls. AP1 beschäftigte sich mit der Verbesserung und Erweiterung ausgewählter Modelle, mit deren Hilfe das Verhalten des Reaktorkerns im Falle eines Unfalls simuliert werden kann. Von zentraler Bedeutung sind dabei die Vorgänge der Kernzerstörung, das damit eng verbundene Oxidationsverhalten sowie die Freisetzung und der Transport der Spaltprodukte, denen jeweils ein eigener Unterpunkt gewidmet wurde.

Im Vorgänger-Vorhaben RS1546 wurden die Nodalisierungsmöglichkeiten für den Kernbereich deutlich erweitert. Die Beschränkung auf eine ringförmige Nodalisierung im Kernbereich wurde aufgehoben, und eine azimutale Unterteilung der Ringsegmente ermöglicht und auch weitere, weitaus freiere Nodalisierungen nutzbar gemacht. Allerdings war es bislang nicht möglich, dass sich im neu implementierten Modell die Schmelze innerhalb einer Ebene, also in radialer oder azimutaler Richtung, ausbreitet, was in der Ringgeometrie möglich war. Um realistischere Ergebnisse der Schmelzevorgänge zu erzielen, wurden diese Wege der Ausbreitung der Schmelze ermöglicht und verifiziert. Außerdem wurden bei der vertikalen Verlagerung die Abstandshalter, die bei der Schmelzeverlagerung eine Blockade bilden können, in der Modellierung berücksichtigt. Weiterhin wurde ein Modell entwickelt, das eine vertikale Verlagerung von Schmelze im Kernbypass, wie es beispielsweise während des Unfalls in der Anlage von TMI-2 geschehen ist, ermöglicht. Schließlich wurden die Möglichkeiten verbessert, Unfälle in Reaktoren des russischen Typs WWER440 zu simulieren, von denen sich einige noch längere Zeit im Betrieb befinden werden. Besonders die Tatsache, dass bei diesem Reaktortyp bei der Schnellabschaltung Brennstäbe aus dem Kern nach unten herausgeschoben werden, machte einige Erweiterungen in der Modellierung notwendig, beispielsweise hinsichtlich der besonderen Geometrie der kombinierten Brenn-/Steuerstäbe.

Hinsichtlich der Oxidationsphänomene und Materialinteraktionen wurden die Oxidationsmodelle erweitert, so dass neue Hüllrohrmaterialien wie beispielsweise FeCrAl berücksichtigt werden können. Dies erfolgt auf Basis des engen Kontakts mit den Experimentatoren, die solche Materialien untersuchen (z. B. beim KIT). Weiterhin wurde für Siedewasserreaktoren die Bildung von Eutektika bei den Borkarbid-Stahl- und Borkarbid-Zirkon-Reaktionen berücksichtigt. In der bisherigen Modellierung wurden hier die Schmelzpunkte der einzelnen Elemente verwendet, nicht aber die reduzierten Schmelzpunkte und geänderte Parameter der Stoffmischungen. Für Luftoxidation wurde die Nitridbildung in der Schmelze modelliert, die bisher bei Siedewasserreaktoren nicht möglich war.

Im Modul für den Spaltprodukttransport SAFT wurde die Steuerung der teilweise recht umfangreichen Datenausgabe weiter verbessert; die durchgeführten Arbeiten basierten auf entsprechenden Anwenderrückmeldungen. Außerdem wurde das Abschmelzen von Strukturen, an denen sich Spaltprodukte ablagern können, modelliert. Bisher hat SAFT das Versagen einer Struktur nicht ausreichend berücksichtigt. Schließlich wurden die

wesentlichen noch im Code befindlichen Limitierungen von SAFT identifiziert und dokumentiert, um die Arbeit der Anwender mit SAFT zu erleichtern und um zukünftige Entwicklungsmöglichkeiten zu konkretisieren.

Ein weiterer wichtiger Punkt war die Überarbeitung einzelner Modelle (Refactoring). Aufgrund der gewachsenen Struktur von ATHLET-CD bereitet die Erweiterung und Pflege von Modellen in zahlreichen Fällen große Mühe, z. B. wenn Rechnungen unrealistische Ergebnisse liefern oder auch wenn Rechnungen numerisch nicht performant sind. Aus dem Grund wurde der Code allgemein besser an die Vorgaben der GRS-Richtlinie zur Softwareentwicklung und an die Programmierrichtlinien der GRS angepasst. Dabei wurden sowohl rein IT-technische Änderungen durchgeführt wie zum Beispiel die explizite Deklaration aller internen Variablen, als auch eine Ersetzung/Überarbeitung einzelner Modelle vorgenommen. Einen größeren Arbeitsaufwand bedeutete die Ersetzung der Module für Inventar- und Zerfallsberechnung (OREST/FIPISO) von ATHLET-CD durch den mit Beteiligung der GRS neu entwickelten Code VENTINA. Für diese Arbeiten wurde ein Aufstockungsantrag gestellt und genehmigt. Damit beinhaltet ATHLET-CD jetzt ein aktualisiertes Modell für die Inventar- und Zerfallsberechnung, das in der Zukunft durch die GRS einfacher verbessert und für alle AC²-Programme implementiert und genutzt werden kann.

AP2: Simulation der Spätphase

Die Simulation der Spätphase eines Unfallablaufs hat in den vergangenen Jahren, gerade seit dem Unfall in Fukushima-Daiichi, immer mehr an Bedeutung gewonnen. Daher war es wichtig, die in ATHLET-CD implementierten Modelle für das untere Plenum weiter zu verbessern.

Das untere Plenum-Modul LHEAD wurde um wichtige Modellierungsoptionen erweitert, die bisher nur in AIDA verfügbar waren, wie z.B. der Leistungserzeugung in der Metallschicht. Außerdem wurde durch die Code-Umstrukturierung erreicht, dass das Einfließen der Schmelze in die Rechenbereiche von LHEAD durch ein „FILL“ möglich ist. Das bedeutet, dass der Benutzer jetzt die Möglichkeit hat, die Rand- und Anfangsbedingungen der Schmelze im unteren Plenum explizit angeben kann, falls er mit LHEAD nur die Phänomene im unteren Plenum untersuchen möchte, ohne vorher ein Unfallszenario im Kern rechnen zu müssen. Somit steht jetzt eine viel einfachere und reproduzierbare Möglichkeit für den Anwender zur Verfügung, um Versuche zur Validierung oder auch

Code-to-Code-Vergleiche durchzuführen. Weiterhin wurden in die unteren Plenum-Module Modelle für einige bisher vernachlässigte thermochemische Effekte implementiert. Programmintern wurden die zwei Module LHEAD und AIDA so harmonisiert, dass Modelle und Routinen für die gleichen Phänomene, soweit sinnvoll, über gemeinsame Routinen aufgerufen werden. Somit sind in der Zukunft die Pflege und Erweiterbarkeit einfacher. Auch wurde die Modellierung des Herausfließens der Schmelze so erweitert, dass das Ausfließen der Schmelze die Stelle des Reaktordruckbehälterversagens berücksichtigt. Ob zuerst eine metallische oder keramische Schmelze in den Sicherheitsbehälter ausfließt, hängt davon ab, wo sich das Leck befindet.

Die bestehenden Modelle zum Versagen des Reaktordruckbehälters infolge des Einwirkens der heißen Schmelze auf die Wand wurden verbessert und erweitert. In diesem Zusammenhang wurden die bestehenden Modelle überarbeitet und – soweit verfügbar – aktualisierte Datenbasen verwendet. Außerdem hat der Anwender die Möglichkeit erhalten, eigene Kriterien für das Versagen des Reaktordruckbehälters zu definieren, um so anlagenspezifische Daten oder Kenntnisse über spezielle Eigenschaften der Wandmaterialien in der Simulation zu berücksichtigen.

Die Gültigkeitsbereiche sowie Anwendbarkeit der bereits in ATHLET enthaltenen Korrelationen für den kritischen Wärmestrom (**Critical Heat Flux, CHF**) für die Wand des Reaktordruckbehälters wurden mit positivem Ergebnis überprüft bzw. getestet. Aktuelle Forschungsaktivitäten mit GRS-Beteiligung wie das EU-Projekt IVMR zeigen, dass das Konzept der Außenkühlung eine wichtige Maßnahme zur Verminderung der Folgen eines Unfalls mit Kernschmelze ist. Die im IVMR-Projekt gewonnenen Erkenntnisse wurden genutzt, um die Modelle zur Simulation der Spätphase im Allgemeinen und zur Außenkühlung im Speziellen zu verbessern. Aus diesem Grund wurde die Kopplung, also der parallele Einsatz von AIDA für den Reaktordruckbehälter und ATHLET für den Kühlkanal an der Außenseite, ermöglicht. Eine weitere Option ist eine Kopplung mit COCOSYS, besonders wenn auch weitergehende Vorgänge im Containment betrachtet werden sollen. Durch entsprechende Testrechnungen wurden der vorhandene Modellumfang auf Funktionsfähigkeit und Plausibilität der Ergebnisse getestet.

AP3: Arbeiten zur Reaktoranzwendung

Das zentrale Ziel der Entwicklung von ATHLET-CD ist am Ende die Anwendung auf nukleare Anlagen wie Reaktoren oder Brennelementlagerbecken. Wichtig ist dabei das Zusammenspiel von ATHLET-CD mit ATHLET und COCOSYS im Rahmen von AC².

Daher wurde hier die Fähigkeit von ATHLET-CD für die Reaktoranwendung gezielt überprüft.

Um neue Modelle schnell testen zu können, wurden im laufenden Vorhaben generische bzw. prototypische ATHLET-CD-Anlagendatensätze für einen Druckwasserreaktor, einen Siedewasserreaktor und einen Reaktor des russischen Typs VVER1000 erstellt bzw. optimiert. Diese Datensätze wurden mit generischen Containment-Modellen von COCOSYS gekoppelt, um so AC² als Gesamtsystem regelmäßig auf Funktionsfähigkeit und Plausibilität testen zu können. Damit sind als Grundlage auch leicht adaptierbare Datensätze vorhanden, die die Verifikations- und Entwicklungsarbeiten unterstützen und für eine ggf. kurzfristig notwendige orientierende Analyse eines Stör- oder Unfallszenarios genutzt werden können.

Durch die vermehrte Zahl der gekoppelten AC²-Rechnungen (also ATHLET + ATHLET-CD + COCOSYS) tauchten viele Anwenderwünsche und Programmschwächen auf. Diese wurden soweit möglich kurzfristig bearbeitet und so eine verbesserte Ablauffähigkeit von AC² erreicht. Nur durch Adressierung dieser Anwender-Rückmeldungen kann die Leistungsfähigkeit des Programmsystems AC² auch für die Zukunft gewährleistet werden.

Seit den Unfällen von Fukushima ist das Interesse an Untersuchungen von Unfällen in Brennelementlagerbecken stark gestiegen. Durch die Ermöglichung der flexiblen Nodalisierung im Vorgängervorhaben ist es jetzt möglich, das Lagerbecken deutlich feiner und adäquater zu repräsentieren. Um weitere Erfahrungen mit den neuen Nodalisierungsparradigmen zu gewinnen, wurde diese Methode tiefer analysiert, optimiert und vermehrt angewendet, um den Benutzern Anwendungsempfehlungen geben zu können. Erste Erfahrungen mit den neuen Nodalisierungsmöglichkeiten zeigten, dass die Eingabe der notwendigen 3-dimensionalen Daten für solche Rechnungen, besonders für Lagerbeckensimulationen, sehr kompliziert und fehleranfällig war. Deswegen wurde in diesem Vorhaben eine Methode entwickelt, die dem Benutzer eine vereinfachte Eingabe der Daten ermöglicht.

AP4: Querschnittsaufgaben

Ein wesentlicher Punkt bei der Weiterentwicklung der bestehenden Modelle war die Zusammenarbeit mit anderen Instituten und Experten auf nationaler und internationaler Ebene, insbesondere auch mit externen Entwicklern an ATHLET-CD. Es wurden neueste Erkenntnisse ausgetauscht und diskutiert, welche dann Eingang in die Programmentwicklung finden konnten. Hierzu trug auch die Arbeit in Gremien und die Begleitung von Experimenten bei.

Ein weiteres wichtiges Ziel des Vorhabens war die Qualitätssicherung sowie die Unterstützung bei der Anwendung von ATHLET-CD. Dazu zählten auch koordinierende Aufgaben sowie gezielte Hilfe bei der Anwendung von ATHLET-CD bei verschiedenen Aufgabenstellungen. Aus diesem Grund entstand während der Projektlaufzeit eine deutlich umfangreichere Dokumentation von ATHLET-CD, die häufig gestellte Fragen von Anwendern beantwortet und diesen einen besseren Überblick über den Code gibt.

Im Rahmen der Begleitung der QUENCH-Versuchsreihe am KIT wurden die Experimentatoren bei der Konzipierung ihrer Versuche unterstützt. Dafür wurden Voraussrechnungen verschiedener QUENCH-Versuche durchgeführt, insbesondere zu den Arbeiten mit **Accident Tolerant Fuel (ATF)**-Material. Die dadurch gewonnenen Erkenntnisse konnten dann in die Programmentwicklung einfließen und zur Verbesserung des Codes genutzt werden.

Veränderungen am Programm mussten jedes Mal wieder ausgiebig getestet werden, bevor eine neue Version freigegeben werden konnte. Um die Qualität des Rechenprogramms ATHLET-CD langfristig aufrechtzuerhalten und weiter zu verbessern, wurden die bisherigen Maßnahmen um neue Verfahren ergänzt, die sich an aktuelle Standards der Softwareentwicklung und insbesondere der GRS-Richtlinie zur Softwareentwicklung orientieren. Dies umfasst in erster Linie die Anwendung und den Ausbau automatisierter Tests, die jeden Entwicklungsschritt automatisiert überprüfen und die Entwickler bei Problemen informieren. Dabei wurden die, unter anderem in dem vorherigen Punkt erwähnten, generischen Datensätze verwendet.

Der Transfer von Wissen an neue Kollegen spielte eine wichtige Rolle für den Kompetenzerhalt bei der Weiterentwicklung von ATHLET-CD im Speziellen sowie im Bereich der Unfallphänomene im Allgemeinen. Um den Einstieg in die Arbeit mit ATHLET-CD

sowohl für neue Kollegen als auch für Anwender zu vereinfachen, wurde ein ausführliches Tutorial erstellt.

ATHLET-CD wird sowohl GRS-intern als auch extern validiert und im zunehmenden Maße von anderen Institutionen angewendet. Aus dem Erfahrungsrückfluss der Programmvalidierung und -anwendung ergaben sich Hinweise zur Verbesserung der Eingabedatenbeschreibung, für zusätzliche Eingabedatensatzkontrollen, zu Modell- oder Programmschwächen, zu notwendigen Modell- und Programmiererweiterungen sowie zur Verbesserung der Rechendatenausgabe und Ergebnisvisualisierung. Die Nutzung des Erfahrungsrückflusses erforderte eine intensive Zusammenarbeit mit den Programmanwendern und deren Betreuung. Hierdurch konnte auch ein erheblicher Nutzen für die Programmentwicklung hinsichtlich der Beseitigung von Programmschwächen und der Verbesserung der Nutzerfreundlichkeit realisiert werden.

Notwendige Arbeiten zur Programmverbesserung, die nicht den ersten zwei Arbeitspaketen zugeordnet werden konnten und ihren Ursprung u.a. in der Betreuung der Programmanwender hatten, wurden unter diesem Arbeitspaket durchgeführt. Dazu zählen auch Programmoptimierungen, allgemeine Arbeiten zur Datenstruktur, Datensatzeingabe, Ergebnisdarstellung und die Beiträge zur Weiterentwicklung von ATLAS bzw. ATLASneo, sowie Programmbeschleunigung.

Durch das Projektmanagement und das Projektcontrolling wurde sichergestellt, dass alle Arbeiten in dem Vorhaben konform zu den GRS-Projekt- und Qualitätsmanagement-Prozessen und -Regeln und im Einklang mit den Vorgaben des Auftraggebers koordiniert und sach- und termingerecht abgewickelt sowie EDV-technisch erfasst, vorgehalten und bedarfsgerecht aufbereitet wurden.

Während der Projektlaufzeit wurden zwei offizielle ATHLET-CD-Versionen als Bestandteile von AC² freigeben und für zahlreiche Anwender zur Verfügung gestellt. Angesichts der COVID-Pandemie wurden zwei AC²-Anwendertreffen als Videokonferenz durchgeführt, bei denen die Neuigkeiten der neuen Freigabeversionen vorgestellt wurden.

Zusammenfassend kann festgestellt werden, dass die Themen und Schwerpunkte des Vorhabens RS1574 zur Weiterentwicklung des Moduls ATHLET-CD des Codepaketes AC² innerhalb der Projektlaufzeit von drei Jahren erfolgreich bearbeitet wurden. Alle wichtigen Projektziele wurden erreicht. Im Rahmen des Projektes wurden zahlreiche

Neuentwicklungen angestoßen und Modellverbesserungen durchgeführt, um die Leistungsfähigkeit und Zuverlässigkeit von ATHLET-CD für die Zukunft im Hinblick auf ein stetig wachsendes Anwendungsspektrum zu gewährleisten. Die weitere Intensivierung der Zusammenarbeit und Betreuung der Programmnutzer sowie die Mitarbeit in internationalen Arbeitsgruppen gaben wichtige Impulse für die Weiterentwicklung von ATHLET-CD, die im Laufe des Projektes aufgegriffen und umgesetzt werden konnten. Einige der Programmverbesserungen wurden bereits im Zuge der Freigabe neuer Programmversionen an alle Nutzer von ATHLET-CD weitergegeben, andere werden mit dem nächsten Release, das für das Jahr 2023 geplant wird, folgen. Die Maßnahmen zur Qualitätssicherung der Programmentwicklung wurden durch fortschrittliche Werkzeuge und überarbeitete Arbeitsabläufe deutlich erweitert, die die Effizienz und Qualität der Codeentwicklung sowie den Know-how-Transfer fördern, so dass ATHLET-CD auch langfristig als qualitätsgesichertes Analysewerkzeug zur Verfügung gestellt werden kann.

Die Entwicklung von ATHLET-CD wird auch nach dem Ende des Projekts RS1574 fortgesetzt, um neuen und kommenden Anforderungen an ATHLET-CD als Programm in AC² gerecht zu werden und bestehende Modelllücken zu schließen, auch im Hinblick auf innovative und evolutionäre Reaktordesigns.

Table of contents

	Abstract	I
	Kurzfassung	II
	Table of contents	XI
1	Introduction	1
1.1	Severe accident code ATHLET-CD.....	1
1.2	Particular objectives and programme of work	3
1.2.1	WP1: Improvement and extension of models for the reactor core	3
1.2.2	WP2: Simulation of late phase	4
1.2.3	WP3: Plant simulation.....	4
1.2.4	WP4: Cross-sectional tasks	5
2	WP1: Improvement and extension of models for the reactor core	7
2.1	WP1.1: Modelling of core degradation	7
2.1.1	Adjustment of the horizontal melt relocation modelling to the flexible nodalisation	7
2.1.2	Model to assess the influence of spacer grids on the movement of molten material	12
2.1.3	Model for melt relocation in the core-bypass channel	28
2.1.4	VVER-440 specific model for “Follower-Assemblies”	38
2.2	WP1.2: Modelling of oxidation.....	50
2.2.1	Oxidation model for ATF material	50
2.2.2	Model for material interaction between stainless steel and boron carbide and between zirconium and boron-carbide.....	56
2.2.3	Model for nitride formation in melt phase	66
2.3	WP1.3: Fission product behaviour (SAFT).....	68
2.3.1	Optimised output handling	68
2.3.2	Melting of SAFT structures	70
2.3.3	Limitations of SAFT	76
2.4	WP1.4: Refactoring.....	85

2.4.1	Refactoring the model for heat transfer between transported fission products and environment	85
2.4.2	Refactoring of the software infrastructure of ATHLET-CD	98
2.4.3	Replacement of the models OREST/FIPISO by VENTINA.....	99
2.4.4	Increasing the usability, fixing limitations, and refactoring of SAFT	109
3	WP2: Simulation late phase	117
3.1	WP2.1: Improvements in LHEAD and AIDA.....	117
3.1.1	Implementing the recent AIDA developments in LHEAD	117
3.1.2	Allowing a “Fill” function for melt for LHEAD	119
3.1.3	Model for decay power calculation in the metallic layer in the lower plenum.....	123
3.1.4	Model for thermochemical effects in the lower plenum.....	125
3.1.5	Model for considering the order of melt relocation from the RPV into the containment after RPV failure	127
3.1.6	Model for elliptical RPV bottom	129
3.2	WP2.2: Modelling of structure failure	130
3.2.1	Implementation of a user-definable failure criteria.....	130
3.2.2	Improvement of the RPV failure models.....	131
3.2.3	New critical heat flux correlations for lower plenum cooling calculations	132
3.3	WP2.3: Ex-vessel cooling	133
3.3.1	Detailed modelling of ex-vessel cooling for IVR	133
4	WP3: Plant simulation	137
4.1	WP 3.1 Generic input decks	137
4.1.1	Improvement of the generic input decks	137
4.1.2	Coupling of the generic input decks to COCOSYS.....	143
4.1.3	Implementing the generic input decks into a continuous integration platform	145
4.2	WP3.2 Maintenance and development of coupling interfaces	147
4.3	WP 3.3 Accidents in spent fuel pools	148
4.4	WP3.4 Input of 3D data.....	155

5	Cross-sectional tasks.....	159
5.1	WP4.1 Documentation and quality assurance.....	159
5.2	WP4.2 Transfer of know-how.....	159
5.3	WP4.3 Program use and code transfer.....	160
5.4	WP4.4 Code maintenance.....	160
5.5	WP4.5 Experimental support and international cooperation.....	161
5.6	WP4.6 Project management.....	162
6	Summary and outlook.....	163
	References.....	165
	Table of figures.....	169
	List of tables.....	175

1 Introduction

Continuously developed computational tools are used to demonstrate the effectiveness of provisions for controlling transients, incidents, and accidents in nuclear power plants. The Federal Ministry of Economic Affairs and Climate Action (BMUV) funds the development and validation of such programs as part of nuclear safety research. GRS develops the program package AC² that consists of three simulations tools: ATHLET, ATHLET-CD and COCOSYS and of the interactive graphical user interface and post-processing tool ATLAS /WIE 19/.

ATHLET (**A**nalyse der **T**hermohydraulik von **L**ecks und **T**ransienten) simulates the thermohydraulic behaviour in the reactor and particularly in the reactor pressure boundary. ATHLET-CD (**C**ore **D**egradation) extends these thermohydraulic modules with models for severe accident phenomena such as core melting and fission product transport. COCOSYS (**C**ontainment **C**ode **S**ystem) can simulate the phenomena occurring in the containment building of a nuclear power plant. AC² integrates the individual programs into one code package that can cover all the relevant phenomena occurring in a nuclear power plant during normal operation, anticipated operational occurrences (AOO), design basis accidents (DBA) and severe accidents (SA).

AC² and its individual programs are used as a deterministic analysis tool by around 60 organisations, research institutes and regulatory bodies worldwide. Primary objective of the project RS1574 funded by the German Ministry for Economic Affairs and Climate Action (BMUV, previously BMWi) on the basis of a decision of the German Bundestag was to continue the development of ATHLET-CD as part of AC² for increasing its capabilities and performance and for adapting the program according to the developing the state of the art.

1.1 Severe accident code ATHLET-CD

ATHLET-CD extends the underlying ATHLET models and inputs with additional modules for the simulation of severe accident phenomena and processes. Consequently, nuclear thermal hydraulics are provided by ATHLET /AUS 21a/. ATHLET-CD has a modular structure, the most important modules of ATHLET-CD are the following (see Fig. 1.1):

- ECORE calculates core heat-up, core degradation phenomena and oxidation effects,
- FIPREM calculates the fission product (FP) release from the fuel rods after cladding failure,
- SAFT calculates the transport and deposition of FP outside of the core region in the cooling circuit through multiple release paths,
- FIPISO calculates the activities of the core material and of released FP and the resulting decay as well as decay power on a nuclide basis,
- AIDA/LHEAD are two modules for simulation of lower plenum processes and ex-vessel cooling.

As a plug-in of ATHLET, ATHLET-CD uses the same numerical approaches as ATHLET. Moreover, ATHLET-CD is fully compatible with the NuT library /STE 21/. All the modules use the timesteps defined by ATHLET, except for the module SAFT, which uses the ATHLET defined time step as input and subdivides this timestep in its own time integration procedure. ATHLET-CD can be coupled to COCOSYS /ARN 21/ as well, to provide input for the simulation of the containment processes during an accident scenario. In such a coupled case, ATHLET-CD provides fission products and other thermohydraulic quantities for COCOSYS.

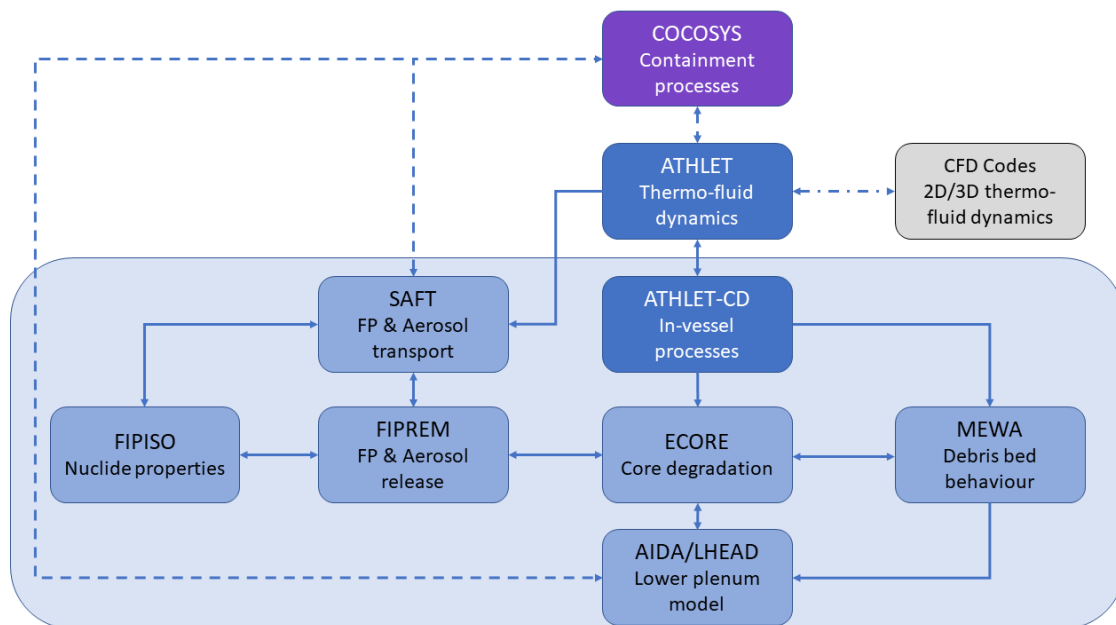


Fig. 1.1 ATHLET-CD code structure and interfaces /LOV 21a/

1.2 Particular objectives and programme of work

1.2.1 WP1: Improvement and extension of models for the reactor core

The models that cover the phenomena occurring during the early phase of a severe accident are very important, because their results impact the whole accident scenario. To improve the overall predictivity of the code the following tasks were specified and have been implemented:

- **WP1.1: Modelling of core degradation**

Tasks in this work package involve developments and improvements to simulate core melting phenomena and the movement of molten materials within the core region up until their relocation to the lower plenum. The aim of these developments was to add several previously missing, but important accident phenomena and to increase the accuracy and stability of the existing models.

- **WP1.2: Modelling of oxidation**

In order to be able to use ATHLET-CD for analysis of accidents in reactors with accident tolerant fuel, models for the oxidation of accident tolerant fuel (ATF) were implemented. Also, due to their importance and due to lack of previous modelling capabilities in ATHLET-CD, the models regarding material interactions and nitride formations were extended.

- **WP1.3: Fission product behaviour**

The objective of the tasks involving fission product behaviour was to improve the user-friendliness of the fission product transport module (SAFT) and to allow its usage also in areas where the structures along the transport path can fail.

- **WP1.4: Refactoring**

Tasks structured around refactoring were aimed to improve the stability and speed of the code. Also, through refactoring some parts of the code were restructured in order to make further developments and maintenance easier. Some models are based on assumptions that are no longer state-of-the-art, therefore replacing these models with more adequate models was also a task in this work package.

The results of the previously mentioned work packages are shown in chap. 2 in detail.

1.2.2 WP2: Simulation of late phase

One important topic of nuclear safety research worldwide are the phenomena occurring in the lower plenum of a reactor vessel (RPV) after the melt from the core relocates to the bottom of the RPV. Models for the currently investigated phenomena and measures had to be developed and implemented in ATHLET-CD in order to be able to use the code in current research activities and to deliver best-estimate simulation results.

The following tasks were identified and fulfilled:

- **WP2.1: Improvements in the models LHEAD and AIDA**

The two lower plenum modules in ATHLET-CD available, LHEAD and AIDA, cover the same physical phenomena but have different depth of detail and range of application. To increase their usability and to improve their maintainability their structures were unified. Also, so far neglected or not well-known phenomena and features were added, such as modelling of elliptical RPV bottom and thermo-chemical effects.

- **WP2.2: Modelling of structure failure**

To fill the previously identified modelling gaps regarding RPV failure, the failure models, as well as the heat transfer related wall ablation models had to be improved.

- **WP2.3: Ex-vessel cooling**

Due to the importance of the in vessel melt retention severe accident management strategy, the lower plenum models of ATHLET-CD had to be further improved and extended so they can simulate the effect of the outside cooling of the vessel on the molten pool and the interaction with the remainder of the containment.

The results of the previously mentioned work packages are shown in chap. 3 in detail.

1.2.3 WP3: Plant simulation

In this work package the primary objective was to create input decks to realistically test on a wide range of applications the existing and newly developed models, to facilitate a quick reaction to potentially occurring nuclear accidents by having already a basic input deck available, and to enhance the user-friendliness of the code.

The following tasks were identified and fulfilled:

- **WP3.1: Generic input decks**
PWR, BWR and VVER reactor input decks were created to test the applicability of the code and to provide a basic input set for the users.
- **WP3.2: Maintenance and development of coupling interfaces**
Maintain and potentially improve the coupling of ATHLET-CD mainly with COCOSYS, but also with other programs.
- **WP3.3: Accidents in spent fuel pools**
The importance of accident simulations in spent fuel pools was more clearly recognised after the accident in the nuclear power plant of Fukushima Daiichi. It was therefore decided that a coupled, ATHLET-CD/COCOSYS calculation is performed, to prove the applicability of AC² for such scenarios.
- **WP3.4: Input of 3D data**
Flexible nodalisation, especially in the spent fuel pool case, required a lot of 3D inputs from the user. A simplified approach was implemented to avoid extensive, error-prone input data by the user.

The results of the previously mentioned work packages are shown in detail in chap. 4.

1.2.4 **WP4: Cross-sectional tasks**

Tasks gathered in WP4 were necessary to allow frictionless work throughout the project and to maintain and improve the high level of quality of ATHLET-CD.

The following tasks were identified and fulfilled:

- **WP4.1: Documentation and quality assurance**
- **WP4.2: Transfer of know-how**
- **WP4.3: Program use and code transfer**
- **WP4.4: Code maintenance**
- **WP4.5: Experimental support and international cooperation**
- **WP4.6: Project management**

2 WP1: Improvement and extension of models for the reactor core

2.1 WP1.1: Modelling of core degradation

2.1.1 Adjustment of the horizontal melt relocation modelling to the flexible nodalisation

Motivation

A model for the horizontal movement of molten material was developed in RS1505 /WEB 14/. At that time only a ring-like nodalisation of the core was possible, therefore the implemented model took advantage of the cylindrically symmetrical nodalisation. Since then, it is possible to nodalize the core also in azimuthal direction, therefore adjustments of the horizontal relocation modelling were necessary.

Developments

The basic idea behind horizontal melt movement did not change due to the new type of nodalisation: melt flows gravity-driven preferentially downwards. During the simulation melt candles downward along the rods within a node. It is first stopped when the melt rivulet reaches a blockage (e. g. blockage due to frozen molten material, ballooned cladding or the lower core support plate), thus preventing its further axial progression. These are the locations where melt can flow horizontally to the neighbouring nodes. Without any changes in the horizontal melt relocation model, previously developed for radial discretisation only, the melt can only move from a node i to its neighbouring node numbers, $i+1$ and $i-1$, as shown in Fig. 2.1.

Considering that the core is now also discretised azimuthally, requiring a different node numbering, this relocation model is no longer appropriate. Therefore, the identification of the node numbers in the model had to be extended, so that the melt can flow to the correct neighbouring nodes, as shown in Fig. 2.2.

Blue = molten node
 Green = node where melt
 Relocates to in case of a
 blockage below the molten
 area

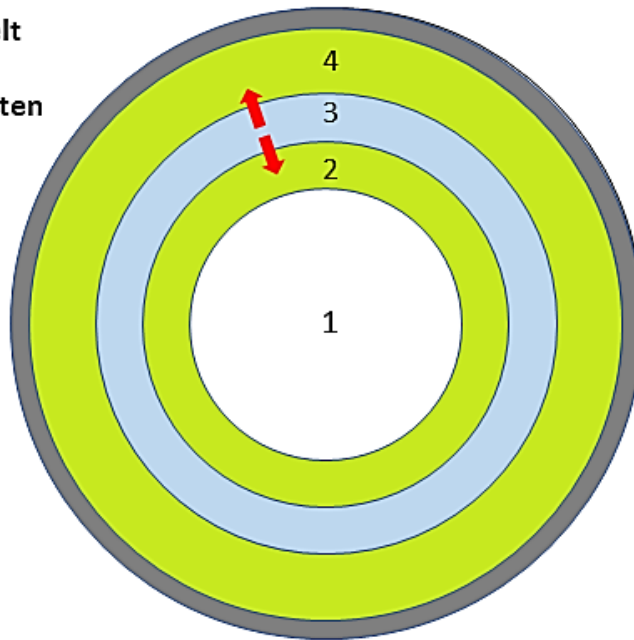


Fig. 2.1 Top view of a core discretised radially only (4 representative rings)

Blue = molten node
 Green = node where melt
 relocates to in case of a
 blockage below the
 molten area

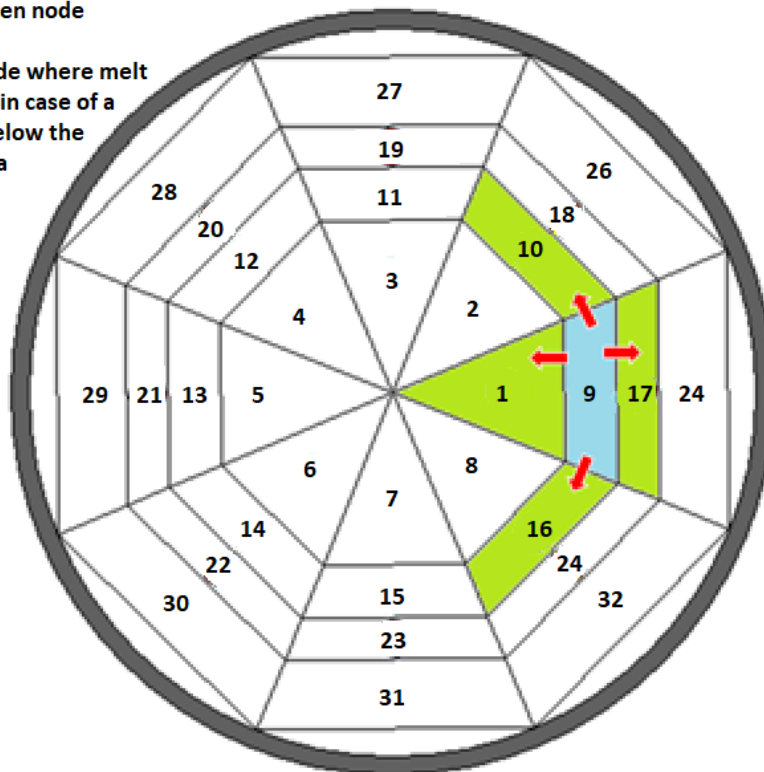


Fig. 2.2 Top view of a core discretised radially and azimuthally (each ring discretised into 8 nodes), with new relocation model

Verification

Verification calculations were performed to check the code capability regarding simulation of horizontal relocation, and more precisely the simultaneous spreading of molten material in the radial and azimuthal direction as specified, as well as the plausibility of the simulation outcomes.

For this purpose, two examples were created, and they were compared to each other. For both cases the same scenario was analysed, however, once with and once without the new horizontal relocation model. The analysed scenario is very simple and hypothetical. It was optimised for the development and verification process to achieve conditions that could lead to horizontal melt relocation. Artificial blockage was created in one of the core nodes, indicated with blue node in Fig. 2.3. Red nodes indicate the porosity of the unblocked zones. The core is deliberately not cooled, and only local power source is defined in the nodes above the blockage (yellow nodes in Fig. 2.3) in order to achieve fast melting of the nodes above the blockage, and thus, allowing for analysis of the different melt behaviours induced by the different model options.

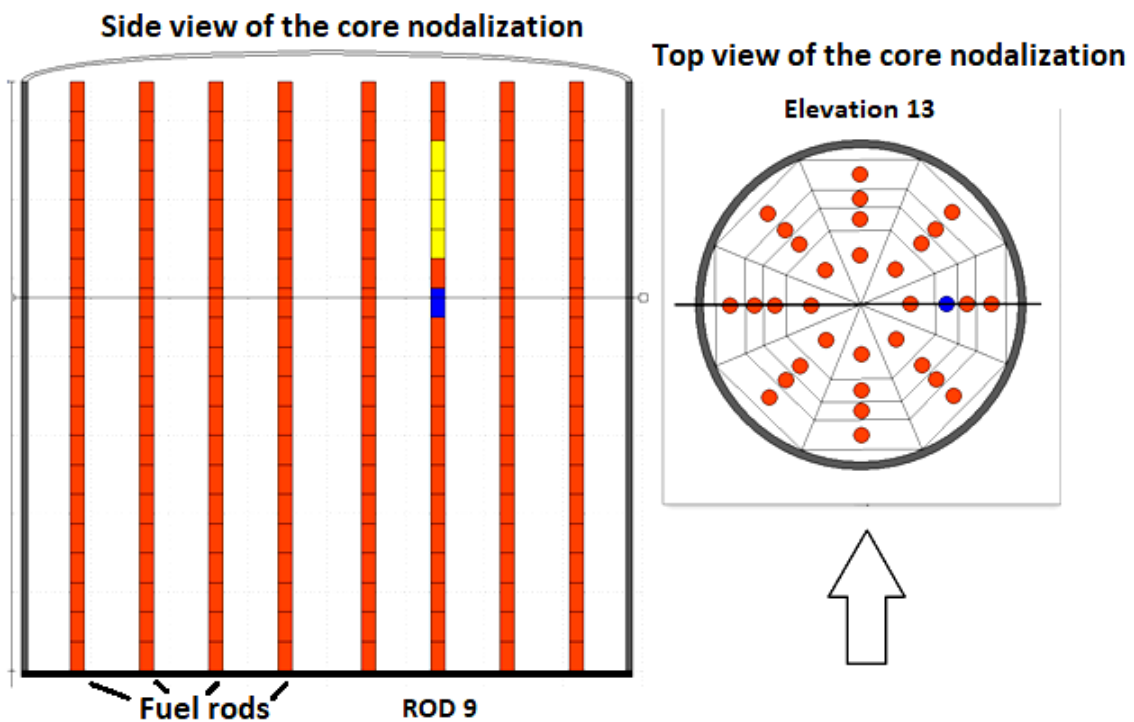


Fig. 2.3 Side and top view of the core nodalisation in the sample input

The results of the two verification calculations can be seen in Fig. 2.4 and Fig. 2.5.

In the simulation without the horizontal melt relocation model (Fig. 2.4) it is visible that due to the local heat up, the nodes above the blockage melt and relocate. The melt candles down the rods until the blockage in ROD9 at elevation 13 (centre of node 13 is approx. 2.6 m above core entry) stops the axial melt movement. The accumulated melt above the blockage creates another blockage (in NODE 14), which leads to further melt accumulation above the newly created blockage. As a result, without horizontal melt relocation, an artificial melt column is formed which remains unrealistically as a column.

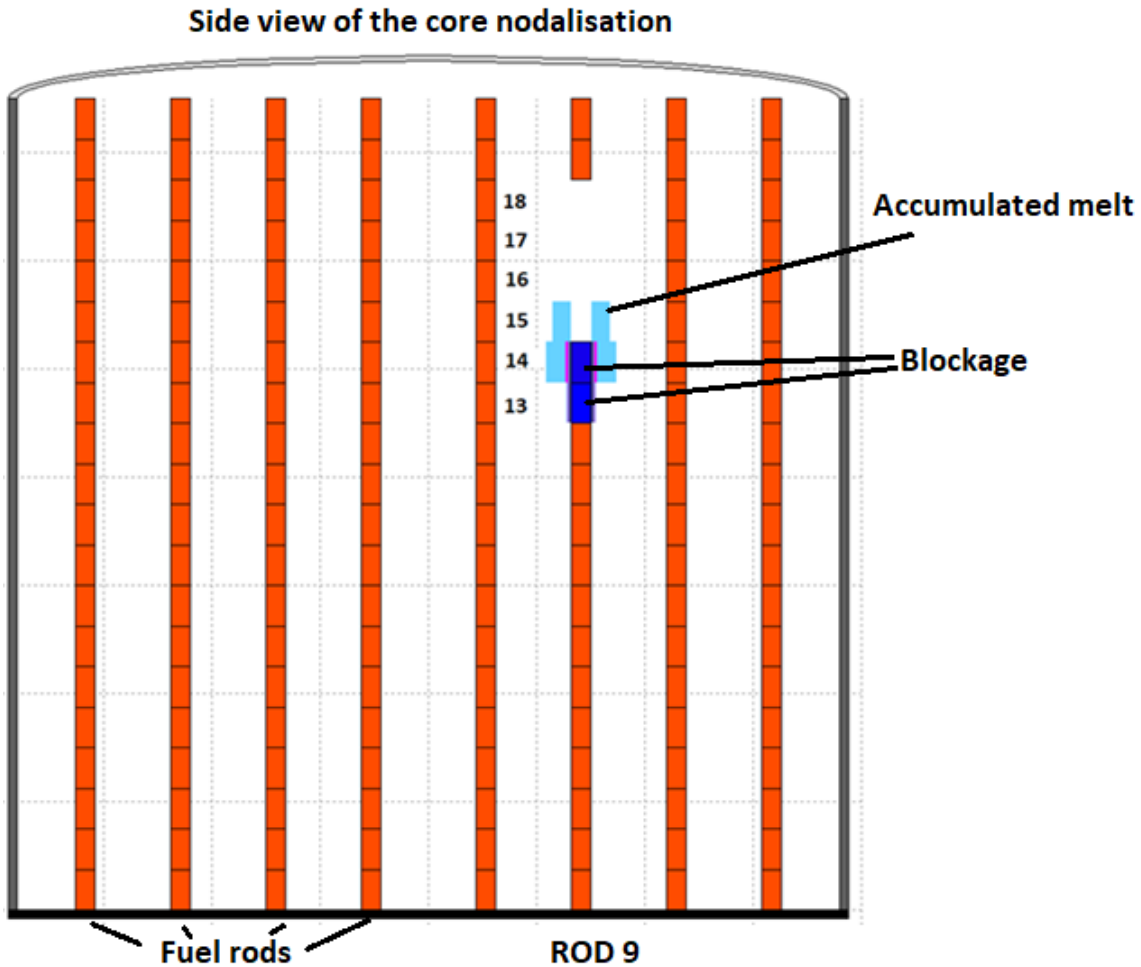


Fig. 2.4 Simulation results of the sample calculation without horizontal melt relocation model

The simulation of the same hypothetical scenario with the horizontal melt relocation model shows significantly different results. Just as in the previous case, the local heat source above the blockage leads to the melting of nodes 15 – 18 (shown as empty nodes in Fig. 2.5). The melt starts to candle down along ROD9. The blockage prevents the melt from further axial movement, the melt starts to relocate horizontally to the neighbouring rods: ROD1, ROD10, ROD16 and ROD17. The melt accumulates at the bottom of the rods, narrows the flow path for the coolant and starts to form another blockage (dark red

nodes in Fig. 2.5). This, however, does not result in a formation of a new blockage as in the previous sample simulation, because the melt was distributed along the four rods. In case a blockage was formed, horizontal relocation of melt would take place again, automatically. The sum of the molten masses in all of the nodes (744 kg) equals the sum of the molten material in the calculation, where the horizontal relocation model was turned off.

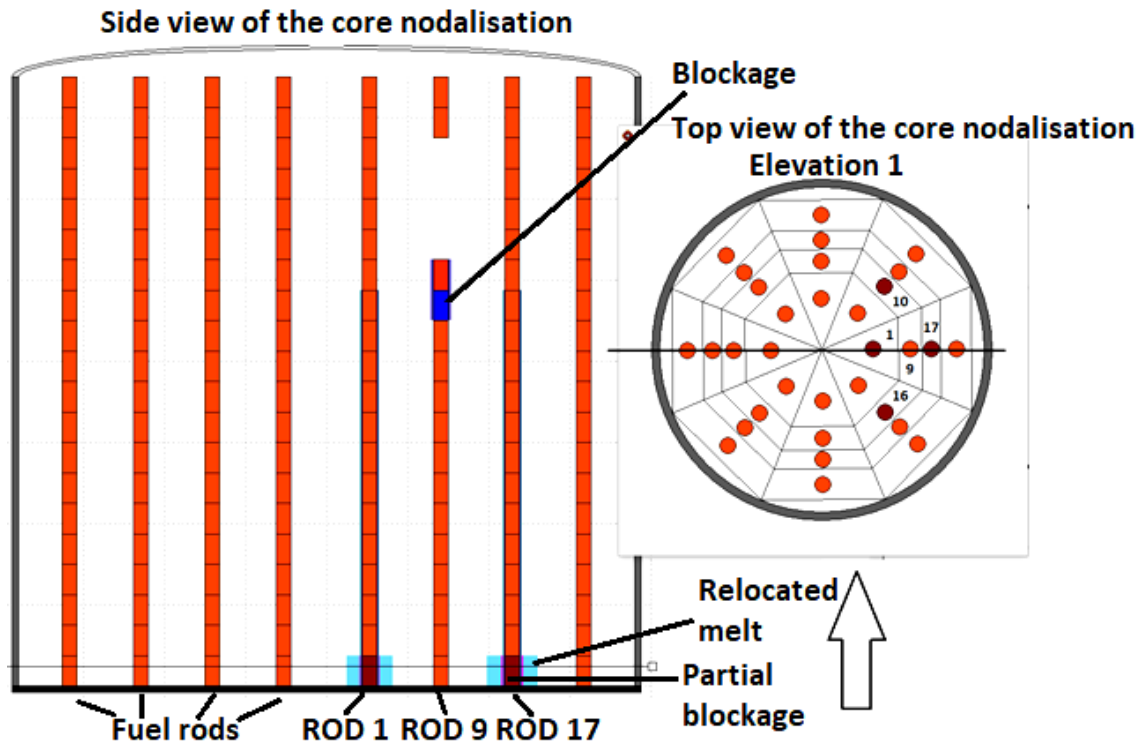


Fig. 2.5 Simulation results of the sample calculation with horizontal melt relocation model

(Left side of the picture shows the cross section of the reactor from the direction of the arrow)

These simple samples delivered the expected results, and thus proved that the model implementation was correct. The simulation results shown above are part of the verification process of the horizontal melt relocation model. Targeted model validation is planned, if experimental data of horizontal melt relocation are available.

2.1.2 Model to assess the influence of spacer grids on the movement of molten material

2.1.2.1 Motivation

According to a model by Siefken and Olsen /SIE 94/, the impact of grid spacers to the core degradation can be categorised into the following groups:

- Chemical reaction with fuel rod cladding leading to premature failure of the cladding and release of fission gases.
- Reacting with fuel rod cladding such that a large amount of cladding is liquefied and slumps due to additional oxidation heat.
- Trapping the slumping material and thus blocking the coolant flow.

These interactions with spacer grid are generally not considered in state-of-the-art severe accident codes, for example, ATHLET-CD. Nevertheless, these effects may significantly affect the core degradation progression sequence.

The spacer grids in the power reactor are made of either Zircaloy or Inconel for PWR and BWR, and stainless steel for VVER. Depending on the material, the failure criteria of the spacer grids can be very different. Strong interactions exist between the Inconel/stainless steel with Zircaloy /SEH 12/. These materials are degraded at relatively low temperatures (i.e. 1500 – 1700 K) due to eutectic interaction between the materials /TRO 00/. The Zircaloy spacer grid will oxidise similarly to the fuel cladding, contributing to the oxidation heat.

For RELAP/SCDAP Mod 2.0, a preliminary grid spacer degradation model was developed /BER 82/ using only the melting temperature as a failure criterion. Also, the temperature of the spacer grid is simply taken as the cladding outer temperature and without any consideration of oxidation or eutectic interaction between spacer grids and fuel/control rods. The stored energy in the spacer grid and the interactions between Inconel and spacer grids /SIE 94/ are considered in the RELAP/SCDAP Mod 3.0 /ALL 92/.

In the previous version of ATHLET-CD, grid and shroud components had to be modelled by non-ATHLET-CD heat conduction objects due to the lack of specific ATHLET-CD models. For these heat conduction objects basic geometric forms such as pipe, sphere, or plate are available. In addition, simulating the temporary blockage of cladding materials is not possible, which may be relevant to the in-vessel core degradation process.

Therefore, the current development project aims to improve the spacer grid modelling in ATHLET-CD with the following:

- Temporary hold-up of candling material at spacer grids' elevation before its failure during core degradation.
- Direct simulation of the spacer grid structure by solving the energy balance equation, including effects of radiation with fuel rod, heat transfer with fluid, heat transfer with melt and crust and oxidation of the spacer grid. These heat source within the spacer grid will be influencing the fuel rod temperature by radiation transfer between them.
- Simple failure model for the spacer grid, where the grid structure is assumed to fail after reaching the melting point or the maximum load it can withstand or the maximum allowable oxidation layer limit (which is a user input).

The eutectic interaction between the spacer grid and the fuel rod is not simulated but can be a future improvement of the model. The model currently does not transfer the additional melt/crust mass due to grids and melt oxidation to the melt in the remainder of the core. Once the grid is failed, the additional energy equation will be turned off and the melt relocation behaviour will be the same as without spacer grid model. Therefore, the current model provides one-way feedback to the core melt behaviour of the rod structure.

2.1.2.2 Development

The new ATHLET-CD model for spacer grid relocation

The new model attempts to model the spacer grid as a separate entity from the core model. In other words, it solves an independent energy equation in each core ring and at each level of the spacer grid. The whole spacer grid model is divided into three parts:

- Energy calculation for the spacer grid (including oxidation)
- Adjustment of the melt velocity at the location of the spacer grid
- Failure criteria for the spacer grid

Modelling of the spacer grid

The spacer grid is modelled as a per-rod entity, rather than a lumped component as was done in the previous approach with ATHLET heat conduction objects (HCO). In the current development version, the grid can be specified as either a square spacer grid (i. e. relevant to PWR and BWR) or a hexagonal grid (i. e. relevant for VVER designs), see Fig. 2.6.

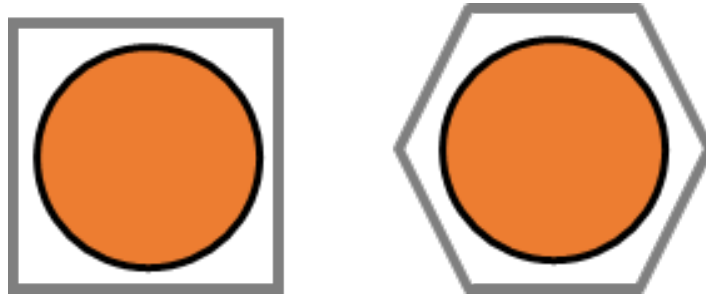


Fig. 2.6 Spacer grid (square and hexagonal shaped) zone per rod

By entering the height, width and thickness of the grid material, the surface area and volume per-rod spacer grid will be calculated. For other specific forms of spacers used in other applications or specific experiments, the user has the option to directly input the surface area and volume of the spacer grids for calculation.

In ATHLET-CD the whole core is divided into different, generally ring-shaped, core sections (e. g. rod 1, 2, ...), so the spacer grid is multiplied by the number of rods present in each ring or core section. For each elevation there is a spacer grid and for each of these elevations a separate energy equation is solved.

Energy calculation for spacer grids

To consider the effect of spacer grid, an additional energy balance equation in ATHLET-CD is evaluated as

$$\rho_{gr}c_{gr}V_{gr}\frac{dT}{dt} = \dot{Q}_{grid\ spacer \rightarrow fluid} + \dot{Q}_{rad \rightarrow fuel} + \dot{Q}_{rad \rightarrow melt} + \dot{Q}_{cond \rightarrow melt} + \dot{Q}_{cond \rightarrow crust} + \dot{Q}_{oxi} \quad (2.1)$$

This energy equation is solved for the whole spacer grid (at a given height) as one entity (no special subdivision of the spacer grid). The density, specific capacity and volume are defined according to the choice of grid material (i. e. zirconium alloy, stainless steel, or control rod materials such as Ag-In-Cd). Nevertheless, in the current development version of ATHLET-CD, oxidation is calculated only when the grid is made of zirconium alloy, since steel oxidation is not yet considered in ATHLET-CD. The problem of steel oxidation is addressed in the next development project of ATHLET-CD.

The heat transfer from grid spacer to fluid is calculated in the same way as the rod to fluid heat transfer,

$$\dot{Q}_{grid\ spacer \rightarrow fluid} = k_{grid\ spacer \rightarrow fluid} A_{grid\ spacer} (T_{grid\ spacer} - T_{bulk}) \quad (2.2)$$

where the heat transfer coefficient (i. e. $k_{grid\ spacer \rightarrow fluid}$) is calculated based on the hydraulic diameter of the spacer grid and the standard heat transfer package in ATHLET is applied. The heat transfer from the melt to the spacer grid is calculated with,

$$\dot{Q}_{cond \rightarrow melt} = k_{melt} A_{\frac{melt}{spacergrid}} (T_{melt} - T_{grid\ spacer}) \quad (2.3)$$

Due to the simplistic layout between the grid and the fuel rod, the view factor can be treated as 1. The radiation fully absorbed by the grid and vice versa. The radiation heat transfer between the spacer grid and fuel is calculated simply as,

$$\dot{Q}_{rad \rightarrow fuel} = \epsilon_{rod} \cdot \epsilon_{grid\ spacer} \cdot 1.0 \cdot A_{rod} \cdot \sigma \cdot (T_{rod}^4 - T_{grid\ spacer}^4). \quad (2.4)$$

$\epsilon_{rod} \cdot \epsilon_{grid\ spacer}$ [-] represent the emissivities of cladding and spacer grid simplifyingly neglecting reflection between the surfaces, while σ is the Stefan-Boltzmann constant [5.6697E-08 W/m²K⁴]. (The conduction heat transfer between the rod and spacer grid is ignored due to the tiny contact area. A rough estimation of the contact area is around 6·10⁻⁵ m², which is at least two orders of magnitude smaller than the surface area of the grid. Similarly, absorption in the fluid is ignored).

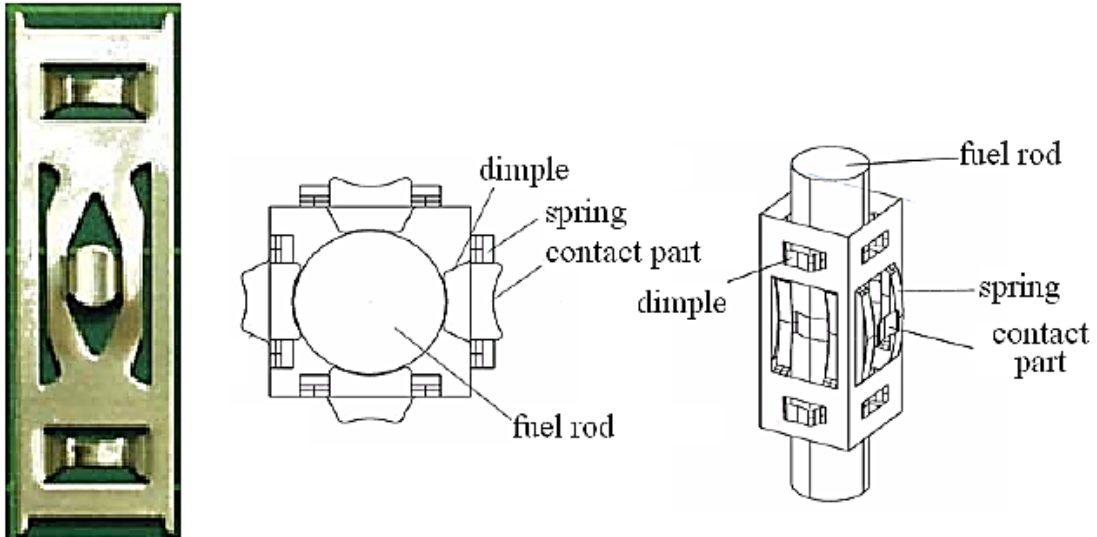


Fig. 2.7 Sample cross-section of the contact support between spacer grid and fuel rod

The oxidation is calculated by lump-summing the whole spacer grid volume into an equivalent pipe object. Due to limitations in the ATHLET-CD oxidation models, an equivalent diameter is calculated in a first approach as

$$D = 2 \sqrt{\frac{V_{gridspacer}}{\pi H_{gridspacer}}}. \quad (2.5)$$

Energy equation for melt

In the subroutine EVENBA, the energy equation of melt is formulated as

$$\frac{\partial(c_p m_{melt} T_{melt})}{\partial t} = \dot{Q}_{all}. \quad (2.6)$$

The convection term (i. e. $\nabla \cdot (c_p m_{melt} u_{melt} T_{melt})$) is ignored in the treatment of EVENBA, as the velocity of the spacer grid melt is assumed to be zero. The heat source (\dot{Q}_{all}) includes the contributions from the following:

- Heat transfer between melt to fluid
- Heat transfer between melt to cladding
- Internal heat source including the additional heat coming from the inflow of melt ($c_{p_{in}}(T_{in} - T)$) and other internal heat sources such as radiation, decay power and oxidation power (\dot{Q})

Thus, the full equation can be written as

$$\begin{aligned} \frac{\partial(c_p m T)}{\partial t} = & \nabla \cdot (\lambda_{clad} A_{fluid} \nabla T) + \nabla \cdot (\lambda_{fluid} A_{clad} \nabla T) \\ & + c_{p_{in}}(T_{in} - T) + \dot{Q} \end{aligned} \quad (2.7)$$

For the internal heat source terms ($c_{p_{in}}(T_{in} - T) + \dot{Q}$), in EVENBA, they are considered as explicit source terms in the computation. The Crank-Nicolson implicit technique is used to solve the discretised version of the energy equation.

$$\begin{aligned} \frac{c_p(m + \delta m_{in})(T^{n+1} - T^n)}{\delta t} \\ = & \lambda_{fluid} A_{fluid} \left[\frac{T^{n+1} + T^n}{2} - T_{fluid} \right] \\ & + \lambda_{clad} A_{clad} \left[\frac{T^{n+1} + T^n}{2} - T_{clad} \right] + c_{p_{in}}(T_{in} - T^n) \\ & + \dot{Q} \end{aligned} \quad (2.8)$$

The melt temperature thus be solved by

$$\begin{aligned}
 T^{n+1} &= \frac{1}{\frac{c_p(m + \delta m_{in})}{\delta t} + \frac{1}{2}[\lambda_{fluid}A_{fluid} + \lambda_{clad}A_{clad}]} \\
 &\cdot \left\{ \left[\frac{c_p(m + \delta m_{in})}{\delta t} - \frac{1}{2}\lambda_{fluid}A_{fluid} - \frac{1}{2}\lambda_{clad}A_{clad} \right] T^n \right. \\
 &\quad \left. + \lambda_{fluid}A_{fluid}T_{fluid} + \lambda_{clad}A_{clad}T_{clad} + c_{p_{in}}(T_{in} - T^n) + \dot{Q} \right\}
 \end{aligned} \tag{2.9}$$

Addition of the spacer grid terms

In EVENBA, an extra term is introduced to the implicit equation as follows:

$$\begin{aligned}
 &\frac{c_p(m + \delta m_{in})(T^{n+1} - T^n)}{\delta t} \\
 &= \lambda_{fluid}A_{fluid} \left[\frac{T^{n+1} + T^n}{2} - T_{fluid} \right] \\
 &\quad + \lambda_{clad}A_{clad} \left[\frac{T^{n+1} + T^n}{2} - T_{clad} \right] \\
 &\quad + \lambda_{spacer}A_{spacer} \left[\frac{T^{n+1} + T^n}{2} - T_{spacer} \right] \\
 &\quad + c_{p_{in}}(T_{in} - T^n) + \dot{Q}.
 \end{aligned} \tag{2.10}$$

The melt temperature thus be solved by

$$\begin{aligned}
 T^{n+1} &= \frac{1}{\frac{c_p(m + \delta m_{in})}{\delta t} + \frac{1}{2}[\lambda_{fluid}A_{fluid} + \lambda_{clad}A_{clad} + \lambda_{spacer}A_{spacer}]}
 \end{aligned} \tag{2.11}$$

$$\left\{ T^n \left[\frac{c_p(m + \delta m_{in})}{\delta t} - \frac{1}{2} (\lambda_{fluid} A_{fluid} - \lambda_{clad} A_{clad} - \lambda_{spacer} A_{spacer}) \right] \right.$$

$$+ \lambda_{fluid} A_{fluid} T_{fluid} + \lambda_{clad} A_{clad} T_{clad} + \lambda_{spacer} A_{spacer} T_{spacer}$$

$$\left. + c_{p_{in}} (T_{in} - T^n) + \dot{Q} \right\}$$

Control of candling material movement in ATHLET-CD

Initialisation routine for the spacer grid model.

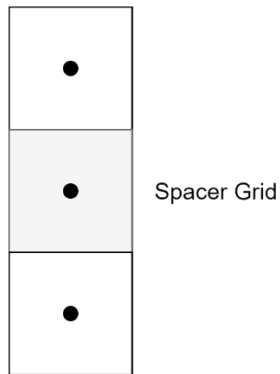


Fig. 2.8 Schematic for spacer grid

KGS(I,J) is used as a flag to indicate whether a spacer grid is present at node J for radial node I. If IGRIDS = 1, subroutine EGSINIT is used to initialise the spacer grid (upon reading of the control keyword RODSPACER). If the spacer grid is in its failure state, KGS(I,J) will be set to zero (i.e. sub-routine EGSFAIL).

Adjustment of melt relocation speed and its movement

At the start of the EGSREL, the code checks to see if the current calculation is using a spacer grid or not (using IGRIDS variable). A re-initialisation of the melt velocity is always performed on non-spacer grid positions (KGS = 0) to remove any residual artifacts from the spacer grid location.

To consider the effect of blockage for the melt at the spacer grid location, the melt velocity is manually adjusted to one-thousandth times of the original melt velocity in the subroutine EGSREL. A small melt flow is still assumed, therefore, the spacer grids slowly let melt through:

$$w_{melt} = \frac{W_{melt}}{1000}. \quad (2.12)$$

The flag ISTOPP is used to store the state of the spacer grid modification, and this will be used to classify whether a reinitialisation of the relocation grid is required at that node level.

Additionally, the subroutine EGSREL is called within the subroutine ERELOC_CML which restricts the bottom of the melt rivulet to the spacer grid location ($KGS = 1$) until the spacer grid fails ($KGS = 0$). Because the additional mass at the spacer grid location is also added to the blockage mass (with flipped index), it is possible that the stoppage of the melt at the spacer grid location triggers the blockage of the melt at that location; thus, one should check the channel's porosity to confirm. Additionally, this is observed in the test calculation.

Failure of the spacer grid

When the degraded material (i. e. melt and crust) comes to a halt at the spacer grid's location, a certain amount of mass accumulates on the spacer grid. Simultaneously, the spacer grid material will be heated by the melt and crust. It is assumed that the spacer grid can fail in one of the following ways:

1. When the spacer grid temperature is higher than its melting temperature. ($T_{spacer\ grid} > T_{melting}$).
2. When the accumulated mass on the spacer grid is higher than the maximum stress that the material can withstand.
3. When oxidation leads to significant weakening of the spacer grid's integrity.

Melting temperature of the common spacer grid materials

Tab. 2.1 Melting temperature of common spacer grid material

	Zr-alloy	Inconel Alloy	Stainless Steel
Melting Temperature [K]	2023	-	1783

Under the input keyword RODSPACER, users must enter the melting temperature. Once the spacer grid temperature reaches the material's specified melting point, the flag KGS is reset to 0. As a result, the ERELOC CML section for spacer grid modification will be deactivated.

Calculation of the maximum load allowable before failure

The total accumulation of the degraded mass is calculated in the subroutine EGSMASS, using the amount of accumulated melt and crust mass located at each elevation times the number of rods. It is compared with the ultimate tensile strength of the material, which is again a required input from the user.

Calculation of oxidation

The standard oxidation routine EOCD is applied to calculate the oxidation power and the hydrogen release of the spacer grid. The hydrogen release is added to the H2Q variable, which is accounted for the hydrogen release by the rod component.

2.1.2.3 Verification

Hypothetical test case for spacer grid effects on core degradation

A hypothetical single rod test case is used to demonstrate and verify the mass balance of the rivulet, which will not be affected by the individual spacer grid. In general, one can see there is a delay of the generation of molten material (see Fig. 2.9), if the influence of spacer grid is not considered.

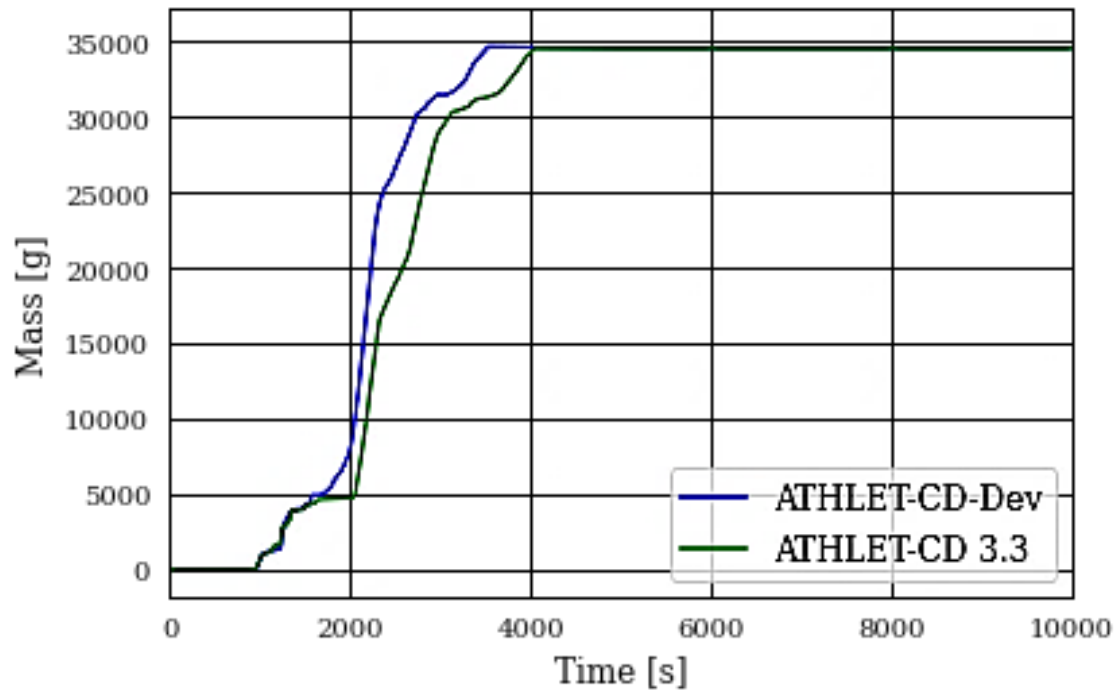


Fig. 2.9 Comparison of the total molten material between the development version and release version 3.3

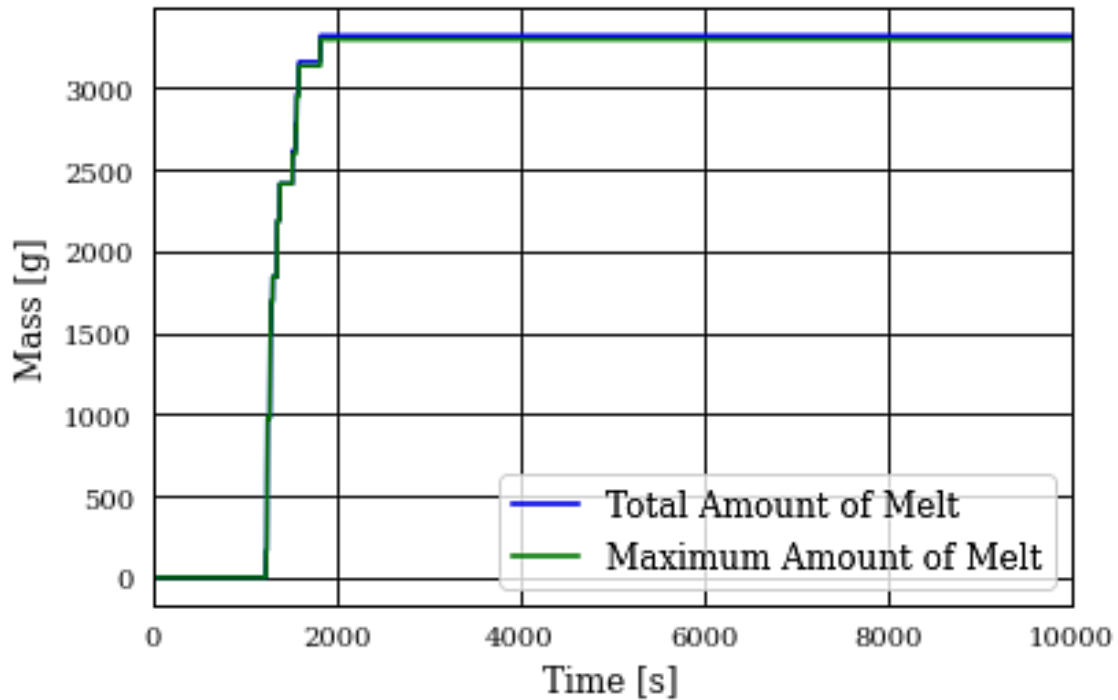


Fig. 2.10 Manual check for total amount of melt

Also, as shown in Fig. 2.10, the stoppage of melt at certain locations did not cause a mass balance error.

2.1.2.4 Validation against QUENCH-11

Adaptation of the input deck

In the existing input for the QUENCH-11 test, the candling velocity of spacer grid was set as 0.001 to limit the movement of the melt out of spacer grids. Due to the lack of the spacer grid model, spacer grids in the QUENCH-11 were modelled as additional heat conduction objects (HCOs). With the new spacer grid model, these spacer grids can be directly modelled by inserting the pseudo-keyword “RODSPACER”. The previously defined ATHLET HCOs for spacer grids were removed and replaced by the manual definition of spacer grid under ATHLET-CD input. Simulation with higher candling velocity might be performed as the melt will be stopped at the spacer grid, although the result may still be dependent on the applied candling velocity. The shroud will still be simulated with ATHLET HCO and the ATHLET oxidation model is still applied to these structures.

As there is no detailed information about the geometric dimension (except for the height) of spacer grids in QUENCH-11, the length and thickness are only approximated values. Therefore, the following comparison maybe subject to uncertainty caused by inaccurate geometric value of grids.

Result with the new spacer grid model in ATHLET-CD

The candling velocity is maintained at the original value used in the reference input for the first comparison of the ATHLET-CD 3.3. (i. e. melt velocity at 0.001 ms^{-1}). In the followings, the effect of the spacer grids on the results is shown and explained shortly.

Fig. 2.11 shows the total amount of H_2 generated by ATHLET-CD structures. The produced H_2 mass is higher if spacer grids are taken into account, compared to the simulation without spacer grids. This is due to three main reasons:

- spacer grids provide additional material to oxidise,
- the extra heat from the spacer grid oxidation heats up the surroundings even more, which leads to more extensive oxidation,
- the melt stops at spacer grids and heats up the surroundings. This was neglected in the simulations without spacer grids.

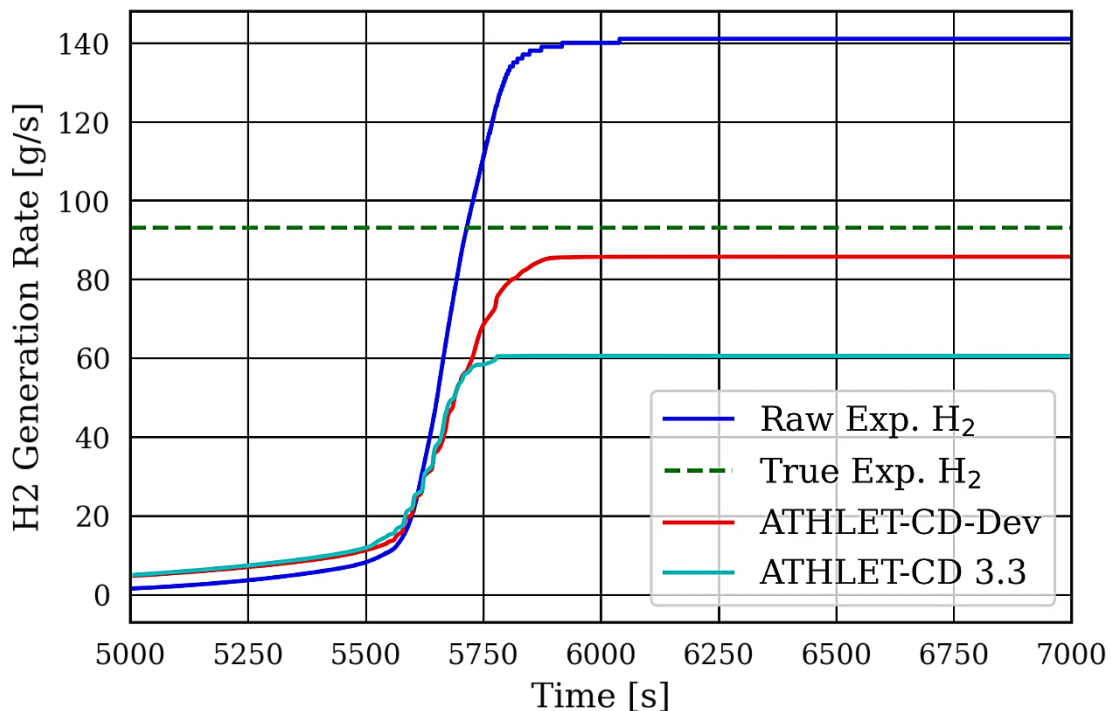


Fig. 2.11 Integral hydrogen generation

Note, that the experimental value should be taken as 94 g instead of 143 g due to the inclusion of non-modelled components in ATHLET-CD. While there is still some under-estimation the hydrogen generation, the target value for the current ATHLET-CD version is actually reproduced at least satisfactorily. This is particularly remarkable as the current development did not attempt to improve the hydrogen generation issue and mainly focused on the pre-failure behaviour. This underlines that a comprehensive consideration of severe accident phenomena is important for a best-estimate severe accident code.

The above-mentioned points lead to an increased heat generation, which is clearly visible in Fig. 2.12 to Fig. 2.14. In these graphs the temperature of the cladding at higher elevations are higher than in the simulations without spacer grids and are therefore closer to the measured values.

The stoppage of the melt at higher elevations has also an effect on the cladding temperatures at lower elevations, as the hot melt does not reach the lower positions (or at least not in such amount). Therefore, the simulated cladding temperatures are colder and are therefore closer to the measured values. This can be seen in Fig. 2.15 and Fig. 2.16.

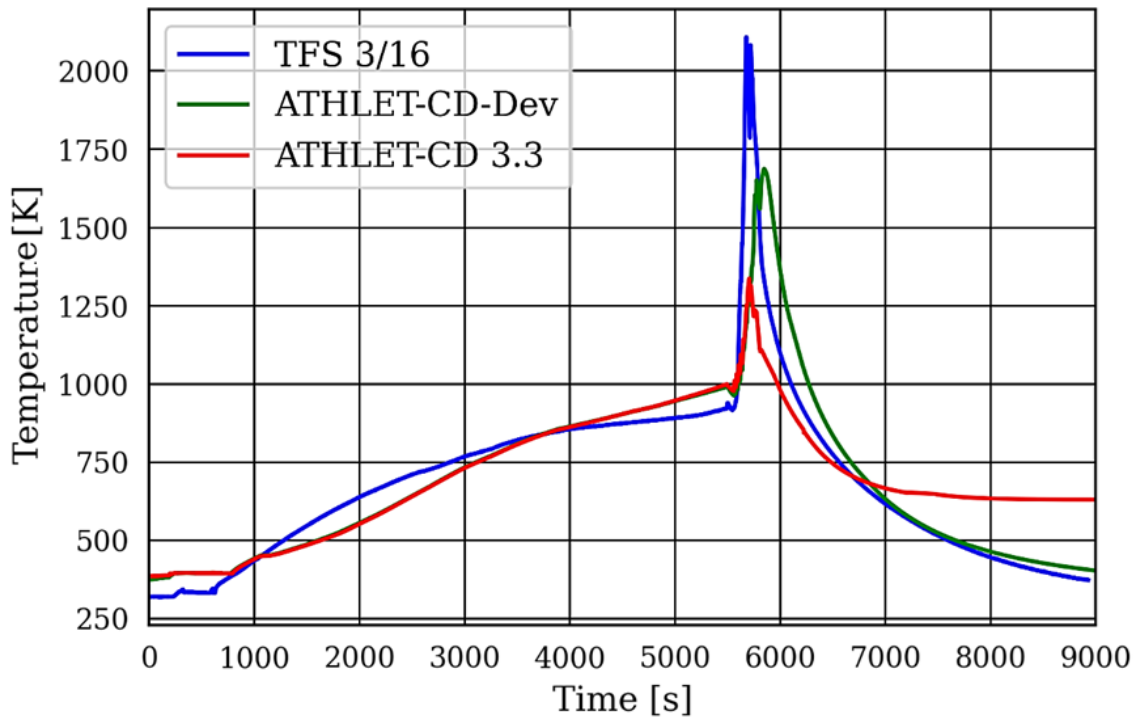


Fig. 2.12 Cladding temperature at 1250 m

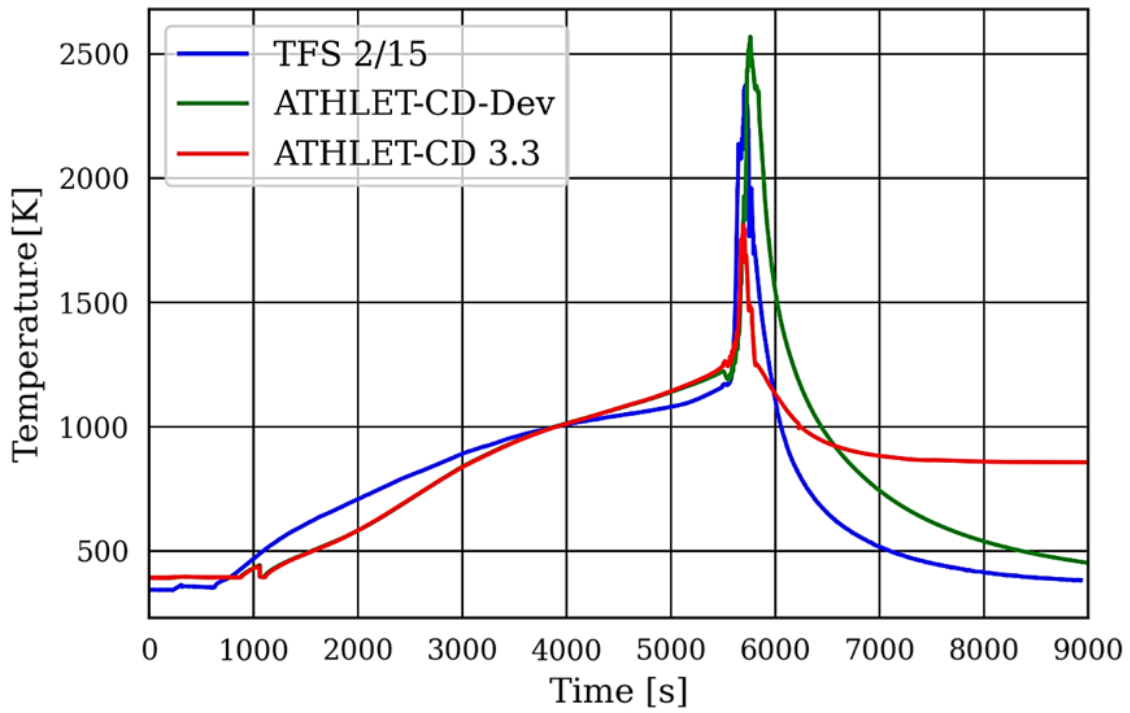


Fig. 2.13 Cladding temperature at 1150 mm

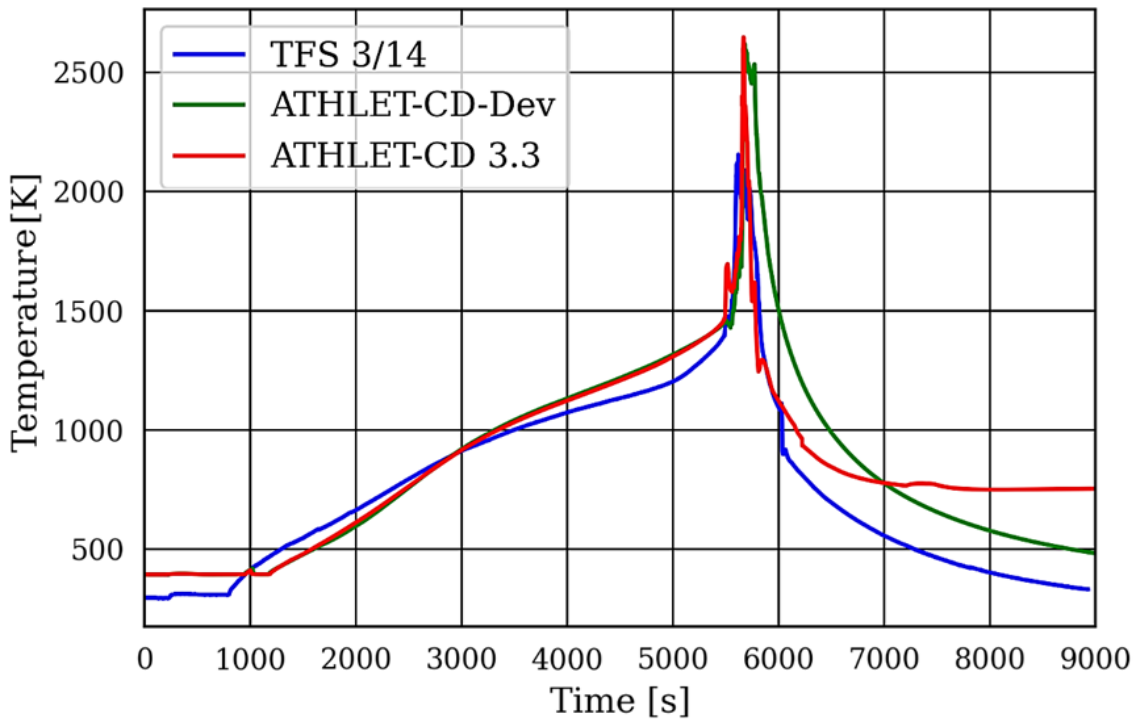


Fig. 2.14 Cladding temperature at 1150 mm

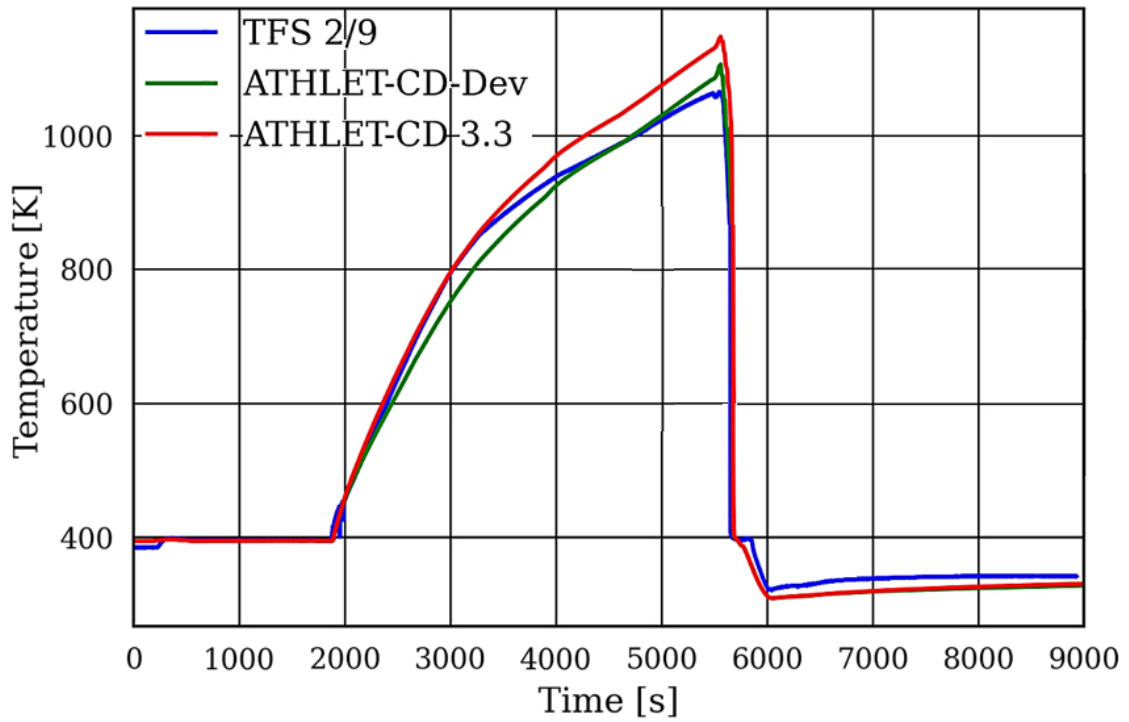


Fig. 2.15 Cladding temperature at 550 mm

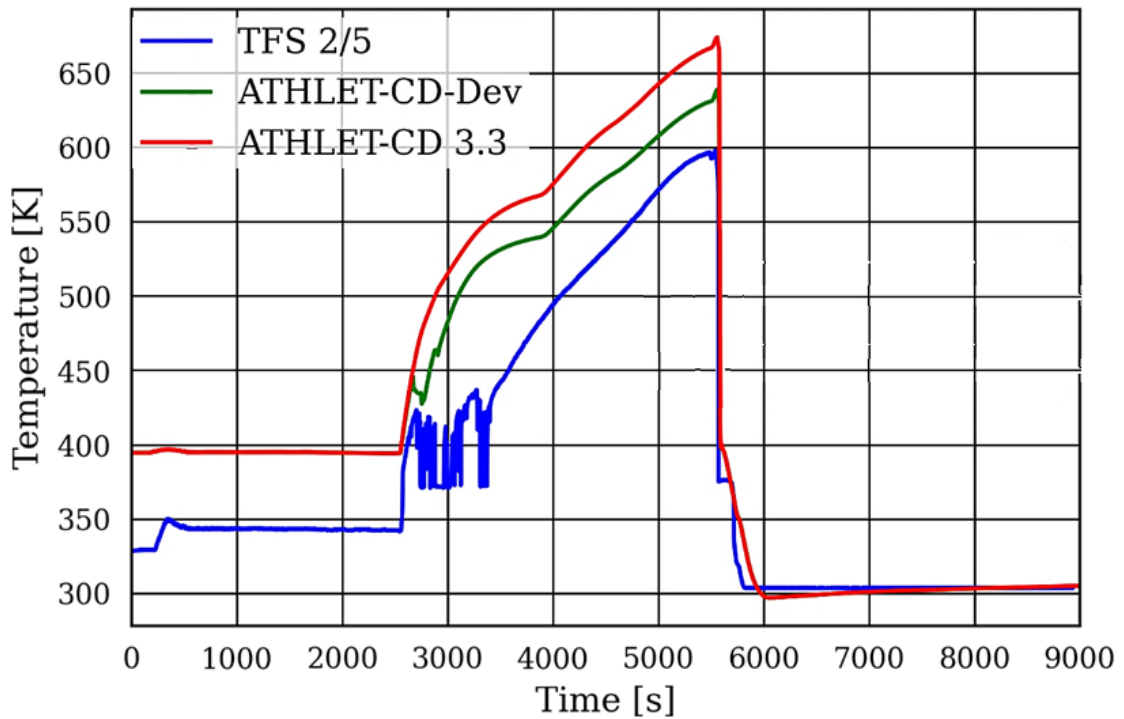


Fig. 2.16 Cladding temperature at 150 mm

The water level predictions (Fig. 2.15) in the development version and ATHLET-CD 3.3 showed no noticeable difference.

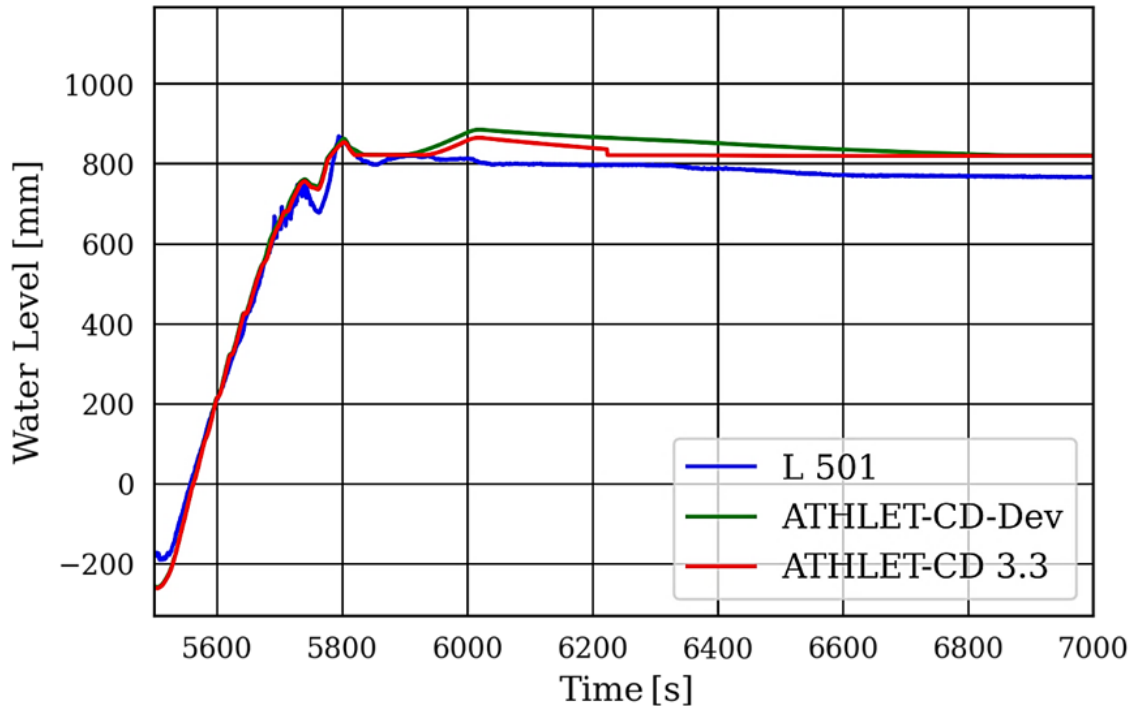


Fig. 2.17 Water level at time interval between 5500 – 6000 s

In general, explicit modelling of the spacer grid provides a more accurate prediction of the thermal hydraulics of the cladding temperature. This is due to the improved prediction of the heat transfer coefficient of grids using the ratio of the volume and area of the spacer grids. ATHLET-CD 3.3 predicted heat transfer between grids and fluid using the fuel rod diameter, which resulted in an underestimation of spacer grid to fluid heat transfer.

2.1.3 Model for melt relocation in the core-bypass channel

Motivation

ATHLET-CD calculates formation of melt due to insufficient cooling and constant heat generation coming from decay of fission products and extensive oxidation processes. Melt can relocate axially along the rod. If it encounters a blockage during its downward movement, it can spread horizontally into neighbouring nodes. However, melt can only relocate within the core region, it is not possible for the melt the spread outside of the core. This is seen as an acceptable limitation in most of the cases, but there are scenarios where melt can attack the RPV internal structures around the core, heat it up and melt through, e. g., the core shroud. Then, there is an additional relocation path for the

melt to move/fall downward to the lower plenum. The most famous example of this scenario is the accident in the TMI-2 power plant in 1979, USA /EPRI 80/, /DRA 05/, /SEH 12/. After core melting the melt attacked the core surrounding and relocated to the lower plenum via volumes next to the core. Fig. 2.18 illustrates the melt path to the lower plenum during the accident.

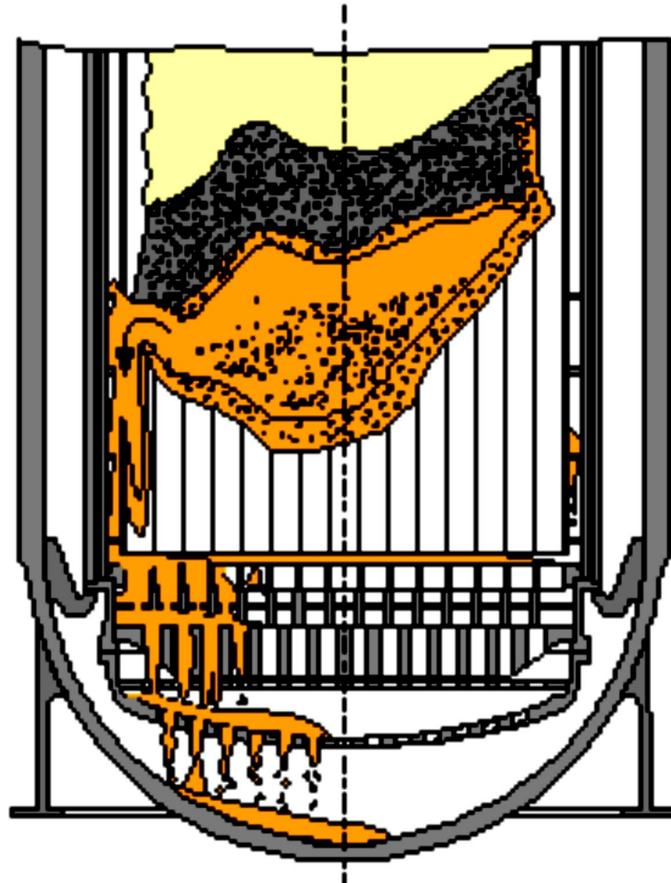


Fig. 2.18 Core melt relocation path to the lower plenum during the TMI-2 accident /SEH 12/

Model development

In order to be able to cover such phenomena in ATHLET-CD, the following model developments, improvements and adjustments were made:

The task can be split into two smaller tasks:

- Melt-core surrounding interaction and core surrounding failure
- Melt relocation outside of the core TFOs and relocation to the lower plenum

2.1.3.1 Melt-core surrounding interaction and core surrounding failure

If the axial movement of melt in the outermost core nodes is hindered due to a blockage and the melt also cannot flow inwards (because the inner nodes are also blocked and/or filled with melt), melt accumulates on the blockage, filling the available space up until “ZMELT” height in the node and gets in contact with the surrounding structure, in this case with ATHLET heat conducting (HECU) objects. The contact area for between the melt and core shroud is calculated via:

$$\begin{aligned} A(i)_{ceramic/metallic} \\ &= ZMELT(i)_{ceramic/metallic} * RSEC(outermost)(i) \\ &* 2.0 * \pi \end{aligned} \quad (2.13)$$

Where

- A(i) is the contact area between melt in the outermost core node i and core surrounding structure [m²]
- ZMELT(i) is the height of melt in the outermost core node I [m]
- RSEC(outermost)(i) is the radius of the outermost core node I [m]
- Ceramic/metallic indicates if the contact area is calculated for ceramic or metallic melt

The conditions for the melt-structure interaction are very similar to the conditions in the lower plenum, where melt also gets into contact with steel, therefore for the calculation of the melt-steel heat transfer equations from the lower plenum module AIDA are used. To calculate the required heat transfer coefficient between steel and ceramic/metallic melt also considering the effects of crust formation the following equations are used:

For contact of ceramic melt with steel /LOV 21a/ the calculation for a node uses:

$$\alpha = \frac{Nu * \lambda_{ceramic}}{ZMELT_{ceramic}} \quad (2.14)$$

where

- Nu is the Nusselt number [-]
- $\lambda_{ceramic}$ is the heat conductivity of ceramic melt [W/mK]
- Ra is the Rayleigh number

$$Nu = 0.55 * Ra^2 \quad (2.15)$$

and

$$Ra = \frac{g * \beta * P_{ceramic} * ZMELT_{ceramic}^5 * \delta_{ceramic} * cp_{ceramic}}{\lambda_{ceramic}^2 * \nu_{ceramic}} \quad (2.16)$$

where

- β is the thermal expansion coefficient = 1.05D-4 [1/K]
- $P_{ceramic}$ is the power of the ceramic melt [W]
- $\delta_{ceramic}$ is the density of ceramic melt [kg/m³]
- $cp_{ceramic}$ is the heat capacity of ceramic melt [J/kgK]
- $\nu_{ceramic}$ is the kinematic viscosity of ceramic melt [m²/s]

For contact of metallic melt with steel /LOV 21a/ for a note:

$$\alpha = \frac{Nu * \lambda_{metallic}}{ZMELT_{metallic}} \quad (2.17)$$

$$Nu = \left(0.825 + \frac{0.387 * Ra^{\frac{1}{6}}}{\left(1 + \frac{0.492}{Pr^{\frac{8}{16}}} \right)^{\frac{8}{27}}} \right)^2 \quad (2.18)$$

where

- Pr is the Prandtl number

$$Ra = \frac{g * \beta * (TSL - HC_{temp}) * ZMELT_{metallic}^3}{\frac{\lambda_{metallic}}{\delta_{metallic} * cP_{metallic}} * \nu_{metallic}} \quad (2.19)$$

where

- β is the thermal expansion coefficient = 1.1D-4 [1/K]
- TSL is the metallic melt temperature [K]
- HC_{temp} is the temperature of the core surrounding structure

$$Pr = \frac{\nu_{metallic}}{\frac{\lambda_{metallic}}{\delta_{metallic} * cP_{metallic}}} \quad (2.20)$$

After obtaining the required heat transfer coefficients the heat transfer from melt to structure can be calculated as follows:

$$Q = \alpha * A * (TSL - HC_{temp}) \quad (2.21)$$

where

- Q is the power exchanged between melt and structure [W]

The amount of the transferred heat is deducted from the melt and added to the surround structure. If the temperature of the surrounding structure reaches a user defined value, the object fails and no longer represents a physical boundary for the melt to relocate outside of the core.

2.1.3.2 Melt relocation towards outside of the core and relocation to the lower plenum

The existing models for horizontal melt relocation had to be adjusted and extended, in order to allow melt to move to volumes without core structures defined in the ATHLET-CD input. A check was implemented into the model that scans in every timestep whether the core structure next to the outermost ring is intact or not. If the structure is not intact, then melt can relocate outwards the same way as for an inner core node towards an outer core node. A description of the horizontal melt relocation modelling can be found in /LOV 21a/.

Melt appears outside of the core, as is depicted in Fig. 2.18. Detailed simulation of the movement of molten material outside of the core was not the aim of this task and so has not been implemented so far. Therefore, if melt leaves the core nodes, it immediately falls into the lower plenum. This simplification is deemed acceptable for this step in the development as flow paths outside of the core shroud have less potential for blockages in several LWR designs. More importantly, the assumption that the melt falls immediately into the lower head of the reactor pressure vessel systematically overestimates the amount of corium in the lower head, which is generally not optimistic with regard to RPV failure in the late phase. Therefore, this assumption is justified, though further development of ATHLET-CD towards a more realistic model would be sensible.

Code structural and internal syntactical changes were made to allow the lower plenum modules to start after (usually) small amounts of melt appear in the lower plenum due to relocation from outside of the core. At the same time, the melt and power relocated from the core are deducted from the in-core quantities.

If the user wants to use the new model, he has to implement the followings into an ATHLET-CD input deck:

- Define ATHLET heat conducting objects, coupled with ATHLET-CD via the keyword "HECUNAMER"
- Allow PW CREEPING under the core surrounding structures
- Set the flag "IDMTLP" to 2, which activates the relocation on the outside of the core

Verification

The new option was verified on a hypothetical severe accident scenario in a PWR. The results of the calculation with the melt-bypass option were compared to a simulation of the same scenario, however, without the melt-bypass relocation.

The important characteristics of the simulated scenario and the analysed reactor were the following:

- PWR with 45548 fuel rods, total thermal power before shutdown was 3.778 GW
- Scenario: station black-out with a cold leg break ($A = 0.055\text{m}^2$), no countermeasures
- Core uncover starts at around 2200 s after the initiating event
- First melt appears at around 3600 s after the initiating event
- For easier comparability the failure of the grid plate is controlled via a time signal, failure is predetermined at 6000 s after the initiating event
- Simulation is stopped at 7000 s after the initiating event, because melt-bypass relevant phenomena are finished at that time

The simulations with and without core-bypass relocation run identically for a long time. First minor differences occur, when melt starts to accumulate at a certain elevation in the outermost core node above a blockage, as shown in Fig. 2.19. With the melt-bypass model active, melt interacts with the core shroud and heats it up. At 5793 s the two simulations diverge, because the core shroud locally fails due to melt-steel interaction and melt starts to relocate into the core bypass, then falls into the lower plenum. The shroud fails at the same position in the simulation without the melt-bypass option, however about 350 s later, as depicted in Fig. 2.20. (Note: core node 5 is assigned to HECU node 6)

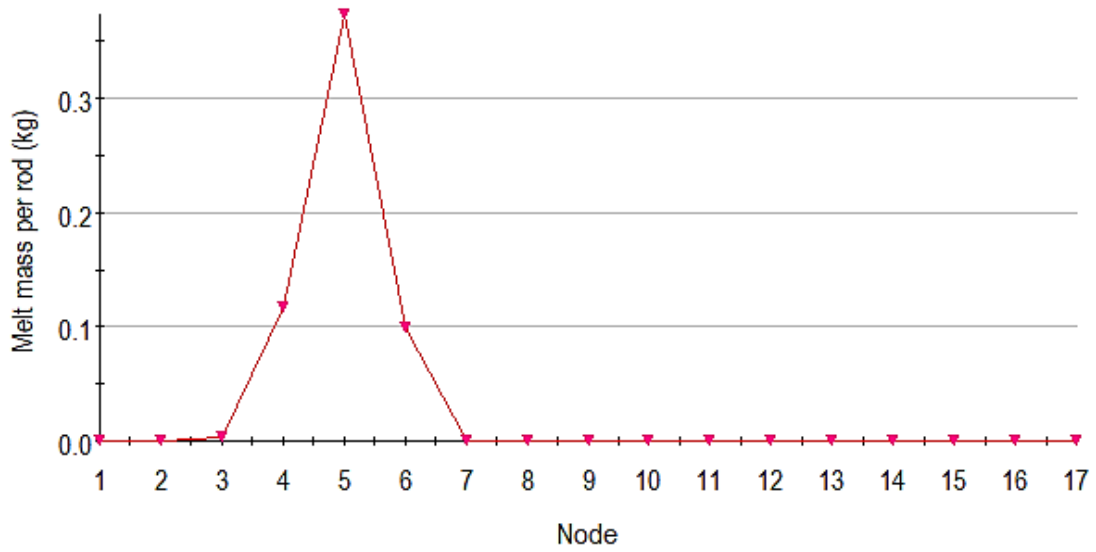


Fig. 2.19 Axial melt distribution in the outermost core node (SUMUOSL = ceramic melt per fuel rod)

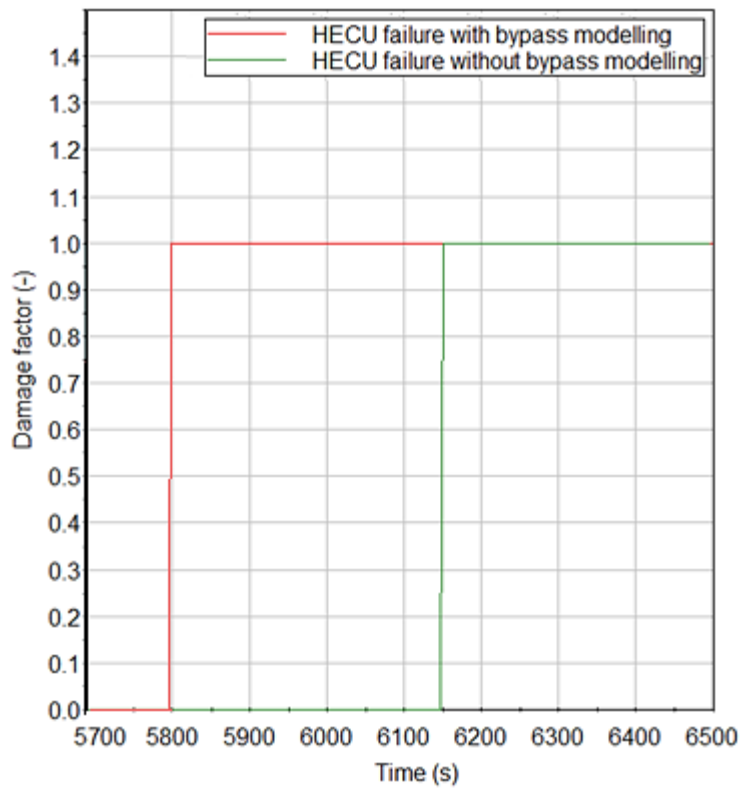


Fig. 2.20 Core shroud failure at elevation 6 with and without modelling of melt bypass

After the shroud fails, melt starts to relocate to the lower plenum only when the option for melt bypass relocation is activated. Melt mass and its associated decay power appear in the lower plenum just after 5793 s, as seen in Fig. 2.21 and Fig. 2.22.

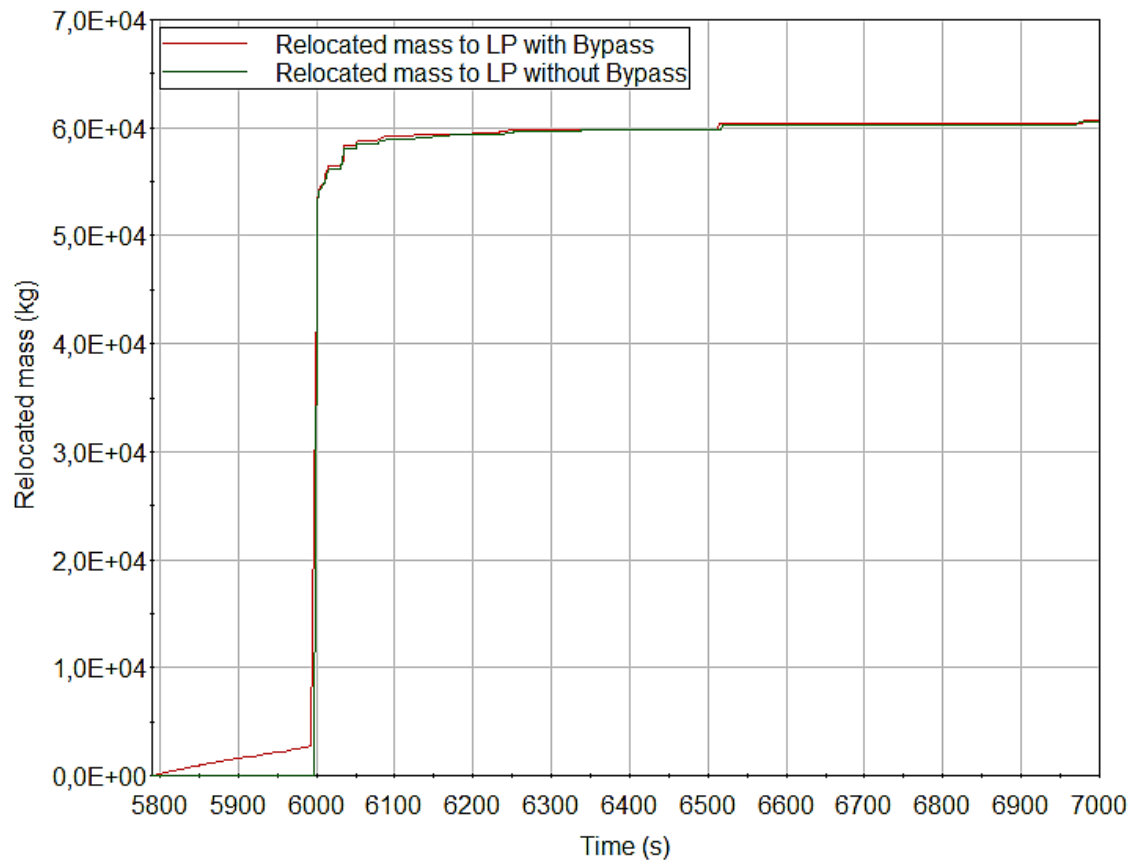


Fig. 2.21 Melt mass accumulation in the lower plenum with and without melt bypass modelling

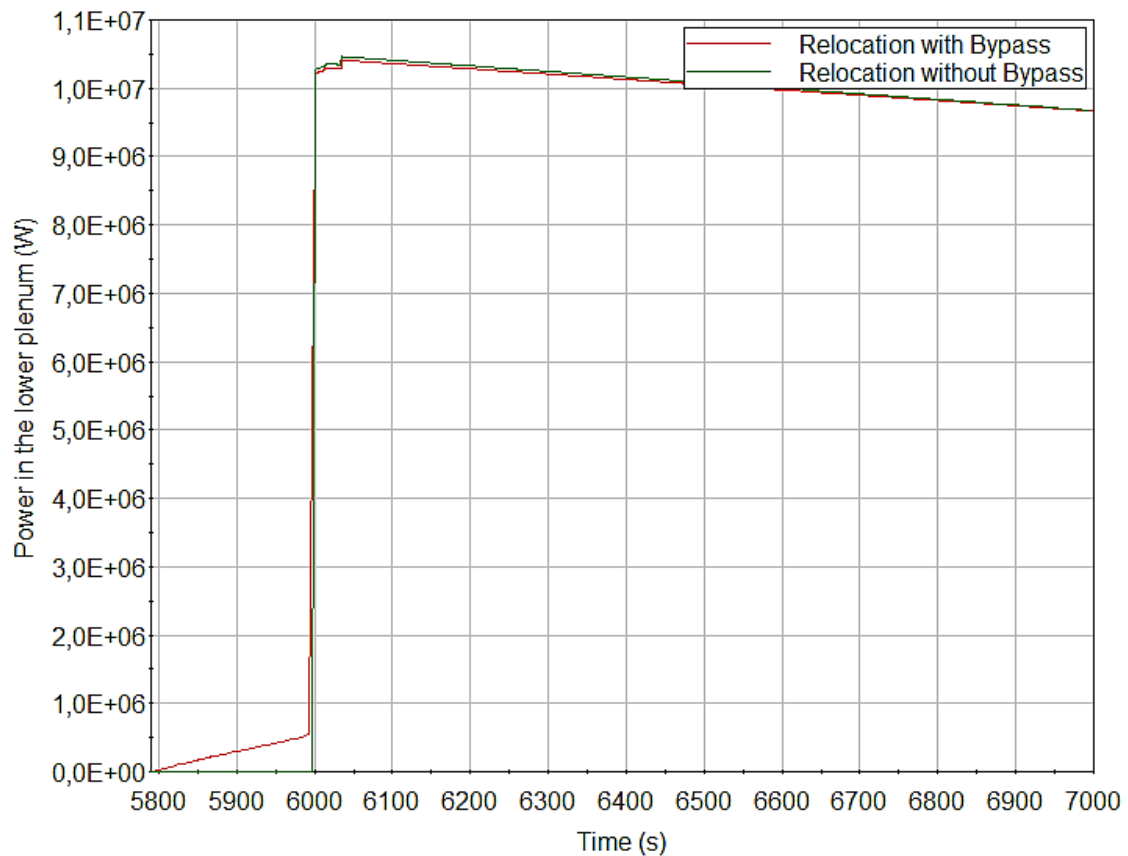


Fig. 2.22 Decay power in the lower plenum with and without melt bypass modelling

Melt mass and its decay power only appear in the calculation without bypass modelling after melt relocation via grid plate failure is initiated at 6000 s. Thereafter, the two calculations behave similarly again, because the sum of all melts in the core is similar, therefore the sum of the total relocated mass is similar, too. So, in this scenario, there are only significant differences in the time period between 5793 s and 6000 s. Overall, the results are reasonable and show that the melt relocated through the bypass is computed reasonably and according to specifications.

The task objective was achieved, the user has now an option to simulate melt relocation to the lower plenum via an alternative path, not just via grid plate failure. Further development work will benefit from user-feedback and targeted validation.

2.1.4 VVER-440 specific model for “Follower-Assemblies”

Motivation

VVER-440 type reactors have a unique shutdown mechanism. Around ten percent of the fuel assemblies consist of two axially different parts and are called “Follower-assemblies”. The upper part is made of absorber material, while the lower part contains fissile material. During normal operation only the fissile material is located within the active core, the absorber material is above the core. If core shutdown is initiated, these fuel assemblies are pushed down completely, thus the fissile material moves below the core, into guide tubes, and the part with absorber material enters the core. The lower part of a VVER-440 reactor is illustrated in Fig. 2.23.

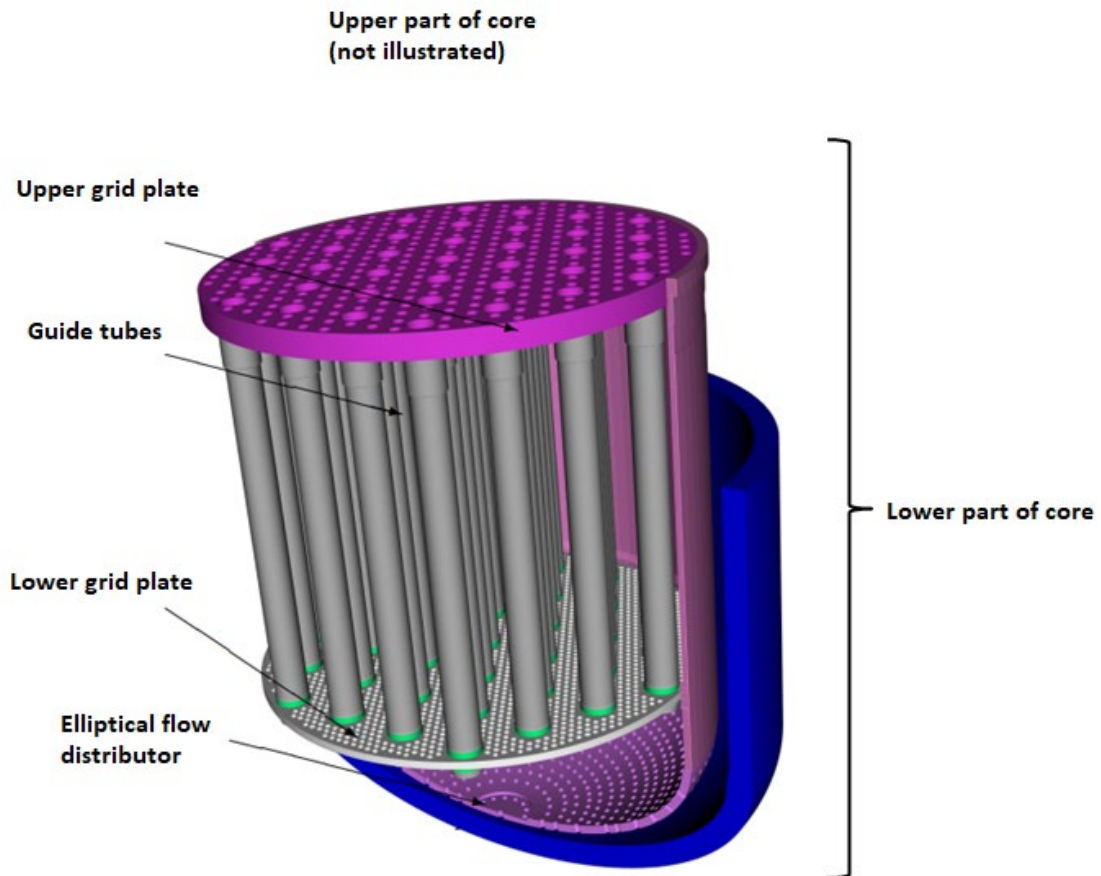


Fig. 2.23 Lower part of a VVER-440 reactor core /PET 15/

This core configuration in shutdown state has some effects on the accident progression. Because 10 % of the fuel assemblies are located below the core, around 10 % of the decay power is generated below the core, while in the core itself only around 90 % remains. Also, as visible in Fig. 2.23, there are two support grid plates, one for the upper core, one for the lower part. Both of them act as a relocation barrier for any core melt, before melt can reach the bottom of the reactor pressure vessel.

Simulating this unique configuration with ATHLET-CD was difficult. It was not possible to define axially different core compositions. A workaround was used for a long time, where only the upper part of the core was modelled as a reduced core (90 % of the fuel assemblies) with ATHLET-CD. The lower part was modelled with ATHLET heat conducting objects, which could simulate the associated heat generation, but could not simulate melting processes or fission product releases. Simulation of oxidation was possible, however, using the ATHLET oxidation models, which are not necessarily the same as the oxidation models implemented in ATHLET-CD. Besides these deficiencies, it was difficult for the user to create an adequate input deck.

Therefore, it was decided to improve ATHLET-CD to allow users to simulate VVER-440 reactors more adequately and in a more user-friendly way.

Model development

A method was developed for ATHLET-CD to simulate the follower assemblies of VVER-440. After the necessary internal changes to the code, the user has to follow these steps to create a VVER-440 specific input deck:

- Define a double length core.
- Subdivide the core into different rings as usual. (Flexible nodalisation is not available for VVER-440 modelling).
- The follower assemblies should be defined in one or two separate, not neighbouring rings (for example Rod 2 and Rod 4 should represent the follower assemblies, as illustrated in Fig. 2.24).
- Innermost and outermost rings are not allowed to be follower rings.

- The number of fuel rods defined in these rings should be equal to the number of fuel rods belonging to those nodes. (Follower rings have usually less fuel rods than normal core nodes).
- The control rods above the follower assemblies have to be distributed to the neighbouring, non-follower assembly rings (control rods of ROD2 shall be distributed proportionally to ROD1 and ROD3 (see Fig. 2.24)).
- Finally, under a new pseudo keyword: "VVER440" the user can define which nodes are active and which are empty. With that it is possible to activate/deactivate certain axial locations in the core.
- Define power (with the help of ----POWERZ) only at locations where fuel is located. This also influences the fission product distribution accordingly.
- Finally, the user has to adjust the fission product distribution under FIPREM input data with appropriate "ATABFN" tables.

An example is provided in in Fig. 2.24. "ROD2" and "ROD4" are the rings representing the follower assemblies. The user defines under PW VVER440, that nodes: 1 – 10 should be empty for "ROD1", "ROD3" and "ROD5". The amount of control rods in Ring 1 is equal to the normal number of control rods (CROD1) and some control rods from the follower assembly ring (CROD2). The number of control rods in ROD3 is equal to its normal amount of control rods and some of the control rods from the two neighbouring follower assembly rings. For "ROD2" and "ROD4", nodes 11 – 20 should be empty.

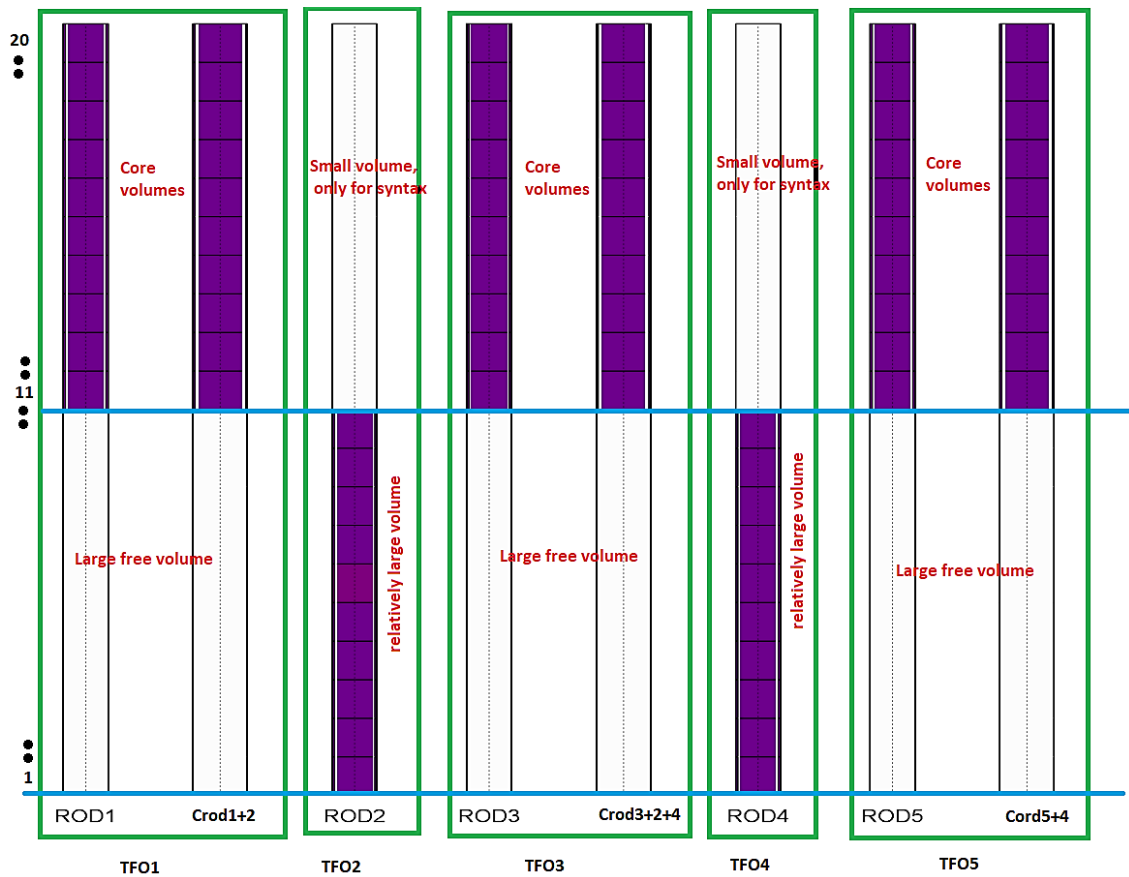


Fig. 2.24 Sample nodalisation for VVER-440

Thermohydraulically, ATHLET TFOs have to be defined for each ring. For the “active” parts of ROD1, ROD3 and ROD5 (nodes 11 – 20), parameters of TFOs should be defined as usual. Below the active part (nodes 1 – 10) a large free space is to be defined.

For the lower parts of the follower assemblies (nodes 1 – 10 in ROD2 and ROD4) the user has to create a TFO with a relatively large free area and volume to depict reality. Only around 10 % of the fuel rods are present below the normal core. The top part of the follower assemblies consists of control rods. In ATHLET-CD, however, they are already defined in the neighbouring rings. Therefore, the top of ROD2 and ROD4 are artificially “empty”. This part of the TFO is irrelevant, should be defined as small as possible, with cross connections, it is only needed due to syntax.

Alternatively, the lower parts of the core could be defined into the same TFO as the upper part. For example, based on the example in Fig. 2.24: “ROD1” and “ROD2” could belong to the same TFO, lower part is a sparse TFO, upper part denser (normal core geometry). With these considerations and additional VVER options the user can create a VVER-440 model.

To allow all these for the user, some code internal changes were necessary.

In the upper core part:

- Heat transfer within one ring is calculated as usual.
- Heat radiation between neighbouring rings is calculated as usual, however, if the neighbouring ring is a follower assembly ring, heat radiation is automatically calculated towards the next normal ring. (From Ring “1” to Ring “1+2” instead of Ring “1+1”).
- Fuel rod deformation, oxidation and melt relocation, fission product release is calculated as usual.
- Melt flows downwards along the rods, until it reaches the upper support plate (upper blue line in Fig. 2.24). Melt is stopped at the elevation of the upper grid plate. For the stoppage of melt the developments from “Model to assess the influence of spacer grids on the movement of molten material” from WP1.1 are used.
- There is no interaction between melt and grid plate(s) (melt-grid plate interaction is neglected also in standard PWR simulations and still needs to be implemented in ATHLET-CD).
- After the upper grid plate fails, the melt is transferred to the lower plenum directly. It is assumed that the falling of multiple tons of molten material destroys the lower grid plate as well. This assumption is also backed by the fact, that the lower grid support plate is not as thick as the upper one.
- The empty nodes from the bottom of the “normal” core assemblies are not calculated, they are considered to be non-existent, they don’t take part in any of the mechanisms.

In the lower core part:

- Heat transfer within one ring is calculated as usual.
- Fuel rod deformation, oxidation and melt relocation, fission product release is calculated as usual.
- Melt flows downwards along the rods, until it reaches the lower support plate (lower blue line in Fig. 2.24). Melt is stopped at the lower support plate, similarly to the upper support plate.
- After the upper plate fails, the lower plate is assumed to fail as well (large impact from above destroys the smaller, lower plate, too). After plate failures melt is transferred to the lower plenum directly.
- All the heat radiation from the follower assemblies is calculated between follower assemblies and core surroundings. Heat radiation between follower assembly rings is not calculated. Due to the relatively sparse distribution of follower assemblies, the heat radiation they emit can pass through the gaps between fuel assemblies and can hit the surrounding wall directly.
- The empty nodes from the top of the follower assemblies are not calculated, they are considered to be non-existent, they don't take part in any of the mechanisms.

Verification

For verification purposes a very simple input deck was created, where all the newly implemented modelling changes and input creation methods could be tested. The objective was to demonstrate the usability of the developed new method. Realistic simulations using this new method is a task for another project.

A VVER-440 reactor core was created, with a core nodalisation shown in Fig. 2.24 and with the modelling considerations defined previously.

INPUT

Under each “Rod” definition the PW VVER440 keyword was added at the end of the section (just before the next rod definition starts). There, the intact parts for each rod (MINVVER, MAXVVER) are defined. For example, based on Fig. 2.24:

- For Rod1 → MINVVER = 11 and MAXVVER = 20 (user variable, shown and used values are based on the example shown here)
- For Rod2 → MINVVER = 1 and MAXVVER = 10 (user variable, shown and used values are based on the example shown here)

An artificially altered axial power profile was defined, to demonstrate the full functionality of the core, especially the effects in the lower part. Axial power profile shown in Fig. 2.25 was used. In “ROD1” power is only defined in the upper part (starting from elevation 2.0 meters). In ROD2 power is only defined in the lower part. An artificial peak in the power was defined between elevation 1.0 and 1.2 meters to clearly demonstrate all the modelling changes. The definition of power profiles also influences the fission product distribution.

K----- POWT1			K----- POWT2		
@	L	POWER FACTOR	@@	L	POWER FACTOR
	0.0	0.0		0.0	0.25
	2.0	0.0		1.0	0.25
	2.0	0.5		1.0	1.0
	2.5	1.0		1.2	1.0
	3.5	1.0		1.2	0.25
	4.01	0.5		2.0	0.25
				2.0	0.000
				4.01	0.0

Fig. 2.25 Axial power distribution in ROD1, ROD3 and ROD5 (left) and ROD2 (right) (effects also fission product distribution)

Fig. 2.26 shows the core nodalisation. The colour of the illustrated nodes shows the temperature of the fuel and control rods at $t = 10$ s. The deliberate power peak (described in Fig. 2.25) leads to a pronounced heat up in ROD2 in the 6th node. The power distribution in ROD2 is also shown in Fig. 2.27, the fission product distribution is shown in Fig. 2.28. It is clearly visible that no power is generated, and no fission product is simulated in the upper part of the follower assemblies. The power and fission product distribution in ROD1

are shown in Fig. 2.29 and Fig. 2.30 Here, different to the “follower-rods”, power and fission products are only simulated in the upper part.

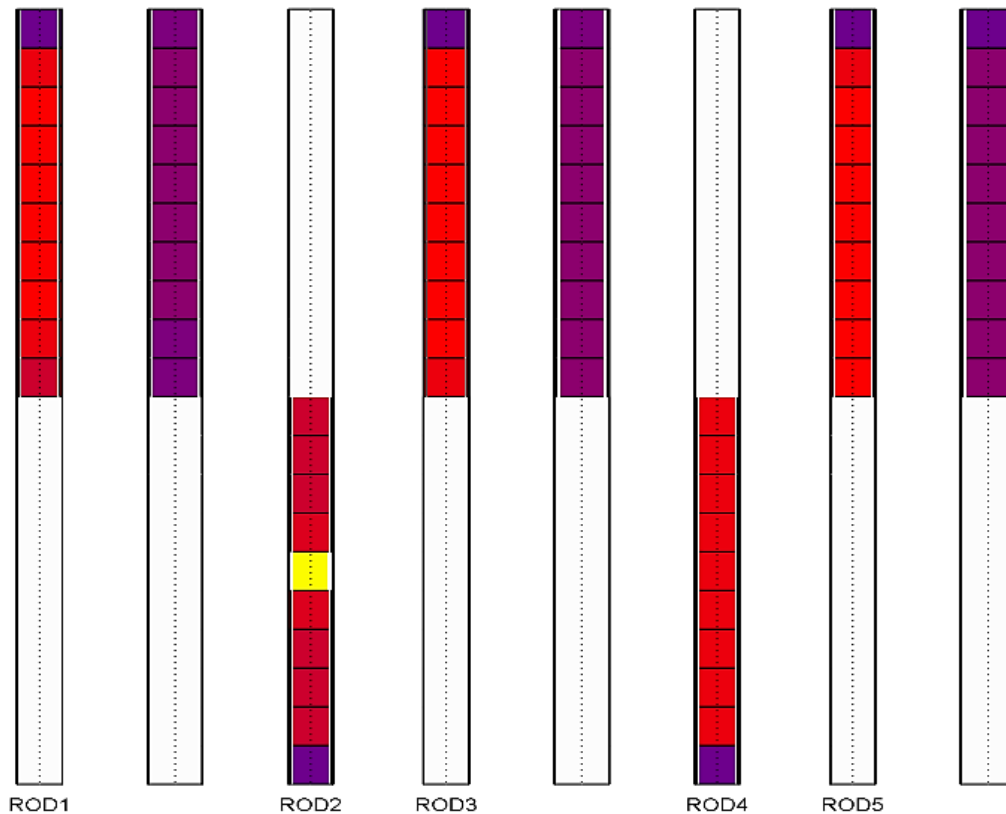


Fig. 2.26 VVER-440 nodalisation, colours depend on the temperature of the structure (yellow-high, red/purple-low)

As visible on Fig. 2.26, node six in ROD2 heats up very quickly (due to the artificially increased power at that elevation). The overheated node radiates its energy, as described in the previous section, directly to the surrounding heat conduction object (ATHLET HECU object). Fig. 2.31 shows that the surrounding structure is extensively heated right at that location. This demonstrates that heat radiation implementation from follower-assembly to surroundings works. Fig. 2.31 Fig. 2.32 show that the large heat-up of one part of the follower-assembly results in extensive H₂ generation and fission product release, proving that the axial extension of the core structures is working as intended. Fig. 2.34 just shows a completely destroyed state of a VVER-440 core, demonstrating that the lower core parts (follower-assemblies) can melt and relocate to the lower plenum, too.

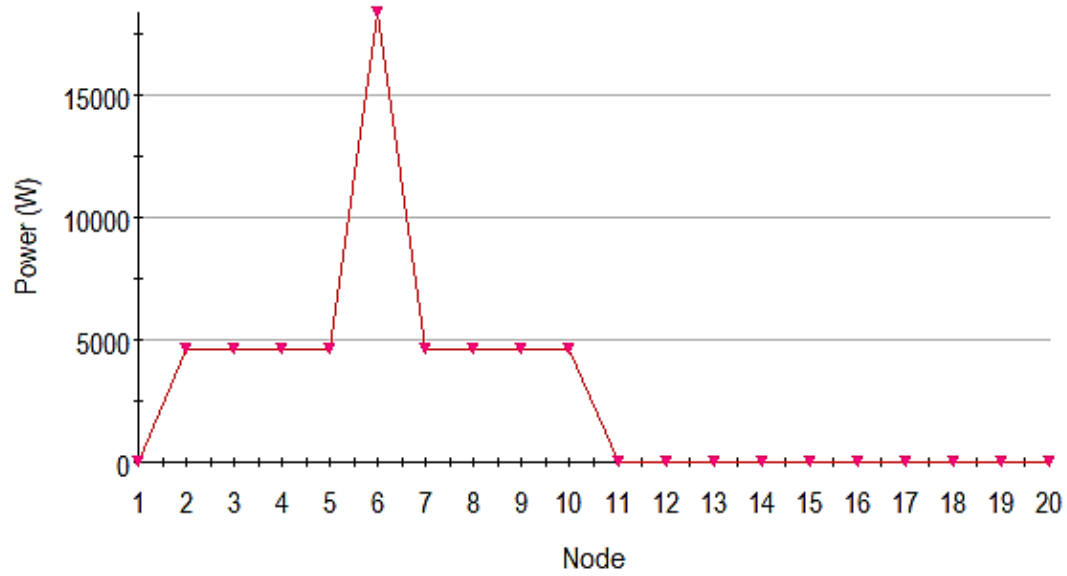


Fig. 2.27 Power distribution along axial nodes for ROD2

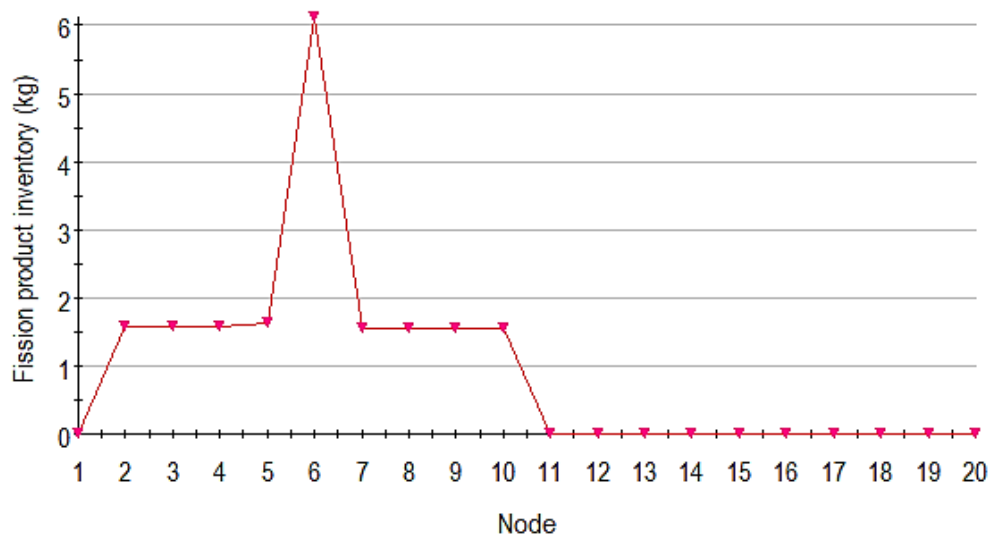


Fig. 2.28 Fission product distribution along axial nodes for ROD2

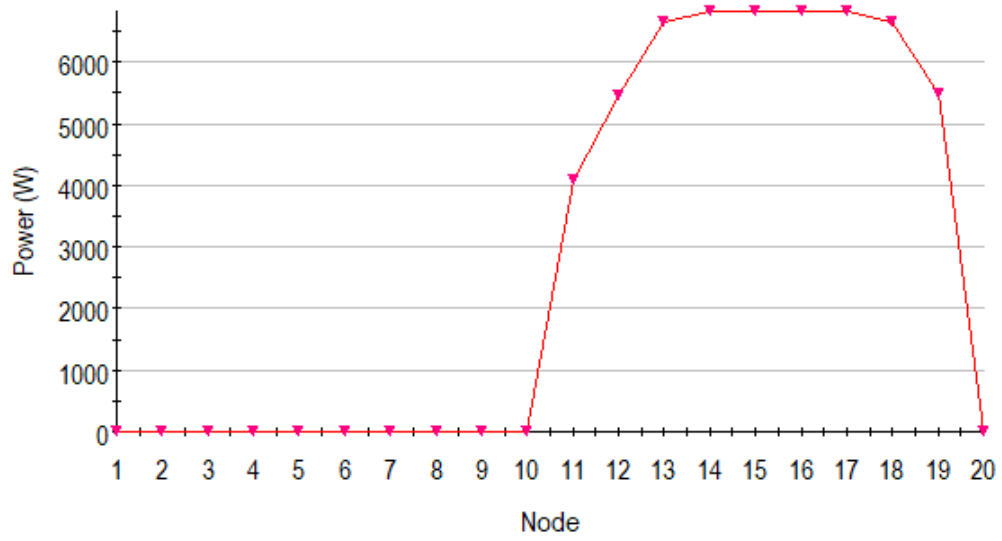


Fig. 2.29 Power distribution along axial nodes for ROD1

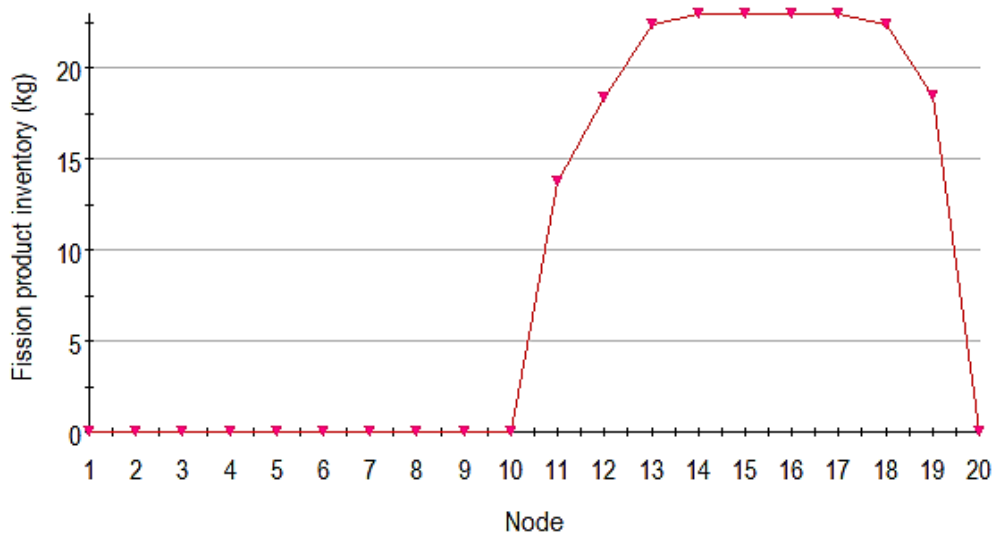


Fig. 2.30 Power distribution along axial nodes for ROD1

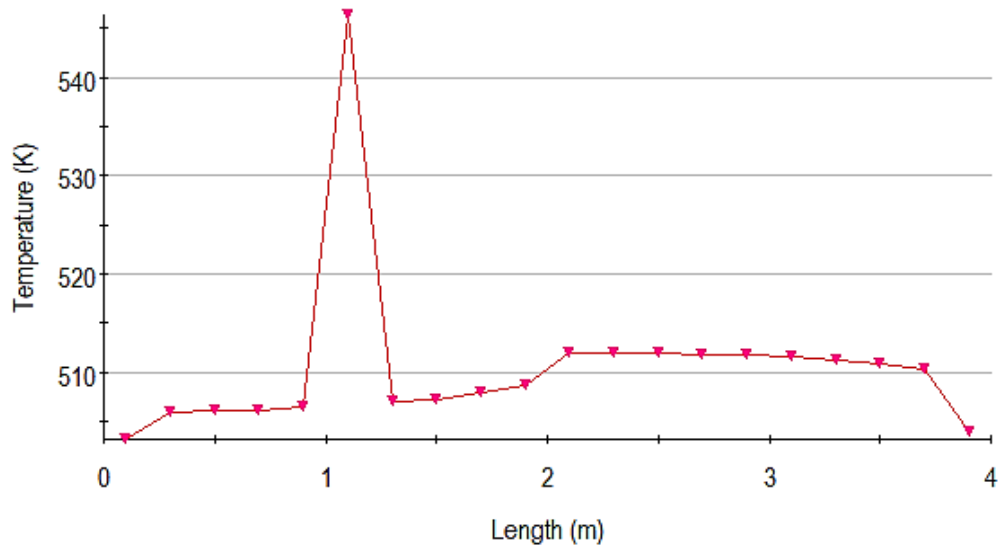


Fig. 2.31 Axial temperature distribution of the core surrounding structure

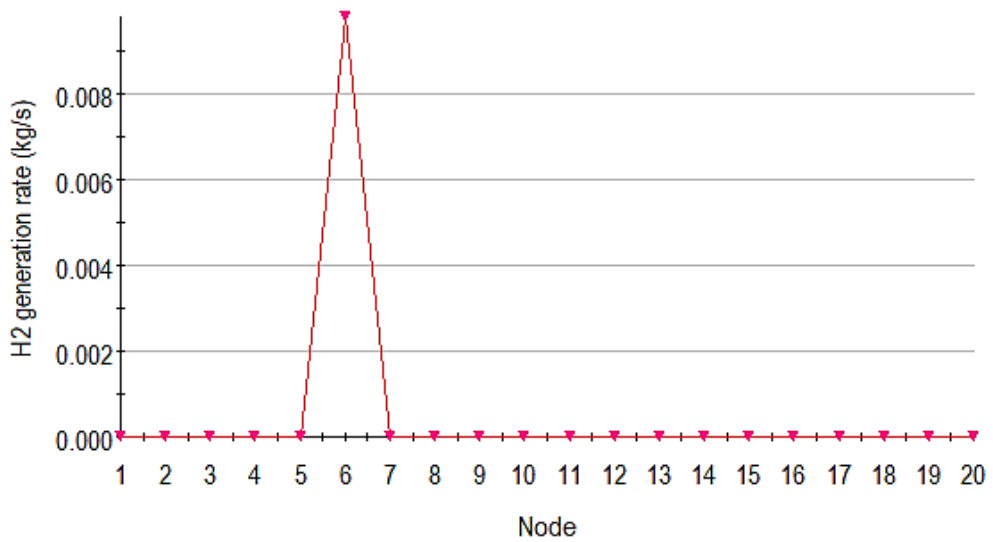


Fig. 2.32 Axial temperature distribution of the core surrounding structure

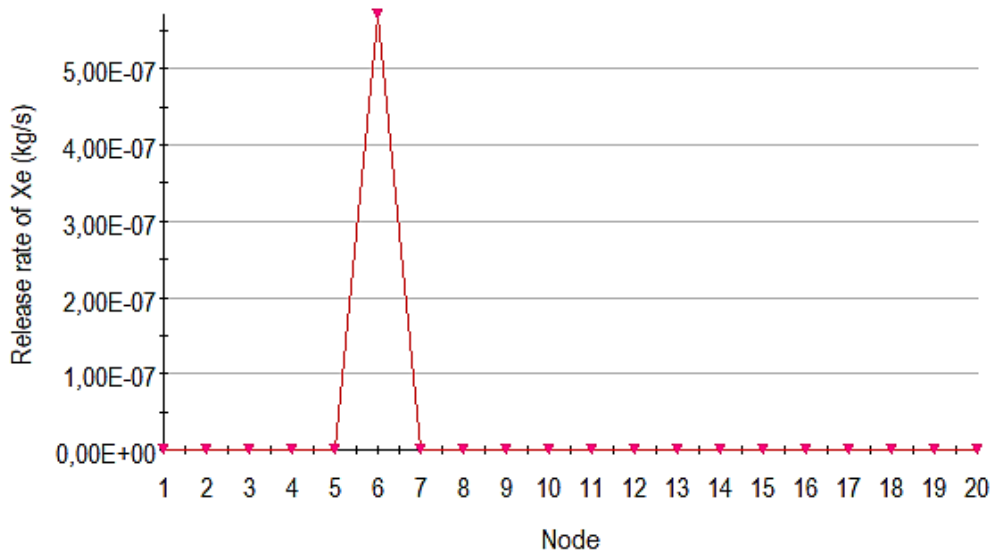


Fig. 2.33 Xe release rate at the hottest part in the follower-assemblies (ROD2)

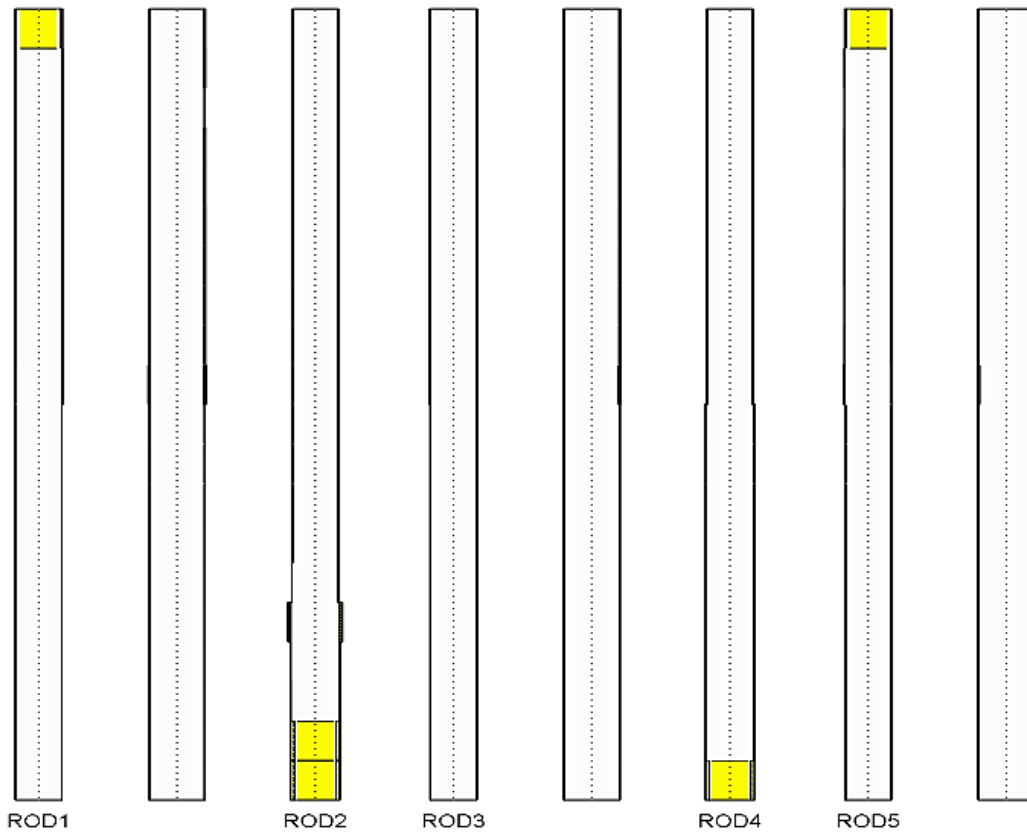


Fig. 2.34 Total core failure in a VVER-440 reactor modelled with the new ATlhET-CD VVER-440 option

With these model developments users can model VVER-440 reactors more adequately and in a more user-friendly way. Further development needs depend on user-feedback and insights from validation.

2.2 WP1.2: Modelling of oxidation

2.2.1 Oxidation model for ATF material

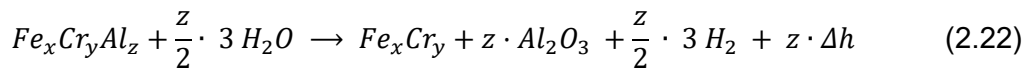
Motivation

Zirconium based claddings have been widely used all over the world for decades due to its good mechanical, corrosion resistant and low neutron absorption properties at around operational temperatures. At higher temperatures, however, the zirconium becomes more reactive, in case of a nuclear accident most likely with the steam in the reactor core, which leads to extensive heat up and hydrogen generation. To mitigate or eliminate this problem, accident tolerant fuel (ATF) designs were developed, that should withstand much larger temperatures without significant oxidation and thus less heat added to the core degradation process. Such materials, however, could not be simulated in ATHLET-CD, therefore, it was decided to implement models so that ATHLET-CD could be used simulate a nuclear power plant with an ATF core loading.

Developments

The selected and implemented model is valid for Kanthal APM (FeCrAl) material with a composition of 69 % Fe, 21.6 % Cr, 4.9 % Al (+ 4.5 % others). It is assumed that due to the oxidation only Al_2O_3 is produced, which then forms a protective layer of $\alpha-Al_2O_3$, i.e. corundum /ORNL 18/.

The oxidation of the specific ATF material can be summarised by the following chemical balance equation:



where

- Δh : energy release during oxidation = $9.3 \cdot 10^5$ J/mol = $9.32 \cdot 10^6$ J/kg_{FeCrAl}
- x, y, z: composition of FeCrAl molar masses of x = 1.307, y = 0.404 and z = 0.215

A parabolic law was used to determine the oxidation rate that was derived from the analytical solution of the diffusion equation, similarly to the method for the oxidation of zirconium:

$$dW^2 = K \cdot dt \rightarrow \frac{dW}{dt} = \frac{K}{2W} \quad (2.23)$$

where

- W = $m_{ox} / (\text{surface area})$ in [kg/m²]
- m_{ox} = mass of the resulting oxide (Al₂O₃) [kg]
- K = reaction rate in [kg²/m⁴s]
- dt = time step [s]

The reaction rate is determined by the following Arrhenius equation:

$$K = A \cdot \exp(-B/RT) \cdot g(ps) \quad (2.24)$$

where:

- R = universal gas constant (J/mol/K)
- T = cladding temperature [K]
- $g(ps)$ = reduction factor to consider steam starvation ($0 \leq g(ps) \leq 1$)

A, B: rate constants as given by KIT for KANTHAL APMT /HOL 19/:

- A = 3.1 kg²/m⁴/s,
- B = 2.78519 · 10⁵ J/mol.

ATHLET-CD uses the material properties (density, heat capacity, melting temperature, etc.) of the cladding, which is user input. If FeCrAl (or any other) material is used, these values have to be changed from the standard Zr values.

The user has the option to implement their own ATF correlation. In this case the user has to explicitly add the following values in the input deck: A, B, Δh and the temperature validity range of the correlation.

Verification/Validation

Altogether three post-test simulations were performed, and their results were compared to the experimental data. All of the simulations were based on the input deck for QUENCH-15 experiment /BAL 09/, which represents the heated part of the QUENCH facility with 10 axial nodes and three concentric rings. The innermost part (ROD1) contains four heated rods, the second ring (ROD2) consists of eight heated rods, while the outermost ring (ROD3) has 12 heated rods. Five spacer grids, 8 corner rods and the shroud insulation with ZrO_2 are also taken into account. Besides the heated part of the facility, steam/ argon flows, and the water quenching are simulated. A more detailed description of the used input is given in /BAL 09/. Differences are caused by the oxidation models. One simulation used the oxidation kinetic defined by constants given by KIT for KANTHAL APMT (Kanthal), the other used the same constants, but the reaction rate was multiplied by 300 (Kanthal*300) derived from /NEA 18/, and the last simulation used the oxidation kinetic model by Cathcart/Prater-Courtright /LOV 21a/ for zirconium (Zr).

The results of the three simulations and experimental data are depicted in Fig. 2.35 – Fig. 2.38. Fig. 2.35 and Fig. 2.36 show the evolution of temperatures in the innermost part of the bundle (ROD1) at elevation 550 mm and 950 mm, respectively. It is clearly visible, as expected, that at lower temperatures the change of the oxidation model doesn't influence the simulated temperatures, as visible at lower elevation in Fig. 2.35. The bundle temperatures are satisfactorily reproduced by ATHLET-CD with the newly implemented ATF oxidation models also at higher temperatures and elevations, there is no significant temperature escalation visible. The simulation with the standard oxidation model for Zr-based cladding resulted in much higher maximal temperatures due to the substantial heat generation during oxidation (Fig. 2.36).

Fig. 2.37 depicts the temperature evolution at different horizontal positions of a simulation at elevation 850 mm. The comparison shows that there is a relatively high radial gradient between internal and external temperatures with a difference of up to ~ 200 °C in the measured data (significantly larger than QUENCH-15; the reason for these differences is not yet fully clarified /STU 18/), while all the simulations result in a flat profile

with a maximum difference of 50 °C. The final report of the experiment might clarify the reasons for such a large horizontal temperature gradient.

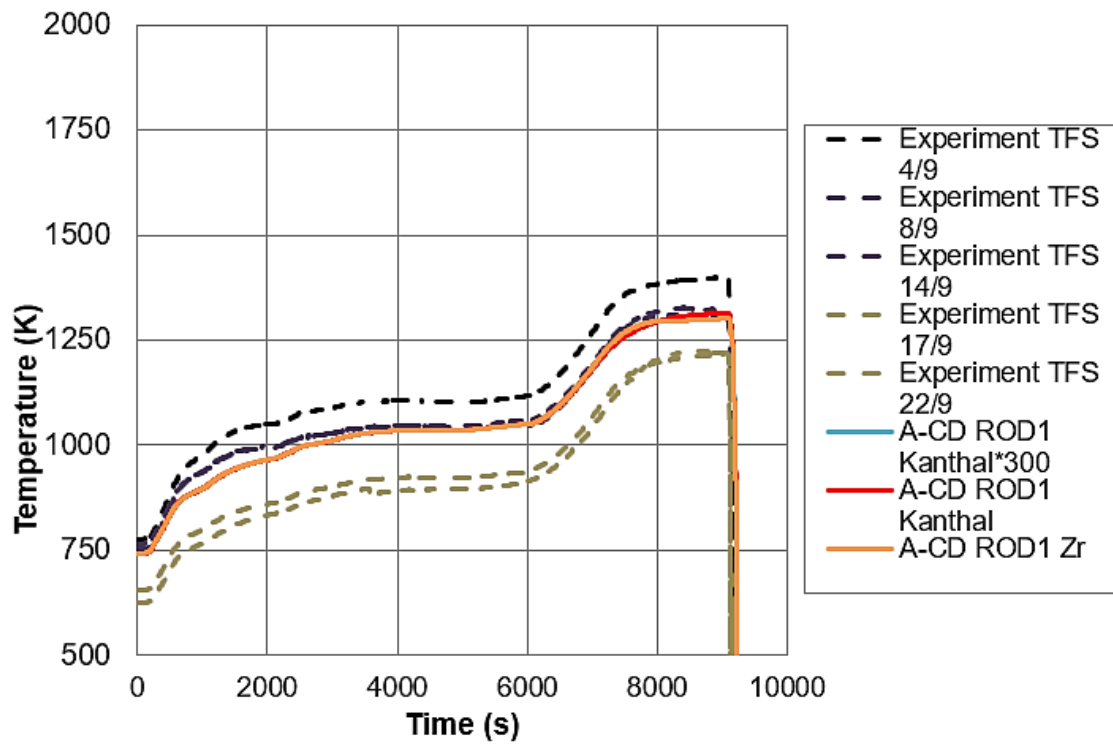


Fig. 2.35 Evolution of temperatures in experiment and in the different simulations at elevation 550 mm

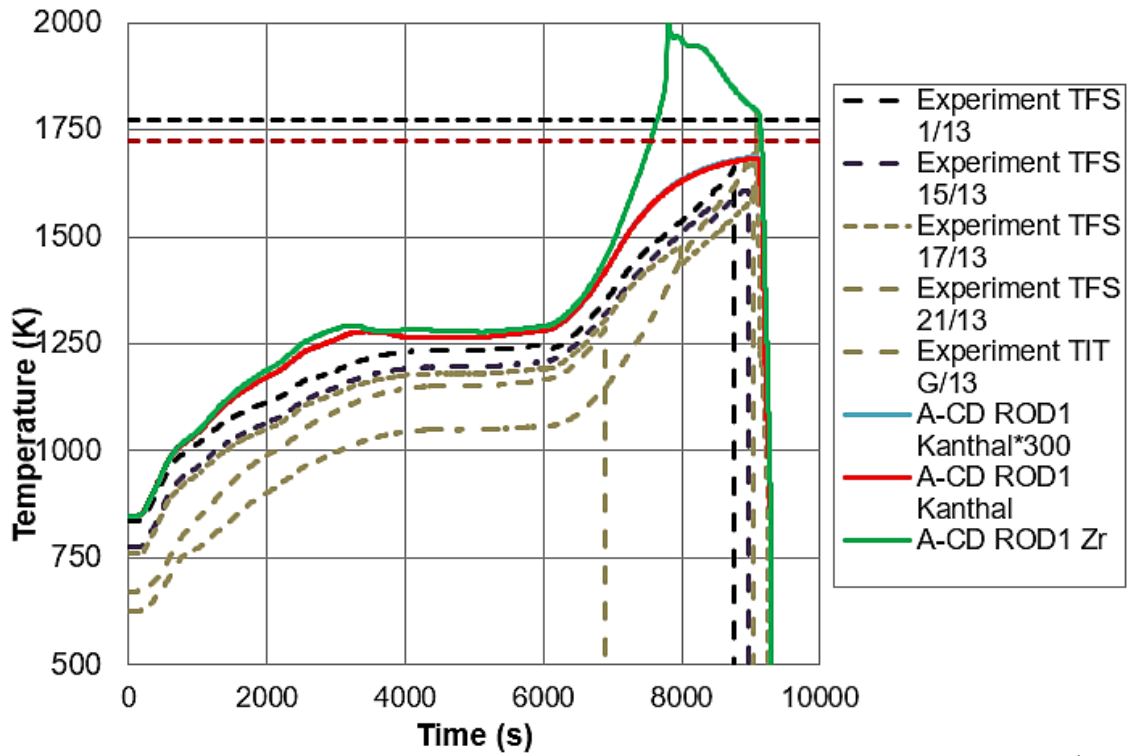


Fig. 2.36 Evolution of temperatures in experiment and in the different simulations at elevation 950 mm

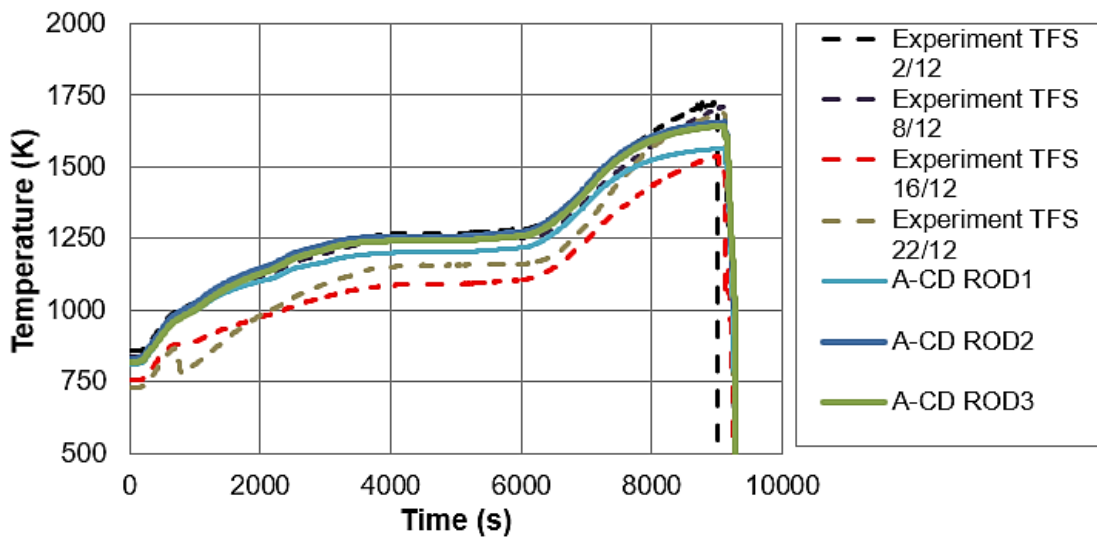


Fig. 2.37 Temperature evolution at different horizontal positions at elevation 850 mm (Kanthal)

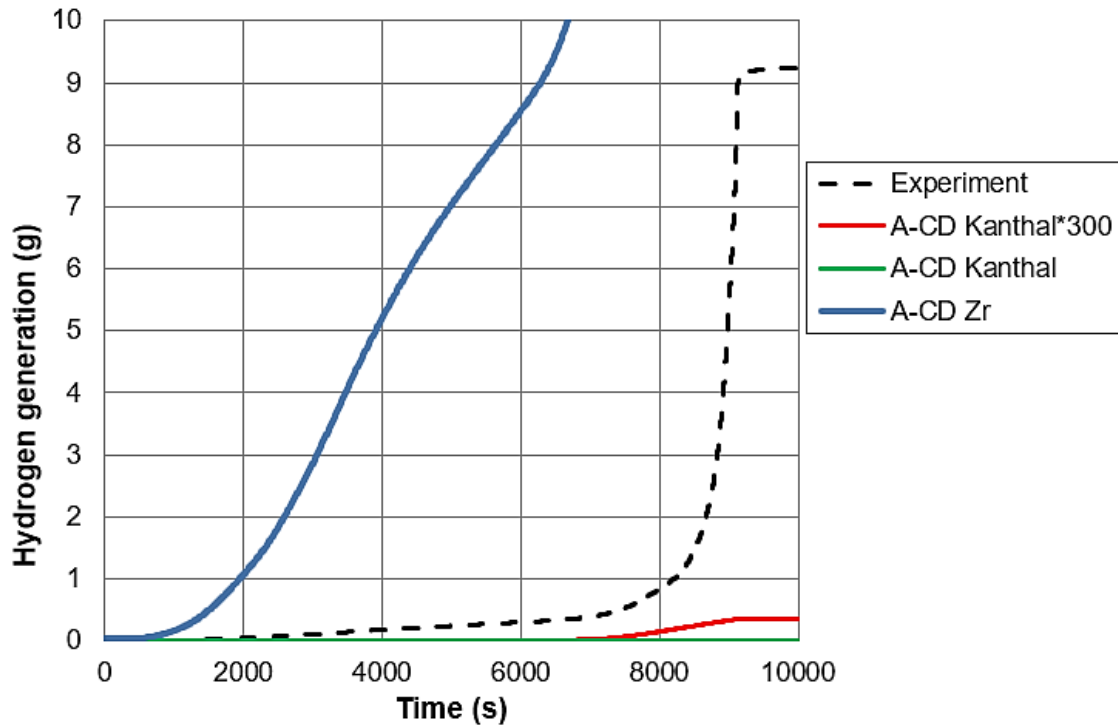


Fig. 2.38 Total hydrogen generated

The total generated mass of hydrogen (Fig. 2.38) shows a significant underestimation of oxidation in the simulations, in particular with the reaction rate given by KIT for Kanthal, but also the Kanthal*300 underestimated the generated hydrogen mass, with 0.008 g and 0.35 g respectively, compared to 9 g in the experiment. The hydrogen generation in the experiment was comparably low until the maximum temperatures was reached (~1400 °C). A sharp increase in the hydrogen release was observed at approximately 800 s before the quenching. One possible trigger for this event could be the failure and melting of the cladding of the steel thermocouples /STU 18/. This was not considered in the post-test calculations.

The understanding of all the governing phenomena during an ATF oxidation is very complex as it is ongoing research. With the previously shown implementation it is possible to test and follow the new scientific results regarding ATF oxidation with a severe accident code. To make further testing of new correlations easier and more accessible for the user, an option was created, where the user can change the parameters of the oxidation kinetics for ATF material. That way, users can implement their own rates, if new data is available, without having to wait for the next official ATHLET-CD release.

2.2.2 Model for material interaction between stainless steel and boron carbide and between zirconium and boron-carbide

Motivation

In the event of a severe accident, the reactor core is heated to an extremely high temperature, resulting in significant degradation of the core materials. However, the reactor core is usually composed of several structural materials, so these materials, depending on this composition of the respective materials, can form different eutectic mixtures when heated. The eutectic reaction leads to a reduction in the overall melting temperature, meaning that the core materials begin to degrade at lower temperatures and thus earlier than expected by the pure materials melting points. ATHLET-CD uses a single component with an artificially lowered melting temperature. This approach has been satisfactory in the past due to limited information available in the past on multicomponent eutectic formation in core materials. Due to more accessible information on binary and ternary phase diagrams and due to shifting of development priorities, the previous approach may be improved by detailed modelling on eutectic mixing.

Apart from the issue of reduced melting temperature, the question of oxidation and mixing enthalpy of these eutectic formations has also remained a challenge due to limited information in the open literature. The goal of the current work is to reconstruct previous attempts to form eutectics and select a viable portion for modelling the selected eutectic reaction in binary form.

The following discusses some of the possible eutectic reaction in BWRs:

1. Zirconium (Zr) – stainless steel (S.S.): the absorber rod cladding may deform by creep at high temperatures and react with the Zircaloy guide tube. Since stainless steel is generally composed of several components, such as Fe, Cr and Ni, there are Fe-Zr, Cr-Zr and Ni-Zr binary systems – and more generally ternary or quaternary systems. The binary eutectic reactions start at different temperatures, Fe-Zr at 928 °C, Cr-Zr at 1332 °C and Ni-Zr at 960 °C.
2. Boron Carbide (B₄C) – stainless steel (S.S.). The B₄C inside the absorber rod can react with the S.S. cladding between 1260 and 1350 °C.
3. Boron Carbide (B₄C) – Zr. In addition, the B₄C can also react directly with the Zr at a much higher temperature of 1650 °C.

In the current version of ATHLET-CD, due to the binary phase diagram used in the code, it is not possible to consider these reactions simultaneously.

In the following, a summary of existing correlations for B₄C-Zr is presented in Tab. 2.2.

Tab. 2.2 Comparison of B₄C-Zr. Kinetic Equation

	Kinetic Equation (K)	Temperature Range (DegC)
JAERI-1 /UET 96/	$K = 2.42 \cdot 10^{-8} \exp(-173000/RT)$	900 – 1500
JAERI-1 /UET 96/	$K = 8.79 \cdot 10^{43} \exp(-1965000/RT)$	1225 – 1350
Nagase-1 /NAG 97/	$K = 4.10 \cdot 10^{-8} \exp(-179000/RT)$	800 – 1550
Nagase-2 /NAG 97/	$K = 6.74 \cdot 10^{43} \exp(-1960000/RT)$	1600 – 1680
KFK-1	$K = 4.15 \cdot 10^{-6} \exp(-122650/RT)/10000$	1000 – 1200
KFK-2	$K = 7.94 \cdot 10^{33} \exp(-1438300/RT)/10000$	1210 – 1340

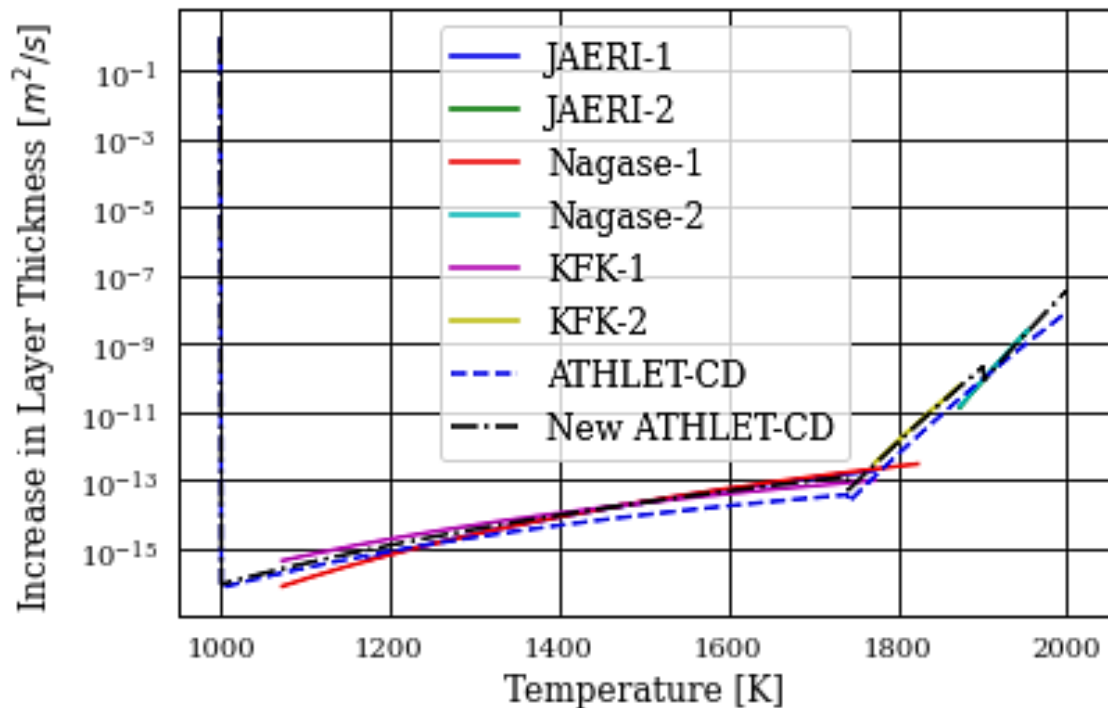


Fig. 2.39 Comparison of different correlations for B₄C-Zr reaction

In the following, a summary of existing correlations for B₄C-S.S. is presented in Tab. 2.3.

Tab. 2.3 Comparison of B₄C-S.S. Kinetic Equation

	Kinetic Equation (K)	Temperature Range (DegC)
JAERI-1 /UET 96/	$K = 1.42 \cdot 10^{-2} \exp(-250000/RT)$	900 – 1500
JAERI-1 /UET 96/	$K = 1.4 \cdot 10^{10} \exp(-549000/RT)$	1225 – 1350
Nagase-1 /NAG 97/	$K = 3.04 \cdot 10^{-1} \exp(-283000/RT)$	800 – 1550
Nagase-2 /NAG 97/	$K = 3.15 \cdot 10^7 \exp(-453000/RT)$	1600 – 1680
KFK	$K = 8.76 \cdot 10^{-6} \exp(-378000/RT)/10000$	1000 – 1200
Belovsky-1	$K = 5 \cdot 10^{20} \exp(-850000/RT)$	1210 – 1340
Belovsky-2	$K = 4.6 \cdot 10^{11} \exp(-544000/RT)$	1210 – 1340

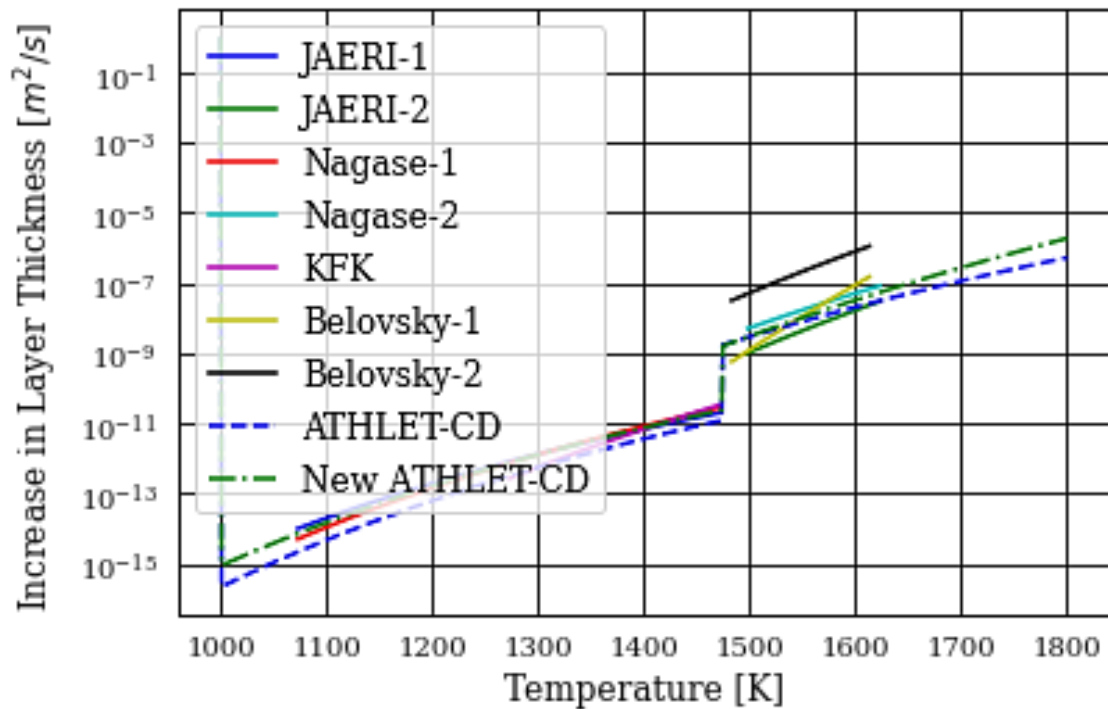


Fig. 2.40 Comparison of different correlations for B₄C-S.S. reaction

Development

In the previous version, the melting temperature of the absorber blade and canister were defined by the user as a fixed temperature. It was defined as the melting temperature of the binary eutectic reaction, since modelling of the eutectic reaction was not possible in

the previous version of ATHLET-CD. In the new version, it is possible to model the eutectic reaction supporting a local calculation of the eutectic modelling and thus a change of the melting temperature in the course of the calculation. The melting temperature entered by the user is changed as the simulation progresses.

The melting temperature is being set to 1550 K in the sample of QUENCH-20 without the activation of eutectic modelling (IEUTECT = 0). In the case with activation of eutectic modelling (IEUTECT = 1), the temperature should be used as the highest melting temperature of that structural component, for example, 2350 K, as the local melting temperature derived from the eutectic modelling will always be compared with the user defined melting temperature, and the lower of the value will be taken in the calculation. Therefore, it is recommended to use a higher melting temperature.

Main driver subroutine for BWR, EHBWR

In the main subroutine for BWR, EHBWR. The eutectic calculation is performed before the main subroutine for liquefaction and thermal behaviour of absorber and vessel wall. When the user provides input information for material interaction, there are three eutectic interactions for BWR structures that can now be modelled in ATHLET-CD:

1. Absorber material with blade
2. Absorber melt/crust with blade
3. Absorber melt/crust with canister

There is no interaction between the intact absorber and the canister wall since it is impossible for the intact absorber structure to come into contact with the canister wall. The interaction between fuel rod cladding and absorber crust is currently ignored.

Manipulation of material interaction

The overall calculation step in these respective subroutine (i. e. EUASWR, EUBSWR and EUCSWR) was implemented in the following order:

1. Define the liquidus temperature based on phase diagram on either B_4C -Zr (EULFBO) or B_4C -S.S. (EULZB4). This is also the position where future development on ternary phase diagram can be implemented. Currently, only a binary phase diagram is available as the reaction rate equation for ternary reaction remains scarce in open literature.
2. Calculate the liquefied mass based on reaction rate equation by calling EUSB4J or EUZYB4.
3. Recalculate the liquidus temperature based on the added mass and mass ratio between the binary species. This depends on local conditions, it may cause feedback to the melting/liquid temperature, for example, for an absorber crust with blade or absorber with canister. The existing input for liquidus temperature for either absorber crust and canister wall will be overwritten during the call in EUASWR and EUCSWR. Therefore, there will be a different liquidus temperature for each elevation. However, there will be no feedback for absorber crust with blade.

Implementation of phase diagram for B_4C -Zr and B_4C -S.S.

There are two standard phase diagrams concerning the current work, the Fe-B diagram for the eutectic reaction between B_4C and stainless steel; and the Zr-B_{0.5}C_{0.5} diagram for the eutectic reaction between B_4C and Zr. (Fig. 2.41 and Fig. 2.42)

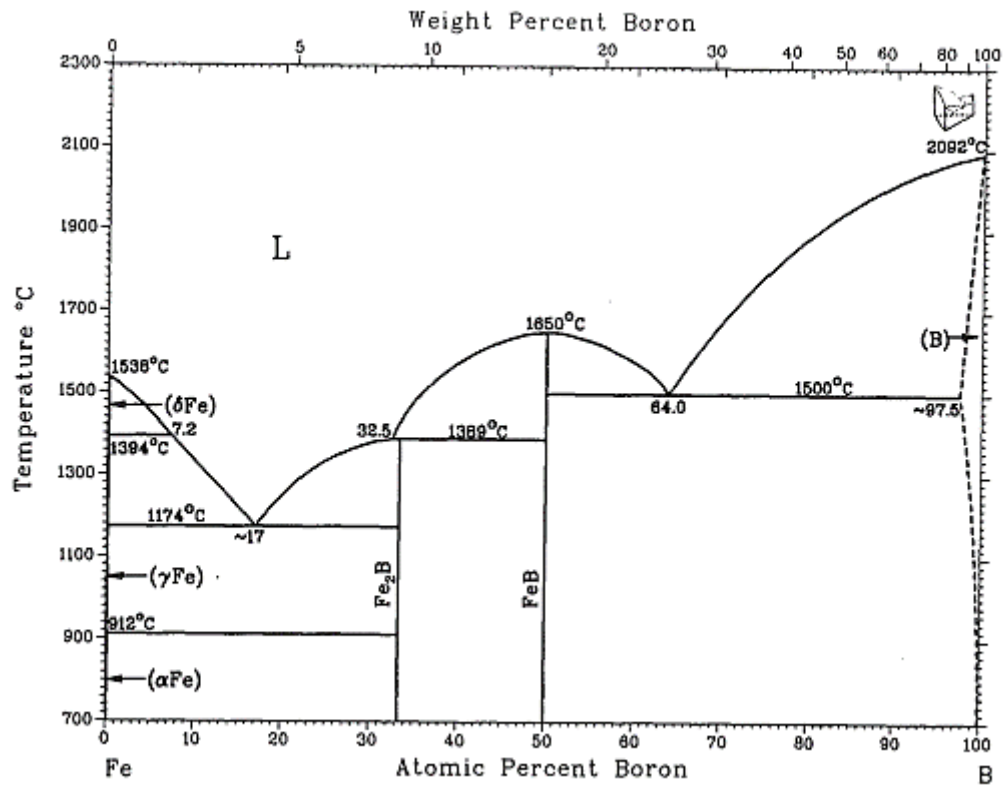


Fig. 2.41 Fe-B phase diagram /OKA 16/

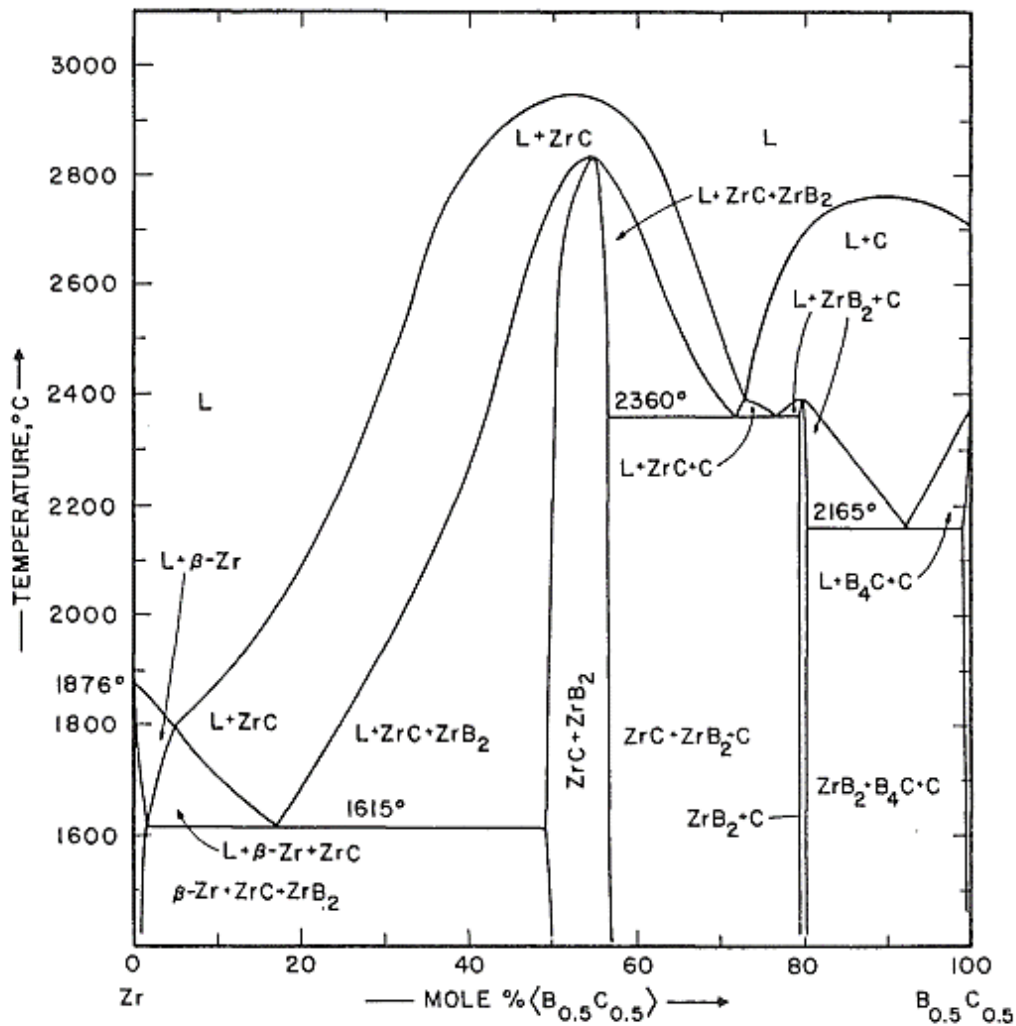


Fig. 2.42 Zr-(B_{0.5}C_{0.5}) phase diagram /HOF 89/

Although one may argue that there are many other constituent elements in stainless steel and the concentration for B and C is not the same as B₄C for the case of B₄C-Zr reaction, the current approach is deemed to be satisfy the current need and a ternary approach would be needed for a general case and with a variety of temperature.

The current implementation selects a set of points with lines between the liquidus and solidus curves based on the figures above.

For B₄C-Zr, the following values are used:

Tab. 2.4 Used values for interpolation for B₄C-Zr eutectic formation

Mass Ratio	Temperature [K]
0.0	2149
0.5	3243
0.632	2673

For B₄C-stainless steel, the following values are used:

Tab. 2.5 Used values for interpolation for B₄C-S.S. eutectic formation

Mass Ratio	Temperature [K]
0.0	1811
0.0382	1662
0.0853	1923
0.2561	1773
1.0	2365

The melting temperature of the eutectic mixture is calculated based on the arithmetic average using the mass ratio of the concerned species. This is a simplified approach, as it does not take into account a partly liquified structure, while being in-between the solidus and liquidus lines. A partly liquified structure would most likely relocate even before reaching the liquidus temperature. This phenomenon has to be addressed in the following project.

Calculation of the mass transfer rate

The mass transfer rate is calculated based on the reaction rate as mentioned in section 1.2 using the new ATHLET-CD formulation that was developed based on the other reported correlations. The mass transfer is assumed to be the same for two reactants involved in the binary eutectic reaction, Zr-S.S. and B₄C-S.S. The adjusted mass transfer rate leads to better numerical stability in QUENCH-20 albeit with a larger melt mass.

Verification

QUENCH-20 is a single bundle core degradation test for BWR representative channel. In the course of verification, the simulation runs with IEUTECT = 0 and 1 are compared. The non-activated eutectic modelling (IEUTECT = 0) represents the standard approach in ATHLET-CD for modelling the core degradation with an artificially lowered melting temperature of the structural components. While the IEUTECT = 1 represents the activation of the eutectic modelling and included a local calculation of the variable melting temperature and feedback to core degradation. Similar to other QUENCH tests, the amount of degraded material is never measured in detail, therefore, the increase of amount of degraded material as shown in IEUTECT will have to be justified by more dedicated validation cases. In the following, we will first compare the overall degradation state of the core via ATLAS in Fig. 2.43 and Fig. 2.44.

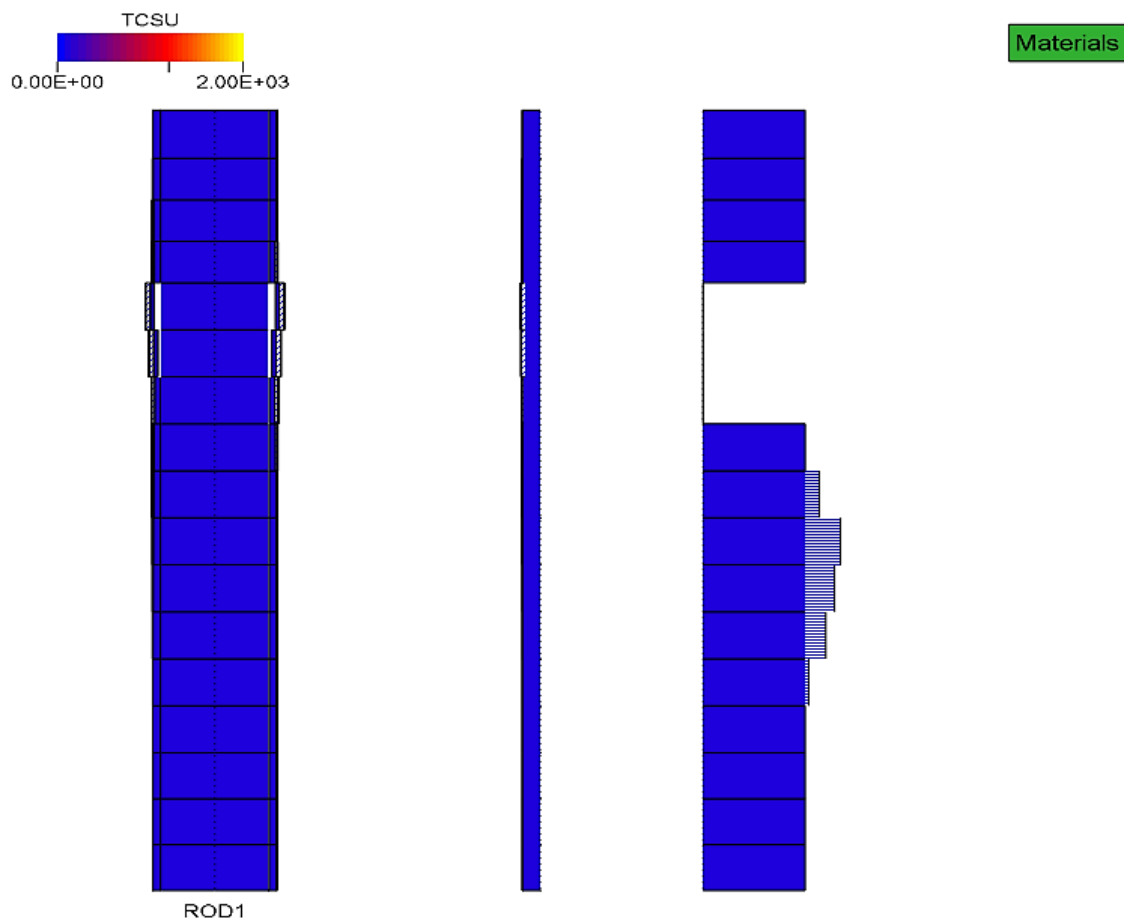


Fig. 2.43 The core degradation state of IEUTECT = 0

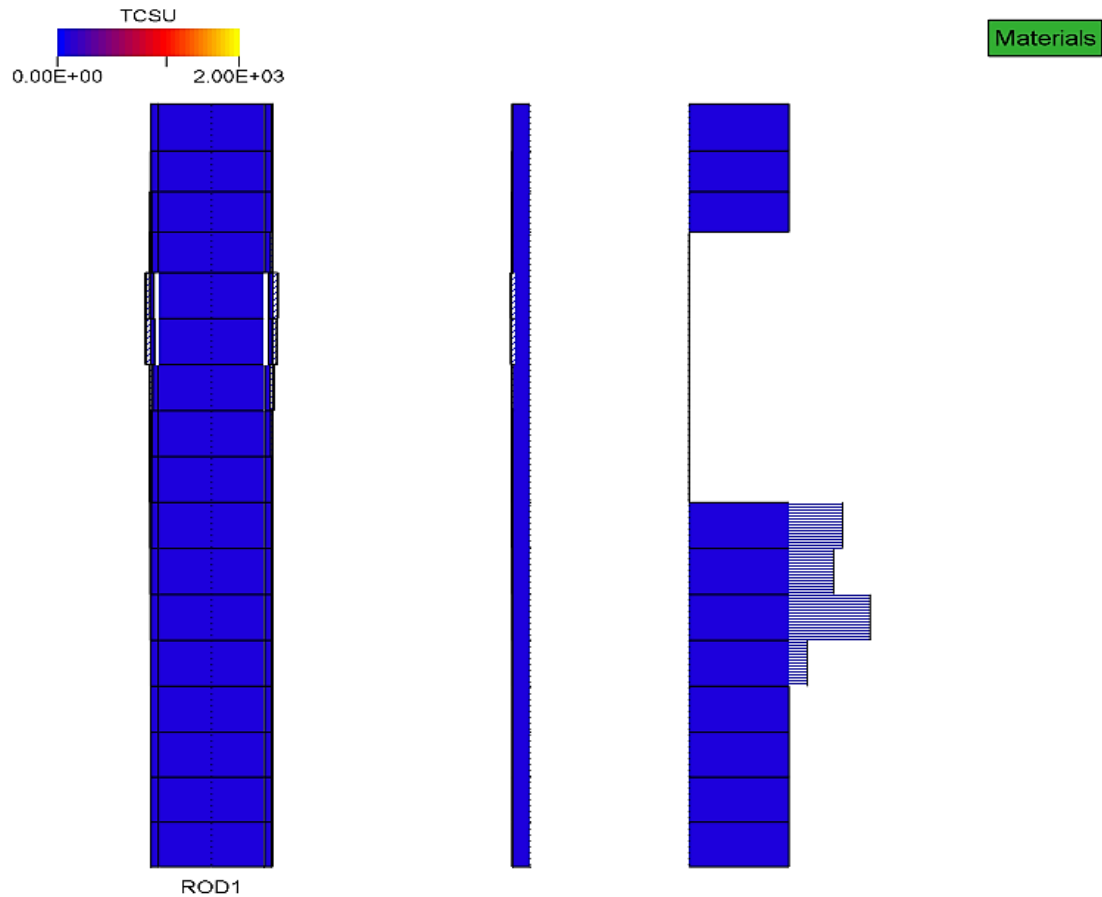


Fig. 2.44 The core degradation state of IEUTECT = 1

In the case with eutectic formation (Fig. 2.44), the degradation state of the canister is more severe than the case with IEUTECT = 0. However, the lowest degraded node as seen in the Fig. 2.44 corresponds to the picture taken from the QUENCH-20 report. Nevertheless, the degradation state of the canister is strongly dependent on the calculation of mass transfer rate of individual species. In the current development version, the individual species of the binary eutectic reaction are assumed to have the same reaction rate.

The temperature evolution of Rod 1 is similar for both versions, and this illustrates the change of eutectic modelling in the code has little feedback to the core temperature as the damage was mostly concerned with the canister and the absorber blade.

For the water level evolution, the core reflood comes a bit earlier in the case with IEUTECT = 1, due to the slightly lower average porosity in the test bundle. This results in a bit lower hydrogen generation than the standard case without eutectic modelling.

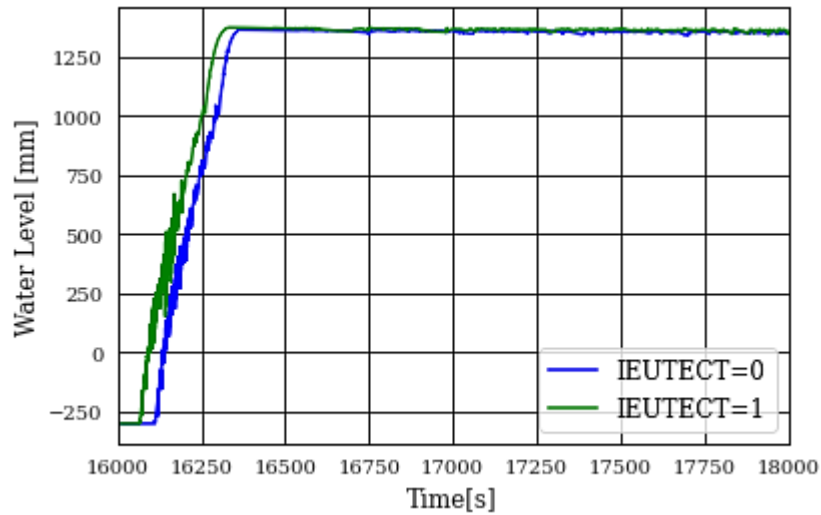


Fig. 2.45 Water level evolution between time interval of 16000 to 18000 s

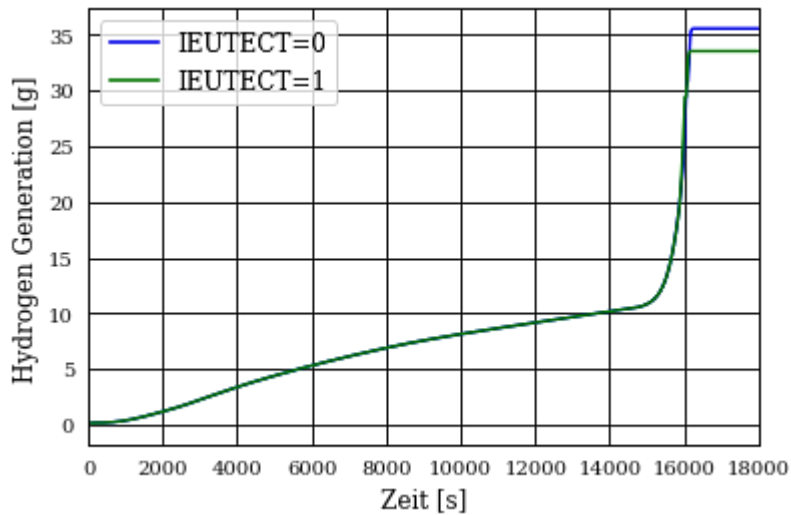


Fig. 2.46 Total hydrogen generation

With these new models, the user has the option to take material interactions between $B_4C - Zr$ and $B_4C - S.S.$ into account.

2.2.3 Model for nitride formation in melt phase

Motivation

During core degradation, a significant amount of degraded material forms at the site where the overheating occurs. These melt streams are therefore subject to oxidation reactions, e.g., the particularly noteworthy interaction between Zr and water. Another interaction worth mentioning is the interaction with nitrogen, i. e. nitride formation. Nitride

formation is more important in accidents where air can get in contact with the cladding. The previous version of ATHLET-CD was not able to simulate the nitride formation process in the melting phase for both PWR and BWR type. The current task is to review the model of nitride formation and to adapt the model for simulating nitride formation in the melting phase for both types of reactors.

Development

Nitride formation due to air oxidation was only considered in the previous version of ATHLET-CD for intact fuel rods.

For PWR, the heat subroutine EHCAL_FR calculates oxidation when the intact fuel rod reacts with available nitrogen. Since there is little information in the literature on nitride formation in the melt, the existing correlation for nitride formation in intact rods is used to calculate the nitride formation in the melt.

Another oxidation subroutine EOCDA, called by ERELOC_PO for the mass and energy distribution in the melt, is used. A separate subroutine EOCDA2 is created to calculate the nitride formation in the melt, which is activated only when the variable INITN2 is greater than zero. Therefore, nitride formation in the melt can now be simulated in conjunction with Zr oxidation in the PWR simulation.

For the BWR, the oxidation of the melt was not previously considered and the subroutine EOCDA2 is added to the subroutine EHBWR to simulate the oxidation of the melt with nitride. The subroutine is accessed only when the melt temperature is greater than zero and the nitride formation flag INITN2 is greater than zero. The additional heat of oxidation from the inner and outer parts of the melt are added to the total oxidation heat flux for the canister, although they are considered much less exothermic than the Zr-vapor interaction counterparts.

2.3 WP1.3: Fission product behaviour (SAFT)

2.3.1 Optimised output handling

Motivation

Multiple users reported that the output handling of SAFT is not user friendly, in some cases it needs simplifications to reduce the amount of data generated, in some other cases more information would be needed. Therefore, an optimisation of the output handling of SAFT was necessary.

Developments

The output parameters available from a SAFT calculation have been extended in order to enable a better overview and help the user in his/her further analysis. Two new key words have been introduced: *M_BAL* and *SXXOBJECT*. Both of them are providing integral data, to help the comparison and analysis especially using detailed neutronic codes or the code COCOSYS. It also serves as a check among the different modules interacting when calculating fission product behaviour in the system. Furthermore, they allow an integral analysis without having to save all detailed information, which would cost a lot of storage. In some applications the detailed information is not necessary, and only the integral behaviour of the system is of interest. Both keywords are present at all times without any further user input.

In case of unexpected, unexplained behaviour in the calculation, it is also advisable to take a look at the detailed information available through these keywords. Therefore, it is recommended to at least have under *SDATA* all species listed, even if due to storage concerns the results within individual objects are only saved in a reduced form, if at all.

The keyword *M_BAL* stands for mass balance and includes integral data of the fission products and aerosols found/transported in the defined SAFT-network. The individual parameters are similar to the ones already available at the detailed level, but they are summed up for the whole system. It also includes a mass error information for quality checks.

The keyword *SXXOBJECT* is also a summary, but instead of the whole system it gives information about the integral data within each object. Alongside the key word *M_BAL* it

helps to have a semi-detailed integral overview of the overall behaviour of the system, without needing too much storage place.

The detailed description of the newly introduced output values is shown in Fig. 2.47.

M_BAL	-	Model name (Mass balance within the whole SAFT Network)
I/J	-	1
SUS_VA(KG)	kg	Total mass of gas (GAS) or Total mass of suspended vapour (gaseous fission product = VOLATILE)
SUS_AE(KG)	kg	Total Mass: Condensed on suspended aerosol
LIQUID(KG)	kg	Total Mass: in Liquid state
DEP_AE(KG)	kg	Total Mass: Condensed on deposited aerosols
SOR_VA(KG)	kg	Total Mass: <u>Sorbed</u> on walls
CONDEN(KG)	kg	Total Mass: Condensed on walls
M_INLET(KG)	kg	Total Mass: Circuit inlet mass
M_OUT_A	kg	Total Mass: Released as aerosol
M_OUT_V	kg	Total Mass: Released as vapor
M_OUT_L	kg	Total Mass: Released in liquid
M_OUT	kg	Total Mass: Release (M_OUT_A + M_OUT_V + M_OUT_L)
SUSPENDED	kg	All suspended species (SUS_VA + SUS_AE)
DEPOSITED	kg	All deposited species (DEP_AE + SOR_VA + CONDEN)
M_DIFF	kg	Mass error in the calculation (M_INLET + MC_IN - SUSPENDED - DEPOSITED - M_OUT)
MC_IN	kg	Total inlet carrier gas mass
SXXOBJECT	-	Model name (Mass Balance within each SAFT Object)
I/J	-	1
SUS_VA(KG)	kg	Total mass: Gas or Suspended vapour (gaseous fission product = VOLATILE)
SUS_AE(KG)	kg	Total mass: Condensed on suspended aerosol
LIQUID(KG)	kg	Total mass: Liquid state
DEP_AE(KG)	kg	Total mass: Condensed on deposited aerosols
SOR_VA(KG)	kg	Total mass: <u>Sorbed</u> on walls
CONDEN(KG)	kg	Total mass: Condensed on walls
SUSPENDED	kg	All suspended species (SUS_VA + SUS_AE)
DEPOSITED	kg	All deposited species (DEP_AE + SOR_VA + CONDEN)

Fig. 2.47 Detailed description of the newly introduced output values

Depending on user feedback and user needs, the output can be further extended/reduced with different output options. Control through user input could be introduced under PW OUTFL with relative ease.

2.3.2 Melting of SAFT structures

For SAFT it is necessary to define structures to be able to simulate the deposition and retention of fission products. Not only their actual area, but their physical (geometry, material, etc.) and thermal (temperature) properties are of great importance.

The structures in ATHLET are the so-called HECU objects, while in ATHLET-CD the ROD objects provide the necessary information within the core region. Both objects might fail during the simulation. For the ROD objects simply by melting and relocation, while in case of the HECU objects a special creeping model can simulate the failure of the structure (see PW CREEPING). The latter, if active, will eliminate the affected HCV from the ATHLET calculation procedure, as if the whole structure would have disappeared. In both cases SAFT would continue the simulation of the fission product deposition, retention and remobilisation in the same way as for an intact structure, even though it would be physically not possible. For this reason, some development work has been carried out improve the simulation capabilities.

The following assumptions have been made:

- If a structure or ROD fails, the phenomenon affected by the presence of the given structure are turned off.
- The deposited mass prior to failure can't be remobilised and is assumed to "stay" in the given CV.
 - This assumption ignores the possible instant evaporation/remobilisation as well as the mixing into the melt. This might be addressed later.
 - Assuming the remobilisation of all deposits would be a clear overestimation of the fission products within the circuit. Furthermore, the fission product release/behaviour within the melt is currently not modelled (also no release from the melt). Therefore, it is the least intrusive way of dealing with structural failures within the SAFT simulation for the moment.
 - Fission products that did not remobilise until the melting temperature are most likely to be incorporated by the melt.

Within a given CV there might be multiple HEAT (ROD), HECU-right and HECU-left surfaces. The three types of surfaces are handled separately due to their possibly significant differences in temperature and other qualities. An averaging of the temperature is done for a given type of surface, which is then applied for all surfaces available for deposition from that specific type.

The failure criteria for the structures are defined by other ATHLET-CD models, those were not changed in this development.

In case of structure failure, it is removed from the temperature averaging and the surface areas are recalculated. After some tests it became clear that there have been some unreasonable simplifications in the modelling up until this point: the change in surface area due to blockades and thermal expansion within the core has been neglected. In this case it led to the situation, where after a structure failure some surfaces became bigger. Therefore, a correction has been introduced, that takes these changes into account.

As for the temperatures: if in a given CV all ROD objects are failed the surface temperature is set to -10; for right-side HECU surfaces to -5, while for left side HECU surfaces to -3. These temperature values are not used in the calculation of any characteristics of phenomena or boundary conditions. They serve the sole purpose of informing the user about the melting.

First verification calculations with the newly implemented features have been carried out. In addition to the fast-running simplified s8 sample model, two Phebus tests were calculated. For testing the new model's functionality, the core was also simulated in the SAFT path, even though that is not yet recommended. For further verification purposes, calculations with no structure failures have been ran as well, and they delivered the exact same results as without the introduced changes confirming that the development work does not affect the code outside its intended domain.

As expected not all elements are affected by the change, since both the DHYI change as well as the melting of the structures take place within the core region, where almost no volatile element deposits. Changes were expected and observed in the low to non-volatile elements such as Pu, U, and Zr.

In the following, the verification calculations are shown and discussed.

The legends on the following diagrams correspond to

- Base – original
- rca – change of surface due to thermal expansion/blockade formation
- final – structural failure and change of surface due to thermal expansion/blockade formation

Since the phenomena governing the deposition and retention of fission products are very complex (availability, compound formation, temperatures, mechanical and thermal flow conditions, etc.) it is difficult to predict the overall effect of changes that influence, e.g., the temperature, area, composition of fission products, etc. Therefore, it is always necessary to test and try to find physical explanations for the observed effects in the simulations. If necessary further changes have to be included, such as the aforementioned necessary change to take into account the changes in surface area.

Generally, the area changes due to the thermal expansions/blockades have a bigger impact on the retention of fission products, than considering the melting and failure of the structures. In the following three cases are presented, which are representative of the different types of elements regarding their transport (and the transport of their compounds) in SAFT. Most of the elements belong to the first two groups, while only a fraction of the elements (mainly low volatile/no volatile elements) belong to the third group.

Group #1: Fig. 2.48 and Fig. 2.49 depicts the iodine release into the containment in aerosol and vapor form. As it can be seen practically no effect of the new modelling can be observed. This is because the changes influence deposition within the core region and iodine is too volatile for being deposited or retained under core conditions.

Group #2: Fig. 2.50 shows the plutonium release into the containment. As it can be seen, taking the possible greater deposition areas due to thermal expansion/ blockades (rca) into account, the released mass decreases as more Pu is retained. At the same time there is no effect when it comes to the failure of structures.

Group #3: The release of zirconium into the containment is shown in Fig. 2.51. Here the effects of all introduced changes can be seen. The changes introduced by the thermal effects are generally positive. Due to the higher temperatures a greater area is available for deposition decreasing the release, as can be seen in Fig. 2.51. Considering the failure

of the structures reduces the area where deposition can take place yielding a higher release into the containment.

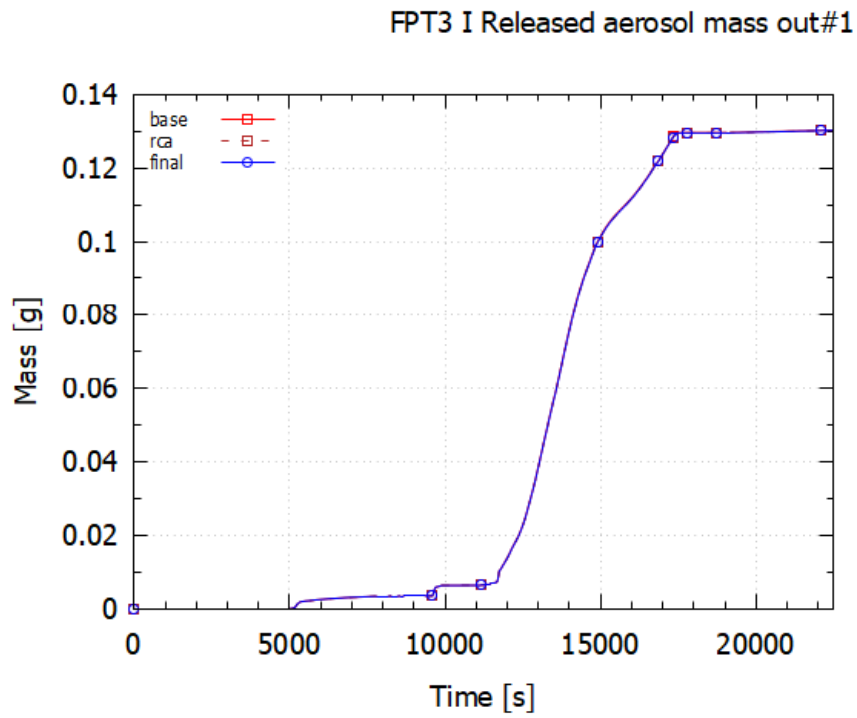


Fig. 2.48 Release iodine aerosol mass

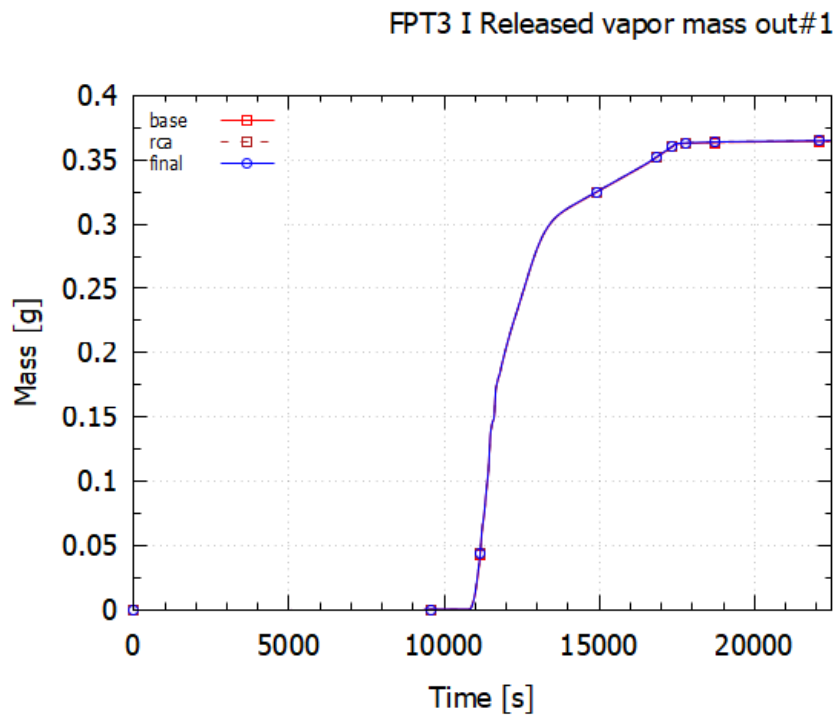


Fig. 2.49 Release iodine vapor mass

FPT3 Pu Released aerosol mass out#1

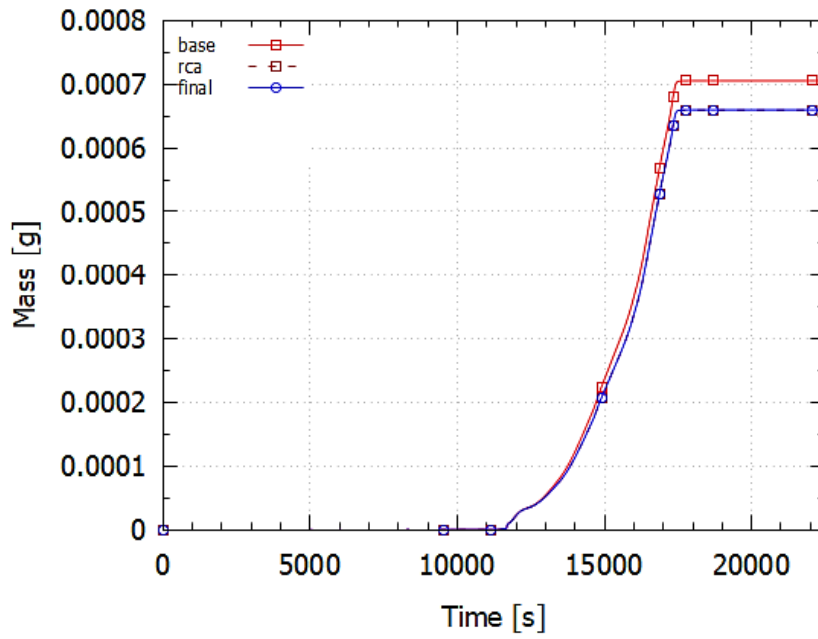


Fig. 2.50 Release of plutonium (aerosol)

FPT3 Zr Released aerosol mass out#1

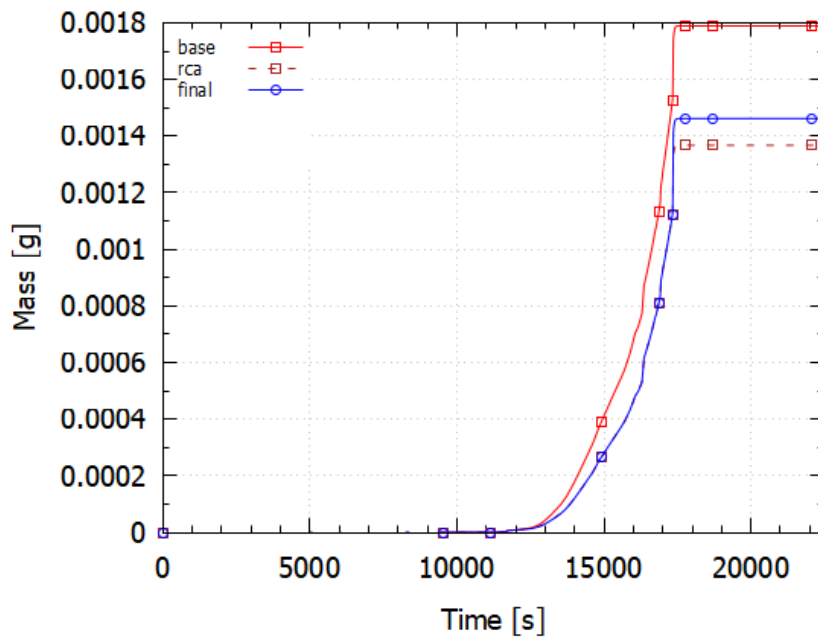


Fig. 2.51 Release of zirconium (aerosol)

Output information in the .out file:

- In case of absolute value of IOPSOP ≥ 2 at the time of the failure, information about the new, as well as all previously failed structure is given. This information is provided for each structure type, but only for those, for which failure occurred. The format for core structure failure is depicted in Fig. 2.52.

```

ETFBK3: FAILURE OF FUEL ROD      IN NODE WITH IRA =  1 AND JAX = 16 AT TIME ZFFKT = 1.73263157618E+04
ETFBK5 CHECK(1) DT : HEAT_UO  1 15 16  0  0 1.73263158E+04 6.751E-01 6.250E-01 5.010E-02 3.361E-01 8.333E-02
New structures within SAFT have melted
List of melted HEAT positions:
Radial core pos.:      1 Axial core pos.:      16
List of melted HEAT positions (all):
Radial core pos.:      1 Axial core pos.:      13
Radial core pos.:      1 Axial core pos.:      14
Radial core pos.:      1 Axial core pos.:      16
Radial core pos.:      2 Axial core pos.:      13

```

Fig. 2.52 Structure failure information

- In case the original SAFT outlet is activated (IOPSOA = 1) information about fully melted structures is given at each output variable, where necessary, as shown in Fig. 2.53.

```

      2      0.0000E+00      0.0000E+00      0.0000E+00      0.0000E+00
13      1      1.1280E-47      0.0000E+00      0.0000E+00      0.0000E+00      0.0000E+00
Note: Surface area of wall #      26 is zero due to melting
      2      0.0000E+00      0.0000E+00      0.0000E+00      0.0000E+00
14      1      6.4954E-21      0.0000E+00      0.0000E+00      0.0000E+00      0.0000E+00
Note: Surface area of wall #      28 is zero due to melting
      2      0.0000E+00      0.0000E+00      0.0000E+00      0.0000E+00
15      1      6.1851E-21      0.0000E+00      0.0000E+00      0.0000E+00      3.9352E-47
      2      0.0000E+00      0.0000E+00      0.0000E+00      0.0000E+00
16      1      5.9179E-21      0.0000E+00      0.0000E+00      0.0000E+00      1.1759E-48
Note: Surface area of wall #      32 is zero due to melting

```

Fig. 2.53 Original SAFT output

The following residual matters and possibilities for future development work have been identified:

- Dealing with the already deposited fission products and aerosols after the failure of the structure on which they are deposited. This would require the modelling of fission product behaviour within the melt, necessitating changes also in AIDA and ECORE.
- The built-in check for the area recalculation in case of thermal expansion/blockades is quite robust, but at the same time not optimal. Due to time constraints no further optimisation took place to avoid multiple calls of the new routine when it is might not be necessary. This could be optimised in the future.

2.3.3 Limitations of SAFT

Motivation

SAFT is the fission product transport module in ATHLET-CD. It is based on the SOPHAEROS version from ASTEC V2.0. During the implementation process, the possibility for fission product transport in liquid water was also created (framework conditions and properties from ATHLET-CD, mass transport equations from Sophaeros). This capability of the code has not yet been tested. This was done within the framework of the current ATHLET-CD further development project.

Accomplishments

First, the capability of the code of simulating transport in water was tested. In an example data set (modified s8, see below), various fission product masses were added to the water phase in debug mode in the mass vector (vol%*xmass*) manually. These then appeared in the calculation in LIQUID (kg) and were transported with the water to the starting point. At the end of the pipe, the entire artificially added mass flowed out, which was stored in the calculation under OUT_L (kg). The mass balance in the water was correct in all sample calculations. These results prove the ability of SAFT to transport fission products in water, provided that such water-soluble species are present. Furthermore, these species must prefer the water-soluble form over other forms (aerosol, gas, etc.) in order to enter the water at all.

For the tests, the general S8 data set was taken as a basis. From 1000 s, the supply of steam was turned off (INFLOW#T = 0.0) and at the same time water was added to the TFO PIPE to flood this pipe (FILL1), but at the same time leave the core free (to allow release from the core). The pipe was flooded within 35 s and remained submerged until the end of the simulation time (Fig. 2.54), only the last CV had a steam-water mixture.

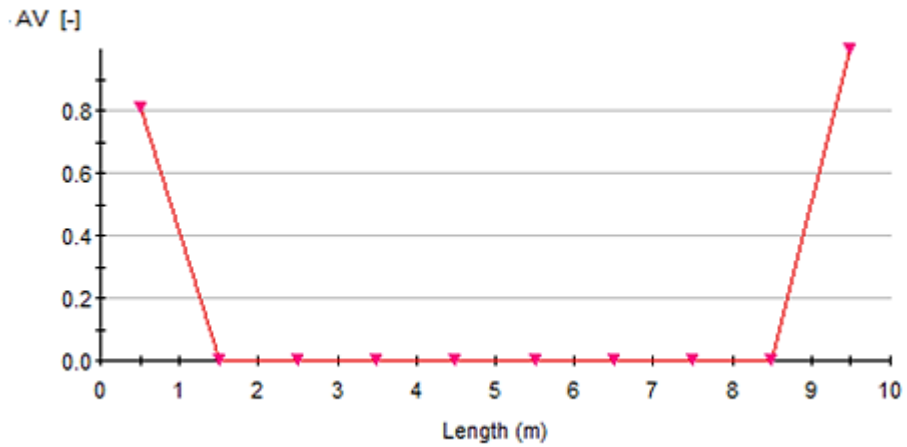


Fig. 2.54 Void in pipe after reflooding

Fig. 2.55 and Fig. 2.56 show two examples, caesium and silver, which were artificially added to the water. The total amount added was then transported through the pipe Fig. 2.55 , Fig. 2.56 and at the end of the pipe they flowed out Fig. 2.57.

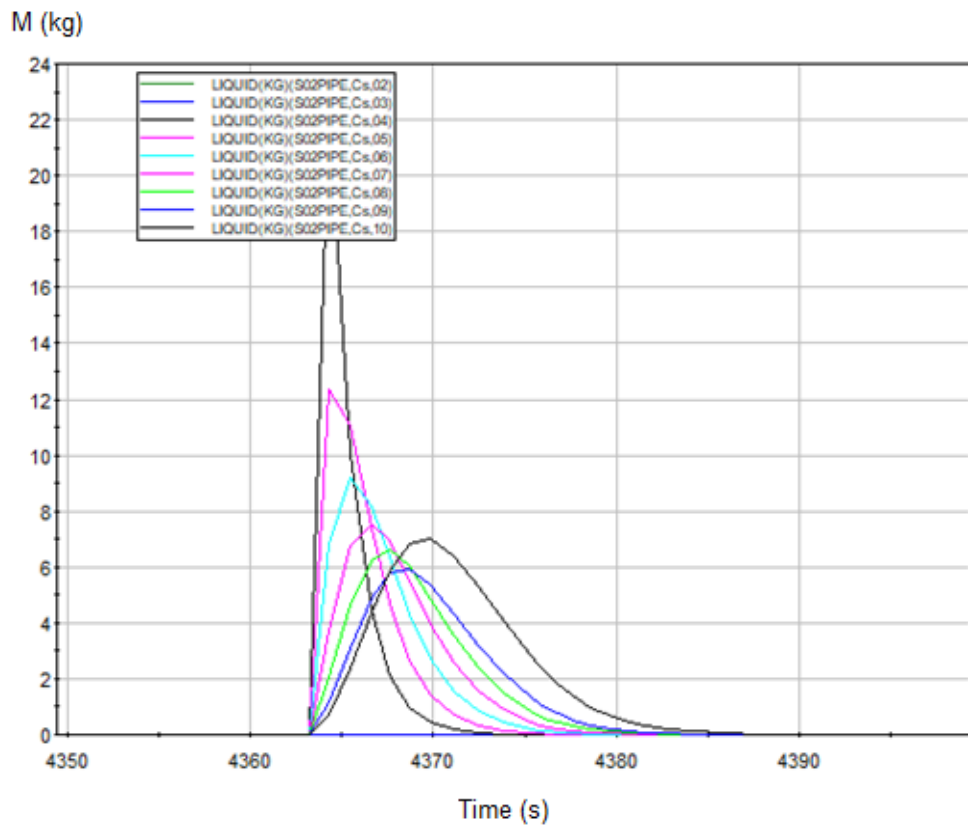


Fig. 2.55 Mass of Cs in liquid phase in different control volumes

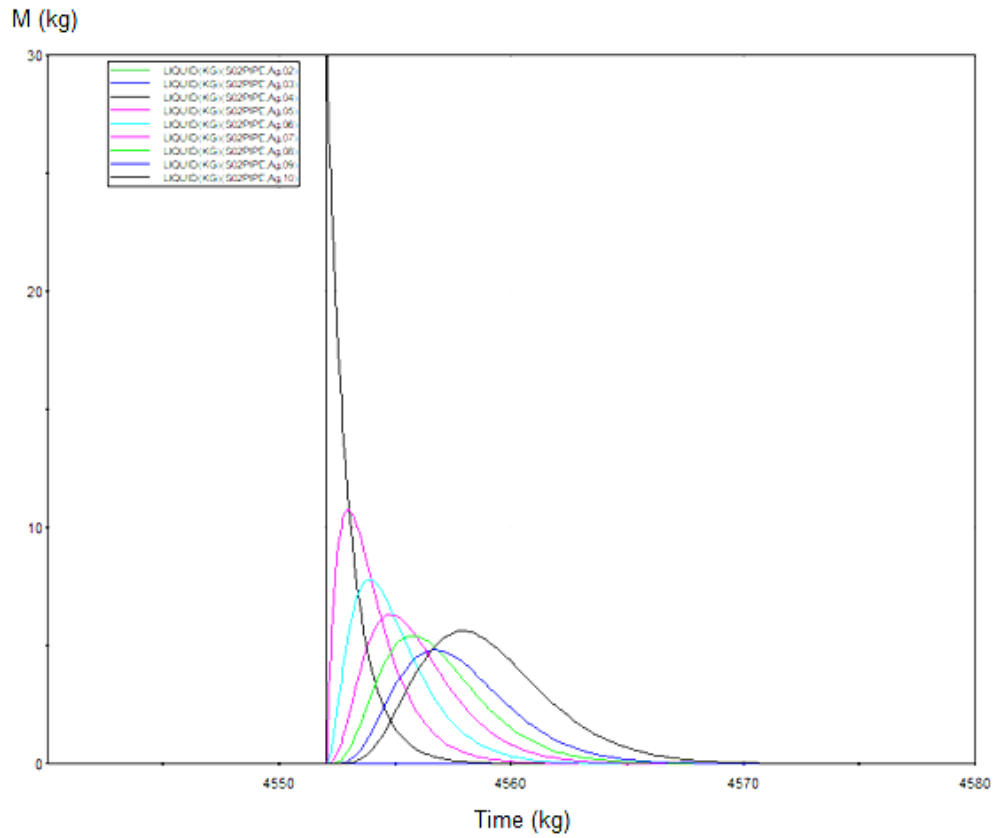


Fig. 2.56 Mass of Ag in liquid phase in different control volumes

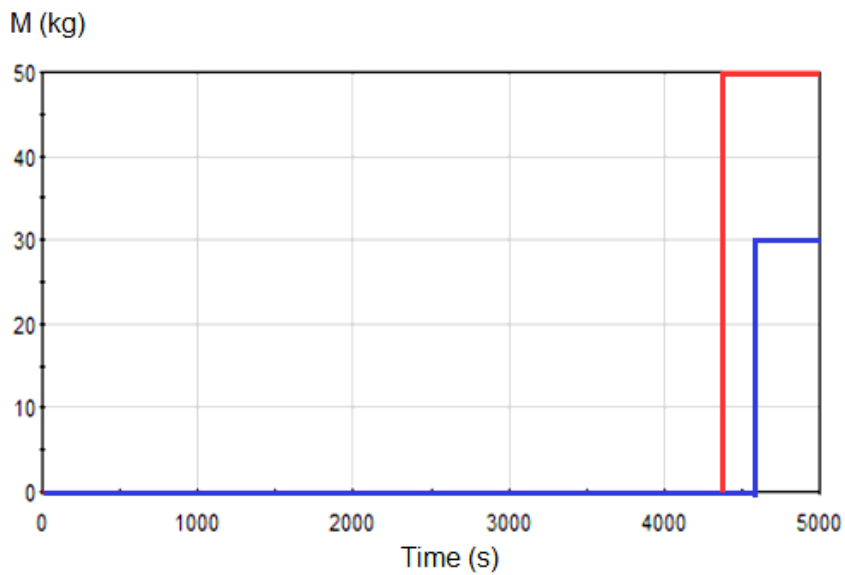


Fig. 2.57 Outflow mass of Cs and Ag at the end of the SAFT-path

Using the example data set (this time without artificial FP in the water), it can also be seen that after flooding the pipe, the fission products are no longer transported further in aerosol and gas form, consequently they also do not flow out (Fig. 2.58 - Fig. 2.61). They

remain in the circuit mainly as suspended vapour/aerosol or as deposited aerosol. After flooding the pipe, these species remain suspended before the flooded part of the circuit (end of the core and first CV in the PIPE). This is probably due to the fact that aerosol and gas transport is essentially simulated in vapour, and entrainment by water is not considered. This needs to be investigated in more detail. Furthermore, realistic assumptions have to be found on how to improve the modelling.

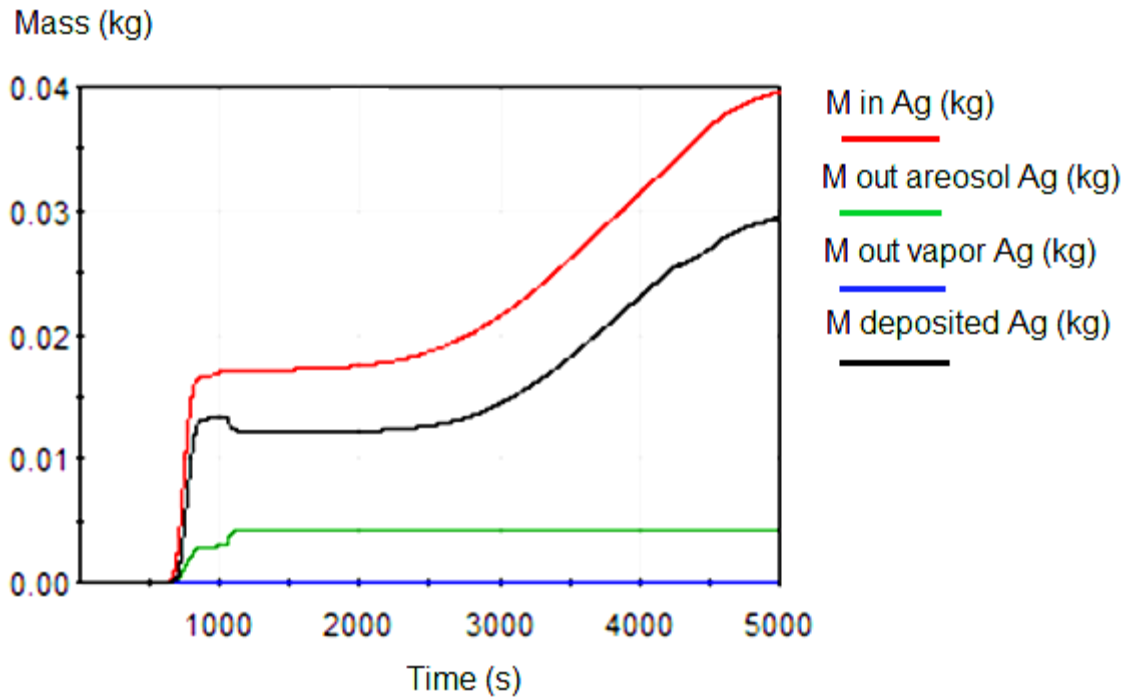


Fig. 2.58 Transported fission products (Silver)

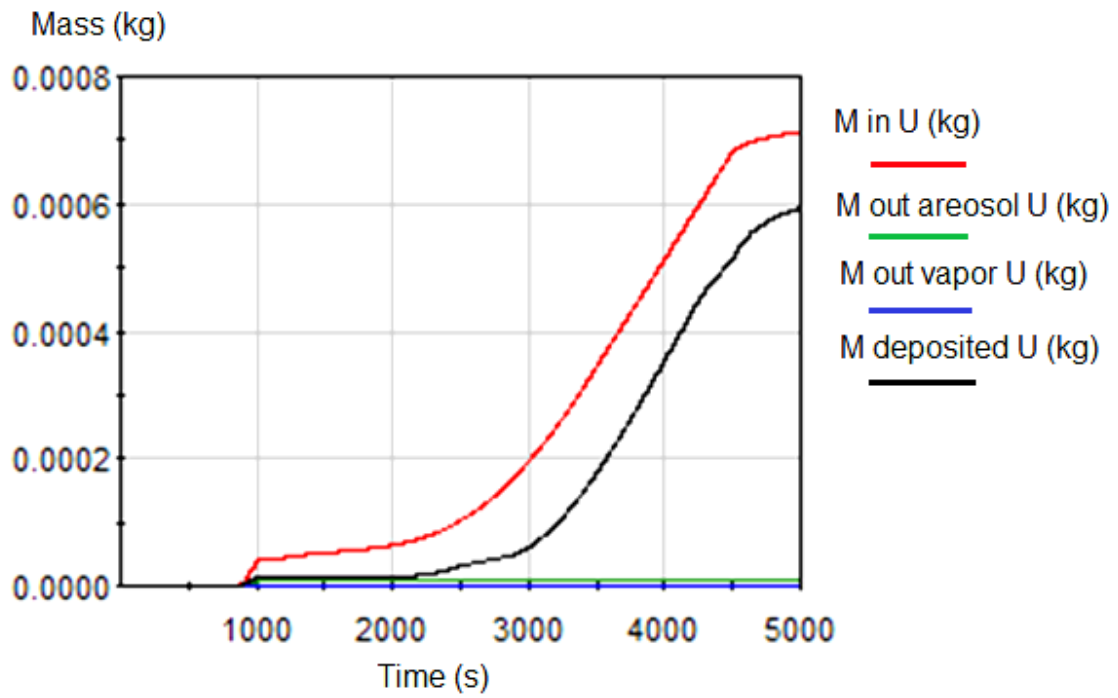


Fig. 2.59 Transported fission products (Uranium)

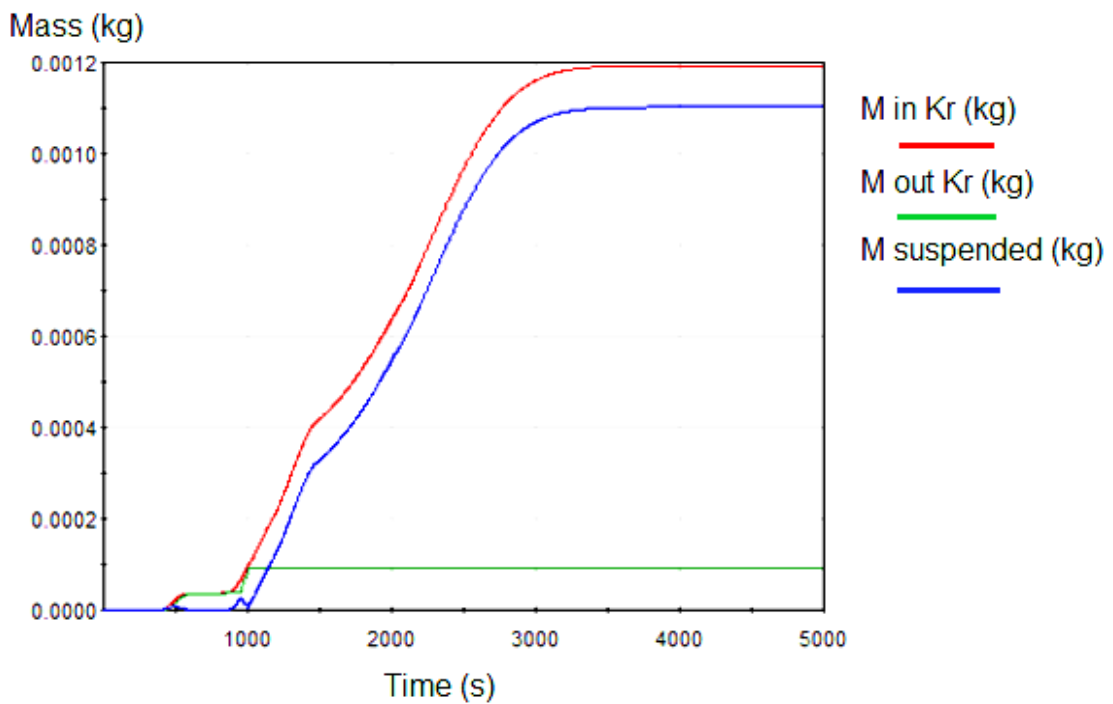


Fig. 2.60 Transported fission products (Krypton)

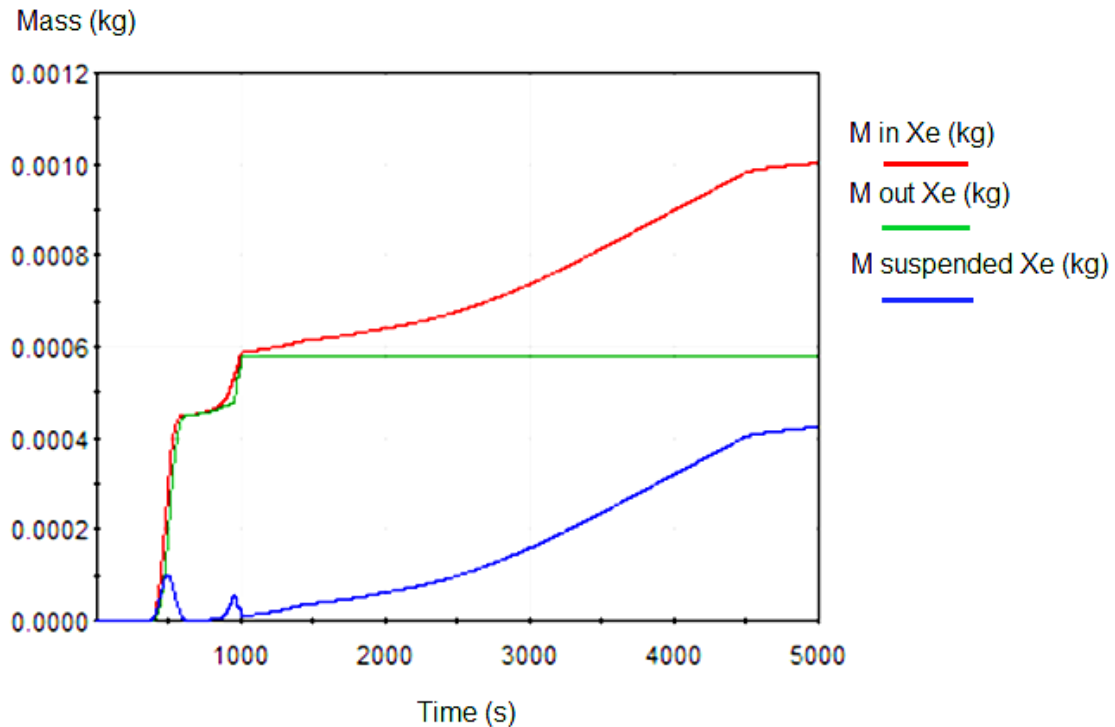


Fig. 2.61 Transported fission products (Xenon)

The next issue is to answer and model how a species gets into the water phase to be transported or deposited. While most elements can theoretically appear in the water phase in elemental form, dissolved transport often involves compounds and consequentially ions, which is also relevant for all non-volatile species as there are numerous water-soluble compounds of most elements. Obviously, noble gases like Xe or Kr would be exclusively transported in the gas phase (forming bubbles). Additionally, solid particles formed of non-soluble compounds could be transported in the water phase as aerosols are in the gas phase.

As a test, the code-internal “ctype” of caesium was changed to ‘OTHER’ to make it water-soluble in the simulation (Fig. 2.62 and Fig. 2.63). After this change, Cs also enters the water phase. However, it is not transported to the end of the pipe but remains in the last CV of the core. This is most likely because, due to the “ctype” change, Cs can only be transported in water in the current implementation. However, there is no water in the core, only steam, which is why it is not transported. Nevertheless, it is accounted for as if it were dissolved in water. This paradox must be eliminated in future.

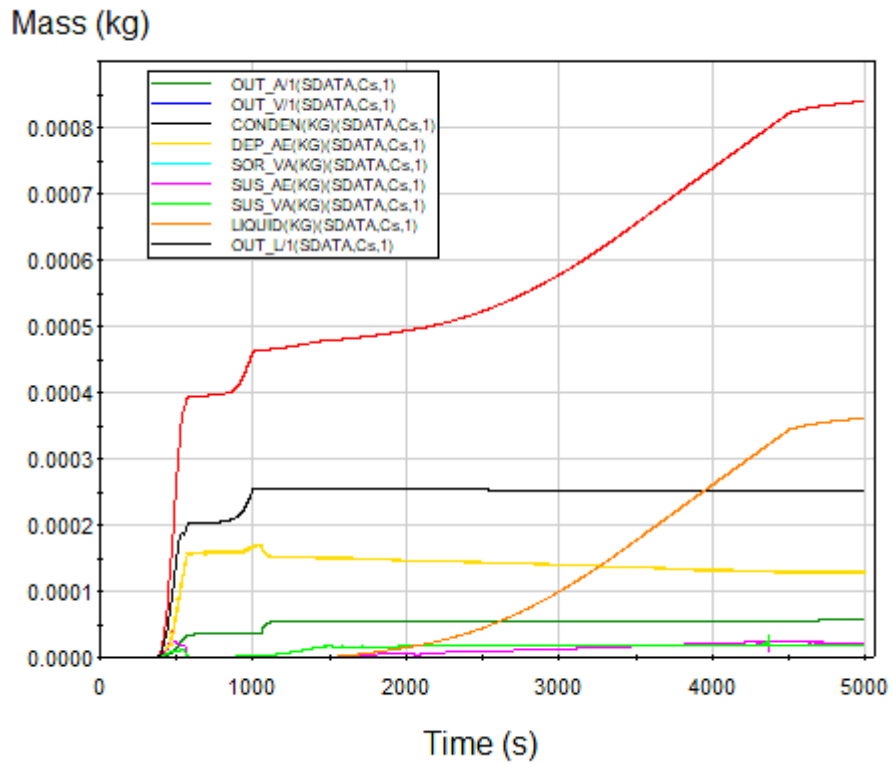


Fig. 2.62 Water solubility of cesium

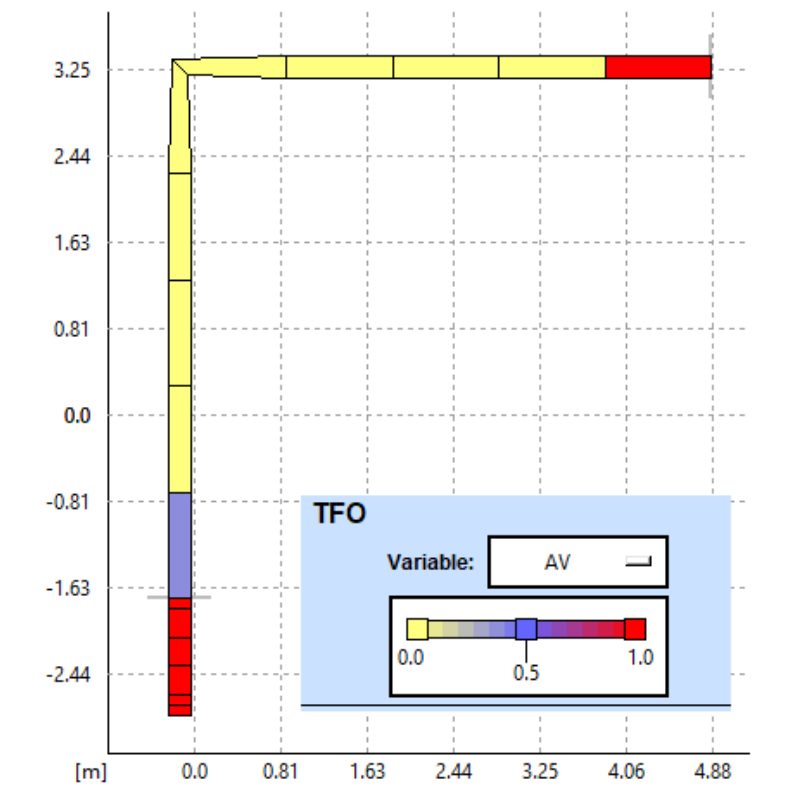


Fig. 2.63 Void fraction in the test section

A further test calculation has shown that xenon and krypton must both be defined as FIPREM elements to avoid a crash at vapour content = 0.0. If they are defined under PW SOURCE in CW SAFT, they are not recognised as carrier gases. This leads to the fact that at vapour content = 0.0 there is no gas phase at all on the basis of which the transport properties could be calculated (division by zero). This problem can be eliminated by considering xenon and krypton as carrier gases, regardless of how they are defined. Alternatively, a check can be included to ensure that xenon and krypton are defined in FIPREM.

Changes have been made to include xenon and krypton as carrier gases in SAFT, even if they are defined under PW SOURCE. A flag was defined (XEKR) which gets the value 1 if xenon and krypton are defined under PW SOURCE, otherwise it is 0 (tmot-scali.f; tsounam.f). This flag is used later to add Xe and Kr to the SAFT carrier gases and to store their properties accordingly (tsofip.f; tvolnet.f). This change requires that Xe and Kr must always be defined together, either in FIPREM or in SAFT.

In another test calculation, both the core and the conduit were flooded (Fig. 2.64 and Fig. 2.65). Some elements were defined under PW SOURCE to ensure that fission products were still released despite the flooded condition. Since none of the species were soluble in water, the LIQUID (kg) values remained zero, but the elements could be released. On the other hand, it was found that no transport of these elements took place. This was probably because transport is envisaged in the vapour and gas mixture, while only water was present in the flooded circuit. Since Xe and Kr were defined under FIPREM, there was a minimum amount of gas everywhere in order to be able to calculate the properties of the carrier gas (in this case Xe and Kr). But since there is no gaseous carrier in ATHLET, the velocities are zero. This leads to a quasi-static state in the SAFT, where the released fission products simply remain where they were released. This result, together with previous experience, suggests that gases and aerosols are transported only in the gaseous carrier, while water-soluble species are transported only in water. The program does not foresee the entrainment of water, or the transport of bubbles and aerosol particles in water. Furthermore, there seems to be a need for checking the rate values. Special attention must be paid to gaseous and liquid velocity calculations.

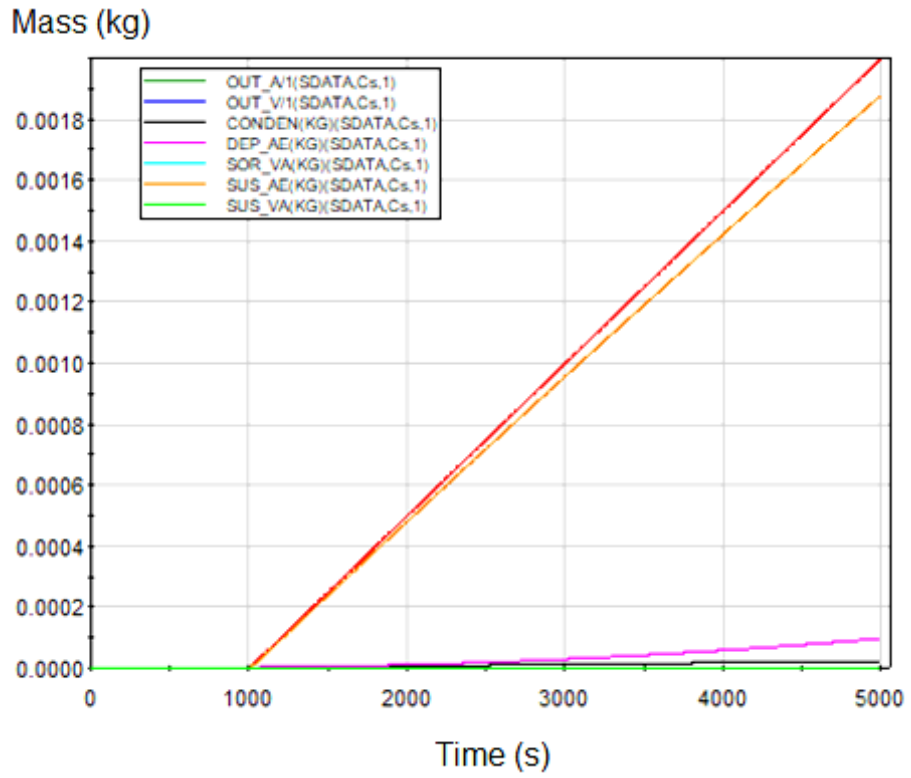


Fig. 2.64 Water solubility of cesium (flooded case)

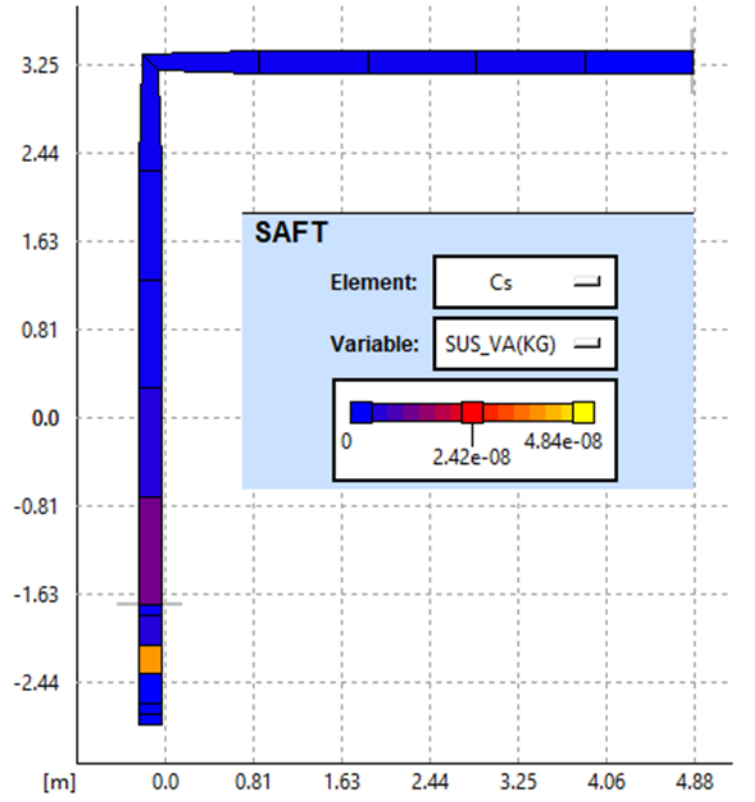


Fig. 2.65 Water solubility of cesium (flooded case)

The following conclusions can be drawn, and the following points need to be considered in the future:

- Inclusion of SAFT carrier gases in the ATHLET equation system.
- Termination of calculations in flooded cases (vapour content = 0.0) occurs. Since this is to be avoided, another solution has to be found in the future.
- Simulation of the entrainment of aerosol and gas in water. This would most likely be the cleanest solution, but at the same time the costliest. It could be considered to rely on ATHLET thermal-hydraulics prediction of entrainment and bubble transport, but this would require a closer integration of SAFT models into ATHLET.
- Rate values should be checked.

With these analyses, several weak points and still undeveloped parts of SAFT were identified, which can be addressed in the future.

2.4 WP1.4: Refactoring

2.4.1 Refactoring the model for heat transfer between transported fission products and environment

Motivation

In ATHLET-CD 3.2 the parts of energy of α -, β - and γ -rays emitted by the fission products and absorbed by either the fluid or the walls were determined without considering physical properties of the particles, namely their absorption coefficient or their range in the fluid (the distance travelled by the particle in the medium until its energy is fully absorbed). This resulted in unrealistic energy repartitions. The existing model was refactored for more realistically differentiating between the interactions of fluid and structures with the different types of decays.

Developments

α - and β -rays are charged particles, unlike γ -rays. α - and β -particles continuously lose energy by interacting with nuclei they encounter during their travel in a medium. In ATHLET-CD, they are handled as one ensemble ($\alpha+\beta$). Considering the pair ($\alpha+\beta$), α -radiation represents barely 1 % of the total ($\alpha+\beta$)-power for typical fission product

releases in a nuclear reactor. Therefore, there is no need to distinguish the absorption of α -rays from the absorption β -rays. α -ray power contribution and α -particle absorption thickness can be neglected.

Knowing the initial energy $E_{\beta,0}$ [MeV] of the β -particle, and the density [g/cm³] of the medium, the distance travelled by the particle in the medium until its energy is fully absorbed, also called “range” in the literature /TUR 95/, and denoted R [cm], can be determined by:

$$R = 0,412 \frac{E_{\beta,0}^n}{\rho} \quad (2.25)$$

with $n = 1,265 - 0,0954 \ln (E_{\beta,0})$

Additionally, the linear energy transfer LET [MeV/cm], i. e. the average absorbed energy of a single β -ray per length unit, can be obtained from the range R:

$$LET_{\beta} = \frac{E_{\beta,0}}{R} \quad (2.26)$$

LET is a determinant value regarding the partitioning of the initial energy of the particle, with respect to the position from which the particle is emitted.

Γ -rays are high energy photons. During its journey through a medium of thickness L [cm], a γ -photon can either encounter an atom and be fully absorbed by it, or encounter nothing and continue its journey, possibly diffracted. Effectively, one can consider a γ -beam as initially consisting of an amount of $N_{\gamma,0}$ γ -rays. A part $N_{\gamma,abs}$ of this γ -beam will be absorbed, while the remaining $N_{\gamma,L}$ ($=N_{\gamma,0} - N_{\gamma,abs}$) get through the medium. $N_{\gamma,L}$ can be calculated, knowing the linear attenuation coefficient μ [cm⁻¹]:

$$N_{\gamma,L} = N_{\gamma,0} \exp (-\mu L) \quad (2.27)$$

The estimation of the energy absorption $E_{\gamma,abs}$ of a γ -beam, initially with $E_{\gamma,0}$, follows analogously:

$$E_{\gamma,L} = E_{\gamma,0} \exp(-\mu L) \quad (2.28)$$

and subsequently,

$$E_{\gamma,abs} = E_{\gamma,0} - E_{\gamma,L} \quad (2.29)$$

The absorbed energy fraction can be easily determined as:

$$\frac{E_{\gamma,abs}}{E_{\gamma,0}} = \frac{E_{\gamma,0} - E_{\gamma,L}}{E_{\gamma,0}} = \frac{E_{\gamma,0} (1 - \exp(-\mu L))}{E_{\gamma,0}} = 1 - \exp(-\mu L) \quad (2.30)$$

The partitioning of the energy obviously depends on the geometry of the TFO and on the position of the emission (whether at the wall or somewhere in the fluid inside the TFO). Still, the attenuation coefficient must be defined. μ depends on the material of the medium, i. e. on its density ρ , and the particle energy $E_{\gamma,0}$. In the energy range favourable to the Compton effect, the attenuation coefficient μ can be expressed by: $\mu = \frac{A \cdot \rho}{E_{\gamma,0}^B}$, where A and B are constant values depending on the medium. It can be also formulated as follows:

$$\mu = A \rho E_{\gamma,0}^{-B}, \text{ with } \begin{cases} A = \frac{1}{15.0} \\ B = 0,47 \end{cases}, \text{ for steam} \quad (2.31)$$

Constant values A and B were deduced for steam by plotting the attenuation coefficient vs. steam density ρ_{steam} (for fixed $E_{\gamma,0}$) and the attenuation coefficient vs. initial energy $E_{\gamma,0}$ (for fixed density), using as basis attenuation coefficients for water that can be found in the literature. Therefore, this correlation is also valid for water ($\rho_{vap} = 1 \text{ g/cm}^3$). For air, it is assumed that the attenuation coefficient is very near to the one of steam for the same density.

Modelling of radiation energy partitioning

In this section, an approach is proposed for the partitioning of the fission product power **to** fluid and **to** walls (to HECU and HEAT structures). This power [in watt] is denoted SPOWAT(ZONE,I,J), which is an intern variable of the program. SPOWAT is indexed by three attributes, that are ZONE, I and J. I refers to the origin of the particles: I = 1 if particles are emitted **from** fluid; I = 2 if emitted **from** the wall. J refers to the type of particles: if J = 2 then γ -particles, and if J = 3 then $(\alpha+\beta)$ -particles.

In other words, SPOWAT(ZONE,I,J) represents the total γ - and $(\alpha+\beta)$ -power from the fission product inventory, that is present in a specific zone. SPOWAT cannot be used directly to determine the range R of β -particles or the attenuation coefficient μ of the γ -particles, since these parameters rely on energy of "single particle".

The average values for $E_{\beta,0}$ and $E_{\gamma,0}$ are chosen as default values:

$$E_{\beta,0} = 1 \text{ MeV}$$

$$E_{\gamma,0} = 2 \text{ MeV}$$

The different energy contributions are defined as follows:

Energy released by β -particles in the fluid:

- F13L: The fraction of SPOWAT(-,1,3) going into the fluid
- F13W: The fraction of SPOWAT(-,1,3) going into the wall

Energy released by β -particles at the fluid:

- F23L: The fraction of SPOWAT(-,2,3) going into the fluid
- F23W: The fraction of SPOWAT(-,2,3) going into the wall

Energy released by γ -particles in the fluid:

- F12L: The fraction of SPOWAT(-,1,2) going into the fluid
- F12W: The fraction of SPOWAT(-,1,2) going into the wall

Energy released by γ -particles at the wall:

- F22L: The fraction of SPOWAT(-,2,2) going into the fluid
- F22W: The fraction of SPOWAT(-,2,2) going into the wall

Before going any further, a remark is necessary on the CV topology, and thus, on the way to compute the ratio of the volume enclosed within R (zone in red) on the whole volume defined by the radius. For simplification reason, we consider the problem in 2D:

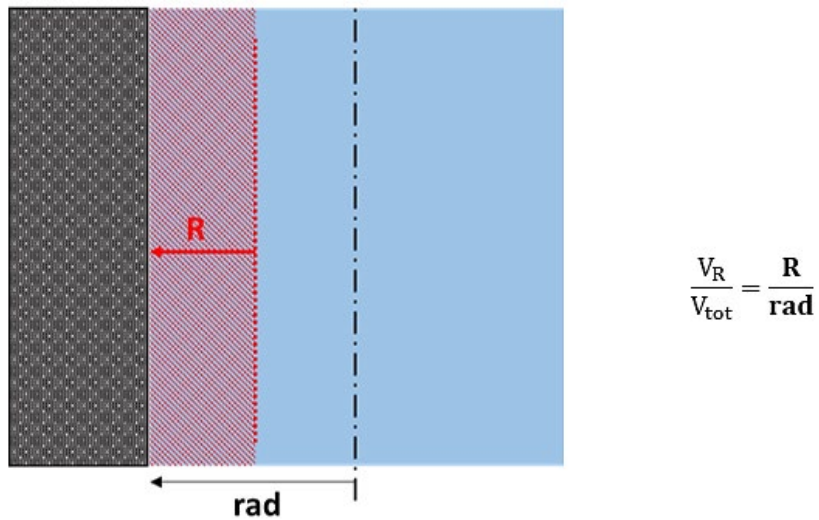


Fig. 2.66 Vertical view of structure, fluid and β -radiation zone

β -ray power from fluid: F13L, F13W

Concerning the β -particles emitted by aerosols in the fluid, three configurations are possible regarding the average range R of the β -rays:

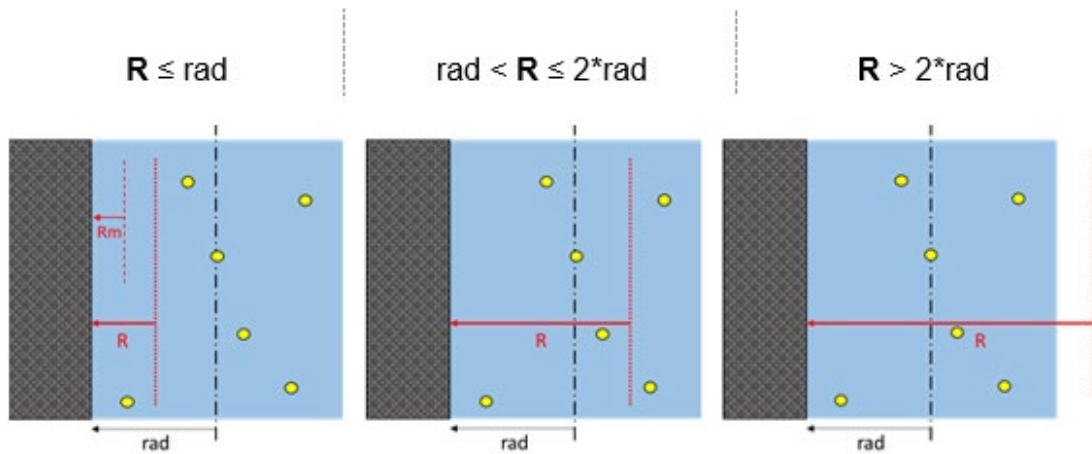


Fig. 2.67 Zones for β -radiation from the fluid towards walls and into fluid

Case 1: if ($R \leq rad$)

- The β -rays from the CV fraction $\mathbf{FRL1} = \left[1 - \frac{R}{rad}\right]$, i. e. volume fraction not enclosed within the range R , go necessarily into the fluid.
- The β -rays from the CV fraction $\left[\frac{R}{rad}\right]$ go partly into the fluid and partly into the wall:
 - 50 % is necessarily directed towards the fluid:

$$\mathbf{FRL2} = 0.5 \cdot \frac{R}{rad} \tag{2.32}$$

- The remaining 50 % are partly absorbed by the fluid while traveling towards the Wall, and thus, the rest goes into the wall:

We define a mean length R_m within the zone of the range R , as depicted above: $R_m = \frac{R}{2}$. For a length R_m , the mean absorbed energy of one single particle:

$$E_{\beta,abs} = LET_{\beta} \cdot R_m \tag{2.33}$$

and its fraction $\frac{E_{\beta,abs}}{E_{\beta,0}}$ can be estimated (basically = $\left[\frac{R_m}{R}\right]$)

Therefore, the fraction going to the fluid is:

$$\mathbf{FRL3} = \left[0.5 \frac{R}{\text{rad}} \right] \cdot \frac{E_{\beta,\text{abs}}}{E_{\beta,0}} \quad (2.34)$$

and the fraction to the wall:

$$\mathbf{FRW1} = \left[0.5 \frac{R}{\text{rad}} \right] \cdot \left[1 - \frac{E_{\beta,\text{abs}}}{E_{\beta,0}} \right] \quad (2.35)$$

Case 2: if ($\text{rad} < R \leq 2 \cdot \text{rad}$)

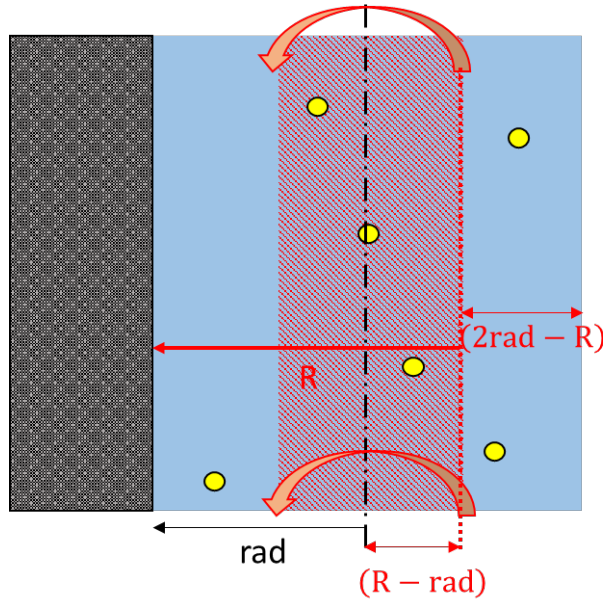


Fig. 2.68 β -radiation zone from the intermediate zone in the fluid

- All the β -rays from the CV fraction $\left[\frac{R - \text{rad}}{\text{rad}} \right]$ go toward the wall, but a part is absorbed during the travel. We define a mean range: $R_m = \text{rad}$, in order to estimate the energy fraction that is absorbed by the fluid:

$$\frac{E_{\beta,\text{abs}}}{E_{\beta,0}} = \frac{\text{LET}_{\beta} \cdot R_m}{E_{\beta,0}}, \text{ and subsequently:}$$

$$\mathbf{FRL1} = \frac{E_{\beta,\text{abs}}}{E_{\beta,0}} \cdot \left[\frac{R - \text{rad}}{\text{rad}} \right] \quad (2.36)$$

- The rest goes to the wall:

$$\mathbf{FRW1} = \left[1 - \frac{E_{\beta,abs}}{E_{\beta,0}} \right] \cdot \left[\frac{R - rad}{rad} \right] \quad (2.37)$$

- As for the remaining $\left[1 - \frac{R-rad}{rad} \right] = \left[\frac{2 rad-R}{rad} \right]$:
 - 50 % is necessarily directed into the fluid:

$$\mathbf{FRL2} = 0.5 \cdot \left[1 - \frac{R - rad}{rad} \right] \quad (2.38)$$

- The remaining 50 % are partly absorbed by the fluid on the way towards the wall. We define a mean length:

$$l_m = \left[\frac{2 rad - R}{2} \right] \quad (2.39)$$

and the absorbed fraction of the energy $\frac{E_{\beta,abs,2}}{E_{\beta,0}} = \frac{LET_{\beta} \cdot l_m}{E_{\beta,0}}$

$$\mathbf{FRL3} = \frac{E_{\beta,abs,2}}{E_{\beta,0}} \cdot 0.5 \cdot \left[1 - \frac{R - rad}{rad} \right] \quad (2.40)$$

The rest goes into the wall:

$$\mathbf{FFRW2} = \left[1 - \frac{E_{\beta,abs,2}}{E_{\beta,0}} \right] \cdot 0.5 \cdot \left[1 - \frac{R - rad}{rad} \right] \quad (2.41)$$

Case 3: if ($R > 2 \cdot \text{rad}$)

We define a mean absorption length: $l_m = \text{rad}$

- This following energy fraction goes into the fluid:

$$\mathbf{FRL1} = \frac{E_{\beta,\text{abs}}}{E_{\beta,0}} = \frac{\text{LET}_{\beta} \cdot l_m}{E_{\beta,0}} \quad (2.42)$$

- The rest goes into the wall:

$$\mathbf{FRW1} = 1 - \frac{E_{\beta,\text{abs}}}{E_{\beta,0}} = 1 - \frac{\text{LET}_{\beta} \cdot l_m}{E_{\beta,0}} \quad (2.43)$$

Overall result after Case 1, Case 2 or Case 3

$$\mathbf{F13L} = \mathbf{FRL1} + \mathbf{FRL2} + \mathbf{FRL3}$$

$$\mathbf{F13W} = \mathbf{FRW1} + \mathbf{FRW2} + \mathbf{FRW3}$$

β -ray power from Wall: F23L and F23W:

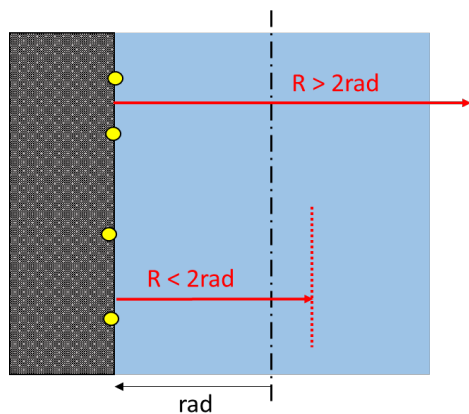


Fig. 2.69 β -radiation zones for radiation from the wall surface

In any case, at least 50 % of the β -rays emitted by aerosols at the wall are necessarily directed towards the wall and fully absorbed by it.

Case 1: if ($R > 2 \cdot \text{rad}$)

- As mentioned above, 50 % goes directly to the Wall:

$$\mathbf{FRW1} = 0.5$$

- As for the remaining 50 %:
 - a part is absorbed by water during the journey

$$\mathbf{FRL1} = 0.5 \cdot \frac{E_{\beta, \text{abs}}}{E_{\beta, 0}} = 0.5 \cdot \frac{\text{LET}_{\beta} \cdot 2 \text{ rad}}{E_{\beta, 0}} \quad (2.44)$$

- the rest goes to the wall on the opposite side:

$$\mathbf{FRW2} = 0.5 * \left(1 - \frac{E_{\beta, \text{abs}}}{E_{\beta, 0}} \right) = 0.5 * \left(1 - \frac{\text{LET}_{\beta} * 2 \text{ rad}}{E_{\beta, 0}} \right) \quad (2.45)$$

Case 2: if ($R \leq 2 \cdot \text{rad}$)

- As mentioned above, 50 % goes directly to the wall:

$$\mathbf{FRW1} = 0.5$$

- The remaining 50 % is fully absorbed by water:

$$\mathbf{FRL1} = 0.5$$

Overall, after Case 1 or Case 2

$$\mathbf{F23L} = \mathbf{FRL1} + \mathbf{FRL2}$$

$$\mathbf{F23W} = \mathbf{FRW1} + \mathbf{FRW2}$$

γ-ray power from fluid: F12L and F12W

We define first a mean length: $l_m = rad$

- Knowing the absorption coefficient, the absorbed fraction by the fluid is obtained by:

$$\mathbf{FRL1} = \frac{E_{\gamma,abs}}{E_{\gamma,0}} = 1 - \exp(-\mu l_m) \quad (2.46)$$

- The rest goes into the wall:

$$\mathbf{FRW1} = 1 - \frac{E_{\gamma,abs}}{E_{\gamma,0}} = \exp(-\mu l_m) \quad (2.47)$$

Overall:

$$\mathbf{F12L} = \mathbf{FRL1}$$

$$\mathbf{F12W} = \mathbf{FRW1}$$

γ-ray power from wall: F22L and F22W

We define first a mean length: $l_m = 2rad$

- 50 % goes necessarily directly to the wall:

$$\mathbf{FRW1} = 0.5$$

- As for the remaining 50 %:
 - knowing the absorption coefficient, the absorbed fraction by the fluid is obtained by:

$$\mathbf{FRL1} = 0.5 \cdot \frac{E_{\gamma,abs}}{E_{\gamma,0}} = 0.5 \cdot (1 - \exp(-\mu l_m)) \quad (2.48)$$

– the rest goes into the wall:

$$RW2 = 0.5 \cdot \left(1 - \frac{E_{\gamma,abs}}{E_{\gamma,0}}\right) = 0.5 \cdot \exp(-\mu l_m) \quad (2.49)$$

Overall

$$F22L = FRL1$$

$$F22W = FRW1 + FRW2$$

Conclusion: power repartitioning:

In each zone I, the energy partitioning between the corresponding ATHLET-TFO IAT, HECU-object IHT and ECORE-Heat structure IHC is calculated as follows:

Isotope power to ATHLET (i. e. to fluid):

$$\begin{aligned} QRAYDR(IAT) = \frac{1}{FPARO} [& F13L * SPOWAT(I, 1, 3) + F23L \\ & * SPOWAT(I, 2, 3) \\ & + F12L * SPOWAT(I, 1, 2) + F22L \\ & * SPOWAT(I, 2, 2)] \end{aligned} \quad (2.50)$$

with FPARO = multiplier for parallel geometries.

Isotope power to ECORE (i. e. to wall defined in ECORE):

$$\begin{aligned} QRAYHT(IHT) = \frac{FAC * FNW}{NDODR} [& F13W * SPOWAT(I, 1, 3) + F23 \\ & * SPOWAT(I, 2, 3) \\ & + F12W * SPOWAT(I, 1, 2) + F22W \\ & * SPOWAT(I, 2, 2)] \end{aligned} \quad (2.51)$$

with

$$FAC = \frac{Area_{HEAT}}{Area_{HEAT} + Area_{HECU,right} + Area_{HECU,left}} \quad (2.52)$$

$$FNW = \frac{1}{\text{number of HEAT structures in } I} \quad (2.53)$$

NRODR = radial number of rods in I.

Isotope power to HECU, left or right wall:

$$Q_{RAYHC}(IHC) = \frac{FAC * FNW}{F_{PAR}(IHC)} \cdot [F13W * SPOWAT(I, 1, 3) + F23W * SPOWAT(I, 2, 3) + F12W * SPOWAT(I, 1, 2) + F22W * SPOWAT(I, 2, 2)] \quad (2.54)$$

with

$$FAC = \frac{Area_{HECU,left \text{ or } right}}{Area_{HEAT} + Area_{HECU,right} + Area_{HECU,left}} \quad (2.55)$$

$$FNW = \frac{1}{\text{number of HEAT structures in } I} \quad (2.56)$$

To sum up, from the radiative power emitted by γ - and $(\alpha+\beta)$ -rays from the fission product inventory in each zone, a redistribution of the power into the walls (Q_{RAYHC}) and/or structures (Q_{RAYHT}) as well as into the fluid (Q_{RAYDR}) has been derived, considering the properties of particle rays and photons, their location of emission (near-to-wall region or inside the bulk region of fluid) and the cell dimension, i. e. the radius of the control volume. The current model is based on a simplified two-dimensional representation of the control volume geometry. The model should be further developed to account for more a realistic geometry of the control volume in three dimensions. Additionally, the default

values for the initial energy of γ - and β -particles, that are currently fixed in the code, could be made available as input parameters to the user or even be estimated for each zone by a model, as a function of the different fission products present in each zone, their concentration, and the typical initial energy of γ - and β -particles for each species.

2.4.2 Refactoring of the software infrastructure of ATHLET-CD

Motivation

Program development of ATHLET-CD began in the 1980s /LOV 21b/, since then the IT infrastructure and the programming language changed a lot. ATHLET-CD had some problems with compatibility, maintenance, and extendibility due to its legacy code nature. It was therefore decided to modernise the source code of ATHLET-CD to fit today's programming standards.

Developments

An initial task was to update the limiting syntax of Fortran 77, called fixed format. This format restricts the user to both a maximum amount of code per line as well as restricts the initial 6 characters of each line to have a unique meaning if used and therefore making them unusable for the majority section of a code file. To remove these limitations all ATHLET-CD files with the extension '.f' had to have their syntax updated to the more modern Fortran 90 standard, which uses 'free-format'. These developments were mainly done within the project RS1572, however with strong coordination and cooperation within this (RS1574) project, to do the verification for the changes made by these maintenance works and to ensure not changing code behaviour or results. After the changes no functional differences were allowed to occur. To ensure that, multiple checks were done. Simulations were performed with and without the refactoring code changes and the results of the simulations were compared. As expected, the results between the old and the refactored versions were exactly the same. This proves the correct implementation of these purely syntactical changes. With that ATHLET-CD now consists of only .F90 files, and allows developers to maintain the code easier and also allows easier future modernisations and developments.

In order to take advantage of newer compiler optimisations and to significantly ease future developments, maintenance, and verification, it was also decided to explicitly declare the type of all variables in every file (in accordance with FORTRAN guidelines).

When working on large codebases, it is easier for the developer to avoid mistakes and use the correct type of values, if all variables have an explicitly declared value type. It also helps when certain operations are applied to variables as they might result in different outcomes if the variable is a float, an integer, or a character. Furthermore, the explicit declaration of variables allows for certain optimisations done by the compiler when transforming the Fortran code into object code. Here, similarly to the previous development, the work was done in cooperation with the project RS1572. After the necessary code changes, checks were done. Simulations were performed with and without the software refactoring and the results of the simulations were compared. As required, the results between both versions were identical.

Besides these larger internal changes to the code, several other syntactical changes were performed, like to update the obsolescent arithmetic IF statements to regular IF statements and to remove the equally obsolescent “go to” order within DO loops in the code. These changes were necessary to keep up with the changing of the FORTRAN guidelines and to be able to use the current (and future) compiler options. Here, similarly to previous tasks, checks showed no differences between results from refactored and unmodified versions, therefore all the tasks were finished successfully.

2.4.3 Replacement of the models OREST/FIPISO by VENTINA

Motivation

The refactoring and further developments of the parts of the code related to the decay of the fission products is difficult because these code parts are old, both programming-wise and model-wise. Towards the end of 2019, it was determined that replacement of OREST/FIPISO by VENTINA was a priority for the further development of ATHLET-CD and also AC². Consequently, this task was added to the scope of this project by a modification of the contract late in 2020. The modernisation will achieve:

- Better maintainability and facilitate further development
- Modern models
- Uniform decay modelling for AC²

The VENTINA program co-developed by GRS and EPFL was selected for replacement of OREST/FIPISO, which are the existing modules for inventory and decay calculation, because the program can meet the requirements of GRS and has reached a sufficient level of development and validation.

Developments

The refactoring work can be grouped in four main subtasks:

1. Adjusting the existing model basis of VENTINA to the needs of ATHLET-CD and COCOSYS
2. Integration of VENTINA into ATHLET-CD
3. Integration of VENTINA into COCOSYS
4. Verification of the integration process

2.4.3.1 Adjusting the existing model basis of VENTINA to the needs of ATHLET-CD and COCOSYS

Supporting work concerning the integration of VENTINA into AC² has been carried out in the associated GRS project "MODENA" (RS1582). The tasks addressed in MODENA comprise the generation of custom nuclear input data as well as the contribution of interface code. These activities are summarised in the following paragraphs. A detailed account will be included in the MODENA final project report.

A self-contained software module (BND, short for "burn-up'n'decay") written in Fortran 2008 has been prepared for AC², which provides an abstract interface for a generic burn-up and decay solver and which addresses VENTINA as a specific back-end library. This approach establishes a loose coupling between the program components and allows for the solver to be easily exchanged in the future. It also serves to hide VENTINA's implementation details as well as to contain the namespace it occupies, which is important, because the program has not been originally designed to be used as a software library.

BND generates and configures a burn-up solver instance. The software reads an assembly loading pattern and accesses an extendable nuclear database of assembly types, which has been specifically designed and created for this project and purpose. This database has been generated using the 3D high-resolution burnup code MOTIVE /HAN 17/, which has been developed at GRS in the last years. MOTIVE couples a Monte Carlo neutron transport code to the inventory calculation code VENTINA and allows for fuel assembly burn-up calculations with pin-by-pin resolution. The database stores nuclide-specific, microscopic nuclear cross sections and fluxes condensed to one energy group. The data are parametrised by burn-up, moderator density and enrichment for several assembly types. For the purpose of creating this database, a special option has been introduced in MOTIVE, which allows to define the steps in burn-up, enrichment and moderator density for which values are to be written into the data base. The data base can then be filled by running several MOTIVE calculations – one for each parameter combination – using the full geometry information of the specified fuel assembly.

Subsequently, the initial nuclide vectors of the fresh fuel elements are calculated from their assembly types and enrichments. Based on the above information and the individual power histories, the solver (VENTINA) is applied to burn each assembly for the determination of the nuclide densities at the beginning of an ATHLET-CD simulation. In order to subsequently take into account, the effects of nuclear decay on the nuclide densities contained in the control volumes, a second, dedicated solver instance is created, which can also be used independently in COCOSYS.

In addition to the data provided for the burn-up solver, the decay solver (VENTINA) requires a fission yield matrix and nuclide decay chain information, provided here in the form of two text files. These have been generated using the GRS nuclear data pre-processor for ENDF6 databases, NuGra. Additional programming efforts have been invested to extend NuGra in order to mitigate the effects of reducing the nuclide information contained in a database to a problem-tailored selection while preserving mass and, approximately, nuclide generation rates.

In addition to a few auxiliary procedures for the handling of data and memory resources, the interface presented by BND to AC² consists mainly of the subroutines "calculateInitialNuclideDensities" and "decayNuclidesInNodes" which populate or modify a nuclide density array owned by AC² for assembly and non-assembly control volumes. The effects of nuclear decay may be restricted to a subset of the control volumes via a user-defined node mask.

After these extensions and adjustments, the VENTINA code can provide input for the initial fission product inventory for ATHLET-CD and can be used to simulate the decay of fission products, which is needed both in ATHLET-CD and in COCOSYS.

2.4.3.2 Integration of VENTINA into ATHLET-CD

VENTINA, through the BND module, is able to determine the initial fission product inventory of a reactor core in stand-alone mode, based on a limited set of input data, and is able to simulate the decay of the previously generated initial fission product inventory. Two main tasks remained for a complete integration into ATHLET-CD:

1. Allowing a two-way communication between ATHLET-CD and VENTINA
2. Removing OREST/FIPIISO (previous models for inventory and decay calculation) and achieving/improving the previously available features using data from VENTINA

For the initial inventory calculation VENTINA requires the following inputs: type of fuel element (e.g., PWR 18x18), enrichment of UO_2 , density of UO_2 , volume of UO_2 , power history of the fuel, and moderator density history. The density and volume of UO_2 can be derived from other ATHLET-CD input data, the new implementation only requires additional data for the remaining properties. The input handling routines of ATHLET-CD were extended, so that the user can provide these data in the input deck.

For the initial inventory calculation, data transfer occurs only once, at the beginning of the simulation from ATHLET-CD to VENTINA and backwards. A coupling interface was created where the required data from ATHLET-CD can be given to VENTINA. Based on these data VENTINA generates the core inventory in the form of more than 1300 relevant isotopes of the first 100 elements and transfers this data back to ATHLET-CD. ATHLET-CD assigns these isotope masses to specific core nodes. Currently, VENTINA cannot provide an axial distribution of the fission products, it has to be explicitly defined by the user. With that, fission product masses are assigned to all core nodes.

To simulate the residual power of the core that is generated by the decay of fission products further and continuous interaction of ATHLET-CD and VENTINA is needed. The isotope masses from ATHLET-CD are given back to VENTINA, where a decay calculation is performed, and a new isotope composition is given back to ATHLET-CD. VENTINA also provides a decay power density (W/kg) for all considered isotopes.

The power generated by the decay of an isotope is calculated as follows:

$$\text{decay power [W]} = \text{isotope mass [kg]} * \text{specific decay power} \left[\frac{\text{W}}{\text{kg}} \right] \quad (2.57)$$

To summarise, VENTINA generates isotope masses based on input data provided by ATHLET-CD and calculates the decay of these isotopes, providing accurate mass and power data for ATHLET-CD via continuous data exchange.

For the replacement of OREST and FIPISO, first, all parts of these modules had to be removed from ATHLET-CD. Instead of naively replacing those parts by VENTINA parameters, a larger refactoring was achieved. The new general logic in ATHLET-CD is the following:

- At the beginning of the simulation, there are isotopes only in the axially/horizontally defined core nodes. These masses are constantly recalculated by VENTINA to address the change of isotope composition (and power) in the core.
- As the core eventually heats up due to insufficient cooling, fission products can be released, after cladding failure occurred. Models for fission product release only take elements into account. It is assumed, that the released fission products have the same isotopic composition as at the location where the fission product originates from.
- The amount of released isotope mass is subtracted from the core inventory.
- The released isotopes form a new entity and are also handed over to VENTINA, separately from the isotopes that remained in the core, for further decay.
- The released fission products (and isotopes) are transported within the cooling circuit using the SAFT models (those remain unchanged). Along the transport path, energy is exchanged between the decaying fission products and the environment. For that, the isotope specific decay powers (alpha, beta and gamma) provided by VENTINA are used.
- Isotope masses that leave the boundaries of ATHLET-CD are provided to COCOSYS, where they can be further transported and further decayed.
- If a node melts, the melt has the decay power and isotope composition of its origin.

- If the molten material relocates to the lower plenum, then a new entity is formed again, and all the isotopes that were relocated to the lower plenum via melt transfer are handed over to VENTINA for further decay.

By implementing the above-described logic, ATHLET-CD can be used together with VENTINA to simulate the effects of the decay of fission products adequately. As a next step, verification calculations were performed.

2.4.3.3 Integration of VENTINA into COCOSYS

The integration of VENTINA into COCOSYS is subject of RS1598, a description of the development is therefore omitted here.

2.4.3.4 Verification of the integration process

The refactoring of the fission product inventory and decay modelling was a large task, the changes had an effect at multiple parts of the code. In order to make sure that the implemented changes and modernisations work as intended, verification calculations were performed. One of such calculations is described here to verify that the first and main phase of the integration of VENTINA into ATHLET-CD was successfully achieved.

A simple sample input deck was constructed to be able to analyse the different important phenomena, where the effects of VENTINA can be checked. The core of the input deck is divided into two rings and axially into 26 nodes. Each ring has 20000 fuel rods assigned to it. The rings are located in the thermofluidic objects (TFO) “Bundle” and “Outer”. The beginning of the core is connected to a “Fill” object, that just delivers a constant steam mass flow during the entire simulation. The ends of the core objects are connected to a TFO “Plenum” that acts as an upper plenum. From here on, a pipe divided into three segments (“HOTPIP”, “STGEN” and “COLPIP”) connects the upper plenum with a time dependent volume “CONTAN” that represents the containment. A schematic representation of the nodalisation of the used model is shown in Fig. 2.70.

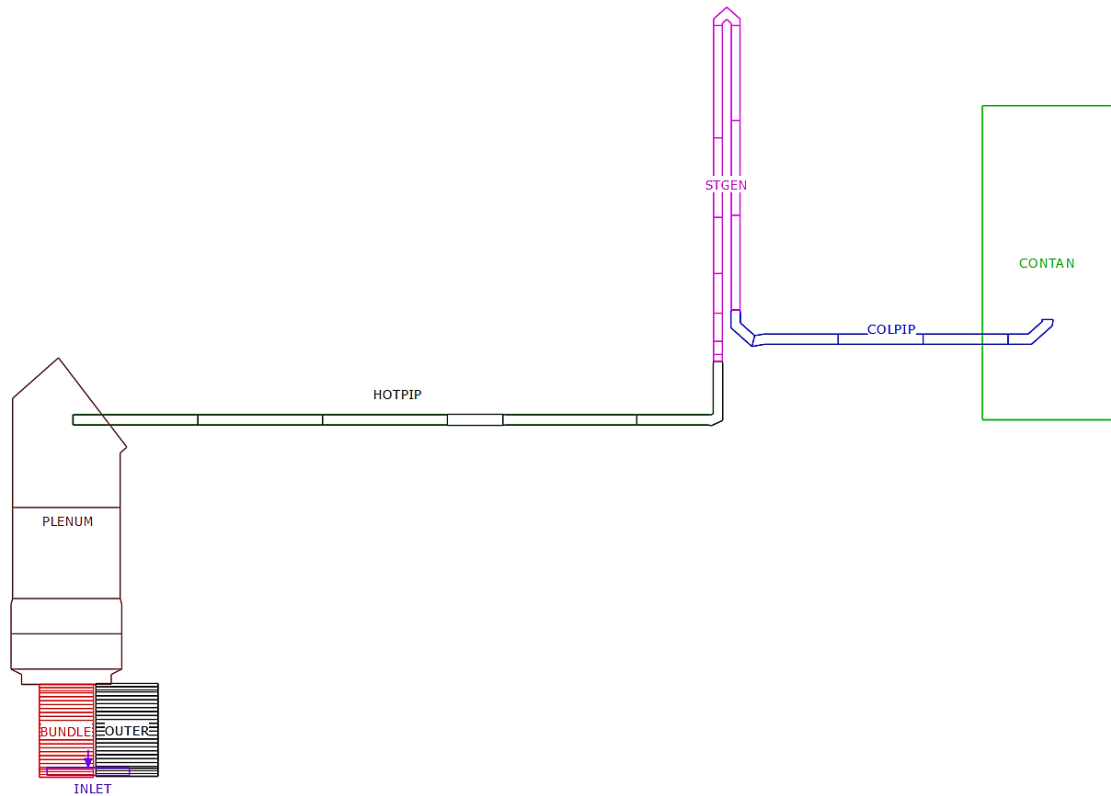


Fig. 2.70 Nodalisation of the verification sample

During the whole simulation the system was only filled with steam, in order to limit cooling of the core and to achieve a fast-running sample, where fission product release and material relocation can be analysed. The two horizontal core nodes (rings) have the same amount of fuel rods assigned to them, however, with different power histories, therefore their isotope composition differs, which also leads to different decay power in the individual rings (Fig. 2.71).

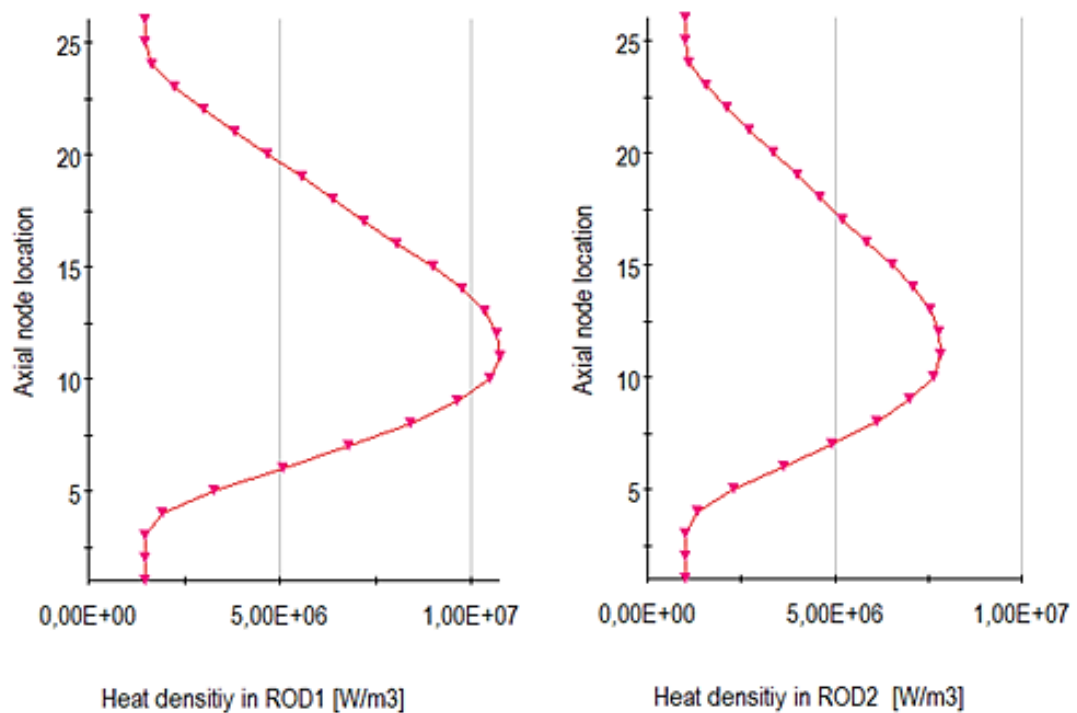


Fig. 2.71 Different decay power distributions in the core due to different power histories

As a result of the decay in the fuel rods and due to insufficient cooling via steam, the core heats up and fission product release starts. Fig. 2.72 shows as an example how Xe is released from the core and simultaneously the mass in the core reduces.

At $t = 375$ s molten material relocates from the core the lower plenum. This results, firstly, in the appearance of decay power in the lower plenum. Simultaneously, the remaining power in the core reduces. Parallel to these events, fission products are continuously released, removing some power from the core. All these power changes can be seen in Fig. 2.73. The figure also shows the sum of all powers (red line). This shows that the energy balance of the system is maintained, and that the decay of isotopes is calculated constantly, as a general decline of the total decay power is visible.

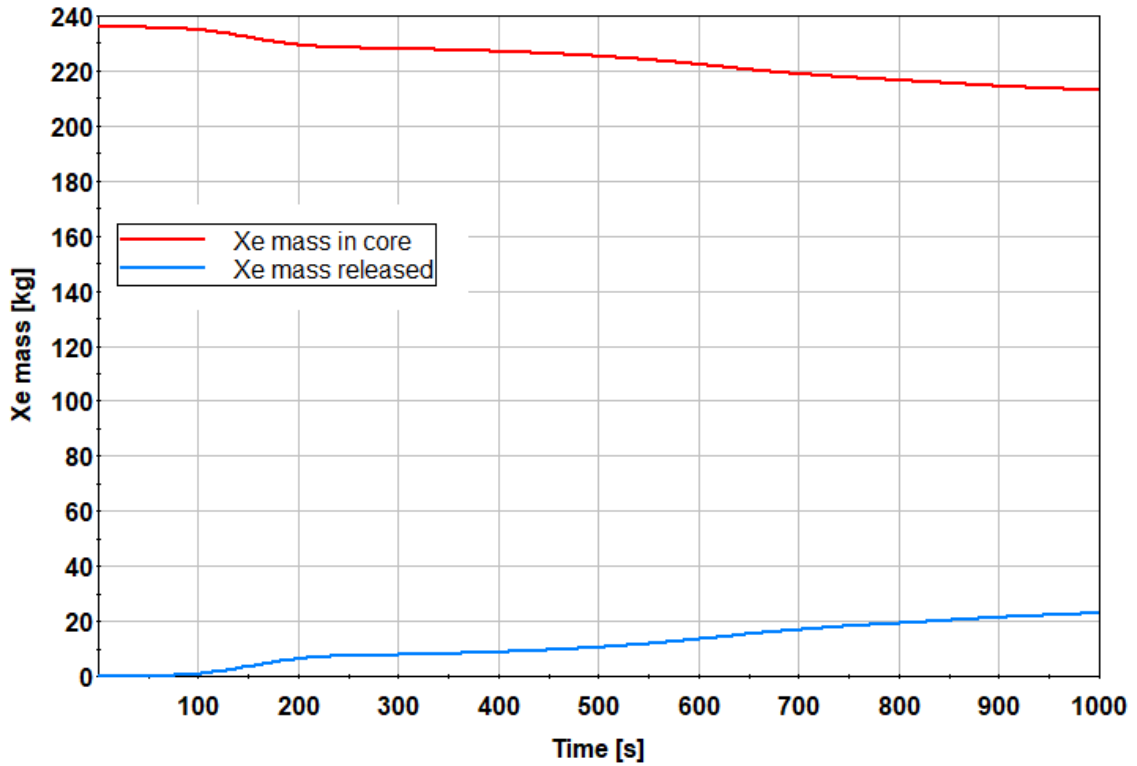


Fig. 2.72 Evolution of Xe mass in the core and in the cooling circuit

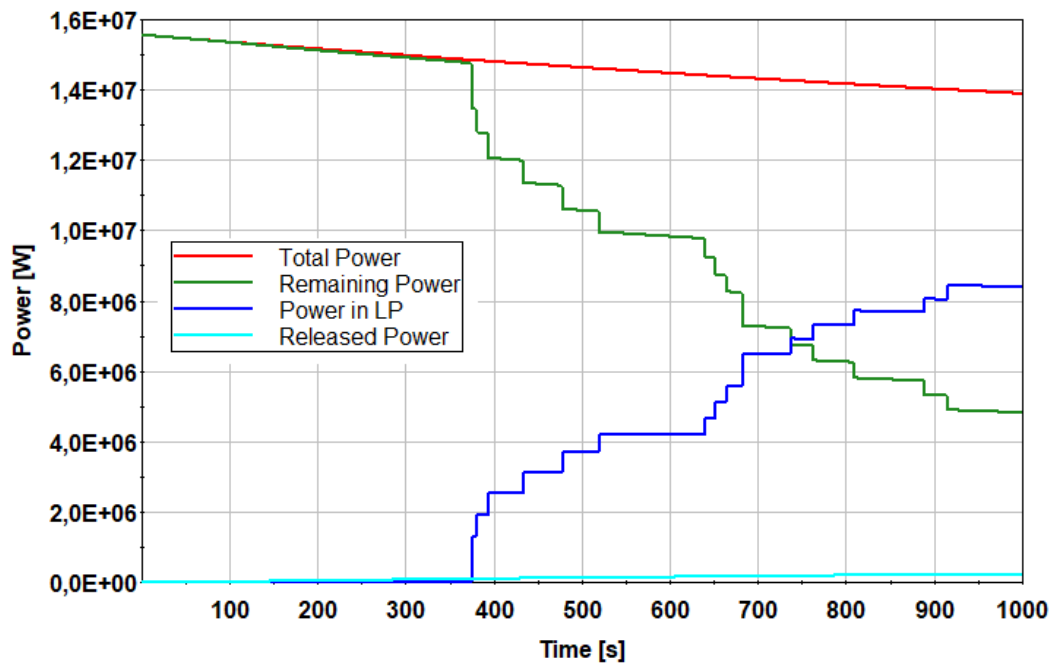


Fig. 2.73 Evolution of the power of the released, relocated and remaining isotopes

The released and transported fission products continue to decay and interact with the environment. Fig. 2.74 and Fig. 2.75 show that the majority of the released fission products give off their decay power to the first 5 wall nodes above the core. This shows, first of all, that the fission products are transported in the cooling circuit. Secondly, it shows that their decay is simulated and assigned to fluid/wall entities. A sudden drop in the power after node 5 is explainable by the fact that a relatively small pipe is the exit from the upper plenum (Fig. 2.70), therefore most of the fission products stay in the large, upper plenum volumes and on its walls and give off their energy there.

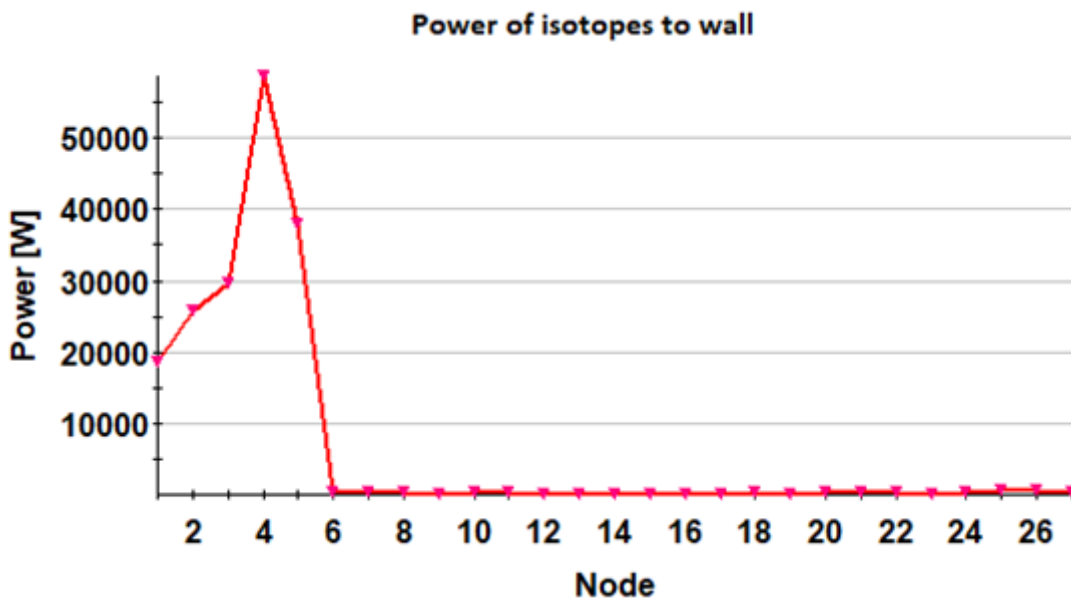


Fig. 2.74 Power distribution in the cooling circuit (to wall)

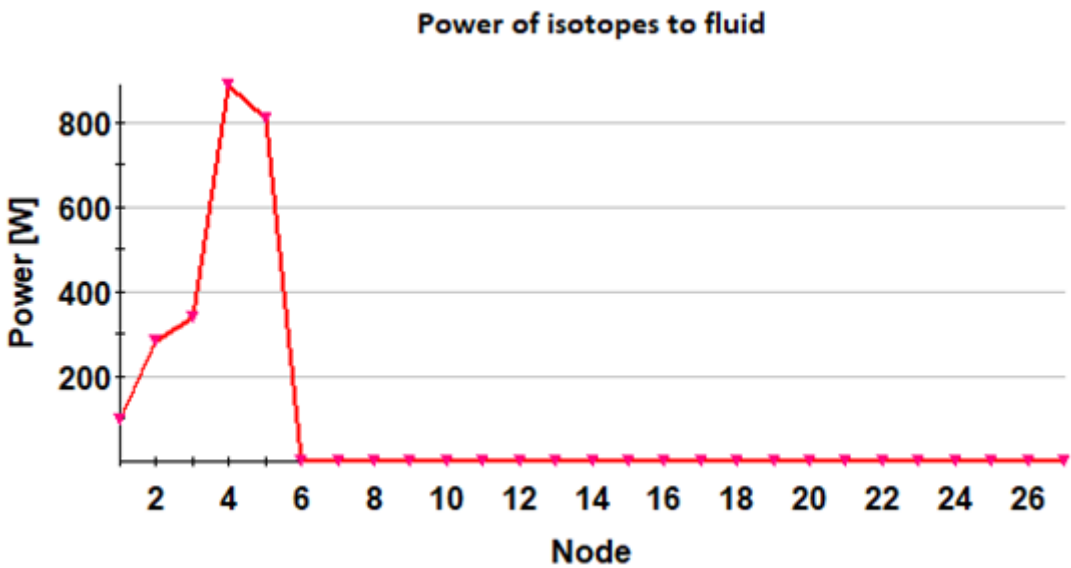


Fig. 2.75 Power distribution in the cooling circuit (to fluid)

Based on this verification, we can conclude that:

- VENTINA generates an initial fission product inventory for ATHLET-CD that is dependent on the defined input (and thus adjustable).
- The generated decay power is released at the adequate locations, leading to heat up and melting of the core.
- The released fission product masses and their associated power are subtracted from the core and transported within the cooling circuit.
- The masses, fission products and their powers are subtracted from the core inventory, when material relocates to the lower plenum.
- The released fission products are transported and can decay at any part of the defined SAFT path.
- The decay of isotopes is successfully calculated with VENTINA, proving the continuous and successful coupling of ATHLET-CD with VENTINA.

With that, the refactoring of the models for inventory and decay calculations is finished. Further tasks for the future are to optimise the whole VENTINA-ATHLET/CD interaction and to adjust/extend the newly implemented models to the needs of the users. Also, an extensive validation is to be done, combined with COCOSYS, before these new models for new fission product inventory and decay are part of the official release of AC²/ATHLET-CD.

2.4.4 Increasing the usability, fixing limitations, and refactoring of SAFT

Motivation

In SAFT, the user only has to specify a list of TFOs that should be considered as possible transport paths in the fission product calculation. However, there are some aspects that need to be considered when defining the network. Among others, the following points were important to allow for a network definition that is consistent and error-free:

- Each SAFT loop must be defined separately.
- A HECU or HEAT object must belong to each TFO.

- A branch in the transport path must be modelled by a branch TFO in order to be able to calculate all paths adequately with the correct thermal-hydraulic states.
- A maximum of one starting point may be defined in a SAFT loop.
- Single Junction Pipes (SJPs) must not be defined as outflow locations.

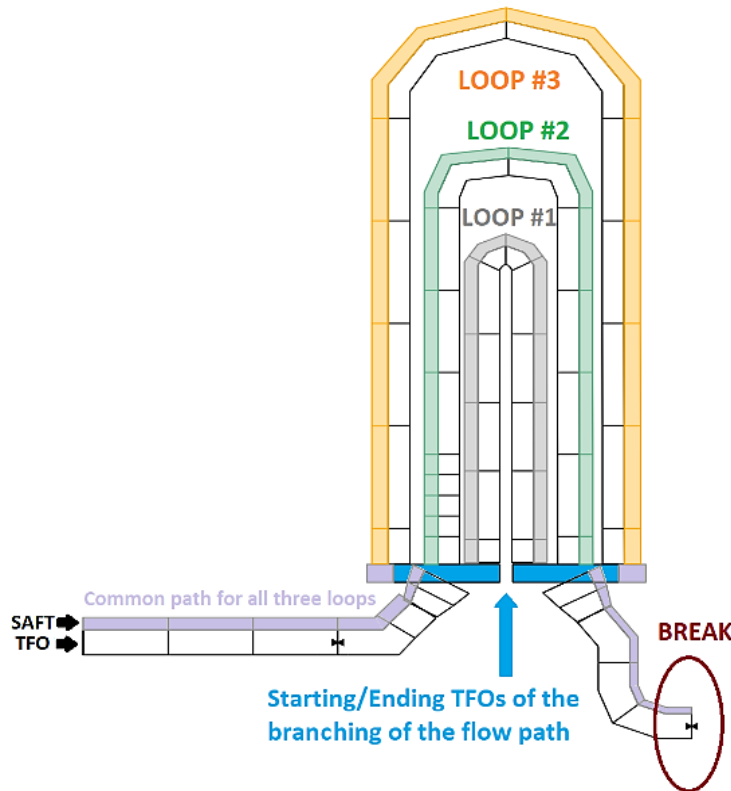


Fig. 2.76 Example of SAFT network

Within the RS1574 project, improvements have been made to make SAFT network construction easier and more comprehensive. Tasks and refactoring needs were deduced from user-feedbacks.

Developments

In order to be able to continue to use existing data sets as unchanged as possible and to keep the conversion effort from ATHLET to ATHLET-CD low, the option of defining a single junction pipe (SJP) as an outflow location was made available.

Outputs: The user is always informed if an SJP has been defined as an outlet. Under the summary data of the SAFT network, both the total number (simple + SJP outlets) and the number of SJP outlets are reported. See Fig. 2.76 and Fig. 2.77.

ATHLET NETWORK DATA

#OBJECT	ATHNAM	L-CON-VOL	R-CON-VOL	L-VOL	R-VOL	IBO	IEO	ITYPO	PRI-C
4	CORE	12	22	15	20	3	5	20	1
5	BRANCH	20	24	22	22	0	0	1	1
6	PIPE	22	31	24	28	5	7	20	1
7	PIPE_A	28	37	31	35	6	8	21	1
18	SJP	28	80	0	0	6	17	22	2
9	PIPE2	22	50	39	48	5	10	20	3
15	PIPE2_B	45	78	73	76	9	16	21	4
11	PIPE3	22	63	52	61	5	12	21	5

Note: There are SJPs, that model OUTLETS.

SAFT NETWORK DATA

NUMBER OF VOLUMES	:	41
NUMBER OF JUNCTIONS	:	45
NUMBER OF SINGLE JUNCTION PIPES	:	1
NUMBER OF INPUT JUNCTIONS	:	1
NUMBER OF OUTLET JUNCTIONS	:	5
Out of which are SJPs	:	1
Created from Dead Ends	:	0

#S-JUN	#S-L-V	#S-R-V	#A-JUN	#A-L-V	#A-R-V	#INP-J
.
.
.
43	41	-1	65	76	-1	0
44	37	-1	51	61	-1	0
-----		SJP OUTLETS	-----			
45	12	-3	71	28	-3	0

Fig. 2.77 Information about single junction pipes in SAFT

Branching of the SAFT Network

A branch object was previously required to create a branching within the SAFT path. In future, this is no longer required. Furthermore, "internal branching" from ATHLET will be transferred to the SAFT path in future. Until now, this has not always happened automatically and not reliably enough. Nevertheless, the user should consider whether a branch object would not be necessary/advisable because of the thermal-hydraulic conditions. There are three types of branching in ATHLET:

- With Branch object (ITYPO=0): several TFOs can be coupled. If necessary, special information regarding the momentum flux can be defined under PW BRANCHING /PW BRANCH2M. (Fig. 2.78). No change is necessary for SAFT.

- Without branch → Changes necessary:
 - At the end of the TFOs: simply append several TFOs at the start or end of a TFO (Fig. 2.79 and Fig. 2.80).
 - Within a TFO, couple another one (Fig. 2.81)

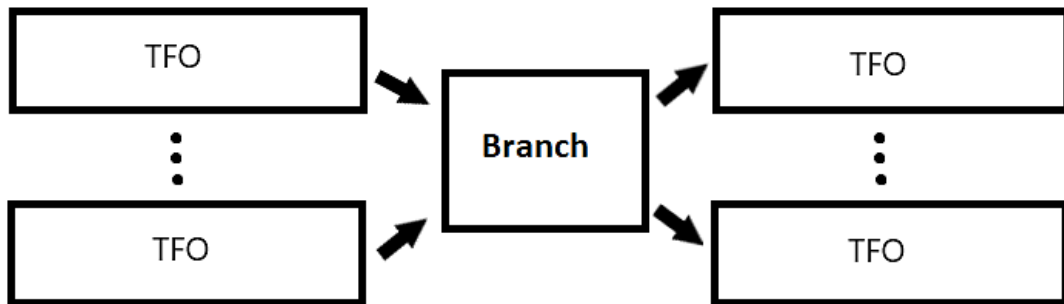


Fig. 2.78 Branching with “Branch” object

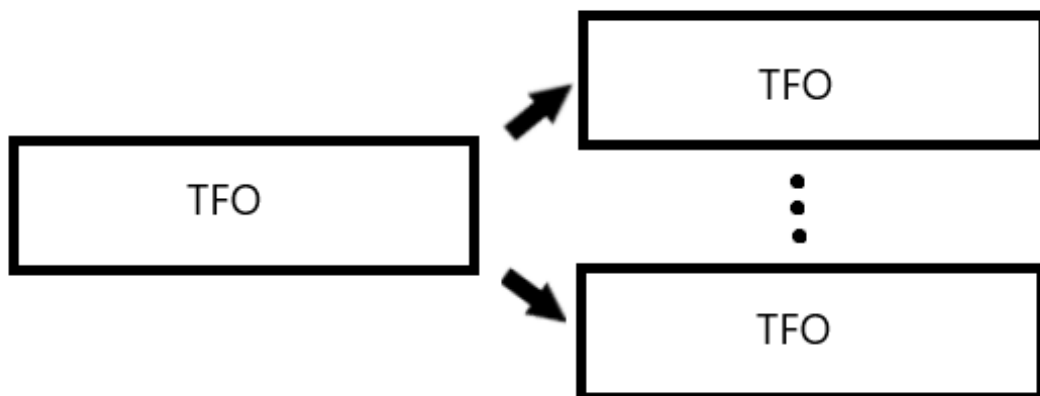


Fig. 2.79 Simple branching without “Branch” object (start)

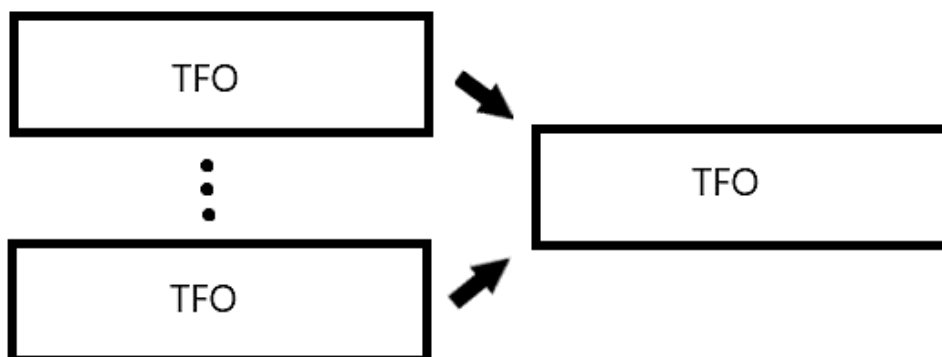


Fig. 2.80 Simple branching without “Branch” object (end)

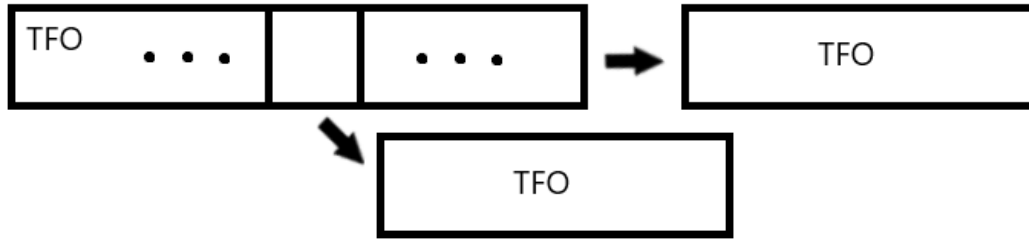


Fig. 2.81 Internal branching

Implementation

JTNET (ATHLET Parameter):

- 1 junction simulating internal branching
 - 0 standard Junction
 - -1 interface junction
 - -2 dead end junction or interface junction
- } Not to be integrated

If $JTNET < 0$ no SAFT connection is to be created. In the case of a simple junction ($jtnet = 0$), the rightmost CV is searched for (either within the TFO or the first CV of the next, rightmost TFO). In the case of $JTNET = 1$, the connection is taken from ATHLET without any change. This allows the simulation of connections as shown in Fig. 2.81. Furthermore, $JTNET = 1$ also models the branching shown in Fig. 2.80. In order to be able to model this in the SAFT, the ATHLET junction is determined in this case as well as the first CV of the TFO attached to the right side. The latter two variants (branching variants shown in Fig. 2.79) occur, for example, in the simulation of steam generators, provided that the steam generator tubes of different lengths are modelled with different TFOs, as shown in Fig. 2.76.

Dead End in SAFT network

There was no check before whether a SAFT path ends meaningfully, e. g. in an exit, or in another SAFT path, or not. This could lead to dead ends for SAFT paths that end without a starting point or connection to other SAFT objects (Fig. 2.82), i. e. at an ATHLET CV. This can cause problems if thermal-hydraulic junctions continue flows from the ATHLET CV even though the SAFT path has ended. In this case, the carrier gas continues to flow but the fission products are not transported further. This can lead to increased deposition at the dead end of this SAFT path or to mass balance errors.

To address this problem, a check has been included to alert the user to this. In addition, the possibility was created to eliminate this automatically. In order to change the network as little as possible, it was decided to convert dead ends into "theoretical" outlets. These outlets work in the same way as normal outlets, i. e. fission products are removed from the ATHLET-CD domain but should not be used when coupling to COCOSYS. The purpose of such outlets is to provide the user with information about the "neglected" path, as well as to maintain the mass balance. If a comparatively large amount of fission products is transported in this direction, the user can see it immediately and define the affected path.



Fig. 2.82 Dead end in SAFT network

Should a real physical dead end be simulated in ATHLET, which is also defined in the SAFT, everything remains as it is, of course, since it is a physical "dead end".

If a dead end occurs in a SAFT path, the ATHLET junction number is searched for. The right control volume is not determined, but the thermohydraulic parameters (flow parameters) linked to the junction are taken over by ATHLET.

If a conversion of the existing SAFT dead end is carried out, the user is informed by a message. Furthermore, detailed information is provided as to where and in what form this conversion has taken place. See Fig. 2.83.

```

WARNING ==> Subroutine TATNOD (Severity Code 4):
           Dead end
Dead end is found in the SAFT network.
Each dead end is turned into an outlet!More information under SAFT Network Data

```

SAFT NETWORK DATA

```

NUMBER OF VOLUMES           : 46
NUMBER OF JUNCTIONS         : 50
NUMBER OF SINGLE JUNCTION PIPES : 0
NUMBER OF INPUT JUNCTIONS    : 1
NUMBER OF OUTLET JUNCTIONS   : 5
Out of which are SJPs       : 0
Created from Dead Ends      : 1

```

```

#S-JUN #S-L-V #S-R-V #A-JUN #A-L-V #A-R-V #INP-J
  :      :      :      :      :      :      :
  :      :      :      :      :      :      :
-----DEAD ENDS-----
  50     42     -2     57     69     -2     0

```

49	OUTLET	JUNCTION	VOL_0046	OUTLET	VOL_0046	OUTL_4	JUN.PRIM	PRIMARY	4	0	46	-1	0	1
50	OUTLET	JUNCTION	VOL_0042	OUTLET	VOL_0042	OUTL_5	JUN.PRIM	PRIMARY	5	0	42	-1	0	1

```

-----
The following outlets are created in order to avoid Dead Ends in the SAFT network:
OUTL_5
-----

```

Fig. 2.83 Information about automatically converted dead ends

As this is a major change, the possibility of controlling it has been made available to the user. The control of the automatic change of the network is done with the help of the input parameter IOPSOP. In order to draw the user's attention to this change, it has been decided that the old entries will lead to a program stop at the dead end. Of course, an error message and a hint to fix the problem in this case will be given (Fig. 2.84).

```
ERROR ==> Subroutine TATNOD (Severity Code 8):  
Dead end
```

```
TRACEBACK NO.      1 PROVIDED BY SRRTRA AT T=  0.00000E+00:  
Image              PC              Routine              Line              Source  
libifcoremd.dll   00007FFB0886820A Unknown              Unknown           Unknown  
athlet.dll        00007FFAFB85A52C c_service_mp_srtr   91               srrtra.F90  
athlet.dll        00007FFAFBC8622E serror_             208              serror.F90  
core_degradation. 00007FFAFA93C839 tatnod_             751              tatnod.F90  
core_degradation. 00007FFAFAB649E2 tsonod_            123              tsonod.F90  
core_degradation. 00007FFAFAAD0690 tsoph_             308              tsoph.F90  
core_degradation. 00007FFAFAC16A91 tsomain_           195              tsomain.F90  
athlet.dll        00007FFAFBDEE5D7 ainl_              665              ainl.F90  
athlet.dll        00007FFAFBBE69E4 athlet_IP_athlet_  219              athlet.F90  
fde.2.8.0.dll     00007FFB24972479 Unknown              Unknown           Unknown  
fde.2.8.0.dll     00007FFB249722B8 Unknown              Unknown           Unknown  
fde.2.8.0.dll     00007FFB248B2734 fde_try_interface  97               exception.fmod  
athlet.dll        00007FFAFBBE59B3 athlet_            14               athlet.F90  
athlet_main.exe   00007FF6E54C103E MAIN_              4                athlet_exe.F90  
athlet_main.exe   00007FF6E54C3162 Unknown              Unknown           Unknown  
athlet_main.exe   00007FF6E54C34C8 Unknown              Unknown           Unknown  
KERNEL32.DLL     00007FFB7C2A7974 Unknown              Unknown           Unknown  
ntdll.dll         00007FFB7CC2A0B1 Unknown              Unknown           Unknown
```

```
Dead end is found in the SAFT network.  
At least one SAFT Loop ends in a dead end, but TFO connections are available.  
For automatically creating outlets instead of the dead ends check IOPSOP!
```

Fig. 2.84 Error message in case of a dead-end detection

IOPSOP controls the output range of the SAFT module. To allow automatic conversion of the dead end to the outlet, this parameter must be negative. The original functionality is determined by the absolute values of the parameter.

3 WP2: Simulation late phase

3.1 WP2.1: Improvements in LHEAD and AIDA

3.1.1 Implementing the recent AIDA developments in LHEAD

Motivation

In the current version of ATHLET-CD there are two modules available to model the late phase in-vessel phenomena in the lower plenum: the modules LHEAD and AIDA. LHEAD is a part of the module ECORE, it allows the 2D nodalisation of the lower plenum (LP) using the core regions of ECORE for vertical node number. LHEAD does not include an own model for the LP wall, heat conduction is calculated via coupled HCO elements from ATHLET. LHEAD does not have built-in LP failure models, the modelling of the wall failure relies on the HCO modelling. AIDA is a separate module, with 0-dimensional solution for the molten pool layers and with an own 2D wall model coupled via GCSM signals. The wall model of AIDA calculates the heat conduction, wall ablation, and wall failure and can be coupled with HCOs in case of external cooling simulations (see chap. 3.3). Furthermore, the GCSM coupling allows to perform fast running stand-alone AIDA calculations.

The two LP module are currently at a different level of development. Basically, in the current code version both modules are capable to simulate a homogeneous molten corium pool until wall failure but without modelling wall ablation, but they have different input and output parameters. Moreover, AIDA has been further developed to enable state-of-art simulation of the lower plenum processes. The most important features in AIDA which are not part of LHEAD module are:

- enhanced modelling of geometry (different LP shapes),
- modelling of stratified molten corium pool, and
- LP wall ablation.

The future goal regarding LP models is to provide one lower plenum module in ATHLET-CD, which includes the more flexible way of pool modelling of LHEAD and the modelling features of AIDA. Within this WP the necessary preliminary work and first steps have been performed to achieve this goal.

Developments

The first step of harmonisation is to build an input deck which allows comparative calculations of the two modules. For this, the sample-s8 has been modified. The modified input allows performing fast running calculations with the two LP module at the same time. This supports the code-development processes very well.

The second step of the harmonisation comprises the preparation of consistent output variables to enable the comparison of the modules. About 20 variables have been identified, which are currently not or not directly available in LHEAD and are necessary for the evaluation. A new output keyword LHEAD-DATA has been defined, which triggers a completely equivalent output of LHEAD variables to the respective AIDA output. The implementation of further LHEAD output variables is ongoing.

The third step of harmonisation is to ensure the common modelling capability for both modules and the harmonisation of the input decks. To ensure this, first LHEAD has to be equipped with the new models of AIDA and the in both modules existing models have to be implement within one common subroutine.

In the project several AIDA subroutines have been modified, split up to be more modular and extended to enable to be called from LHEAD and acting as a common routine. The changes have been made for the routines for simulating:

- upper pool surface heat transfer,
- crust formation, and
- melt discharge.

Since several modelling features are related to the LP wall, the concerned AIDA subroutines have been written in a way, which facilitates a future separate LP wall model, which can be used from both modules. These routines handle the modelling of:

- LP geometry,
- wall heat conduction, and
- wall ablation.

With the current modifications it is possible to run and compare calculations with the two modules, which is the prerequisite of further code development. The modifications of the subroutines in some cases already allow using common routines supporting the further code development processes and maintenance. Moreover, the restructured AIDA routines can be more easily connected to LHEAD and to extend it with new models.

Further development is contingent on substantial structural changes of ATHLET-CD, this is one of the topics of the follow-up project.

3.1.2 Allowing a “Fill” function for melt for LHEAD

Motivation

LHEAD is one of the lower plenum modules of ATHLET-CD. LHEAD is strongly coupled with the core structures and nodalisation, therefore it receives its input parameters (relocated melt mass and its properties) directly from the core. These parameters depend on the simulated scenario. The user cannot define these parameters via the input.

If the user wishes to simulate an experiment to verify and validate LHEAD models and/or if he wants to compare reactor scenarios with predefined parameters (for example: benchmarks), then an option for definable LHEAD input parameters is needed. Without this option, the user has to artificially adjust the core melting scenario to get to the desired LHEAD boundary conditions. This “workaround”, however, is very time consuming and difficult to achieve. Therefore, it was decided to implement an option, where the user can define LHEAD input parameters in the input deck.

Model development

Before any code changes were done, the following considerations for the stand-alone option were decided:

- Due to the structure of LHEAD, users still have to define a core, however, if the standalone option is activated, then the core power is set to zero and it does not influence the simulation.
- The user has to define the boundary conditions and nodalisation for LHEAD, just as in coupled mode.

- A stand-alone calculation starts with melt already in the lower plenum. The parameters of the melt have to be defined by the user via the input deck.
- Additional melt can relocate to the lower plenum also in stand-alone mode, their parameters also have to be provided by the user.

The required code changes to provide this option to the user are of structural nature. The already existing routines had to be extended, so that they don't receive their parameters directly and automatically from the core melt models but are read from the input deck. The following required input parameters were identified:

- Initial melt mass of ceramic (INITCER), metallic (INITMET), control rod (INITCONT) and structure (INITSTEEL) material [kg]
- Further melt mass flow (MCER, MMET, MCONT, MSTEEL) versus time [kg/s]
- Temperature of the inflowing molten ceramic (TCER), metallic (TMET), control rod (TMCONT) and structure (TMSTEEL) material [K]
- Power of melt versus time (DECLP) [W]
- Density (RHO-CER/MET/CONT/STEEL), heat capacity (CP-CER/MET/CONT/STEEL) of molten ceramic, metallic, control rod and structure material versus temperature [kg/m³], [J/(kg K)]

The user has to provide this information via table input at an already existing location in the input deck, under the pseudo keyword HEATINPTAB (as shown in Fig. 3.1):

```

----- HEATINPTAB
3
3  T-RHO          T-CP          time-T
3  HCONC          DENS          HTCAP
   'RHOCER'      'CPCER'      'TMCER'
   'RHOMET'      'CPMET'      'TMMET'
   'RHOCONT'     'CPCONT'     'TMCONT'
   'RHOSTEEL'    'CPSTEEL'    'TMSTEEL'
3  time-kg/s
   'MCER'        'MMET'        'MCONT'
   'MSTEEL'      'DECLP'      'DUMMY'
   'DUMMY'       'DUMMY'
3  time- W
   'DUMMY'
   'DUMMY'
   'DUMMY'

```

Fig. 3.1 Definition of input parameters for LHEAD stand-alone calculation

This location originally reads parameters for the core region, but in stand-alone mode that information is unnecessary, therefore they can be used to provide data required by LHEAD. Additionally, the user has to define whether he wants to use the stand-alone option or not (STANDALONE = 1, option active, STANDALONE = 0, option not active), and he also has to define the initial melt masses in the lower plenum. This is done under the pseudo keyword "LPAC", like shown in Fig. 3.2:

```

----- LPAC
@
@ NDIVLP      ILHMOD      Standalone
   4          2          1

@ INITCER,      INITMET,      INITCONT,      INITSTEEL
  1.8437D+01    2.4252D+00    5.4462D-01    0.0

```

Fig. 3.2 Activation of stand-alone option and definition of initial masses

The tables in Fig. 3.1 are defined under the keyword "Tables" as shown in Fig. 3.3.

```

~
]C----- TABLES
@
@ DENSITY
@      temperature      density
K----- RHOSTEEL
      273.D0      7000.D0
      2000.D0     5000.D0
@
@ HEAT CAPACITY
@      temperature      heat capacity
K----- CPSTEEL
      273.D0      800.D0
      2000.D0     500.D0
@
@ TEMPERATURE OF STEEL
@      time      temperature
K----- TMSTEEL
      0.00      1666.D0
      473.D0     2666.D0
~

```

Fig. 3.3 Sample of the used tables

Verification

To check if the newly implemented stand-alone function works as intended, two simple sample calculations were performed. First a calculation with LHEAD was started. The purpose of this simulation was only to verify the newly implemented option; therefore, the whole calculation uses a very coarse, fast running input deck. First, melt was formed after around 300 s, relocation to the lower plenum and activation of LHEAD was initiated via a time signal at 1500 s. The simulation was terminated after 3000 s. Based on the results of the coupled calculation a new input deck was created, where LHEAD is started via the stand-alone feature. The initial input parameters were the parameters the coupled calculation had at 1500 s. This can be seen in the first 1500 s of Fig. 3.4 and Fig. 3.5. In the coupled case, values are only available from 1500 s, while for the stand-alone case the values are already present from the beginning. The same amount of melt is in the core as after relocation in the coupled case and the initial power in the melt matches the core melt power in the lower plenum after melt relocation in the coupled case. This time shift in the melt power is correct given the modelling assumptions. For test purposes, in the stand-alone case additional melt was added to the lower plenum, to prove the possibility of continuous melt relocation. This is the reason why melt masses and power of melt increases between 1900 and 2000 s in the stand-alone case.

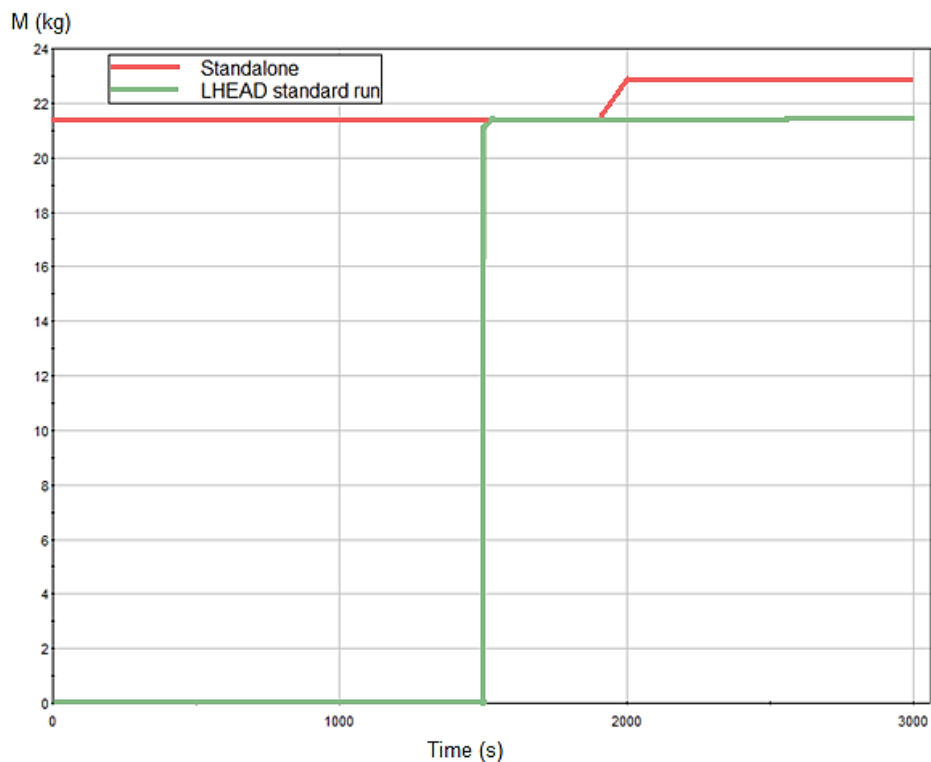


Fig. 3.4 Melt mass in the lower plenum: stand alone and coupled calculation

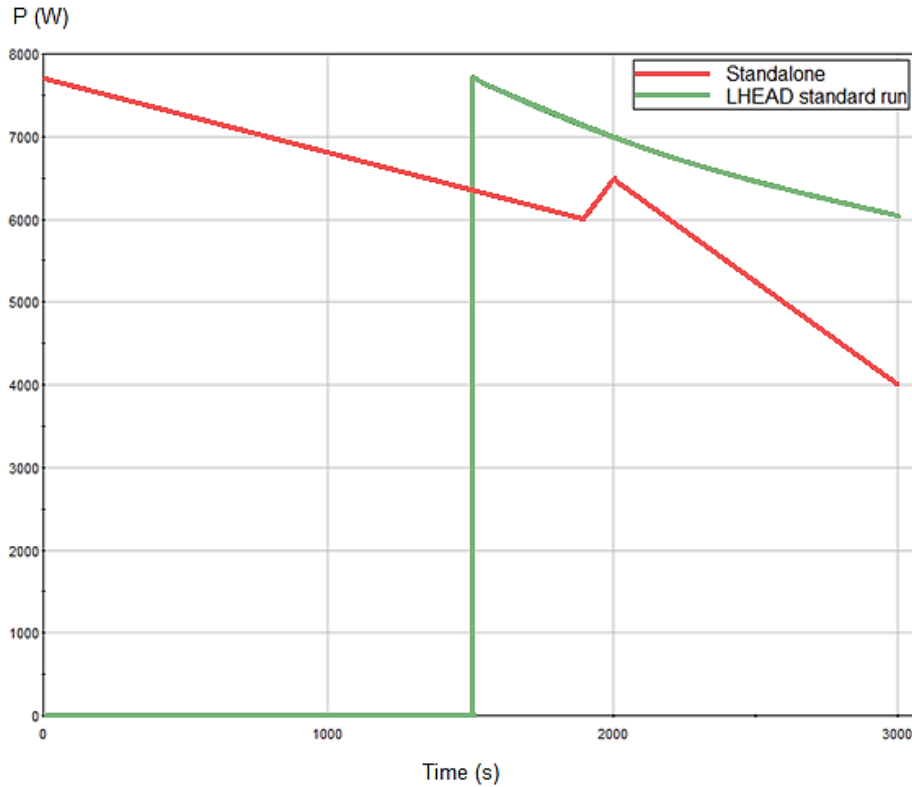


Fig. 3.5 Decay power of melt in the lower plenum: stand alone and coupled calculation

With the aforementioned assumptions and implementations, proven by some simple verification calculations, the user has now an option to define the LHEAD input parameters independently from the core. This allows easier code-to-code comparisons, recalculations of LP phenomena experiments, and facilitates future improvements.

3.1.3 Model for decay power calculation in the metallic layer in the lower plenum

Motivation

In the previous versions of ATHLET-CD, users had to predefine the ratio of fission products (and the associated decay power) in the metallic layer of the corium pool in the lower plenum, although this information would be available from the simulation. The objective was to allow the code to gather this information internally, instead via explicit user input.

Developments

In order to efficiently achieve this objective, the replacement of OREST/FIPIISO with VENTINA (see chap. 2.4.3) had to be finished first. Therefore, the final implementation had to wait for that step.

In the core, during the melting process the code assigns to each new melt rivulet a variable, that describes the fraction of fission products in that melt:

- $FP_ceramic(I,J) = X$, FP fraction in ceramic melt at location I, J is X
- $FP_metallic(I,J) = 1-X$, FP fraction in metallic melt at location I, J is 1-X

Of course, the sum of these two variables equals one, as they together represent all the fission products a node has. If the corium relocates from the core to the lower plenum an average of $FP_metallic$ was needed. To do so, the following was done:

$$FP_{metallic_{avg}} = \frac{\sum_{i=1}^{i=number\ of\ rings} \sum_{j=1}^{j=number\ of\ axial\ nodes} FP_metallic(i,j) * MELTMASS(i,j)}{\sum_{i=1}^{i=number\ of\ rings} \sum_{j=1}^{j=number\ of\ axial\ nodes} MELTMASS(i,j)} \quad (3.1)$$

With that, we have the average FP fraction in the metallic layer in the lower plenum. We also know the amount of fission products (and power = $Q_{decay_{LP}}$) relocated to the lower plenum. With that, the amount of fission products in the metallic phase and therefore also the accompanied decay power can be determined via:

$$Q_{metallic_layer} = FP_{metallic_{avg}} * Q_{decay_{LP}} \quad (3.2)$$

With this relatively simple improvement the user has one less input variable to define. This leads to easier input generation, more realistic and adequate power distribution in the lower plenum and a reduction of the user-effect.

3.1.4 Model for thermochemical effects in the lower plenum

The relocated corium in the lower plenum is a mixture of degraded core material and consists of UO_2 , partially oxidised zirconium (ZrO_2 , Zr) and steel (from the molten structures). The composition of the corium in the lower plenum has a significant effect on the heat flux distribution along the lower plenum wall and with this also on wall damage and failure.

In a standard simulation, the corium pool is assumed to be a well-mixed homogeneous molten pool or a two-layer stratified pool. In the second case, as a consequence of the poor solubility of the metallic material in the oxidised material, a metal layer forms on the top of the oxidised layer due to density difference. In the lower plenum modules of AC² (AIDA and LHEAD) the stratification happens immediately based on the metallic and oxidised material masses provided by ECORE. The current version of AIDA and LHEAD does not consider any thermochemical phenomena between the different materials in the corium pool, the phases are considered chemically independent.

The composition of the corium pool is strongly depending on the Zr oxidation ratio /BAR 21/. The above mentioned two-layer model describes a case with fully oxidised Zr. In case of sub-oxidised corium, at high temperatures the free metallic Zr could chemically interact with the UO_2 and with this reduce the oxide mass. In case of a low quantity of molten steel (e.g. initial phase of relocation), enough Zr and U could be added to the metal layer that it becomes heavier than the oxide phase and settles on the bottom of the lower plenum /SAL 04/. In case of wall ablation or further molten metal addition also a three-layer configuration with a dense metal layer, an oxide layer and a light metal layer is possible. These thermochemical processes affect the heat flux distribution to the vessel wall and the focussing effect. Additional to this interaction, fission products which have affinity with the metallic materials will accumulate in the metal layer and determine the decay heat partitioning between the layers /SAL 04/, /SEI 01/. While the formation of three layers is only assumed for a short term, when steel mass is added, and not for a later steady state configuration, it could lead to a significant increase of wall thermal loads. Therefore, the modelling of the thermochemical effect and the layer transitions are important.

Since these are very complex phenomena, which need the development of several sub-models suitable both for LHEAD and AIDA, first a corresponding developer branch has been created based on ATHLET-CD 3.3. In the first step the development has been carried out for AIDA but under consideration of the later easy application of the models for LHEAD. The first step of modelling the separation process is to provide the complete data of the corium composition (mass of UO_2 , ZrO_2 , Zr, Steel) for the lower plenum modules. For this purpose, the common subroutine of LHEAD and AIDA has been extended with the necessary quantities (metallic Zr).

The thermohydraulic modelling of the migration of Zr and U from the oxidic phase required a complex modelling of chemical reactions or access to a relevant database. However currently there are quite extensive experimental data available (e.g. MASCA tests /SAL 04/, /ASM 04/, /BAR 21/). For the development of a first model of the thermochemical separation a simple correlation has been derived from the available experimental data considering of pool configuration, composition and temperature. The development of the correlation is not finished yet and is planned also to be enhanced with new insights from the already ongoing IAEA CRP project (J46002 "*Developing a phenomena identification and ranking table (PIRT) and a validation matrix and performing a benchmark for In-Vessel Melt Retention*"). After the separation calculation, the amount and the density of the layers can be determined. With this, it is possible to evaluate the initial configuration. The modelling of further molten material addition and the transient behaviour of layers towards reaching a thermal equilibrium can be modelled using additional simplified correlations and models derived from further investigations /BAR 21/ (e.g. the U transport is closely related to free Zn and steel addition).

Since the current lower plenum modules can only handle the standard two-layer configuration (oxide on the bottom, metal on the top), introducing a third, heavy-oxide layer is necessary. The module LHEAD already uses horizontal nodalisation for the corium pool and can solve the thermal equilibrium for each node separately. In principle this method allows to simulate more layers if the nodes are assigned to the appropriate layer and if the nodalisation is fine enough. Whereas AIDA models each layer 0-dimensionally and separately. The goal is to reach a common way of pool modelling that also can consider a possible three-layer (or more) configuration. For this, first the modelling scheme of the AIDA has to be replaced with the modelling scheme of LHEAD. This work is ongoing.

The partitioning of the decay heat between the layers is currently defined via user input in AIDA. A new method has been introduced in the correspondent developer branch based on the U/Zr partition in oxide and metal layer. See also chap. 3.1.3.

The implementation and the verification of the above-mentioned models could not be finished in the project because one of the key influencing parameters, the oxidic mass, is not yet properly modelled. A detailed modelling of the fragmentation of the relocating melt is needed to predict the amount of oxidic mass in the lower plenum adequately. The modelling of the fragmentation of the melt when it gets into contact with water is a topic of the follow-up project. Since the modelled phenomena are strongly interconnected, verification is only feasible after the complete implementation of all the several sub-models, including the residual oxidation of the relocated molten material, has been finished. The current version in the developer branch is prepared for the necessary input data and the separation model is tested with a two-layer model.

3.1.5 Model for considering the order of melt relocation from the RPV into the containment after RPV failure

Motivation

The existing discharge model in LHEAD and AIDA has been developed for a homogeneous melt pool in the lower plenum. However, modelling of a segregated molten pool in the lower plenum is now possible in LHEAD and AIDA, but this was not taken into account when RPV failure occurred, and melt relocated to the reactor cavity.

Developments

During the project, the RPV failure model has been extended towards consideration of a segregated (in the current version 2-layer) molten pool. The new model allows simulating not only total failure but also a partial failure of the PRV and considering the position and size of the leak as well as the configuration and amount of the molten pool. The discharged amount, composition and decay power is still provided to COCOSYS as a code-internal vector. Since AIDA is more suitable for segregated pool calculations, the model has been implemented into the AIDA routines. However, during the development and implementation a high compatibility with LHEAD has been considered.

The new model shares the input variables with the old one, to make it easier to handle the input data sets but has an extended applicability. The user must define

1. the mode of calculating or definition the leak area,
2. the mode of failure and the way of consideration of segregation during the discharge calculation,
3. the melt discharge coefficient, and
4. the melt discharge velocity (calculation or constant user input).

The new model features are coupled to the second point. The new model provides three options to the user:

1. melt stratification at the leak position is not considered,
2. melt stratification will be considered, but all molten material will be discharged from the lower plenum, and
3. melt stratification will be considered, but only the molten material above the leak position will be discharged.

In all cases the mass flow of the discharge is calculated with the leak area and the discharge velocity.

Option 1 is basically the already existing option from the former code version. In this case the discharged volume will be calculated from the homogeneously mixed molten volume in all configuration cases. In case of a stratified configuration, the discharged mixed molten volume will be calculated in accordance with the oxide/metal ratio. The discharge will be stopped when no more molten material is in the lower plenum. In case of further melt relocation from the core the discharge will start instantaneously.

Option 2 and 3 are new options with consideration of the stratification. In option 2 a total failure is assumed, so independent from the leak location, all of the molten material will be discharged (corresponds to a leak at the bottom or a ring form LP failure). The discharge starts with the material which is above the leak position. If it is pure metal, then the metallic material above the leak will be discharged. If above the leak there is a mixed material, first this mixed material will be discharged in accordance of the oxide/metal

ratio. After no more material is above the leak the discharge will be continued with the rest of the material.

Option 3 assumes a local failure without complete LP wall failure. In this case, in the same way as in option 2, only the molten material above the leak will be discharged. If there is no more molten material above the leak, the discharge will be stopped and the calculation continues. Note that further wall ablation or melt relocation of the core is possible. If a new leak is opening or the existing leak widens, the discharge starts again until there is no molten material above of the lowest leak position.

This new modelling method allows a wide range of options, which cover all the possible failure modes which can be taken into account in a pseudo-2D lower plenum model and enables a more realistic modelling of severe accident scenarios with ATHLET-CD.

3.1.6 Model for elliptical RPV bottom

Motivation

The correct modelling of the LP shape affects the heat transfer calculations from the corium pool as well as the modelling of progressive wall ablation and failure. The important geometrical solution variables are

- top surface area,
- interface area between the corium layers,
- wetted area and height of the layers, and
- position of wall damage and failure.

In the former code version, the modelling of the lower plenum wall geometry has been limited to a hemispherical shape. This geometrical assumption is suitable, amongst others, for the German Konvoi Type and for AP-1000 and HPR-1000 designs but leads to distortions for reactor types with an elliptical lower plenum shape like VVER-440, VVER-1000 or BWR-69.

Developments

During the project, the module AIDA has been enhanced to simulate also elliptical, truncated elliptical and truncated hemispherical lower head shapes. The detailed description of the new modelling approach is documented in /LOV 21a/.

The new, enhanced LP geometry modelling approach of AIDA has been demonstrated with the simulation of a severe accident scenario in a generic VVER-1000 type reactor. The results show very well that the consideration of LP shape affects the corium pool evolution in the LP and has a significant influence on major late phase key points like remaining wall thickness or vessel failure.

3.2 WP2.2: Modelling of structure failure

3.2.1 Implementation of a user-definable failure criteria

Motivation

In ATHLET-CD the implemented mechanical failure criteria for the reactor vessel wall are simple and are not necessarily valid for all reactor types and configurations. User feedback suggested the implementation of a user-definable failure criterion, in order to adjust the criterion to different configurations and/or to test new failure criterion models.

Developments

Since the already provided four failure models in AIDA don't completely cover the user requests and because in some simulations an exact failure time is foreseen (e. g., Fukushima Daiichi plant simulations), the possibility of a user-defined LP failure has been implemented in AIDA. This allows the user to create his own failure criterion using the GCSM module of ATHLET. The input data have been extended under the damage keyword with a new GCSM signal, which results in an instant LP failure if its value is set to 1. The leak area as well as the discharge parameters are modelled after the leak opening following the standard input data. With GCSM the user has access to multiple relevant properties, like fluid/wall temperatures, pressures and other material parameters. With the help of those the user can define his own, unique failure criterion. The user defined criterion can also help in the future when the melt and fission product transfer from the ATHLET-CD domain to the COCOSYS domain is to be tested. A time-signal controlled

failure initiation can accelerate the verification process of the coupling between ATHLET-CD and COCOSYS.

For future developments a plug-in interface was prepared, to allow the coupling/usage of a more detailed failure criterion model in the future.

3.2.2 Improvement of the RPV failure models

AIDA has been extended with a new failure model, which considers the ablation of the LP wall. Since the remaining wall thickness in case of a severe accident with melt relocation into the LP is one of the most important solution variables, the newly implemented model is the currently recommended option in case of a low-pressure accident scenario. With the new model, four different failure options are available in the current AIDA version:

- IDAM 1: Simple failure criteria considering the wall ablation
- IDAM 2: ASTOR approximation
- IDAM 3: Larson-Miller approach
- IDAM 4: Rupture model

The implemented simple failure criterion considers the in-vessel and ex-vessel pressure difference, the mass of the corium and the LP wall, the temperature and the remaining wall thickness. With this, the tangential stress (σ_t) is calculated in every axial section (i) of the wall in every timesteps (t):

$$\sigma_t(t, i) = \frac{F_g}{A_r(t)} + \frac{(p_{RPV} - p_a) * D_i}{4 * d(t, i)} = \frac{m_g * g}{d(t, i) * D_i} + \frac{(p_{RPV} - p_a) * D_i}{4 * d(t, i)} \quad (3.3)$$

Here, A_r is the LP surface below of the position i , F_g is the weight force, p_{RPV} is the in-vessel pressure (coupled mode: SIG2, stand-alone: PLH), p_a is the ex-vessel pressure (PCAV in input, GCSM signal), m_g the mass of the wall below the position i , D_i the diameter of the LP, d the wall thickness and g the gravitational constant.

As failure criterion the tensile stress of the RPV (σ_{RPV}) wall is used. Depending on the user variable TENSLSTR:

- TENSLSTR > 0, the user defined constant value has been used (Pa)
- TENSLSTR ≤ 0, a temperature dependent tensile stress for the material 20MnMoNi55 has been calculated with the Boltzmann distribution

A failure of the LP wall is modelled if the following criterion is true in one of the wall sections:

$$\sigma_t(t, i) \geq \sigma_{RPVi} \quad (3.4)$$

The output variable DAMAGE shows in case of IDAM 1 the ratio of the remaining wall thickness to the intact wall thickness. In case of a failure, it reaches the value of 1 in the concerned section. For further details, see /LOV 21a/.

Further collaborative investigations are ongoing with the structure mechanic department and with the ATHLET developer team to develop new more comprehensive and harmonised failure models, which can be used also for LHEAD and AIDA.

3.2.3 New critical heat flux correlations for lower plenum cooling calculations

The critical heat flux (CHF) on the external vessel surface is an important parameter to evaluate the success of an in-vessel-retention (IVR) via external reactor vessel cooling (ERVC) strategy. CHF is strongly dependent on the power in the melt as well as on the shape of the LP, therefore usually full-scale experiments are necessary to determine it. However, for approximative calculations there are some correlations derived from experiments available. Within the newly developed calculation strategy of IVR-ERVC of AC² (see chap. 3.3.1) the external cooling channel is modelled in detail with ATHLET. ATHLET already has correlations for CHF, however the applicability of this correlations in IVR-ERVC case has to be still investigated. During the project, possible correlations derived for IVR-ERVC have been collected. For further information of available CHF correlations for ex-vessel cooling see the ATHLET manuals /AUS 21b/, /AUS 21a/.

3.3 WP2.3: Ex-vessel cooling

3.3.1 Detailed modelling of ex-vessel cooling for IVR

Motivation

Ex-vessel flooding and cooling of the RPV from the outside is currently in the focus of the nuclear safety research. Ex-vessel cooling is already implemented in some newer reactor designs (AP1000) and some of the existing nuclear power plants are applying this strategy to mitigate the consequences of a severe accident. Therefore, it is important to model the ex-vessel cooling with AC²/ATHLET-CD in an adequately realistic manner.

Developments

The newly developed detailed IVR-ERVC modelling approach of AC² consist of three main parts: modelling of the primary and secondary circuit together with the control systems including in-vessel severe accident phenomena, modelling of the external cooling channel or cavity in an adequate level of detail and modelling of the containment thermal-hydraulics, including flooding of the cavity.

The first main part is calculated with ATHLET-CD and can further be divided into a thermo-hydraulics and a severe accident model. The modelling of thermal hydraulics of the primary and secondary circuit and the control systems is carried out by ATHLET. The severe accident phenomena are modelled with further specific ATHLET-CD modules. The dedicated module for simulation of the corium behaviour in the LP, the heat transfer from corium to ERVC through the LP wall and for wall ablation is the module AIDA.

The ERVC channel is a part of the reactor cavity. The reactor cavity is generally modelled with COCOSYS since it is a part of the containment. However, the ERVC channel has usually a relatively small volume and a complex shape compared to other containment compartments. Due to the relatively coarse spatial resolution and model limitations of COCOSYS, it is not possible to model the exact channel geometry and the complex multiphase processes within it in a realistic manner. On the other hand, ATHLET can simulate the geometry of the cooling channel with the necessary level of detail under consideration of the exact channel shape and the complex multiphase phenomena during IVR. Therefore, in the IVR modelling strategy, the ERVC channel is modelled with

ATHLET. The ATHLET ERVC model is coupled through the LP wall to AIDA and gets its boundary conditions from COCOSYS.

In the developed coupled method (IFLOCROUP = 1), the lower plenum wall is the interface between the ATHLET-CD and the ERVC thermal-hydraulic model. The heat conduction in the wall, wall ablation and wall temperature are calculated in the module AIDA. For these calculations, the outer wall boundary conditions are provided by the ATHLET ERVC model. Therefore, the LP wall is also modelled with a representative HCO in the ERVC model, which will automatically get the wall temperatures from AIDA. The ATHLET ERVC model calculates the heat transfer coefficient and the surrounding coolant temperatures (T_{sur}) along the wall nodes, considering the flow regime in the ERVC channel /AUS 21b/. The calculated HTC value and temperature will be averaged in each node and will be given back to AIDA to calculate the total heat flux from the corium through the LP wall into the external cooling channel. Fig. 3.6 shows the coupling schema between AIDA and the ERVC model.

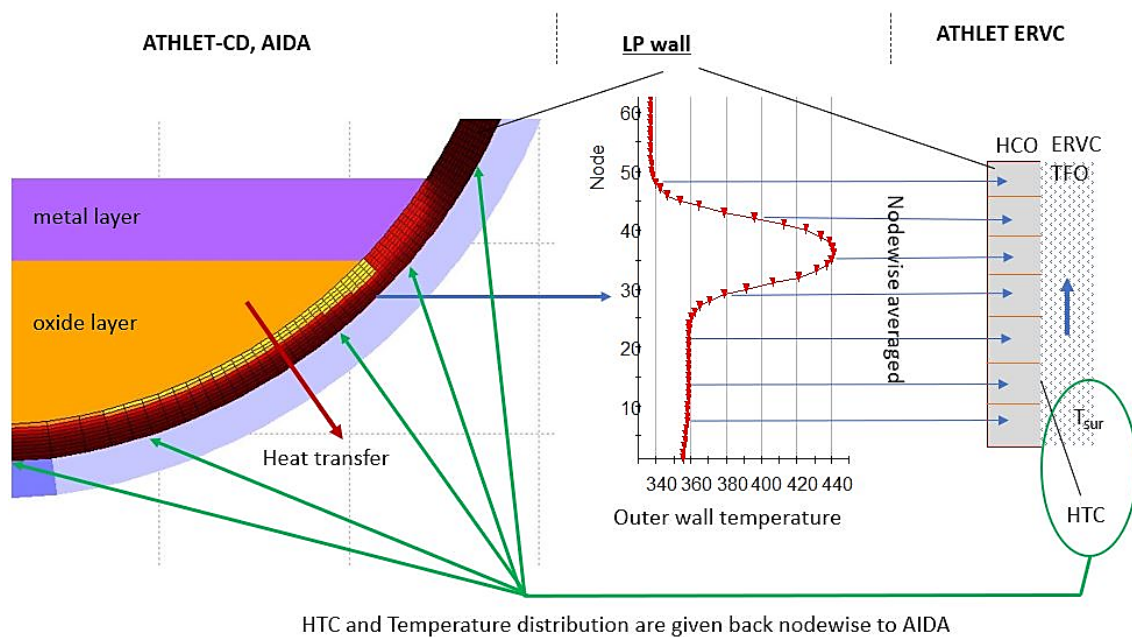


Fig. 3.6 Scheme of the coupling between AIDA and the ERVC model

The AIDA wall and the HCO are modalised differently. To ensure a nodewise transfer of the wall temperature from AIDA to the ERVC model and backwards, an internal coupling algorithm has been developed, where the basis for the algorithm is the surface of the nodes. The data transfer is carried out in every time step automatically. However, due to the numerical setup of ATHLET-CD, the AIDA calculations are carried out at the end of

each timestep, after the thermal-hydraulic solution. Therefore, the temperature and HTC values for the AIDA calculation are from the previous time step. Given current experiences and as the ECRV model will impose adequate time step sizes due in two-phase flow conditions, this causes only an acceptable numerical error in the simulations.

After AIDA activates, the volumes of the coupled HCO (TT) receive nodewise averaged the outer wall temperatures (TWO) from AIDA at the end of the timestep. The right side of the coupled HCO is flooded (the left side should be set adiabatic).

The new method has been successfully demonstrated with the simulation of IVR-ERVC scenario in a Generic PWR, more details about the simulations are published in /PAN 22/.

4 WP3: Plant simulation

4.1 WP3.1 Generic input decks

4.1.1 Improvement of the generic input decks

Motivation

ATHLET-CD consists of numerous models that cover different phenomena, often interacting with each other. Changes made to a model can have an undesirable effect in another model. In order to test ATHLET-CD, whether along the new developments, bug fixes and improvements, such undesirable effects were unintentionally implemented, extended verification calculations are needed. The best way to do that is to use complex input decks. However, most complex input decks contain confidential data, therefore it was decided to use generic reactor input decks for such verification purposes. Existing generic input decks constantly need to be adjusted to new developments and new generic input decks needed to be created.

Developments

During the project period three generic input decks were created/adjusted, one for each major type of LWR designs that are used worldwide: PWR, BWR and VVER. The objective for the creation and maintenance of these input decks was to create stable input decks that cover most of the phenomena that ATHLET-CD can simulate. These input decks were developed and adjusted so that they incorporate most of the characteristics of the different reactor types, however, without the elaborate I&C modelling for operational systems and several safety features. The initiating event in all cases was a station blackout, accompanied with a break in the coolant system. This scenario leads quickly to core degradation, where the models of ATHLET-CD can be analysed, and also doesn't require the implementation of most of the safety systems (as they are unavailable due to station blackout). These input decks can be used for further model verifications during the ongoing development and can also be integrated into an automated testing system (see chap. 4.1.3).

An example is shown based on the PWR generic input deck to demonstrate this generic input deck and to show their use in practice. The other generic input decks are built and used similarly.

The developed input deck is a model for a generic pressurised water reactor, with four loops, simplified secondary circuit (only the steam generator is modelled, no turbine and other secondary systems). The core is divided horizontally into six concentric rings. The 50 cm² leak is defined in the cold leg of the loop “P2”. The pressuriser is connected to the hot leg of the same loop. A simplified view of the generic reactor nodalisation is visible in Fig. 4.1.

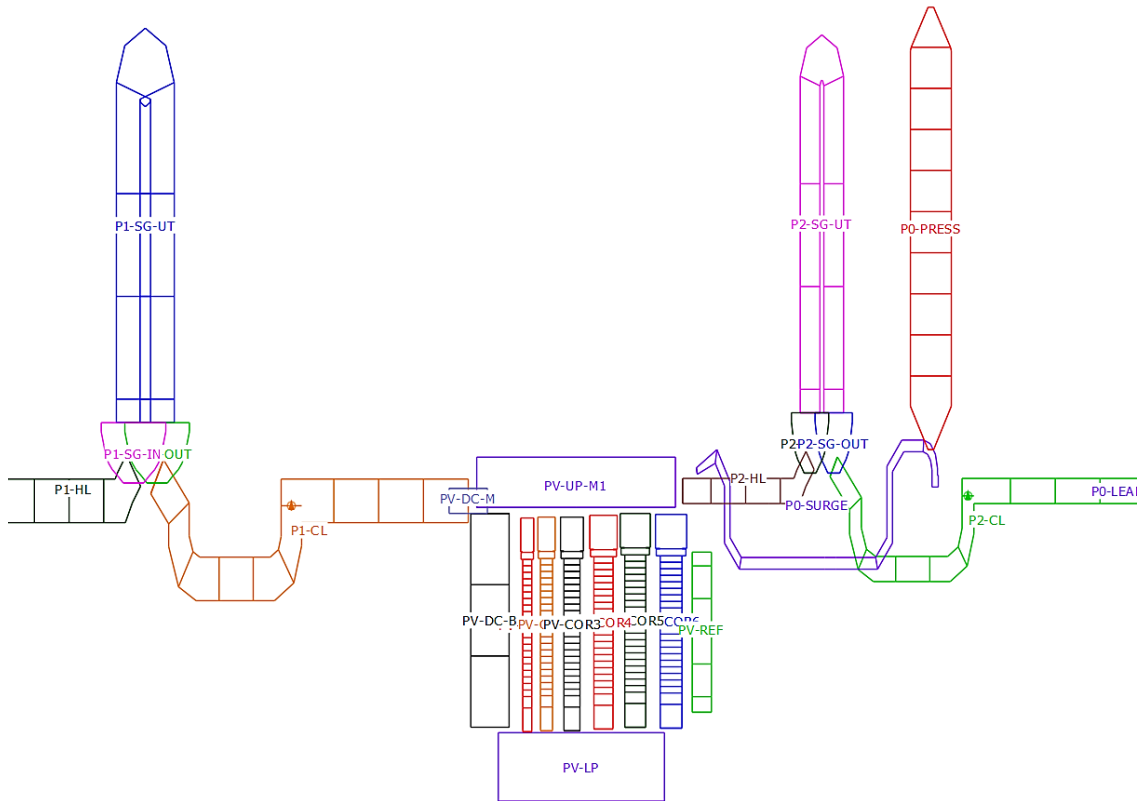


Fig. 4.1 Nodalisation used in the input deck for the generic PWR

The initial core thermal power was 3.85 GW. SCRAM was initiated after 500 s of stationary calculation, when the pipe in the cold leg breaks (leak was activated). This leads to a severe core melt scenario, where most of the core structures melt and relocate. A detailed analysis of the accident evolution is not described here, because this is not necessary for this task. Instead, it is now demonstrated how the results of this simulation (and the other simulations with the other reactor types) are used to help the development process and ensure the high quality of ATHLET-CD.

If the simulation successfully reaches its predefined end (and also if the calculation crashes), multiple checks are made. First of all, several built-in checks are examined. In Fig. 4.2 the evolution of the ceramic melt accumulation is visible. Two graphs would be visible, their evolution is, however, identical, which is the expected behaviour. One graph

(red, covered by the green curve) shows the theoretically possible sum of ceramic melt mass, the green graph shows the sum of all ceramic melt in each timestep. As they run identically, this means that conservation of mass is achieved. There are several other similar basic checks, that are looked at first.

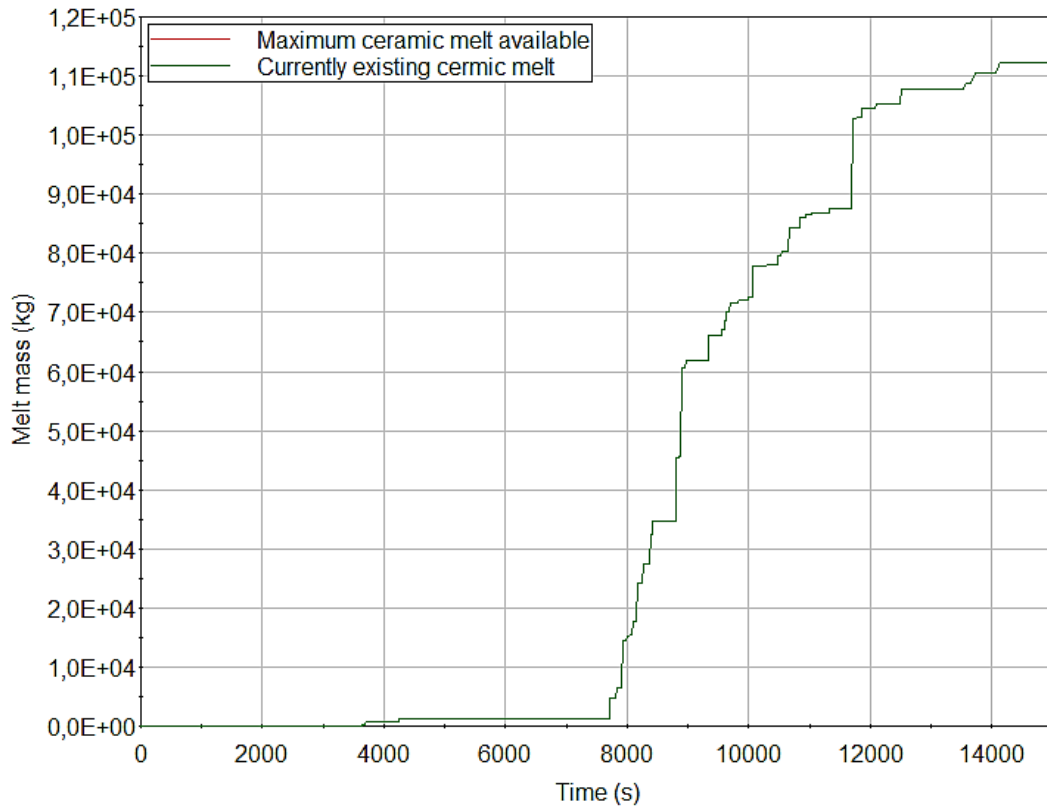


Fig. 4.2 Mass balance check for ceramic melt

If the basic physical laws are proven to be correct (conservation of mass, energy, etc), then it is examined whether the results of the calculation are plausible. The first indication about the correctness of the calculation is a successfully finished simulation. There are many in-built checks that stop the calculation if unrealistic values (extreme temperatures, pressures) occur. So, if a run succeeds, it is unlikely to have totally unrealistic values. Nonetheless, there might still be some hardly explainable results, therefore, some key parameters are checked.

A good indicator for the whole accident process is the mass of the generated hydrogen. In Fig. 4.3 we can see a realistic accumulation of the produced hydrogen due to the oxidation process. We know from scientific literature that 500 – 600 kg of hydrogen are produced during a severe accident for such a scenario. If the values would be significantly lower or higher, a deeper look into the simulation would be necessary.

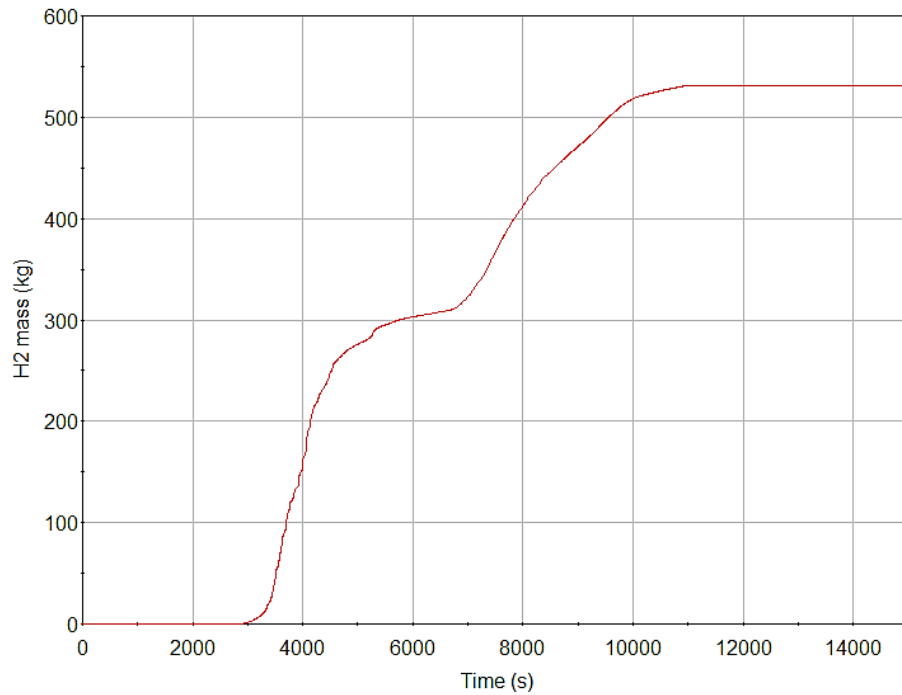


Fig. 4.3 Accumulation of the produced hydrogen

Other key parameters to check are related to the fission products. Fig. 4.4 shows the remaining xenon mass in the core. It is visible that xenon is continuously released from the core from around 3500 s, until it is almost completely removed from the core. The graph indicates that the fission product release models work as intended.

Fig. 4.5 shows the relocation of corium from the core to the lower plenum. The relocation starts if a user defined criterion is reached. In this case, the grid plate fails if 50 t of melt is accumulated on the grid plate. It is clearly visible that this criterion is reached at around 8300 s, where 50 t of melt is relocated to the lower plenum. After the relocation, further melt formed in the core also relocates to the lower plenum.

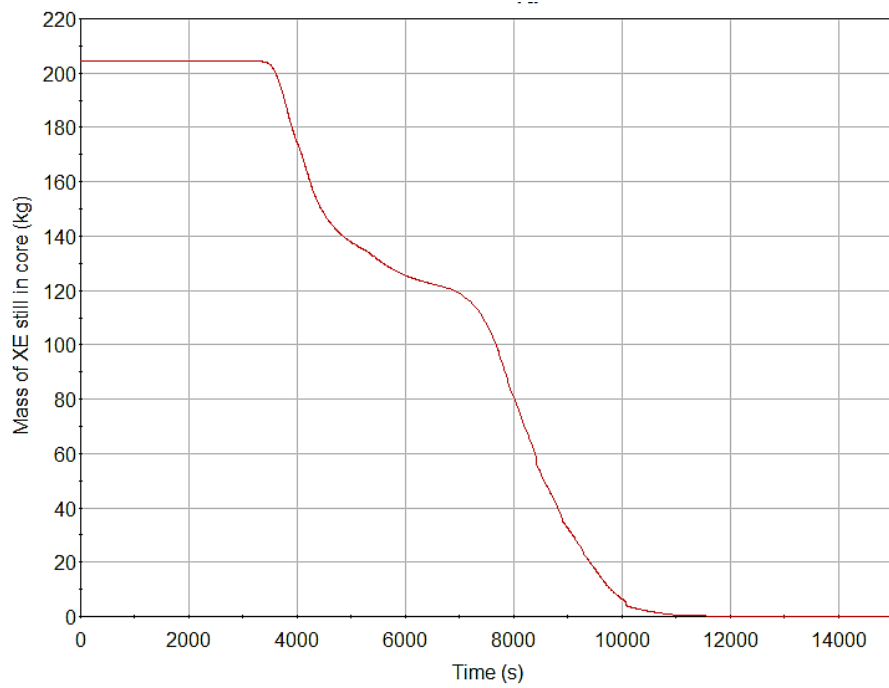


Fig. 4.4 Remaining mass of XE in the core

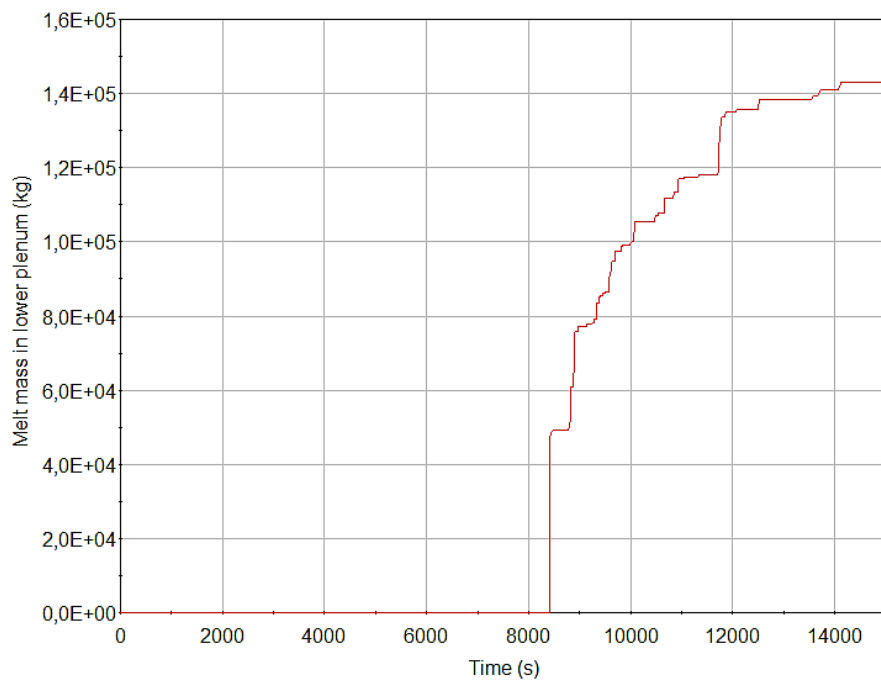


Fig. 4.5 Melt mass accumulation in the lower plenum

Finally, the end state of the core is checked, optically, which is shown in Fig. 4.6 It shows that most of the core melted and relocated to the lower plenum. Also shows that some nodes remain “floating” in the core, which is an ongoing issue and is a topic for future developments.

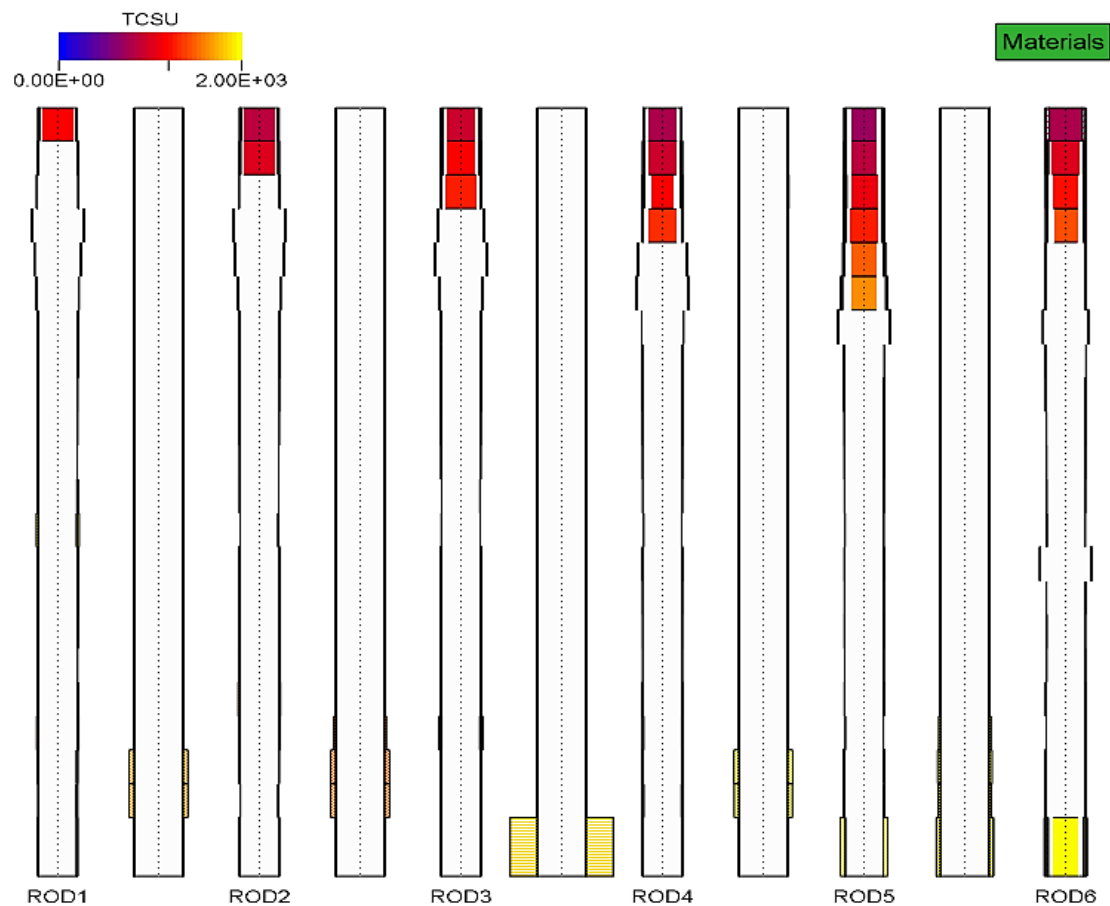


Fig. 4.6 End state of the core in the demonstrated example

One additional parameter of interest is the numerical performance of ATHLET-CD, so that the number of time steps is checked, whether there is an unexpected increase in run-time and thus loss of performance. With the previously briefly shown variables (and with many more unshown variables) and methods, the results of some complex simulations are checked regularly to constantly assess the quality of ATHLET-CD. The generic input decks are essential for these kinds of jobs. Currently, the checks are made by GRS experts. The running of the simulations was made automatic (see chap. 4.1.3), however, the analysis of the results still needs to be done manually. For the future, an automatic results-comparison tool is planned.

4.1.2 Coupling of the generic input decks to COCOSYS

Motivation

The motivation behind connecting COCOSYS to the existing generic ATHLET-CD input decks is similar as it is for the standalone generic input decks. Due to the closer integration of ATHLET-CD into AC² and due to more frequent usage of AC², it is important to keep the coupling interface between ATHLET-CD and COCOSYS up to date and to demonstrate its functionality. Therefore, it was decided to attach a simple COCOSYS input to each of the generic ATHLET-CD input decks.

Developments

A very simplified COCOSYS input deck was developed for a generic pressurised water reactor and one for a generic boiling water reactor. These inputs then were connected to the already existing generic PWR, VVER and BWR ATHLET-CD stand-alone input decks. All the input decks simulate a hypothetical accident, where the initiating event is a station black out scenario, combined with a loss of coolant accident. The new AC² input decks are used to constantly check the functionality of the coupling. Currently, these checks are performed manually, however, in the short-term they are going to be part of the continuous integration system (CI), which is described in chap. 4.1.3. Here, only the simulation of the PWR AC² input deck is briefly introduced, focusing only on the coupling functionality.

The general evolution of the accident is not described here, as it is summarised in chap. 4.1.1, and the coupling of COCOSYS to the input deck did not influence the accident evolution significantly. The coupled simulation was, however, used to check the functionality of the coupling between ATHLET-CD and COCOSYS.

Fig. 4.7 shows the evolution of the pressures in the primary circuit and in the containment. It is clearly visible, that the break is initiated at $T = 500$ s. Up until that time, the pressures in the primary circuit and in the containment are approximately constant. A sudden drop in the pressure is visible in the primary circuit, at the same time the pressure starts to increase in the containment, which proves the arrival of steam in the containment. From around 3000 s the pressure starts to oscillate in the primary circuit. The reason for that is still to be analysed. A similar behaviour would also be expected in the containment, which shows a relative smooth pressure increase. However, if zoomed in,

as seen in Fig. 4.8, the pressure oscillation also occurs in the containment, its amplitude is only smaller as in the primary circuit due to the much larger volume of the containment. The simulation runs smoothly and stable.

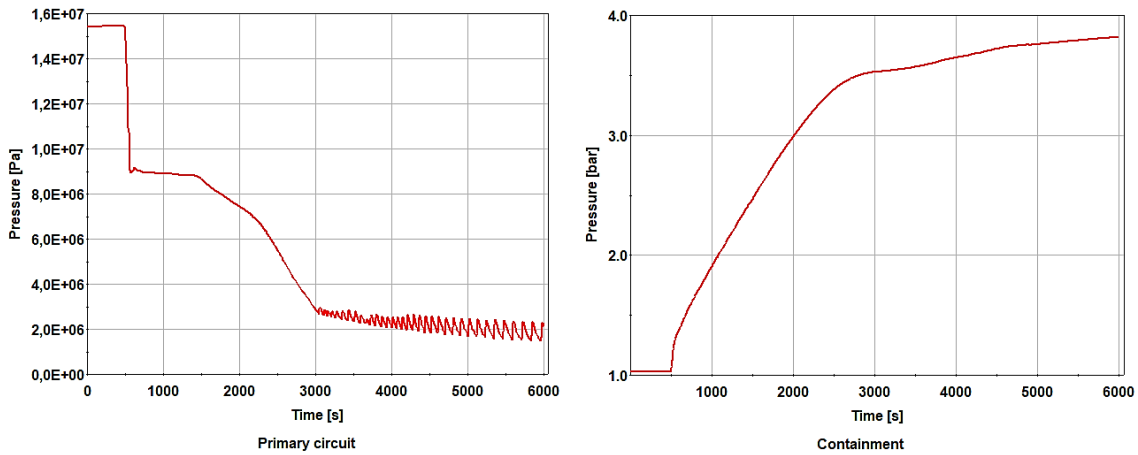


Fig. 4.7 Evolution of pressure in the primary circuit (left) and in containment (right)

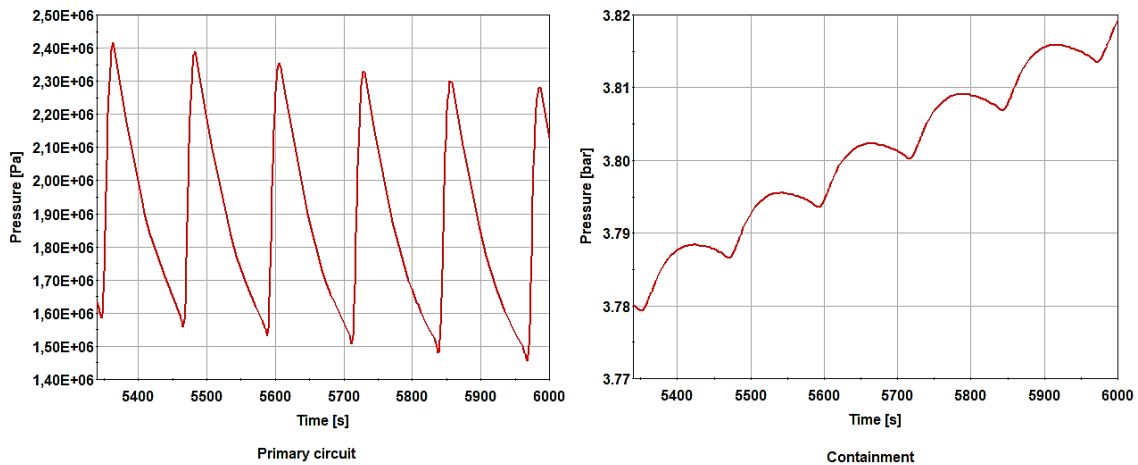


Fig. 4.8 Oscillation of pressure in the primary circuit (left) and in containment (right)

If we look at the transport of fission products, we can see also some indications that the coupling interface works as intended. Fig. 4.9 shows the evolution of Xenon mass that leaves the primary circuit (green) and enters the containment (red) through the leak. The two curves almost run identically, which is the expected and plausible result, as the fission products that leave the primary circuit can only appear in the containment. Slight differences can be seen in the evolution of the masses. This is due to numerical differences and these are, as visible, not significant.

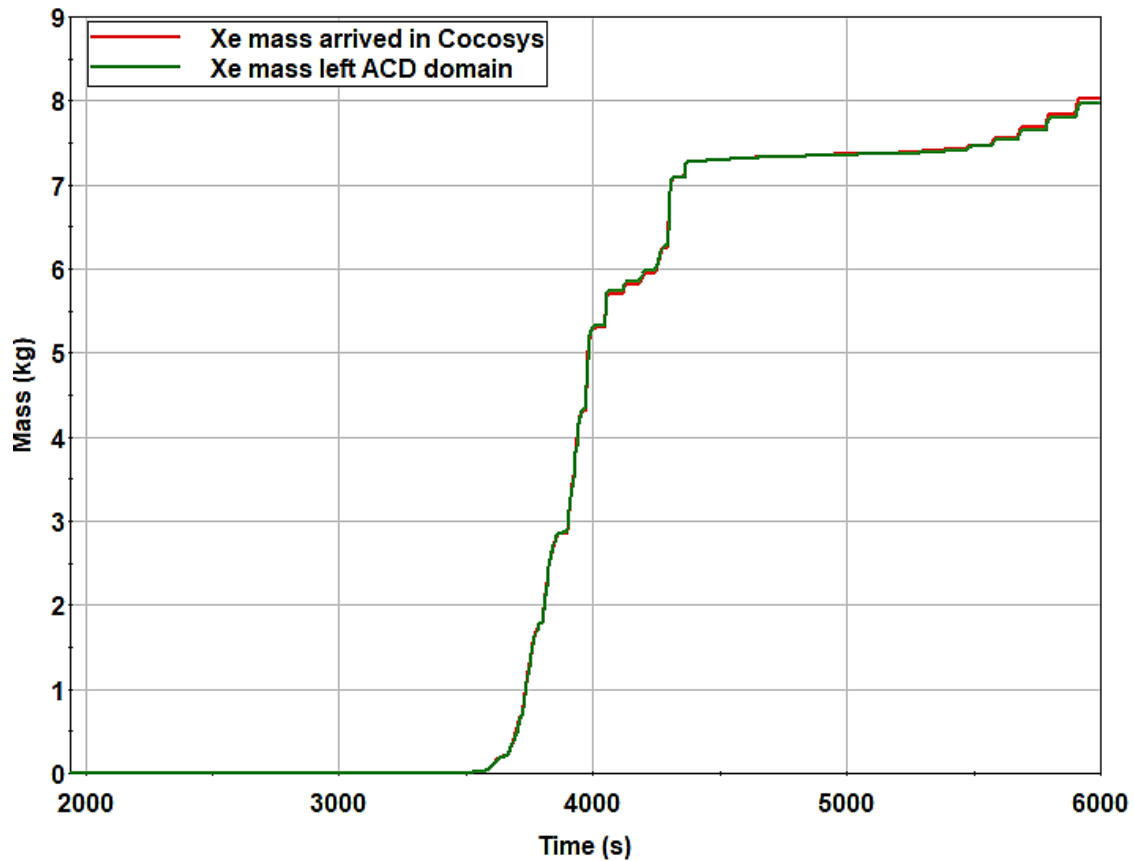


Fig. 4.9 Mass of xenon leaving ATHLET-CD domain and entering COCOSYS

As briefly described here, the coupling interface works as intended, even if there are indications for some numerical instability. To ensure correct simulations also in the future, these coupled calculations are going to be repeated regularly, in the short term manually, medium term using the continuous integration system (see next chapter).

4.1.3 Implementing the generic input decks into a continuous integration platform

Motivation

Newly developed models and bug fixes are tested by the developer against several, for the current topic relevant cases. However, the changes made can have an unwanted effect in other parts of the core, on other unchanged models. These problems only be detected before the official release of ATHLET-CD, which is why an extensive validation process has been specified. It was decided to set up an automated system, that frequently performs simulations on a predefined set of data, allowing the developer to catch unwanted failures faster and more thoroughly.

Developments

For version control of the source code of ATHLET-CD (and AC²) GitLab is used, its Continuous Integration (CI) and Continuous Development (CD) was used also for creating an automated system to check the ATHLET-CD input decks.

GitLab automatically compiles and delivers every night the latest ATHLET-CD version. At this stage all the syntactical errors show up and the developers are informed. The idea was to use the latest available automatically generated ATHLET-CD version to test multiple input decks at once. The following input decks were chosen to be tested regularly:

- Generic PWR, BWR and VVER reactor input deck
- Input decks for experiments: Phebus-1, Phebus-3, multiple Quench and CORA experiments
- Input deck for the TMI-2 accident
- Simple sample input decks

Due to the larger number of input decks (15 in total) and because some of the simulations can last for about a day, an extended automated test is performed only once a week, starting on Friday night, using the ATHLET-CD version automatically generated also on Friday.

If a simulation fails, the developers are contacted, showing immediately the failed simulation. The output generated during the simulation is saved and is made available for download. This makes the analyses of the problem faster and easier.

If the simulations succeed, the output is still saved for a period of two weeks, so that anyone who wishes to analyse the produced results can have a look at it. So far, there is no automated checking of the produced results, thus a successful run only indicates that there is nothing fundamentally wrong with the used version and input deck. It is an objective for the future to implement an automated way of checking the simulation results.

Fig. 4.10 shows an example of the output overview of the automated system. It shows that most of the simulations succeeded, but, at the moment of the screenshot, two simulations failed. The failed jobs are highlighted and the developers are automatically contacted, therefore they can start fixing the problems immediately.

The automated system helps a lot to keep and to increase the quality standards of ATHLET-CD.

	linux: [CI_Test_files/PWR_generic/PWR_generic.in , PWR_generic]	#88796 linux docker	🕒 11:55:50 📅 5 days ago	 
	linux: [CI_Test_files/Qu06/qu06.in, qu06]	#88786 linux docker	🕒 00:06:10 📅 5 days ago	 
	linux: [CI_Test_files/Qu10/qu10.in, qu10]	#88787 linux docker	🕒 00:21:52 📅 5 days ago	 
	linux: [CI_Test_files/Qu11/qu11.in, qu11]	#88788 linux docker	🕒 00:24:06 📅 5 days ago	 
	linux: [CI_Test_files/Qu13/qu13.in, qu13]	#88789 linux docker	🕒 00:24:48 📅 5 days ago	 
	linux: [CI_Test_files/Qu16/Qu16.in, qu16]	#88790 linux docker	🕒 00:48:46 📅 5 days ago	 
	linux: [CI_Test_files/s10/s10-aida.in, s10]	#88793 linux docker	🕒 00:00:19 📅 5 days ago	 
	linux: [CI_Test_files/s7-cora-bwr/s7-cora-bwr.in, s7]	#88791 linux docker	🕒 00:06:54 📅 5 days ago	 
	linux: [CI_Test_files/s8/s8_large.in, s8]	#88792 linux docker	🕒 00:09:25 📅 5 days ago	 
	linux: [CI_Test_files/TMI/tmi2.in, tmi2]	#88794 linux docker	🕒 03:44:39 📅 5 days ago	 
	linux: [CI_Test_files/WWER_generic/WWER_generic.in , WWER_generic]	#88797 linux docker	🕒 12:00:00 📅 5 days ago	
	windows: [CI_Test_files/BWR_generic/BWR_generic.in , BWR_generic]	#88810 windows docker	🕒 03:52:40 📅 5 days ago	 

Fig. 4.10 Example of the output of the continuous integration system

4.2 WP3.2 Maintenance and development of coupling interfaces

Motivation

ATHLET-CD has multiple coupling interfaces to other programs; however, the two most important ones are the interfaces to ATHLET and to COCOSYS. These have to be kept up to date, to follow each development in these codes and also any possibly occurring bugs and performance issues have to be addressed. Therefore, a continuous improvement/maintenance of the coupling interfaces is necessary.

Development

Regarding ATHLET, multiple new variables were made visible via the coupling interface for ATHLET-CD and vice versa, that were needed for new models, for example of the model of ATF oxidation. Also, some structural changes in ATHLET were made, that required the re-dimensioning of some already existing vectors.

Towards COCOSYS, the existing coupling interface proved to be stable and robust, no additional developments were needed during the project timeframe. Some minor bug corrections were implemented, which had an impact on the melt transfer from the failed lower plenum to the cavity of the containment, which is simulated by COCOSYS.

Besides all of these, AC² and therefore the coupling interfaces were used more frequently than before this project. This led to an extensive testing and maintaining of the coupling interfaces.

4.3 WP3.3 Accidents in spent fuel pools

Motivation

Particularly since the accidents at Fukushima, interest in investigations of accidents in spent fuel pools has increased considerably. Corresponding analyses have already been carried out with ATHLET-CD, but only few experiences have been gained so far when coupled with COCOSYS /BAN 18/. Therefore, existing model gaps and weaknesses in coupled calculations needed to be identified and, if possible, eliminated. Therefore, it was necessary to test the coupling on a relatively complex but generic data set for spent fuel pools. In the following, the results of this calculation are briefly shown, and the approaches used and experiences gathered are discussed.

Development

The concept of the coupling of ATHLET-CD and COCOSYS for investigating accidents in spent fuel pools (SFP) is the following.

The calculated mass and energy release rates from the degraded SFP by ATHLET-CD are transferred to COCOSYS. All components taking part in the process of mass and energy transfer have to be defined in both input decks by application of the so-called

“discharge coupling”. The standard fluid components which are released by ATHLET(-CD) are water and steam and in case of the Zr reaction of the fuel assemblies (FA) with steam the produced H₂. Additional components have to be defined also for re-injection to ATHLET from the containment. These components are O₂ and N₂ in the containment atmosphere. These fluid components have to be specified in COCOSYS, too. The heat losses of the structures modelled in ATHLET can be considered in COCOSYS. Therefore, the outer surfaces of structures have to be coupled to containment zones. Each structure (heat conduction object in ATHLET) can only be coupled to one control volume of COCOSYS, where the temperature of the control volume is exchanged via the GCSM COCOSYS library. The necessary boundary conditions are exchanged between COCOSYS and ATHLET(-CD) via GCSM. The coupling is located just above the water level of the SFP. With this approach the gas phase of the SFP is mainly simulated in COCOSYS, ATHLET-CD simulates the decreasing water level and the generated steam up to that height, and additionally the core degradation phenomena.

Using the approach described above, the following accident scenario was simulated for testing AC²:

A spent fuel pool of a generic VVER-1000 reactor was simulated, with a total of more than 70000 fuel rods with a total power of approximately 3.25 MW. The fuel rods are distributed among four core nodes. Initially, the fuel rods were completely covered with water, the water level above the top of the fuel assemblies was set to 2 m (the comparatively low water height is chosen to accelerate the accident evolution for test purposes). Above this elevation a generic containment model was connected. The chosen and analysed scenario was a loss of coolant accident, accompanied with a long-term station blackout, without any mitigating interventions in order to bring AC² to its limits and test its applicability and plausibility.

In the following the simulation results are presented, focusing on the applicability and plausibility of the results, a detailed analysis is omitted as the objective in this development project was to identify and eliminate problems related to spent fuel pool simulations and/or to the coupling between ATHLET-CD and COCOSYS.

Mostly due to the leakage, but partly also because of evaporation, the amount of water in the spent fuel pool decreases (Fig. 4.11). The dropping of the water level has two

consequences: firstly, cooling of the fuel elements not covered by water becomes insufficient and these start to heat up, and secondly air from the containment atmosphere takes up the space of the water that is no longer in the spent fuel pool.

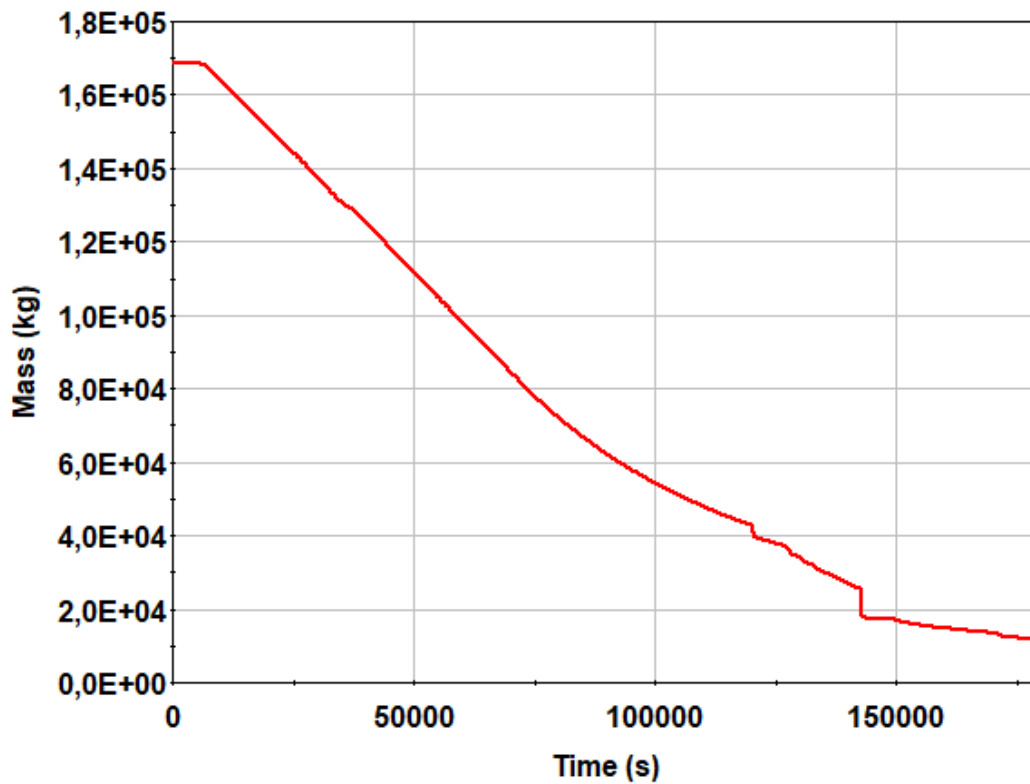


Fig. 4.11 Evolution of the liquid mass in the spent fuel pool

At around 108000 s after the initiating event, the surface of some of the fuel rods reaches 1200 K and an extensive oxidation between Zr of the cladding and air/steam starts. This results in the generation of hydrogen (Fig. 4.12), which is then added to the surrounding ATHLET objects and is transported away. Almost all the available Zr was oxidised by air by the end of the simulation, generating about 1070 kg of H₂. The combined effect of the decay power, oxidation power and the insufficient cooling results in the melting of large parts of the fuel in the SFP, as seen in Fig. 4.13. Parallel to these events, fission products are also released, after the integrity of the cladding is damaged due to the heat-up. Fig. 4.14 shows the evolution of the xenon mass remaining (green line) in the core and the mass released (red line) from the core. As visible, practically all the available xenon was released.

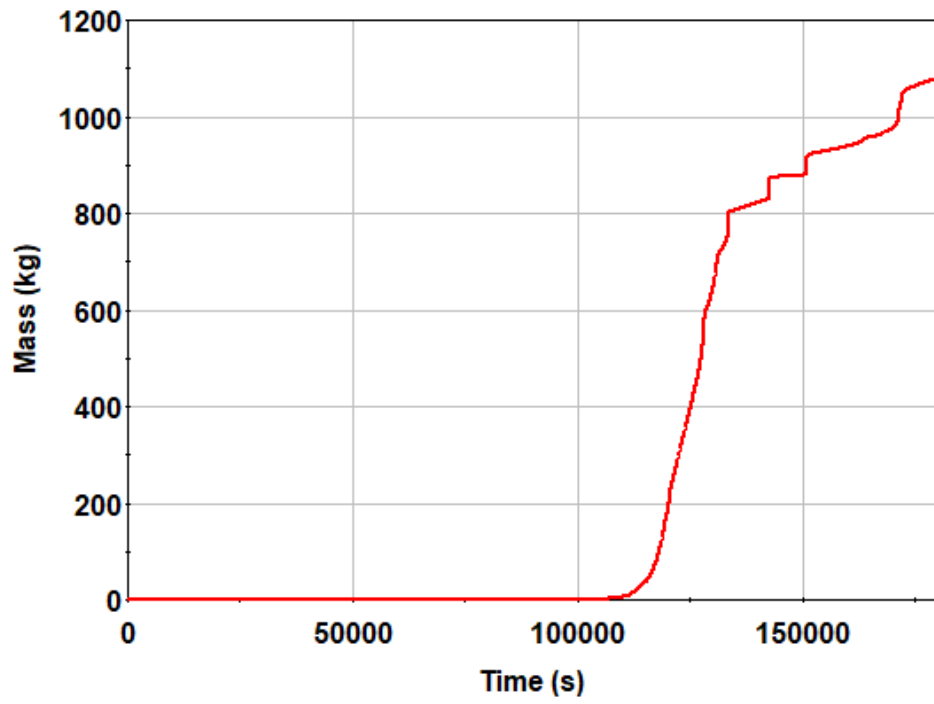


Fig. 4.12 Evolution of the produced H₂

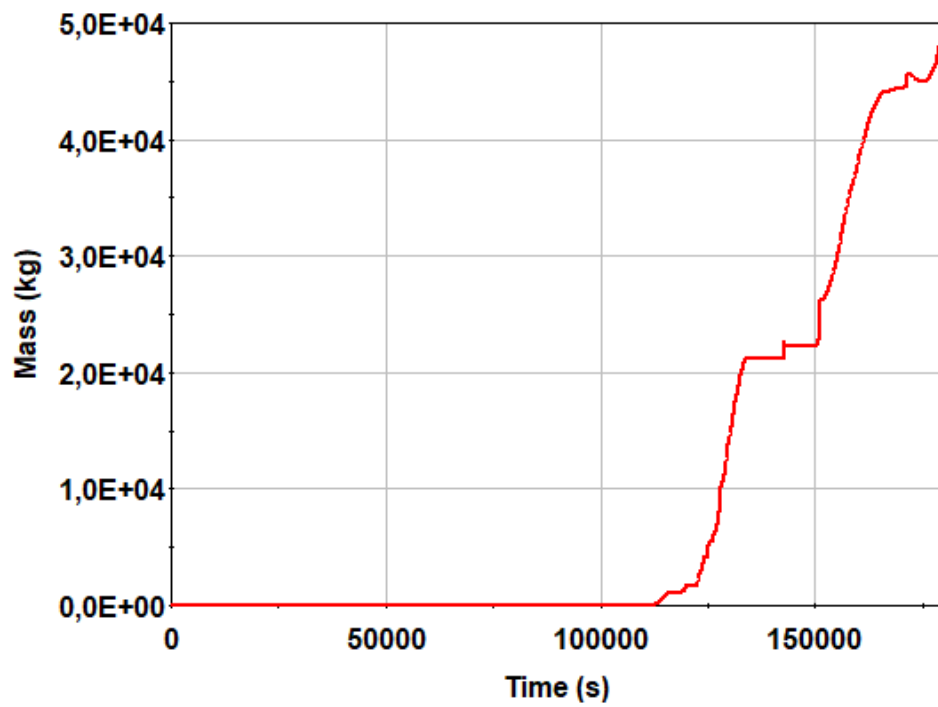


Fig. 4.13 Evolution of molten mass in the spent fuel pool

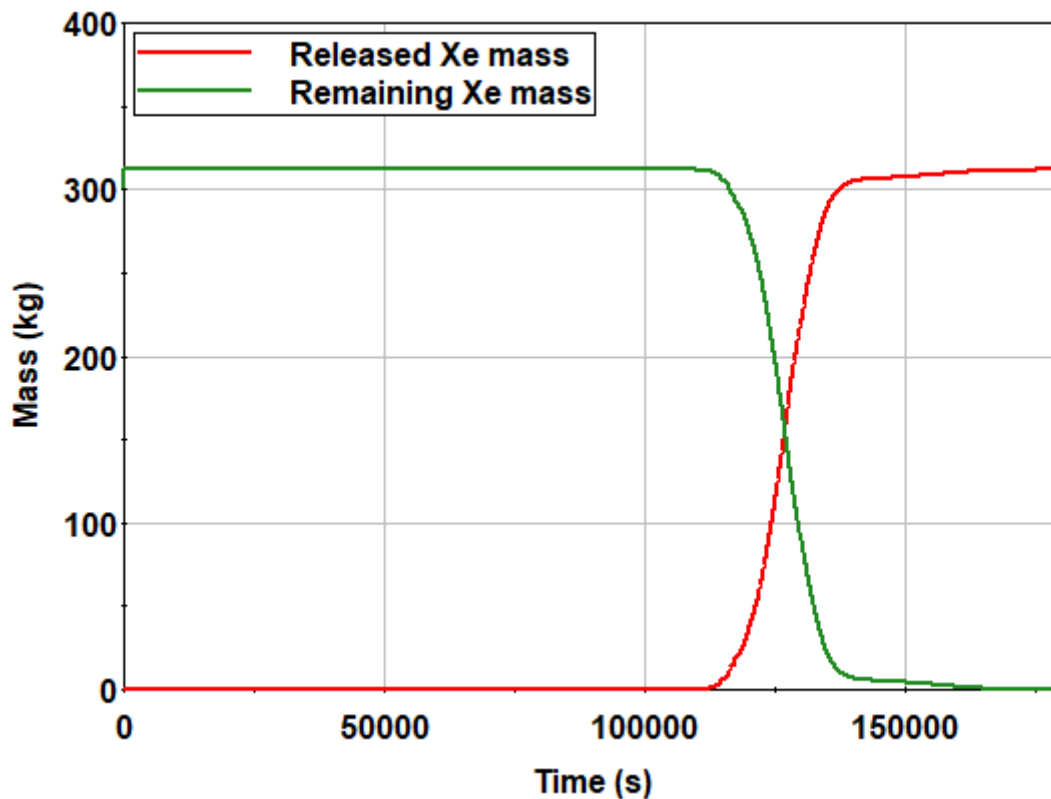


Fig. 4.14 Evolution of the remaining (green) and released (red) Xe mass

The simulation was terminated at $T = 180000$ s due to a lack of late-phase models for the SFP, an issue which has to be addressed in the future. At this time, approximately 50 t of molten material have accumulated at the feet of fuel assemblies. Due to lack of melt relocation modelling to the bottom of the spent fuel pool and due to the absence of the feedback of melt from the bottom of the spent fuel pool back to the fuel region, relocation of melt below the fuel assemblies is not considered. The accumulated melt stays until the end of the simulation at the feet of the fuel assemblies. 50 t of molten material would, however, most likely relocate and interact with the thin SFP liner and then experience molten corium-concrete interaction., Therefore, the calculation was stopped, as the results would become increasingly unrealistic. The value of 50 t is arbitrarily chosen and is about a third of the whole fuel mass in the SFP.

Nonetheless, 180,000 s were enough to check the coupling interface, identify some bugs and modelling deficiencies.

First, we look at the evolution of hydrogen mass in the containment. As already depicted in Fig. 4.12, hydrogen production starts at around $T = 108,000$ s, almost at the same

time hydrogen starts to appear in the containment. The green curve in Fig. 4.15 shows the evolution of mass of hydrogen in the containment. The transport path from the location of the oxidation to the COCOSYS domain is short, therefore an almost instantaneous appearance of hydrogen is plausible. After some hydrogen accumulation, the hydrogen-recombiners in the containment start to work and reduce the amount of hydrogen in the containment (red curve). At the end of the simulation, around 1000 kg hydrogen was recombined and around 70 kg hydrogen remained in the atmosphere of the containment. This means that in total around 1070 kg hydrogen entered the containment, which correlates very well with the amount of hydrogen produced through steam-oxidation in the core-region (Fig. 4.12). Regarding the coupling, this shows a correct mass transfer of hydrogen from ATHLET-CD to COCOSYS.

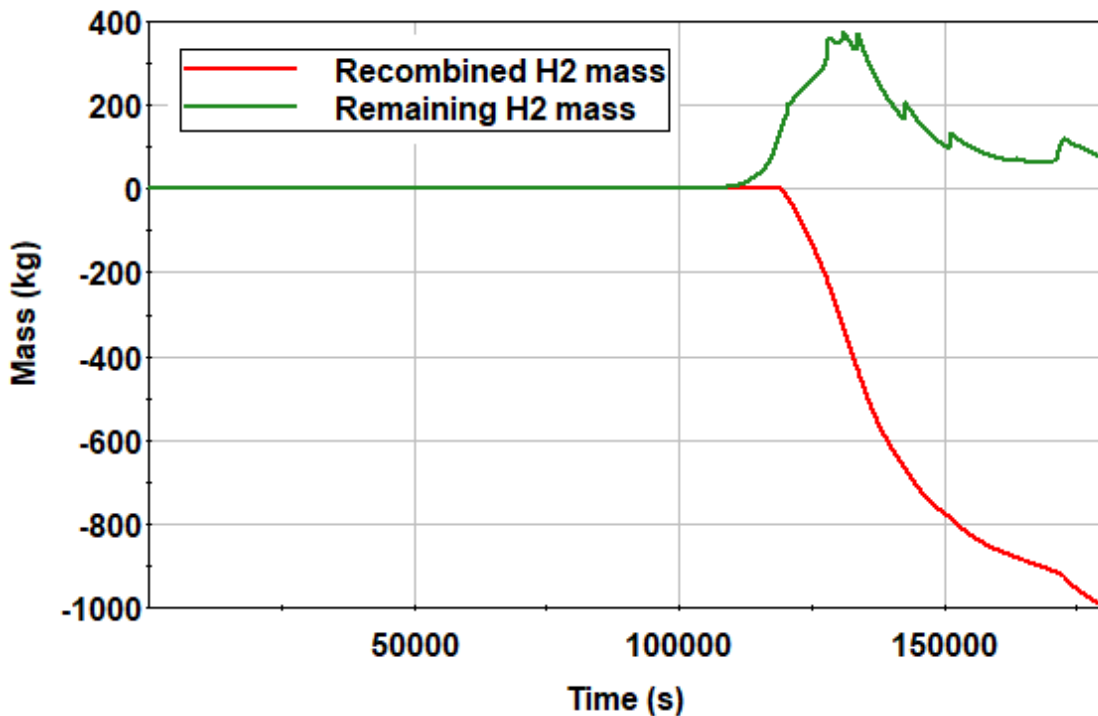


Fig. 4.15 Evolution of recombined (red) and remaining (green) H₂ mass in the containment

Another check for the correctness of the coupling interface is the evolution of xenon mass in the containment. Like hydrogen, xenon appears in the containment shortly after the first fuel rod bursts and starts to release xenon. This can be very well seen in Fig. 4.16. At the end of the simulation, the same amount of xenon is in the containment as was released from the core, meaning that the transport of xenon was successfully calculated between ATHLET-CD and COCOSYS.

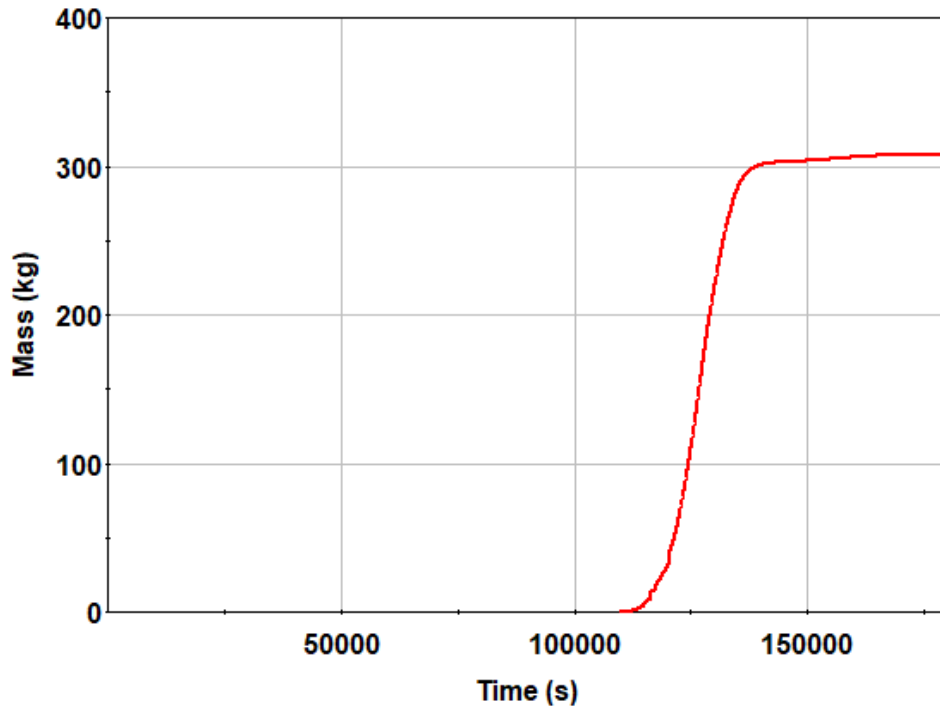


Fig. 4.16 Evolution of xenon mass in the containment

Based on this simulation, the following was achieved:

- Bugs were identified and fixed.
- Limitations and further development needs were identified.
- Experience was gathered regarding spent fuel pool calculations using ATHLET-CD+COCOSYS.

Several iterations and some bug fixes were necessary to achieve the desired final calculation time. The convective heat transfer from the cladding to the fluid became unstable under certain conditions in the spent fuel pool, resulting in extremely small-time steps and/or code stops. After investigation it turned out that the partitioning of the heat flux from the structures and corium was incorrectly assigned to the fluid if multiple structures with different temperatures had contact to the same fluid volume. A small but very practical improvement was implemented that allows the user to initialise air as “AIR-N2O2” in the input deck, instead of an initialising nitrogen and oxygen separately.

One important limiting factor to conduct detailed late-phase analyses of a SFP accident is the absence of melt relocation models in ATHLET-CD and COCOYS suitable for the floor of a SFP. The user has currently two options: he assumes that the melt stays at the

bottom of the fuel assemblies indefinitely, impacting the rest of the core region more conservatively. Or he removes the melt from the core region. However, after that the feedback from melt to the still intact structures disappears completely, even if through some creative user-input melt can be transferred to COCOSYS domain. In addition, as the space below the fuel assemblies is small, there would likely have to be some geometric overlap in the geometries of a reasonable ATHLET-CD and COCOSYS domain, which is also impossible at the moment. These issues have to be addressed in the future.

The experience gathered with this simulation is very valuable. We can see that the coupling is working as intended. The calculation time for 50 hours of simulation time ($T = 180,000$ s) was around 28 hours, so the coupled calculation was performant. It has to be noted though, that the scenario was mainly driven by the leakage. A complete boil-off of the SFP would have been more costly computationally, and residual water at the bottom of the SFP during core melt would have strongly influenced both scenario development and numerical performance. Experience was also gathered how to optimise the input deck to achieve fast, stable and adequate simulation of an accident in a SFP.

In the future, the simulation should be repeated using the flexible nodalisation to see the effects of the nodalisation. Also, the input deck should be further optimised, and it should be included in the generic input decks that are tested automatically via the CI infrastructure (see also chap. 4.1.3).

4.4 WP3.4 Input of 3D data

Previously, if the user wanted to investigate an accident in the SFP with a flexible nodalisation, the coordinates and the initial configurations of the neighbouring nodes had to be specified for each core node. This gave very great flexibility in the nodalisation, as can be seen, for example in Fig. 4.17. Each node covers a part of the storage basin that is approximately equal within the range of a node. This way the nodalisation better reflects reality.

The disadvantage of this option is that a lot of information has to be specified manually and correctly: the coordinates of the corner points of all nodes and which side sees which neighbour. This much information requires a great deal of concentration on the part of the user and this input method is very error prone.

This input method has not been removed, but a new automated input method has been developed as another option. The user only has to specify the number of rows and columns of nodes he wants to have and the size of the rows of nodes. This automatically creates a nodalisation visible in Fig. 4.18.

This creates more nodes, but:

- the creation of the nodalisation is very fast and produces consistent results,
- the user does not have to define an ATHLET object for the thermo-hydraulics behind each core node, you can define several core nodes in one ATHLET object. This way, the slowdown of the code due to the multiple ATHLET objects is reduced, and
- if the irradiated areas are similar in size, the calculation of the view factors is faster and more accurate.

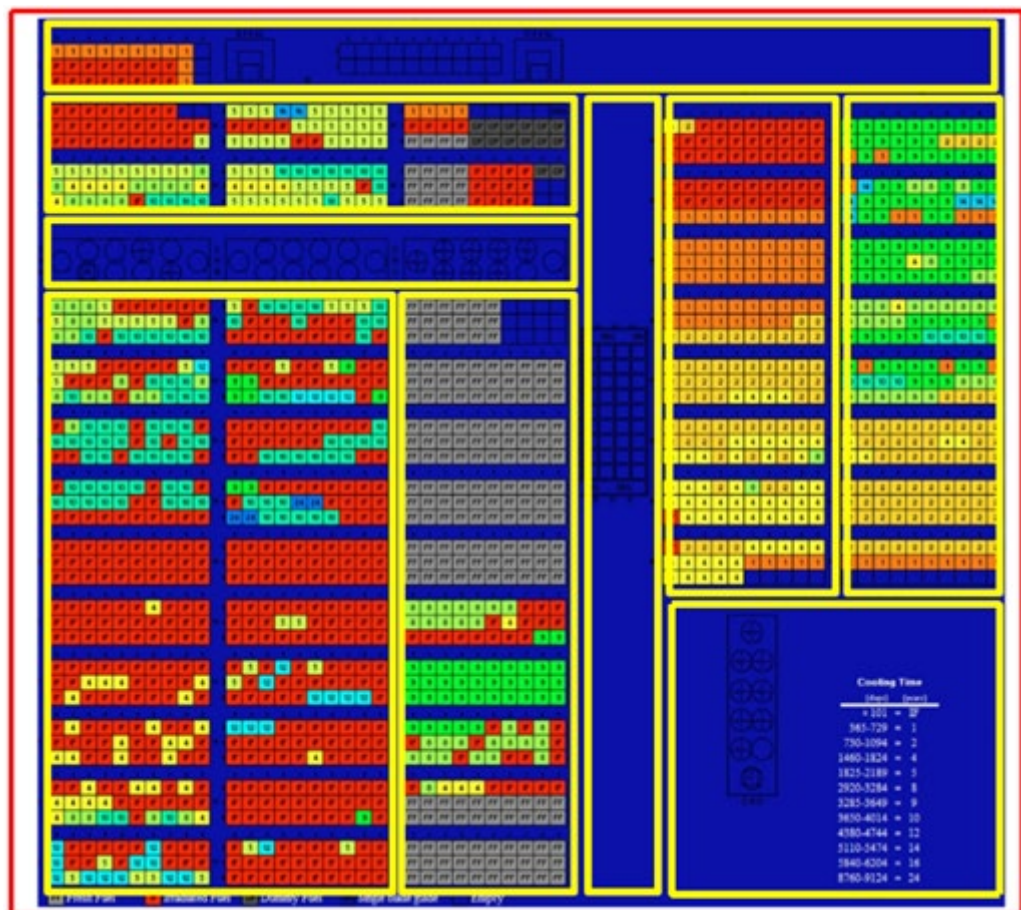


Fig. 4.17 Old nodalisation of the spent fuel pool (left) and the new, automated nodalisation of the spent fuel pool (right)

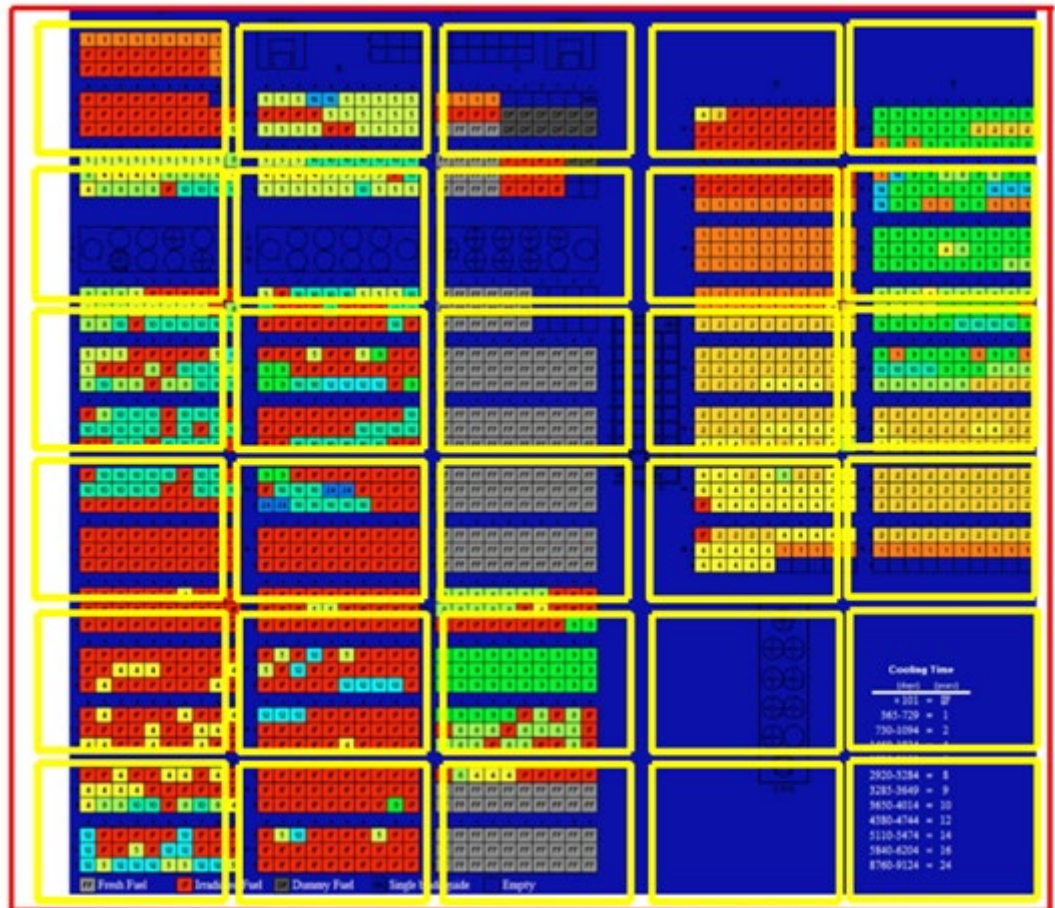


Fig. 4.18 Old nodalisation of the spent fuel pool (left) and the new, automated nodalisation of the spent fuel pool (right)

With that, the user can still flexibly modalised a spent fuel pool, however, in a much faster and in a less error-prone way.

5 Cross-sectional tasks

5.1 WP4.1 Documentation and quality assurance

For user guidance, ATHLET-CD includes program documentation in English. These describe the usage of ATHLET-CD and the underlying model basis. During the project, there were two official ATHLET-CD releases and code documentation had to be updated. Also, some gaps in the documentation were filled to make the code more convenient for the user.

For quality assurance during programming and in accordance with the quality guidelines of GRS /GRS 21/, a number of measures were carried out. An important element is the test calculations on the Continuous Integration of Gitlab, with which, among other things, ATHLET-CD source code can be compiled, and data sets can be started automatically. The set of ATHLET-CD datasets in the Gitlab server were expanded and are planned to be extended further.

With the release of new AC² versions, additional portability tests were carried out on all computer types and compilers available in the GRS.

Also, creating this final report in English was a key point in this WP.

5.2 WP4.2 Transfer of know-how

During the project, new colleagues started using and developing ATHLET-CD. As ATHLET-CD is a very complex program, new users and developers need time and support to be able to effectively start working with ATHLET-CD.

In order to simplify the start with ATHLET-CD a tutorial was created, with a step-by-step guide how to create an ATHLET-CD input deck from an existing ATHLET input deck. This tutorial as provided with the release AC² 2021 to all users. Additionally, the program documentation for the release ATHLET-CD 3.3 was extended significantly.

Newcomers were tutored on the tasks described previously in the report.

5.3 WP4.3 Program use and code transfer

ATHLET-CD is validated both internally and externally and is increasingly applied by other institutions. The feedback of experience regularly resulted in hints for further improvement of the models, elimination of program weaknesses, optimisation of auxiliary programmes and the need for further developments. The intensive cooperation and support, especially with users at German research institutions, both in application and in external developments, also directly benefited the training of young researchers. In particular, support for the installation of new versions of the MEWA module by IKE Stuttgart and further developments by PSS Bochum should be mentioned here. This kind of support facilitates the successful completion of master theses and dissertations at external research institutions. Furthermore, the preparation and participation in the regular AC² user meetings took place here.

Besides receiving models, feature requests and bug reports from external users, this WP also involved consulting tasks, to help the users. Consulting needs occurred, when:

- a simulation showed surprising results and its plausibility had to be checked,
- erroneous simulations, typically program stops, where it had to be determined if the root cause of the problem is in the input deck or in the source code, and
- deeper knowledge about the used models was needed than what is available in the ATHLET-CD documentation for external validation or development.

During the timeframe of the project there were two official releases of AC²/ATHLET-CD, versions 3.2 and 3.3. For each release an extended validation was performed, accompanied with a deeper analysis of the plausibility of the code.

5.4 WP4.4 Code maintenance

Necessary and unplannable program improvement work that cannot be assigned to WP1, WP2 and WP3 was carried out under this task. This mainly includes the elimination of program weaknesses and the short-term implementation of user requirements. Other AC² developments (in ATHLET, COCOSYS but also tools such as ATLASneo) required limited program adaptations, which were implemented here at short notice.

For a detailed list of improvements please see the document “Program updates” in ATHLET-CD 3.3.

5.5 WP4.5 Experimental support and international cooperation

The strong and fruitful cooperation with KIT continued during the project period. As the COVID pandemic halted or delayed several planned experiments, the cooperation consisted mainly of exchange of new correlations, methods and experience regarding the QUENCH-19 ATF experiment /HOL 19/.

GRS participated actively in the already finished European H2020 project IVMR (In Vessel Melt Retention /CAR 20/). During the project, GRS was involved in the elaboration of a PIRT (phenomena identification ranking table) to support severe accident code development, participated in a benchmark exercise for the AP 1000 reactor, performed IVR analyses for a BWR reactor and supported IVR analyses of PWR reactor designs. The participation in these tasks actively supported the development of AC², helped to identify existing uncertainties and further development needs. Moreover, the participation in the benchmark exercise provided the basis of the verification on the new models implemented in AIDA.

The IVMR project identified further research needs to support an international harmonised understanding of the safety demonstration of IVR. Therefore, IAEA launched in 2020 a Common Research Project (CRP) with the topic: *Developing a phenomena identification and ranking table (PIRT) and a validation matrix, and performing a benchmark for In-Vessel Melt Retention*, with 23 organisations from 14 IAEA member states. The project aims to harmonise the international understanding of the scientific and technological bases underpinning crucial parts of the safety demonstration of IVMR. The four tasks of the CRP are to develop a PIRT, develop a validation matrix, perform benchmark on individual phenomena and analytical benchmark calculations. GRS participates actively in the project and took the lead for the task 1 PIRT development. The participation in the different tasks supports the code development process and provides access to validation and verification data.

5.6 WP4.6 Project management

The subject of this work package were the tasks of project management and project controlling. Project management and project controlling ensured that all work in the project is coordinated in accordance with the GRS project and quality management processes and rules and in line with the specifications of the client, and that it is carried out properly and on schedule, and that it is recorded, stored and processed in line with requirements. Project management included all administrative tasks that arose in connection with contact with the client and project support. The tasks of project management were, in particular, the continuous coordination, implementation and monitoring of the contractually agreed administrative tasks, which included, among other things, the application for non-European business trips, budget control, the submission of change requests and the initiation of quarterly deductions. The project management supported the project manager in the planning of resources and personnel, the allocation of work in view of the available budget, and the approval of funds after checking for contractual compliance. Finally, the project management was responsible for the formal quality assurance of all work results, the review of the work resulted with regard to compliance with the GRS quality standards as well as the final release of all results that are to be sent externally or published. Project controlling was responsible for the IT input, maintenance and continuous updating of the contract-relevant data as well as the IT recording and storage of the project-relevant documents (offers, contracts and modification services). Project controlling ensured that GRS is able to provide the client with all project-relevant information electronically at any time as required. This work package did not include all technical research tasks including the documentation of the research results in semi-annual and annual reports and the preparation of the final report as well as the technical management of the research project. Corresponding costs for this were included in the technical work packages.

6 Summary and outlook

The topics and focal points of the project RS1574 “Further development of the module ATHLET-CD of the code package AC²” were successfully dealt with within the project duration of three years. All important project goals were achieved. Within the framework of the project, numerous new developments were started and model improvements were implemented in order to guarantee the performance and reliability of ATHLET-CD for the future with a view to a constantly growing range of applications. The further intensification of the cooperation and support of the program users as well as the cooperation in international working groups gave important impulses for the further development of ATHLET-CD, which could be taken up and implemented within the project. Some of the program improvements have already been distributed to all users of ATHLET-CD via the release of new program versions; others will follow with the next release, which is expected in 2023. The measures for quality assurance of the program development were significantly extended by advanced tools and revised workflows, which promote the efficiency and quality of the code development as well as the know-how transfer, so that ATHLET-CD can also be provided as a quality-assured analysis tool in the long term.

The development of ATHLET-CD will also be continued after the end of the RS1574 project in order to meet new requirements on the part of the program application and to close existing model gaps, also with a view to new and evolutionary reactor designs. Based on the experience gained from this project and user feedback, various topics for future developments were identified. For example, the structures of ATHLET and ATHLET-CD are to be more closely unified and coupled in the future to ensure better applicability, maintainability and expandability of the code. It is also planned to develop models for previously neglected phenomena (such as the dynamically changing melt velocity, eutectic formation or melt fragmentation) and to incorporate them into ATHLET-CD. The quality assurance measures achieved in this project (automated testing) are to be further expanded in the future. Based on the progress also achieved in this project regarding the modelling of the phenomena in the lower plenum, the models will be further improved, maintained and harmonised.

In addition, the work in international groups will be continued. This concerns in particular work in committees on the topic of in-vessel melt retention. In addition, contacts with national and international partners will be further expanded and maintained.

Many of the model developments carried out within the framework of the present project RS1574, but also developments from other research projects that were not released in the program version AC²-2021. They will be, however, available to all program users in the planned future releases. These program improvements will ensure that the numerous users trained in the use of ATHLET-CD will continue to have a powerful, reliable and user-friendly tool at their disposal in the future, which will allow safety analyses to be carried out in accordance with the current state of science and technology.

References

- /ALL 92/ Allison, C. M., Siefken, J. L., Coryell, E. W.: SCDAP/RELAP5/MOD3 code development. EG and G Idaho, Inc., Idaho Falls, ID (United States), EGG-M-92630; CONF-921007-14, 31 December 1992.
- /ARN 21/ Arndt, S., Band, S., Beck, S., Eschricht, D., Iliev, D., Klein-Heßling, W., Nowack, H., Reinke, N., Sonnenkalb, M., Spengler, C., Weber, G.: COCOSYS 3.1 User Manual. Gesellschaft für Anlagen- und Reaktorsicherheit (GRS) gGmbH (GRS), GRS-P-3 / Vol. 1, 2021.
- /ASM 04/ Asmolov, V. G., et al.: PARTITIONING OF U, Zr AND FP BETWEEN MOLTEN OXIDIC AND METALLIC CORIUM. Ed.: OECD Nuclear Energy Agency (NEA), Kurchatov Institute, MASCA Seminar 2004, 2004.
- /AUS 21a/ Austregesilo, H., Schöffel, P. J., von der Cron, D., Weyermann, F., Wielenberg, A., Wong, K. W.: ATHLET 3.3 User's Manual. GRS-P-1/Vol. 1 Rev. 9, November 2021.
- /AUS 21b/ Austregesilo, H., Lee, J., Schöffel, P. J., Skorek, T., von der Cron, D., Weyermann, F., Wong, K. W.: ATHLET 3.3 Models and Methods. GRS-P-1/Vol. 4 Rev. 6, November 2021.
- /BAL 09/ Bals, C.: Post-test calculation of QUENCH-15 with ATHLET-CD. Presentation, KIT Karlsruhe, 15th International Quench Workshop: Karlsruhe, November 2009.
- /BAN 18/ Band, S., Richter, C., Sogalla, M., Sonnenkalb, M.: Unfallablauf- und Quelltermanalysen zu den Ereignissen in Fukushima im Rahmen des OECD/NEA BSAF-Projektes Phase II. Gesellschaft für Anlagen- und Reaktorsicherheit (GRS) gGmbH (GRS), GRS-, vol. 485, ISBN 978-3-946607-69-4: Köln, 2018.
- /BAR 21/ Barrachin, M.: Corium Experimental Thermodynamics: A Review and Some Perspectives, A Review and Some Perspectives. Ed.: Thermo 2021, Institut de Radioprotection et de Sûreté Nucléaire (IRSN), 2021.

- /BER 82/ Berna, G. A.: Grid-spacer removal model. [PWR; BWR]. EG and G Idaho, Inc., Idaho Falls (USA), EGG-CDD-5831, DOI 10.2172/5338728, 1982.
- /CAR 20/ Carénini, L., Fichot, F., Bakouta, N., Filippov, A., Le Tellier, R., Viot, L., Melnikov, I., Pandazis, P.: Main outcomes from the IVR code benchmark performed in the European IVMR project. *Annals of Nuclear Energy*, vol. 146, pp. 107612, DOI 10.1016/j.anucene.2020.107612, 2020.
- /DRA 05/ Drath, T., Kleinhietpaß, I. D., Unger, H. E., Koch, M. K.: Simulation des TMI-2-Unfalls mit dem Programmsystem ATHLET-CD (Teil 2). Ruhr-Universität Bochum (RUB), LEE-26, June 2005.
- /EPRI 80/ Electric Power Research Institute (EPRI): Analysis of Three Mile Island-Unit 2 Accident. NSAC-80-1, 1980. ed., 448 p., DOI 10.2172/5598769, 1980.
- /GRS 21/ GRS gGmbH: Managementhandbuch Kapitel 2.2.3.5: Softwareentwicklung (TKP 03-05). Gesellschaft für Anlagen- und Reaktorsicherheit (GRS) gGmbH (GRS), Managementhandbuch, Kapitel 2.2.3.5, Rev. 2, 2021.
- /HAN 17/ Hannstein, V., Behler, M., Sommer, F.: MOTIVE - A New Modular Burn-up Code. In: American Nuclear Society (ANS): International Conference on Mathematics & Computational Methods Applied to Nuclear Science & Engineering. M&C 2017, Jeju, Korea, 16 - 20 April 2017, ISBN 978-1-5108-5645-5, Curran Associates, Inc.: Red Hook, NY, USA, 2017.
- /HOL 19/ Hollands, T., Lovasz, L., Bals, C.: Status of ATF Modelling in AC2, Proceedings of 2019 International Topical Meeting on Accident Tolerant Fuel, Shenzhen, China. 2019.
- /LOV 21a/ Lovasz, L., Bals, C., D'Alessandro, C., Hollands, T., Köllein, C., Austregesilo, H., Pandazis, P., Tiborcz, L., Weber, S.: ATHLET-CD 3.3 Models and Methods. Gesellschaft für Anlagen- und Reaktorsicherheit (GRS) gGmbH, GRS-P-4/Vol 2 Rev. 0, November 2021.

- /LOV 21b/ Lovasz, L., Austregesilo, H., Bals, C., Hollands, T., Köllein, C., Luther, W., Pandazis, P., Schubert, J.-D., Tiborcz, L., Weber, S., Wielenberg, A.: ATHLET-CD 3.3 User's Manual, Input Data Description. GRS-P-4/Vol. 1 Rev. 8, November 2021.
- /NAG 97/ Nagase, F., Uetsusa, H., Otomo, T.: B4C/Zircaloy Reaction at Temperatures from 1,173 to 1,953 K. *Journal of Nuclear Science and Technology*, vol. 34, no. 4, pp. 367–374, DOI 10.1080/18811248.1997.9733676, 1997.
- /NEA 18/ OECD Nuclear Energy Agency (NEA): State-of-the-Art Report on Light Water Reactor Accident-Tolerant Fuels. *Nuclear Science*, NEA No. 7317, 372 p., ISBN 9789264308343, DOI 10.1787/9789264308343-en, OECD Publishing: Paris, 2018.
- /ORNL 18/ Oak Ridge National Laboratory (ORNL): Handbook on the Material Properties of FeCrAl Alloys for Nuclear Applications, ORNL/SPR-2018/905. U.S. Department of Energy (DOE), 18. ed., 68 p., 2018.
- /PAN 22/ Pandazis, P., Lovasz, L.: Coupled ATHLET - ATHLET-CD Simulation of In-Vessel Retention Scenario in PWR. In: American Nuclear Society (ANS), SCK-CEN (Eds.): 19th International Topical Meeting on Nuclear Reactor Thermal Hydraulics. NURETH 19, virtual, 6 - 11 March 2022, 2022.
- /SAL 04/ Salay, M., Fichot, F.: Modelling of corium stratification in the lower plenum of a reactor vessel. Ed.: OECD Nuclear Energy Agency (NEA), Institut de Radioprotection et de Sûreté Nucléaire (IRSN), MASCA Seminar 2004, 2004.
- /SEH 12/ Sehgal, B. R. (Ed.): Nuclear safety in light water reactors, Severe accident phenomenology. 1. ed., xvi, 714, ISBN 978-0-12-388446-6, Elsevier Academic Press: Amsterdam, Boston, 2012.
- /SEI 01/ Seiler, J. M., Froment, K.: SCALING MATERIAL EFFECTS IN LATE PHASES OF SEVERE ACCIDENTS. Ed.: ICONE, CEA, ICONE-9: Paris (France), 2001.

- /SIE 94/ Siefken, L. J., Olsen, M. V.: A model for the effect of Inconel grid spacers on progression of damage in reactor core. Nuclear Engineering and Design, vol. 146, no. 1, pp. 427–437, DOI 10.1016/0029-5493(94)90348-4, 1994.
- /STE 21/ Steinhoff, T., Jacht, V.: NuT 2.0 Numerical Toolkit User's Manual. GRS-P-10 / Vol. 1 Rev. 4, November 2021.
- /STU 18/ Stuckert, J., Große, M., Laier, J., Moch, J., Peters, U., Stegmaier, U., Steinbrück, M., Terrani, K. A.: First results of the bundle test QUENCH-19 with FeCrAl claddings. Ed.: Karlsruher Institut für Technologie (KIT), 24th International QUENCH Workshop: Karlsruhe, November 2018.
- /TRO 00/ Troyanov, V., Pomeschikov, A., Sougonjaev, V., Ponomarenko, V., Scheglov, A.: High temperature study of the control rod behaviour under accident conditions. 2000.
- /TUR 95/ Turner, J.: Atoms, Radiation and Radiation Protection, 2nd edition. Wiley & Sons. Inc., 1995.
- /UET 96/ Uetsuka, H., Katanashi, S., Ishijim, K.: Research activities at JAERI on core material behaviour under severe accident condition. In: International Atomic Energy Agency (IAEA) (Ed.): Behaviour of LWR Core Materials, Proceedings of a Technical Committee Meeting held in Dimitrovgrad, Russian Federation, 9-13 October 1995. Dimitrovgrad, Russian Federation, 9 - 13 October 1995, IAEA-TECDOC-, no. 921, 1996.
- /WEB 14/ Weber, S., Austregesilo, H., Bals, C., Band, S., Hollands, T., Köllein, C., Schubert, J.-D.: Weiterentwicklung des Rechenprogramms ATHLET-CD, Further development of the code ATHLET-CD. Gesellschaft für Anlagen- und Reaktorsicherheit (GRS) gGmbH (GRS), GRS-A-, No. 3736, March 2014.
- /WIE 19/ Wielenberg, A., Lovasz, L., Pandazis, P., Papukchiev, A., Tiborcz, L., Schöfel, P. J., Spengler, C., Sonnenkalb, M., Schaffrath, A.: Recent improvements in the system code package AC2 2019 for the safety analysis of nuclear reactors. Nuclear Engineering and Design, no. 354, pp. 110211, DOI 10.1016/j.nucengdes.2019.110211, 2019.

Table of figures

Fig. 1.1	ATHLET-CD code structure and interfaces /LOV 21a/	2
Fig. 2.1	Top view of a core discretised radially only (4 representative rings).....	8
Fig. 2.2	Top view of a core discretised radially and azimuthally (each ring discretised into 8 nodes), with new relocation model	8
Fig. 2.3	Side and top view of the core nodalisation in the sample input	9
Fig. 2.4	Simulation results of the sample calculation without horizontal melt relocation model	10
Fig. 2.5	Simulation results of the sample calculation with horizontal melt relocation model	11
Fig. 2.6	Spacer grid (square and hexagonal shaped) zone per rod.....	14
Fig. 2.7	Sample cross-section of the contact support between spacer grid and fuel rod.....	16
Fig. 2.8	Schematic for spacer grid	19
Fig. 2.9	Comparison of the total molten material between the development version and release version 3.3	22
Fig. 2.10	Manual check for total amount of melt	23
Fig. 2.11	Integral hydrogen generation	24
Fig. 2.12	Cladding temperature at 1250 m.....	25
Fig. 2.13	Cladding temperature at 1150 mm.....	26
Fig. 2.14	Cladding temperature at 1150 mm.....	26
Fig. 2.15	Cladding temperature at 550 mm.....	27
Fig. 2.16	Cladding temperature at 150 mm.....	27
Fig. 2.17	Water level at time interval between 5500 – 6000 s	28
Fig. 2.18	Core melt relocation path to the lower plenum during the TMI-2 accident /SHE 12/	29
Fig. 2.19	Axial melt distribution in the outermost core node (SUMUOSL = ceramic melt per fuel rod)	35
Fig. 2.20	Core shroud failure at elevation 6 with and without modelling of melt bypass	35

Fig. 2.21	Melt mass accumulation in the lower plenum with and without melt bypass modelling	36
Fig. 2.22	Decay power in the lower plenum with and without melt bypass modelling	37
Fig. 2.23	Lower part of a VVER-440 reactor core /PET 15/.....	38
Fig. 2.24	Sample nodalisation for VVER-440.....	41
Fig. 2.25	Axial power distribution in ROD1, ROD3 and ROD5 (left) and ROD2 (right) (effects also fission product distribution)	44
Fig. 2.26	VVER-440 nodalisation, colours depend on the temperature of the structure (yellow-high, red/purple-low)	45
Fig. 2.27	Power distribution along axial nodes for ROD2.....	46
Fig. 2.28	Fission product distribution along axial nodes for ROD2.....	46
Fig. 2.29	Power distribution along axial nodes for ROD1	47
Fig. 2.30	Power distribution along axial nodes for ROD1	47
Fig. 2.31	Axial temperature distribution of the core surrounding structure.....	48
Fig. 2.32	Axial temperature distribution of the core surrounding structure.....	48
Fig. 2.33	Xe release rate at the hottest part in the follower-assemblies (ROD2)	49
Fig. 2.34	Total core failure in a VVER-440 reactor modelled with the new ATlhET-CD VVER-440 option	49
Fig. 2.35	Evolution of temperatures in experiment and in the different simulations at elevation 550 mm.....	53
Fig. 2.36	Evolution of temperatures in experiment and in the different simulations at elevation 950 mm.....	54
Fig. 2.37	Temperature evolution at different horizontal positions at elevation 850 mm (Kanthal)	54
Fig. 2.38	Total hydrogen generated.....	55
Fig. 2.39	Comparison of different correlations for B4C-Zr reaction	57
Fig. 2.40	Comparison of different correlations for B4C-S.S. reaction	58
Fig. 2.41	Fe-B phase diagram /OKA 16/.....	61
Fig. 2.42	Zr-(B0.5C0.5-) phase diagram /HOF 89/.....	62

Fig. 2.43	The core degradation state of IEUTECT = 0	64
Fig. 2.44	The core degradation state of IEUTECT = 1	65
Fig. 2.45	Water level evolution between time interval of 16000 to 18000 s	66
Fig. 2.46	Total hydrogen generation	66
Fig. 2.47	Detailed description of the newly introduced output values	69
Fig. 2.48	Release Iodine aerosol mass	73
Fig. 2.49	Release Iodine vapor mass	73
Fig. 2.50	Release of plutonium (aerosol)	74
Fig. 2.51	Release of zirconium (aerosol)	74
Fig. 2.52	Structure failure information	75
Fig. 2.53	Original SAFT output	75
Fig. 2.54	Void in pipe after reflooding	77
Fig. 2.55	Mass of Cs in liquid phase in different control volumes	77
Fig. 2.56	Mass of Ag in liquid phase in different control volumes	78
Fig. 2.57	Outflow mass of Cs and Ag at the end of the SAFT-path	78
Fig. 2.58	Transported fission products (Silver)	79
Fig. 2.59	Transported fission products (Uranium)	80
Fig. 2.60	Transported fission products (Krypton)	80
Fig. 2.61	Transported fission products (Xenon)	81
Fig. 2.62	Water solubility of cesium	82
Fig. 2.63	Void fraction in the test section	82
Fig. 2.64	Water solubility of Cesium (flooded case)	84
Fig. 2.65	Water solubility of Cesium (flooded case)	84
Fig. 2.66	Vertical view of structure, fluid and β -radiation zone	89
Fig. 2.67	Zones for β -radiation from the fluid towards walls and into fluid	90
Fig. 2.68	β -radiation zone from the intermediate zone in the fluid	91
Fig. 2.69	β -radiation zones for radiation from the wall surface	93

Fig. 2.70	Nodalisation of the verification sample.....	105
Fig. 2.71	Different decay power distributions in the core due to different power histories.....	106
Fig. 2.72	Evolution of Xe mass in the core and in the cooling circuit.....	107
Fig. 2.73	Evolution of the power of the released, relocated and remaining isotopes.....	107
Fig. 2.74	Power distribution in the cooling circuit (to wall).....	108
Fig. 2.75	Power distribution in the cooling circuit (to fluid).....	108
Fig. 2.76	Example of SAFT-network.....	110
Fig. 2.77	Information about single junction pipes in SAFT.....	111
Fig. 2.78	Branching with "Branch"-object.....	112
Fig. 2.79	Simple branching without "Branch"-object (start).....	112
Fig. 2.80	Simple branching without "Branch"-object (end).....	112
Fig. 2.81	Internal branching.....	113
Fig. 2.82	Dead end in SAFT network.....	114
Fig. 2.83	Information about automatically converted dead ends.....	115
Fig. 2.84	Error message in case of a dead-end detection.....	116
Fig. 3.1	Definition of input parameters for LHEAD stand-alone calculation F.....	120
Fig. 3.2	Activation of stand-alone option and definition of initial masses.....	121
Fig. 3.3	Sample of the used tables.....	121
Fig. 3.4	Melt mass in the lower plenum: stand alone and coupled calculation.....	122
Fig. 3.5	Decay power of melt in the lower plenum: stand alone and coupled calculation.....	123
Fig. 3.6	Scheme of the coupling between AIDA and the ERVC model.....	134
Fig. 4.1	Nodalisation used in the input deck for the generic PWR.....	138
Fig. 4.2	Mass balance check for ceramic melt.....	139
Fig. 4.3	Accumulation of the produced hydrogen.....	140
Fig. 4.4	Remaining mass of XE in the core.....	141

Fig. 4.5	Melt mass accumulation in the lower plenum.....	141
Fig. 4.6	End state of the core in the demonstrated example	142
Fig. 4.7	Evolution of pressure in the primary circuit (left) and in containment (right).....	144
Fig. 4.8	Oscillation of pressure in the primary circuit (left) and in containment (right).....	144
Fig. 4.9	Mass of xenon leaving ATHLET-CD domain and entering COCOSYS...	145
Fig. 4.10	Example of the output of the continuous integration system	147
Fig. 4.11	Evolution of the liquid mass in the spent fuel pool.....	150
Fig. 4.12	Evolution of the produced H ₂	151
Fig. 4.13	Evolution of molten mass in the spent fuel pool	151
Fig. 4.14	Evolution of the remaining (green) and released (red) Xe mass.....	152
Fig. 4.15	Evolution of recombined (red) and remaining (green) H ₂ mass in the con-tainment.....	153
Fig. 4.16	Evolution of xenon mass in the containment.....	154
Fig. 4.17	Old nodalisation of the spent fuel pool (left) and the new, automated nodali-sation of the spent fuel pool (right)	156
Fig. 4.18	Old nodalisation of the spent fuel pool (left) and the new, automated nodali-sation of the spent fuel pool (right)	157

List of tables

Tab. 2.1	Melting temperature of common spacer grid material	21
Tab. 2.2	Comparison of B ₄ C-Zr. Kinetic Equation	57
Tab. 2.3	Comparison of B ₄ C-S.S. Kinetic Equation	58
Tab. 2.4	Used values for interpolation for B ₄ C-Zr eutectic formation	63
Tab. 2.5	Used values for interpolation for B ₄ C-S.S. eutectic formation.....	63

**Gesellschaft für Anlagen-
und Reaktorsicherheit
(GRS) gGmbH**

Schwertnergasse 1
50667 Köln

Telefon +49 221 2068-0

Telefax +49 221 2068-888

Boltzmannstraße 14

85748 Garching b. München

Telefon +49 89 32004-0

Telefax +49 89 32004-300

Kurfürstendamm 200

10719 Berlin

Telefon +49 30 88589-0

Telefax +49 30 88589-111

Theodor-Heuss-Straße 4

38122 Braunschweig

Telefon +49 531 8012-0

Telefax +49 531 8012-200

www.grs.de